storage is occurring over much of the porous interval, at least two-thirds of the net pay. This conclusion is supported by the 12 and 24 hour shut-in runs that show injection into porosity below depth B at 5,516 feet. The slowly recovering temperature below depth A, 5,530 feet, is the result of the vast majority of the injected fluid entering porosity below this depth. The bottom ten feet of net pay is the location at which long term injection has taken place. The 12 and 24-hour shut-in surveys reveal conditions that were hidden by conduction cooling on the 1 and 3-hour runs; namely, fluid storage signatures appear at depth C, which is located in the porous interval immediately above the injection interval. The small indicated "loss" at depth E on the injecting survey may, indeed, be of significance and some injection is now taking place at this interval due either to a casing leak at this depth or to a loss behind pipe from the injection zone below. Subsequently, examination of a radioactive tracer survey will suggest that this flow occurs behind pipe.

TABLE 3. MINIMUM SHUT-IN PERIODS NECESSARY TO DETECT LEAKS BEHIND PIPE INTO ZONES ABOVE THE INJECTION INTERVAL

Prior Length of Continuous Injection	Minimum Shut-In Time to Detect Leaks of Several Weeks Standing
1 Month	6 - 12 Hours
6 Months	12 - 24 Hours
1 Year	24 - 48 Hours
5 Years	48 - 96 Hours
10 Years	96 - 192 Hours

Figure 7 (page 10) illustrates that lithology influence is such that porous dolomitic intervals will tend to lag non-porous intervals; so how would one differentiate what is seen at depth C on Figure 20 as being the result of injection at this depth rather than the influence of lithology? Two aspects of behavior rule against lithology. First is the "growth" of the signature with time on the 12 and 24-hour surveys. This is backwards to both the time progression indicated on the hypothetical Figure 7 and the actual behavior seen on Figure 16 at depths E and F. The second, and stronger, negative aspect is the shut-in behavior above the suspect depth C, Figure 20. Above 5,470 feet are located much thicker porous and non-porous intervals. Furthermore, the 1-hour shut-in survey shows a muted influence of this lithology on the slight "lead" in recovery evident in the tight section between 5,400 and 5,450 feet. Thus, lithology cannot account for the signature at depth C.

Nevertheless, uncertainty about lithology has made it a common practice to add a radioactive tracer survey to the temperature surveys when checking for confined injection. The tracer tool has incredible sensitivity to flow behind pipe, a feature not present in the injecting temperature survey when flow is upwards behind pipe. This practice, however, has caused the loss from industry of the original philosophy behind running surveys of the type shown on Figure 20. If

one intends to run the tracer tool anyway, then why run anything beyond the 1 and 3-hour shut-in surveys? The reason is contained in the discussion that follows.

Figure 20 is the first example of non-confined injection into a deep disposal zone. It also illustrates how problems typically develop. Quite likely, only the bottom fifteen feet of the perforations "broke" down to injection when the well was initially completed. The pressure increase associated with continued injection into a limited interval has caused the hard rock to fracture up into the next porous interval capable of relieving the pressure. These fractures may leave the wellbore with sufficient rapidity that they intersect the next porosity at a distance from the well that exceeds the range of all tools used for the injecting survey, temperature, radioactive tracer, and neutron activation survey. Only the long shut-in temperature surveys reveal this placement of fluid in porosity away from the well.

On Figure 20, the 1 and 3-hour shut-in surveys depict the influence of completion at depth D, 5,345 feet, in the same fashion as Figure 8 (page 11), frame A, at the casing shoe. On both figures, the extra insulation above the indicated depths causes a more rapid return to static. On Figure 20, this influence is already attenuated on the 3-hour survey and is practically absent from the 12 and 24-hour runs.

Finally, the astute reader may have noticed a "peculiar" behavior to the shut-in logs below depth A on Figure 20. The temperature warms during the first hour more than it does during the next 24 hours. This behavior merely means that the water currently injected is slightly cooler than the long-time "average" injection temperature. This particular set of logs were run in mid December in West Texas. Quite obviously, the temperature of water injected into a formation at any particular time may also be warmer than average zonal temperature in an old injection well. This was the situation when the temperature surveys in Figure 21 were recorded. During injection, water arrived at the disposal perforations about 2°F warmer than the average temperature of the injection zone which has received water for many years. The injecting survey shows losses at only two depths, A and B, inferring that most of remaining perforations are plugged. The "catch-up" shifts below each of these depths is to the cooler side because, as the shut-in surveys show, the "static" condition for current injection is a cooled formation, not one at normal temperature for this depth. Above 5,425 feet , the recovery is in the normal direction, i.e., from the cool side. The shut-in surveys all show the "warmed" storage porosity receiving current injection. The continued "growth" of these injection signatures for 12-hours of shut-in proves that the "current" injection profile has existed for some time and is not something that happened just recently. On Figure 21 is the relic, at depth C, of an earlier period of disposal into the zone immediately below the current completion.

The surveys in Figure 21 also refute the old saw, still being played, that an injecting temperature survey from an old injector "don't show you nothing." This is an outgrowth of the old, all too common procedure that tolerates a recording sensitivity of more like 10 °F/inch rather than the 1°F/inch employed for surveys of Figure 21. The figure further shows, on the 12-hour shut-in survey, that injection has taken place into the porosity over the entire interval during times past.

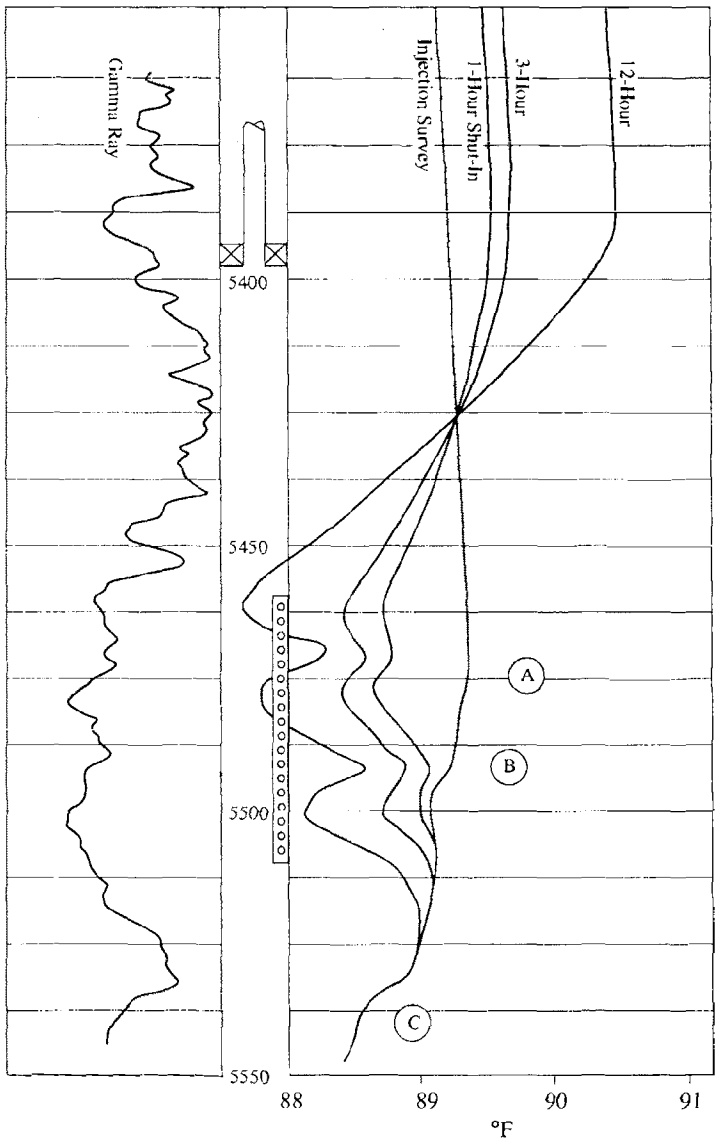

Figure 21. Temperature surveys from a well on 600 BPD injection at a water temperature 2°F warmer than average from long-term injection.

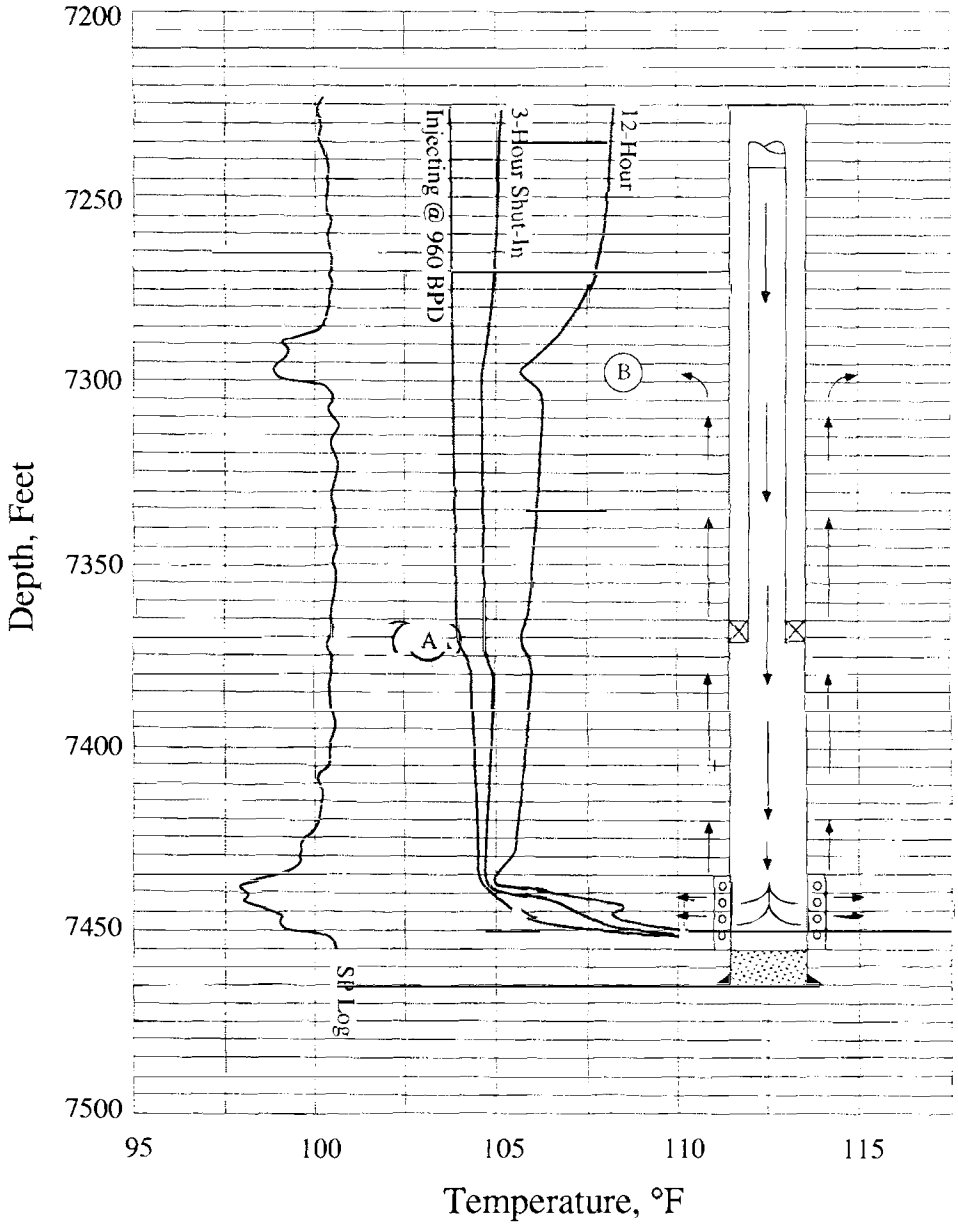

Figure 22. **Temperature surveys from a well on injection at 960 BPD with flow behind pipe even on shut-in status.**

Finally, the shut-in surveys show that over the lifetime of this well, the completion has prevented any injection into the thin porous interval located only three feet above the designated injection interval and only seven feet above the top of the perforations.

The following comments are best understood by reference to Figure 9 (page 12) that contains three computed injection surveys. The insulation offered by the stagnant annular fluid effectively hides from the thermometer during injection any flow that occurs behind pipe above the packer, i.e., above depth A on Figure 9. Consequently, the most one should expect to see on an injection survey is the type of change at the depth of the packer that is evident on Figure 17 (page 24) at the thief zone. The "loss" would appear to occur at a depth that corresponds to the end of the tubing string. This type of behavior is evident on the injecting survey of Figure 22 where the first "loss" appears at depth A, the end of the tubing. The 12-hour shut-in survey, however, clearly shows the storage porosity located at depth B, some seventy-five feet above depth A. This same survey also shows flow from the injection interval up to depth B as continuing after the well is shut off injection. Actually, the warm up on the injecting survey of Figure 22 is located some ten feet below the end of tubing. The thermometer hangs free usually until the entire tool clears the tubing, thus thermal contact with the casing wall typically does not occur for some 10 - 20 feet below the end of the tubing.

The same insulation that shields the thermometer in the tubing string also protects any behind-pipe flow from the injected stream flowing in the tubing. Once the leaking fluid goes above depth A on Figure 9, then it tends to carry its temperature upward with the flow in the same manner that injection inside the tubing carries its temperature downward. Thus, if one turns Figure 9 upside down and locates the tubing packer at zero depth, then survey 1 can be viewed as the temperature in a stream flowing behind casing upward into two shallow zones at depths B and C, respectively. This is not, however, the temperature profile that the thermometer in the tubing string will measure while the well is on injection. The influence of the behind-pipe flow will show up primarily as storage signatures on the shut-in surveys. Suppose that the leak charged zones on Figure 9 at 500 feet . The shut-in residual at this depth depends on the surface temperature of the injected water. Consequently, the storage signature on the shut-in surveys is dependent on injected fluid temperature. This fact is illustrated by the two frames of Figure 23, each computed for a month old injection well that has a behind-pipe leak from an injection interval at 5,600 feet up to a shallow zone at 500 feet. Injection rate into the well is 500 BPD while the leak rate is the value listed for each of the eleven shut-in surveys on the figure. Each frame is for a particular surface temperature for the injected water. The leak crossflow ceases when the well is shut in.

Frame A shows surveys run after a 6-hour shut-in following one month of injection of water at the surface temperature of 80°F. The 250 and 500 BPD leaks arrive at 500 feet at a temperature that is hotter than static at that depth. The 100 BPD leak, however, has cooled to nearly static temperature at 500 feet. It is evident on the survey simply because the 6-hour shut-in temperature on either side of 500 feet is still to the cool side of static. The leak would be hidden on a single, long-time shut-in survey. Leak rates less than 100 BPD are cooled by the injection and arrive at 500 feet colder than static temperature.

The behavior of the 12-hour shut-in surveys of frame B, Figure 23, after injection of water at 110°F is unusual at first glance. The variation, of course, is the result of a hot residual left from the hot water injection. At the 500-foot thief zone, this residual keeps the wellbore temperature at about 98°F after 12 hours of shut-in. The 500 BPD leak arrives at the thief zone about 2°F hotter than this residual and thus appears as a hotter signature on the survey. The 250 BPD leak, however, reaches the thief zone cooler than the 98°F residual. Thus, the wellbore temperature is reduced at the thief zone, the location where the cooler leak fluid is stored in porosity surrounding the wellbore and extending laterally away from it. The 100 BPD leak arrives at about static temperature. Lesser rates of leakage are warmed by the injection of hot water prior to shut-in. For this reason, the 20 and 10 BPD leaks give surveys on frame B of Figure 23 that progress to the hot residual as the rate decreases.

The lesson of Figure 23 is that one does not know exactly what to expect as a result of behind-pipe leakage from a deep disposal zone to shallow strata. It is therefore a wise procedure to run at least two shut-in surveys to ascertain any portions of the shallow wellbore that appear to be "locked" at a relatively unchanging temperature as a result of injection. Furthermore, the surveys on frame B of Figure 23 suggest that the appropriate shut-in times are at the tail end of the intervals of times listed in Table 3.

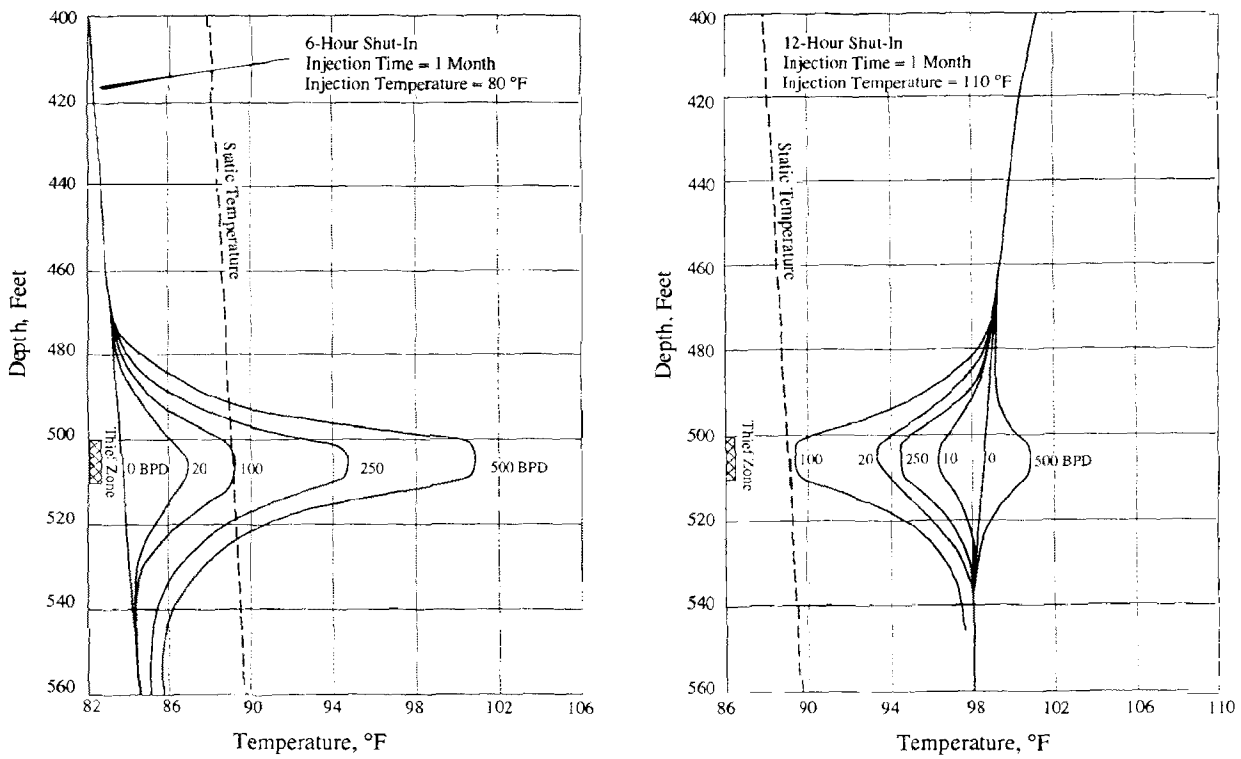

(A) Injection Water Temperature of 80°F

(B) Injection Water Temperature of 110°F

Figure 23. Shut-in temperature surveys across a thief zone at 500-510 feet charged by flow behind casing from injection interval at 5,600 feet.

In reality, deep disposal zones hardly ever leak into shallow strata as a result of flow behind pipe. Deep injectors pollute at shallow depths mainly as a result of tubing, packer and casing leaks. External corrosion can reduce casing wall thickness to the point that annular pressure from a tubing or packer leak will cause the casing to rupture. Subsidence and fault instability are common causes of casing failure in parts of the USA. Tubing and casing leaks are easy to detect on both injection and shut-in surveys as Figure 24 illustrates. The injecting survey shows a slope change at depth A but very little "catch-up" because the loss from the tubing continues downward in the casing. The typical "loss" signature occurs at depth B where the leak exits the casing. The 12-hour shut-in survey places the storage porosity at the same depth as the casing leak. From the relative positions of the static temperature and the injection survey, one can tell how the storage areas should appear on the shut-in runs. The loss at depth B on Figure 24 should cool any porosity in the neighborhood of the leak. This situation can be contrasted with the computed injection survey 1 on Figure 9 (page 12), where any casing leaks above 1,500 feet would add fluid that is warmer than the static temperature of receptor porosity. The storage signature on shut-in surveys would then appear as a "hot spot." The variability evident on Figure 23 for leaks behind pipe is thus removed for casing leaks.

Temperature Behavior in Shallow Injection Wells: These are the type of disposal wells most likely to pollute fresh water sands by loss from the injection zone. The temperature behavior in these wells is no different from the theory and examples that have already been examined for deep injection wells. Therefore, the reader should once again refer to the computed injection

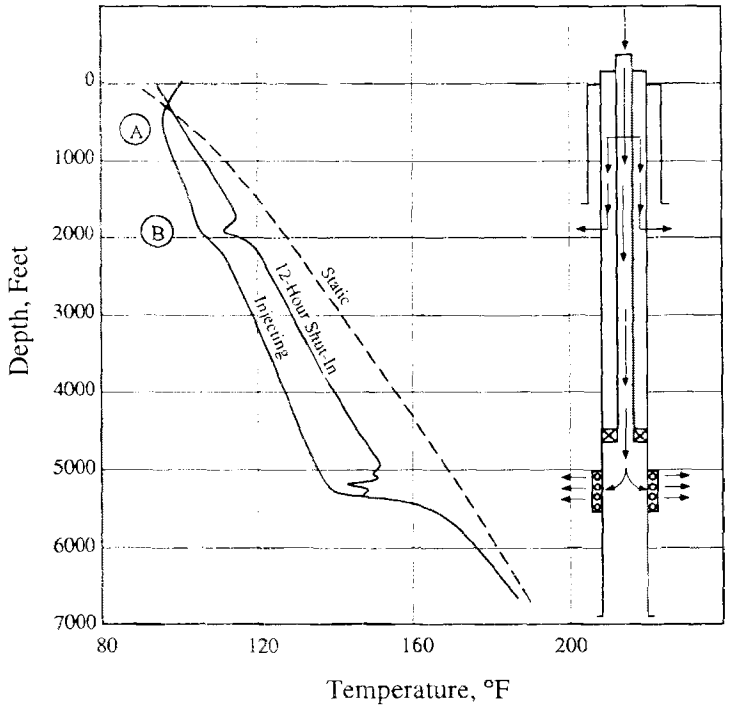

Figure 24. Temperature surveys from deep injector with shallow tubing leak at A and casing leak at B.

profiles on Figure 9, and, this time, imagine that the injection zone is located at 1,000 feet rather than at the deeper locations of the figure. Two things are then evident: First, the contrast in temperature between the injected water and the static wellbore is reduced. Temperature surveys must now be recorded at high sensitivity as a matter of course. Second, the type of storage signatures that one can expect depends entirely on the surface temperature of the injected water. These two facts are illustrated by the computed injecting and shut-in surveys appearing on frames A and B of Figure 25. In each frame, the well has been on injection for one month at a rate of 500 BPD into perforations opposite a 25-foot thick disposal zone at 975 to 1,000 feet. During this same month water has leaked from the perforated interval behind pipe up to a 10-foot thief zone located at 800 feet on frame A and at 825 feet on frame B, respectively. The two frames are computed for different water temperatures at the surface, frame A for water at the surface temperature of 80°F and frame B for 110°F water which is 30°F hotter than surface temperature. Each frame contains, as solid lines, two surveys with the well on injection at 500 BPD. One survey is for no leakage from the injection interval, 0 BPD leak, whereas the other allocates all 100% of injection, 500 BPD leak, to the flow behind pipe. Each frame also contains four surveys taken 12 hours after both injection and flow behind pipe has ceased. These surveys, shown as dashed lines, are for leak rates of 0, 10, 50, and 500 BPD.

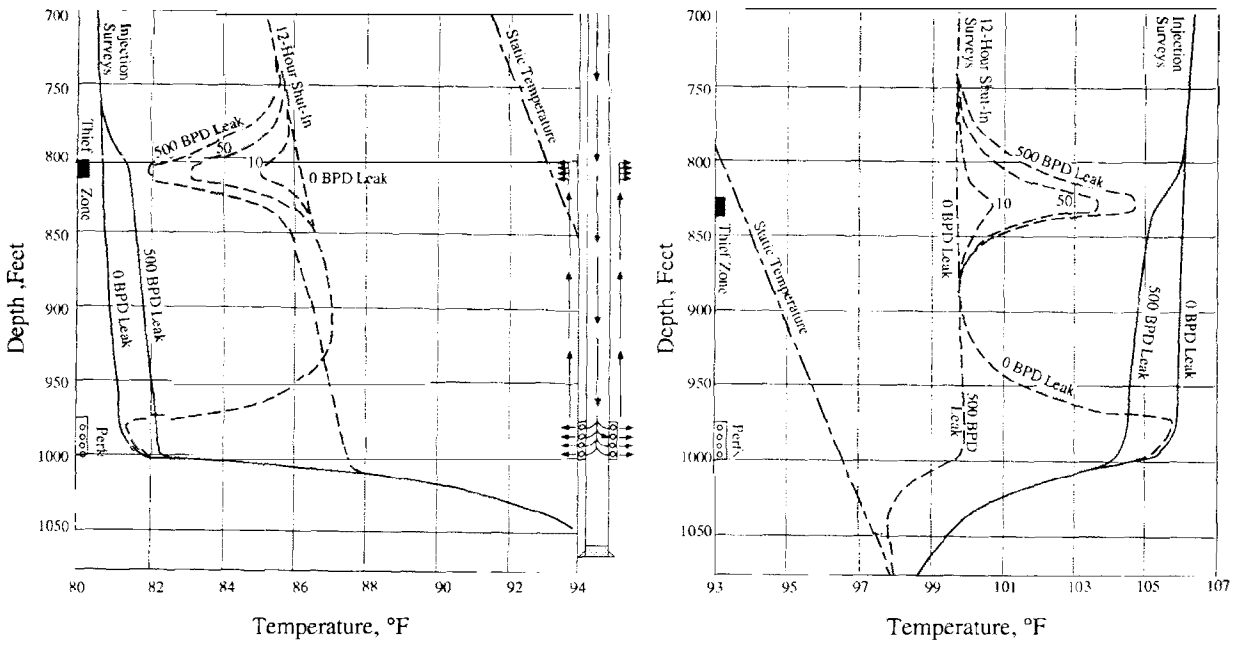

(A) Injection at 80°F Surface Temperature

(B) Injection at 110°F Surface Temperature

Figure 25. Computed temperature surveys injecting (—) and shut-in (---) from a well receiving 500 BPD water with various leaks behind pipe from injection perforations up to a shallower thief zone.

The length of the crossflow interval on Figure 25 is the same 200 feet, approximately, as that on Figure 19 (page 26) for loss from a deep injection zone. Furthermore, the rate of charge per foot of thief zone thickness is the same for the two figures. Yet twice the shut-in time is required on Figure 25 to produce storage roughly the same size as those of Figure 19. This additional time is a direct consequence of the decreased contrast between injected water temperature and static temperature. The second feature, dependence on surface temperature of injected water, is responsible for the cooler storage signatures on frame A and the warmer ones on frame B.

Shut-in temperature surveys for the two situations are given on Figures 26 and 27. Injecting surveys were not run for the four situations depicted on these figures. At the sensitivity used for the surveys, 1°F/inch or 2°F/inch, the injection surveys would be off scale anyway. In each figure the two frames contrast profiles for confined injection, frame A, with profiles for behind pipe leakage into porous intervals immediately above the injection zone, frame B. On the surveys of Figure 26, the injected water is at or near surface temperature. The resulting storage signatures are therefore cooler than the non-storage areas. The only new feature to these logs is the "nose" evident on frame B, Figure 26, at 2,180 feet, the top of the topmost injection zone. This "nose" is a signature of confinement of injection to depths below its location and is not an uncommon feature in clastic environments. It arises because of the interaction of two conditions: the decreased thermal conductivity of shale rich sediments and the change in direction of heat

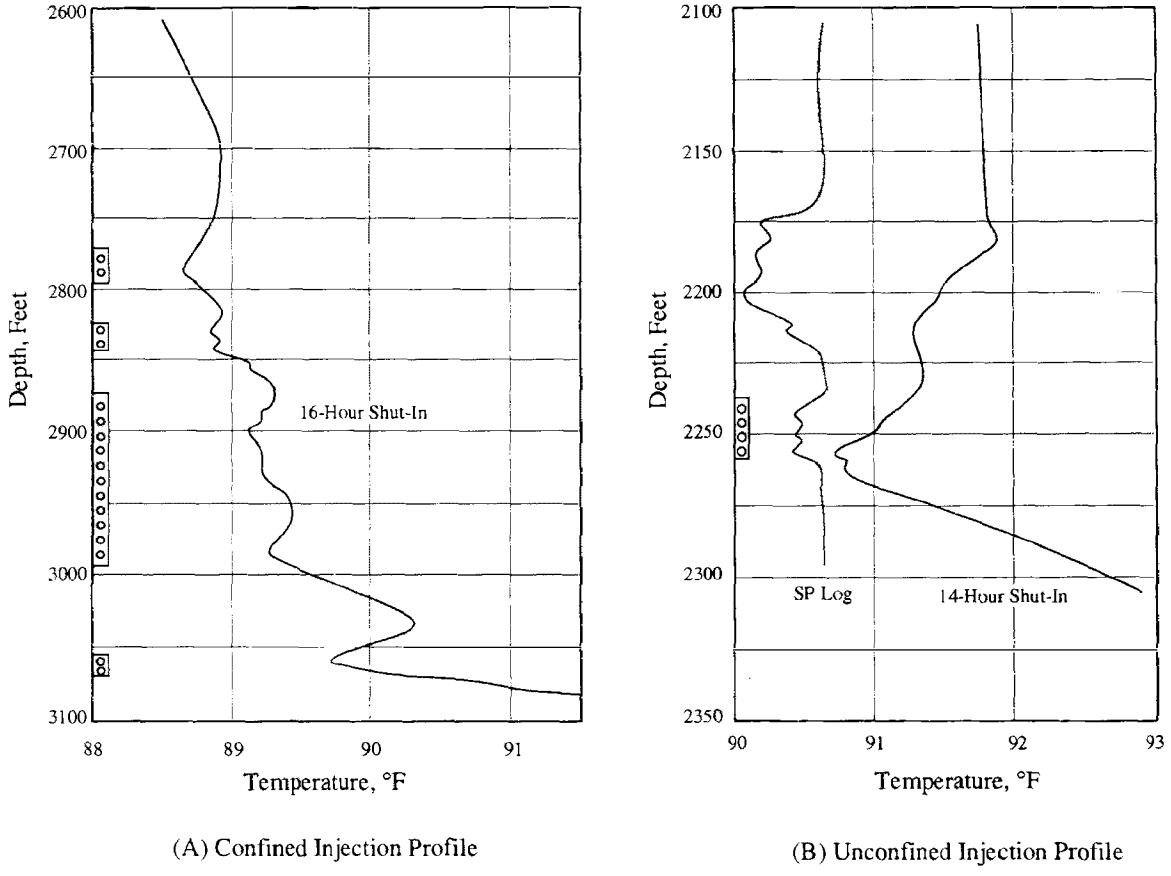

(A) Confined Injection Profile

(B) Unconfined Injection Profile

Figure 26. Shut-in temperature surveys for wells injecting near surface temperature.

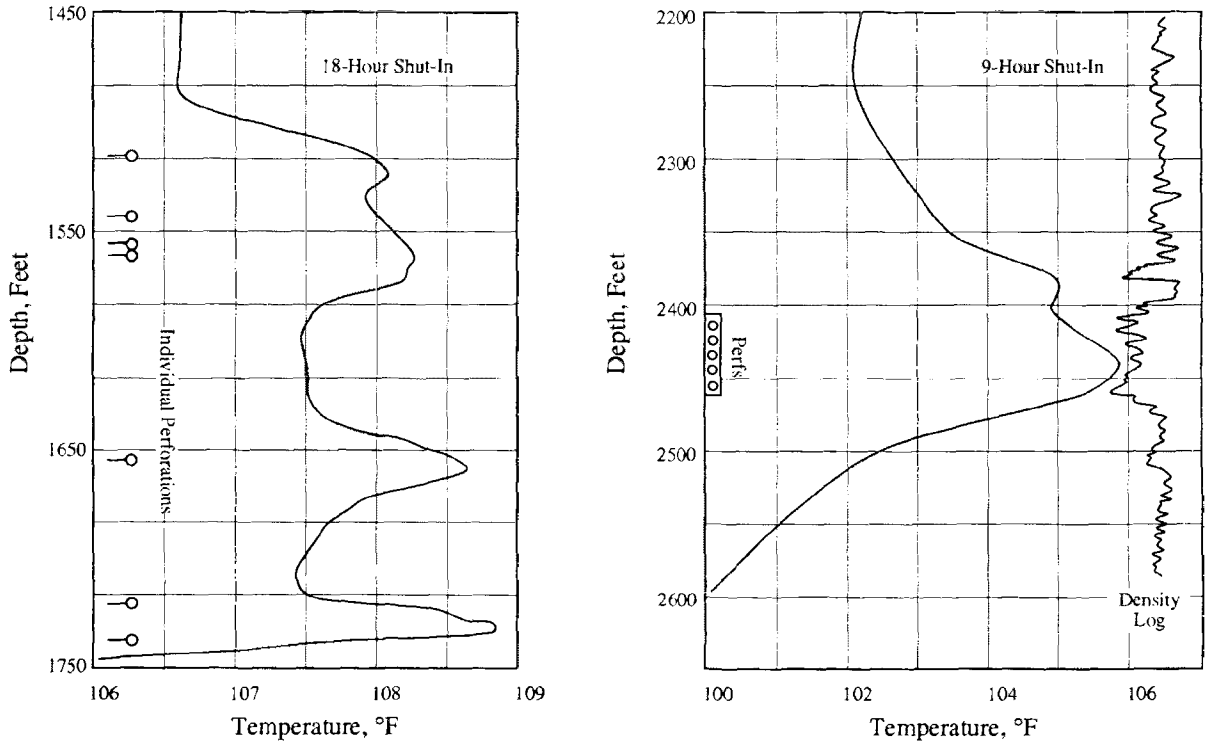

(A) Confined Injection Profile

(B) Unconfined Injection Profile

Figure 27. Shut-in temperature surveys for wells injecting hot water.

flux with vertical depth. Above an injection zone, heat flows to the well bore in a nearly lateral direction whereas this flow acquires a large vertical component at the top of an injection zone. Thus, the vertical temperature gradient must increase accordingly. The rapid change in thermal properties with depth restricts the variation to relatively small vertical intervals, thereby making the "nose" more noticeable in clastics. Like the signatures of lithology and completion, the presence of this "nose" is a matter of proper timing and is not necessarily present on any particular survey. As has already been noted, a "nose" could also be caused by the presence of a fracture, but for different reasons.

The storage signatures on Figure 27 are warm "spots" as the result of water injection at a temperature above surface temperature. These signatures are similar to those already observed on Figure 21, for a deep injector. The warm spots on Figure 27 are smeared more by vertical heat conduction due to longer injection times.

Before leaving related injection well problems, there is a need to discuss two additional reasons for loss in survey resolution besides the digitizing noise illustrated in Figure 3 (page 5). These additional reasons are excessive inertia in the recording system and the practice of logging upward rather than downward. Both are trademarks of the novice operator who does not know how to run a temperature survey, and accordingly, should not be a problem. That these problems

do exist, however, is evident from the surveys on frames A and B of Figure 28, two sets of surveys from the same injection well. Frame A shows an injecting survey at 700 BPD and a 9-hour shut-in survey after injection is stopped. Although both surveys were logged in the correct direction, downward, both show the "stairstepping" characteristic of excessive recording inertia. On an older analog panel this inertia is usually the result of failure to properly set the driving circuit that just overcomes recording pen friction. On a digital truck the stairstepping results from a sampling interval that is too long relative to the logging speed, or, in trade jargon, too large a time constant for the logging speed. Stairstepping can also occur if the display sensitivity exceeds the resolution of the tool. This is clearly not the case for the survey of frame A, Figure 28 because the steps amount to nearly 1/2 degree Fahrenheit! As a consequence of the inertia, the first loss on the injecting survey that can be called "real" is the major loss at depth A, located about midway down the perforated interval. Higher exits are lost in the inertial threshold.

In frame B of Figure 28, the thermometer is jerked off bottom and then moved upward at a constant speed. In this particular situation, such a procedure compounds all errors, those due to stabilization time necessary for the tool to track borehole fluid temperature and those due to mixing of borehole fluid ahead of the sensor. The result is a total loss of injection detail across the perforated interval.

The best of procedures can still produce the kind of temperature log appearing on Figure 29 to the right of the wellbore sketch for an old injection well. These surveys are of the seemingly

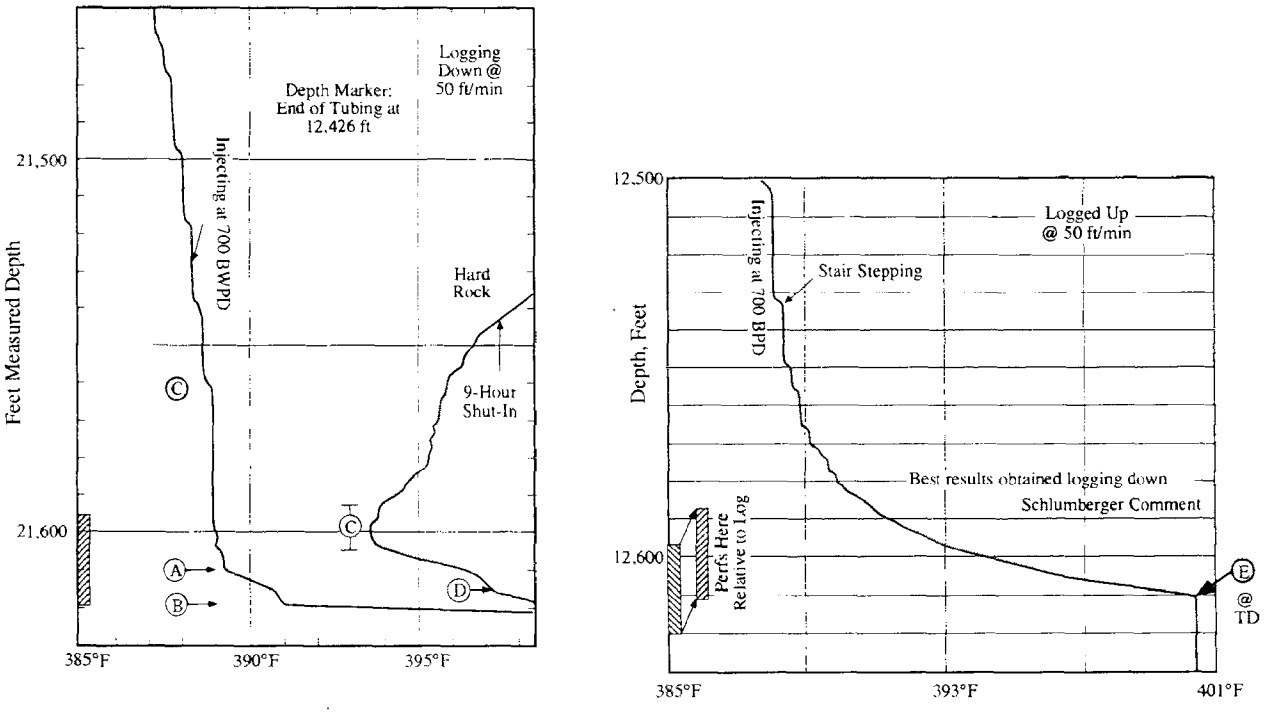

Figure 28. Loss in survey resolution due to "stairstepping" (excessive recording inertia) and to logging upward.

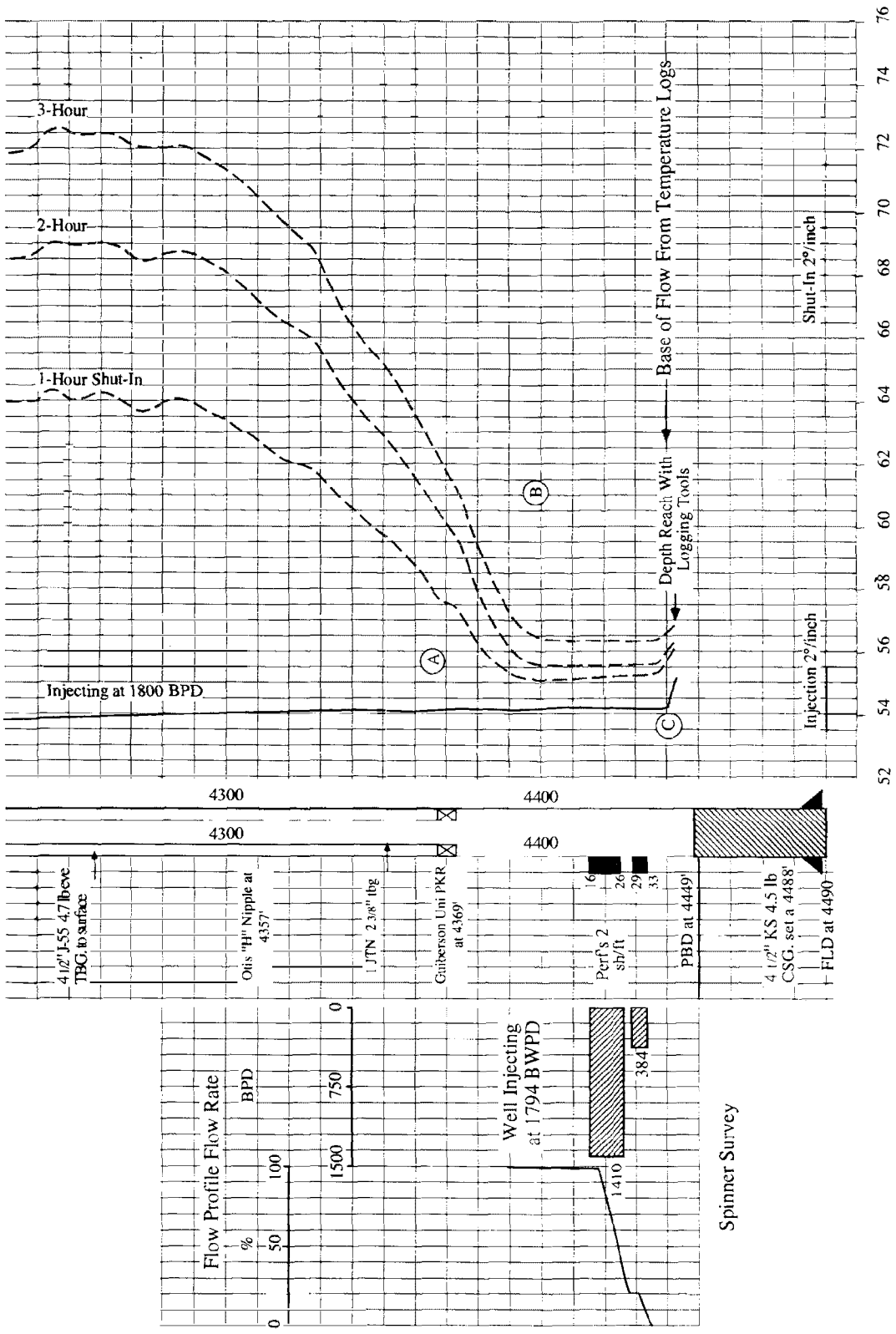

Figure 29. Surveys from an old injection well taking 1,800 BPD water.

"don't tell us nothing" variety. Actually, this is not the case. At depth A, the 1-hour shut-in survey shows the correct response to the completion. Furthermore, this response attenuates with time as it should. With these quality control checks as assurance, we should ask what sort of well conditions can produce the type of surveys we see. First, the injecting survey shows that the majority of the injected fluid reaches depth C, which is seven feet below the deepest perforation. The spinner survey, to the left on the wellbore on Figure 29, shows that 79% of the injected water leaves the wellbore at the top perforated interval. Finally, the shut-in temperature surveys show injection cooling up to depth B, a location some fifteen feet above the topmost perforation. This indicates a fractured wellbore situation, although probably not an intentional condition. The timing of the shut-in surveys is such that the influential storage is in the fracture, not the formation. One would expect a more or less uniform storage in the fracture, which is what the surveys show. The deficiency, thus, lies with the user, not with the tool.

Temperature Signatures For Noninjection Related, Behind-Pipe Flow: An effective cementing operation is more difficult if the wellbore passes through either very depleted or abnormally pressured zones. Cement opposite a depleted zone tends to dewater by filtrate loss to the low pressure zone. The cement then shrinks badly upon setting or fails to set at all in the sense of developing any strength to speak of.

Abnormally high-pressured zones tend to flow into the wellbore in regions where there is premature setting of cement above and below the zone. In this manner, crossflow behind-pipe can be set up before the cement has ever cured. If the cement is weighted too much, then one runs the equally bad risk of fracturing a formation and not being able to even pump cement to the desired height behind pipe. There are well known areas in the U.S. where primary cementing is nearly impossible across certain zones.

Depletion in water zones typically occurs at shallow depths, 1,000 feet or less, as a result of production for municipal, agricultural, or industrial usage. Their locations are generally known before a new well is drilled. Consequently, it is usually the old wells that were not completed so as to cover these zones that pose the major threat to these zones. Even worse, many of these old wells were abandoned years ago!

The mountainous areas of the U.S. are the only locations that have artesian, naturally over pressured water zones at shallow depths. A much more extensive problem is the charging of shallow strata by wells that blow out of control during drilling or by casing leaks in both production wells and injection wells. The first indication of these formations is usually an unpleasant surprise for the driller. Shallow disposal zones, of course, may become significantly over-pressured as a result of years of injection.

Temperature surveys are the most sensitive of the various production logging methods for locating noninjection related crossflow behind pipe in shut-in injection wells or in recently completed wells that are no more than a couple of months old. This sensitivity arises from the fact that these types of wellbores are not at static temperature. Flow into the wellbore region, however, brings its temperature along with it. If this flow is not at true geothermal, it will at least be at a temperature that is different from that caused by injection down the well. Thus,

even during injection, the non-related flow will "clamp" the back side of the casing at a temperature that is constant and different from values elsewhere. This is particularly the case at the source where the flow completely surrounds the wellbore. During injection, the heat transfer at shallow depths from the earth into the water flowing inside tubing that is inside casing typically amounts to only 15 btu/hr per foot of wellbore length. If the noninjection related flow rate per foot of wellbore is designated as q', then the temperature change caused by the 15 btu/hr - ft heat transfer is

$$\Delta T = \frac{15}{\rho c_p q'}, \text{ with q' in cu.ft./hr,}$$

$$\Delta T = \frac{15 \times 24}{62.5 \times 1 \times 5.615} \frac{1}{q'}, \text{ with q' in BPD,}$$

$$\Delta T = \frac{1.03}{q'}$$

A 5 BPD flow from a 10 foot zone, q' = 0.5, will thus only change temperature by about 2°F. Furthermore, this flow will continue once the well is shut-in. After about six hours, the fluid temperature in the tubing string will have almost equilibrated with the temperature of the source zone. Once an injection well that has noninjection related flow behind casing is shut-in, then the wellbore temperature will quickly change to a value reflecting the source temperature at the source depth. It will then change very slowly, if at all, at this location. This behavior, unlike injection related problems, is relatively insensitive to the length of time the well has been on injection. The only planning necessary is to allow sufficient shut-in time for the tubing fluid temperature to reflect conditions on the back side of the casing. Generally, surveys after about 6 hours shut-in will accomplish this.

These ideas are illustrated by the shut-in surveys of Figure 30 that are from a middle eastern oil production well. A shallow, artesian aquifer at depth A is flowing behind pipe down to a lower pressured water zone at depth B. The wellbore temperature at the source depth is at a nearly static value already on the 3-day shut-in and remains at this value. The true perspective of the "injection" from A to B is only evident on the 30-day shut-in survey. This perspective, however, is not necessary to comprehend the nature of the problem.

Frames A and B on Figure 31 show noninjection related flow signatures on single-pass temperature surveys after relatively short periods of shut-in time. Injection zones are below the deepest log depth on the figures so that static temperature lies off scale to the warmer side. In each frame, the shifts toward static are the result of water flow upward behind casing into hydrocarbon formations badly depleted by years of production.

Newly drilled or worked over wells show the same type of noninjection related flow signatures as those from deep injection wells. If no flow occurs in a new well, then three to six months after a well is completed the wellbore fluid is still a degree or so removed from static temperature. The bottom two-thirds of the wellbore is cooler than static whereas the top third is generally warmer.

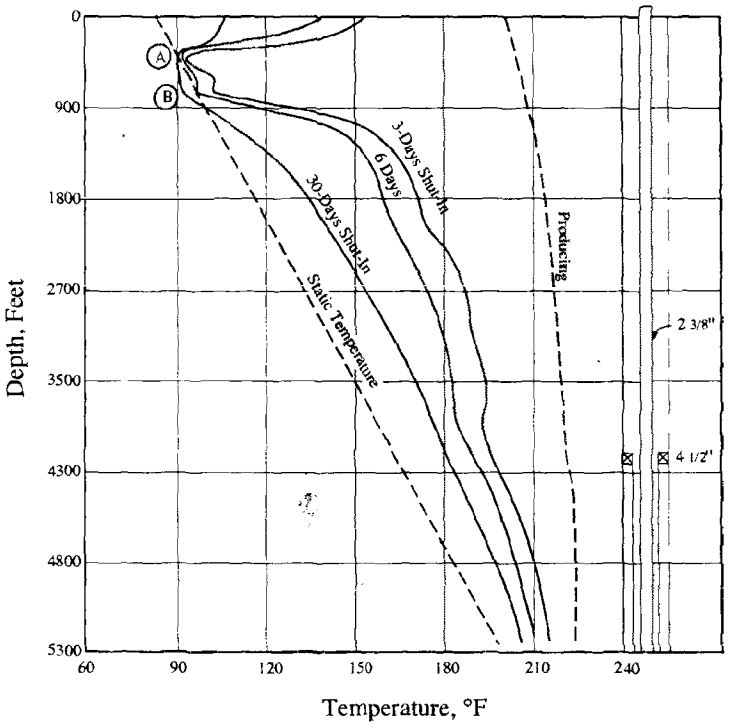

Figure 30. Temperature surveys from an old production well with water flow behind casing from Depth A to Depth B.

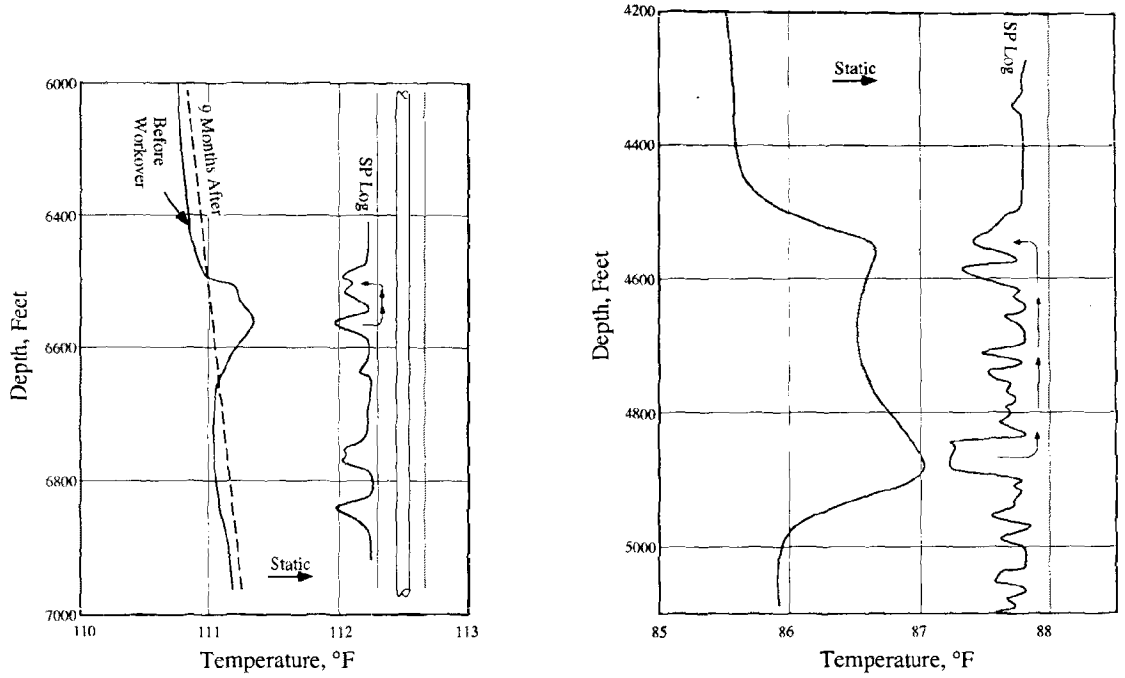

(A) Six-Hour Shut-In Surveys Before and After Workover

(B) 12-Hour Shut-In Survey

Figure 31. Behind-casing water flow into depleted hydrocarbon sands penetrated by wells with deeper injection zones.

This profile is the residual from the relatively long period of mud circulation during the drilling operation. Any flow to the wellbore counters this residual and shifts the wellbore temperature towards static conditions.

This type of behavior is shown on the temperature surveys of Figure 32. Frame A on this figure contains a curve labeled curve-1 that is a survey at a sensitivity of 2°F/inch from a one-month old well that has not yet been perforated for production in the formation whose top shows on the gamma ray log at 8,140 feet. Oil flow into the vicinity of the wellbore is clearly evident on the log by the warming behavior at depth A, 8,150 feet. Furthermore, the log shows that this oil flows upward behind pipe to depth F, 7,976 feet. Numerous losses, presumably to fractured zones known to exist in the 174-foot crossflow interval, are indicated by labels B through E. The validity of these signatures can be judged by the noise-free character of the survey on either side of the crossflow interval. The heating over the entire interval is a result of the wellbore still being cooler than static temperature in those areas free of flow to the wellbore. A six-foot interval was perforated on either side of 8,150 feet and the zone was tested. Wide open, it would only flow 94 BPD of oil. The leak rate recorded on frame A of Figure 32 can then be no more than 10 to 15 BPD based on the maximum pressure drop available over a 174 foot column of oil replacing water.

Once the completion tested oil, the well was killed in preparation for a workover. One day after the kill, another logging company ran the temperature survey appearing on frame B of Figure 32, this time at a sensitivity of only 4°F/inch. Moreover, stairstepping is evident in the trace for temperature at the locations marked by arrows. The quality of the record is so poor that only the gross crossflow interval from depth A, 8,152 feet, to depth C, 7,959 feet, is evident along with the one major loss at depth B, 7,991 feet. The intermediate losses evident on frame A, cannot even be detected on the differential trace of frame B. The response of the differential trace at the source depth A, 8,152 feet is also of interest. The temperature curve shows that this response is due to a rapid two degree Fahrenheit decrease in temperature below depth A. A comparison of this differential response with that on Figure 2 (page 4) at depth B, the location of rapid one-half degree temperature increase, shows how easily quality control is lost if diligent control is not maintained.

The preceding examples show that the only new feature in the use of temperature surveys to detect noninjection related flow behind pipe is the reliance on shut-in surveys alone. It is wise to have at least two run at shut-in times in the range of 12 to 36 hours. Use of such a timed sequence makes it possible to detect leaks that amount to only a few barrels a day. As we have pointed out, this sensitivity is a consequence of the well not being at static conditions when logged.

In regard to this sensitivity, the influence of lithology is usually greater at shallow depths due to increased variation in thermal properties. Furthermore, shallow sands that are on production near a given well often flow past the well at a drift velocity sufficient to add their signature to a shut-in temperature survey from the well. Consequently, it is a good practice to log a well in a given area purely for background data.

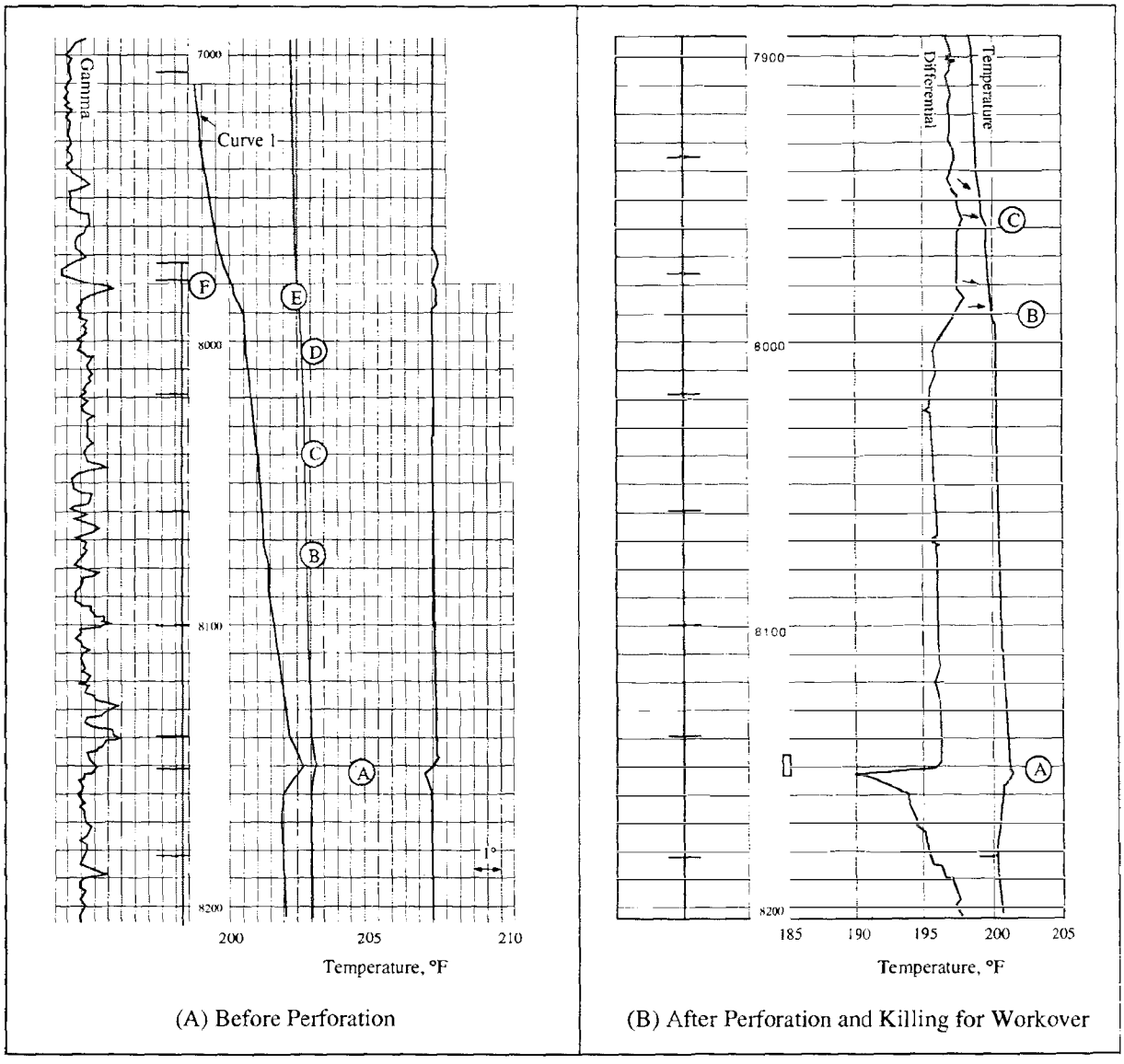

Figure 32. Behind-casing crossflow of liquid (oil) in a new well still slightly cooler than static temperature.

Logging for Lithology Influence: The next sequence of temperature surveys illustrate a logging sequence that was run during the first day of operation of a new injection well at a low enough injection pressure to insure water entry only into the depleted zone that had been perforated for water flooding. The logs were run as a reference for the influence of lithology because the well penetrated a potpourri, as evidenced by the lithotype labels appearing on the left-hand side of Figure 33. This mix clearly influences the short shut-in time surveys shown on the right of the figure. From the top, there is the tendency of the shale above A to lag the sand at B in recovery. The sand, in turn, lags the siltstone in the interval below C. Further, the carbonate section between D and E has a temperature survey reflecting the porous and non-porous pattern of the SP and gamma ray logs. The completion influence is seen at depth F. Finally, the carbonate

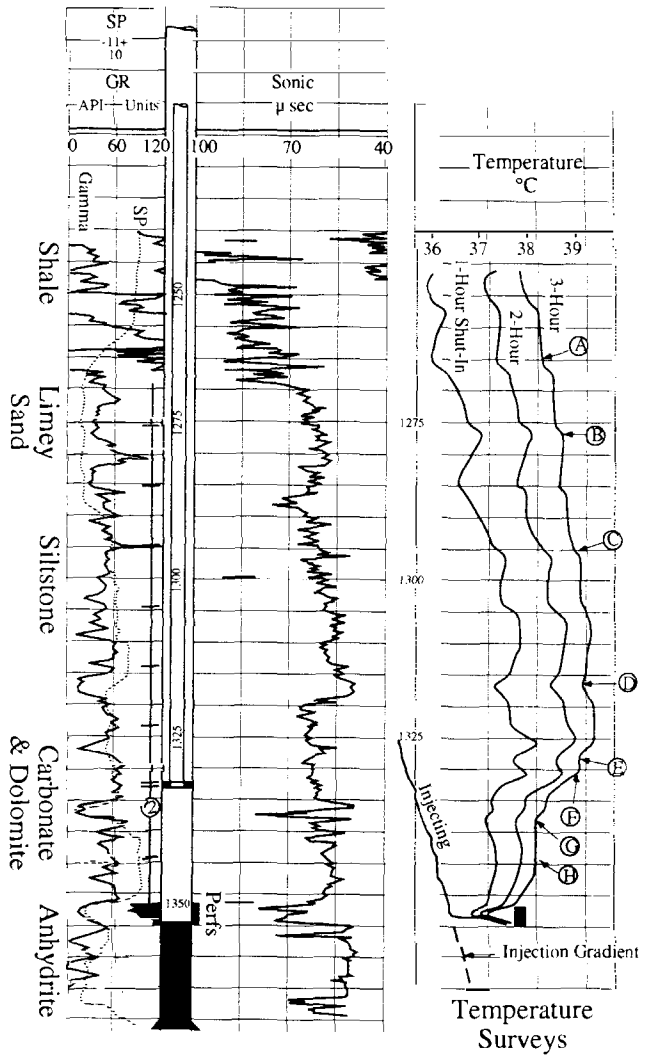

Figure 33. Temperature logging a new injection well for lithology signatures.

porosity is again reflected in the interval GH below the tubing packer. Because of limited daylight in the winter, the three shut-in runs are about one day's work in themselves. Consequently, the base information continued in Figure 33 is essential to any interpretation of injection confinement on future surveys. In particular, the next zone up, zone 2 on Figure 33, had already been charged by leaks in older injection wells in other parts of this field.

This last example ends the discussion, formally at least, of temperature logging and leads to the second tool, the radioactive tracer logger. This tool is the most sensitive instrument for the detection of fluid movement inside and immediately outside of pipe. Fractional barrels per day of movement can be detected outside pipe provided it can be tagged and then pumped behind the casing. Fortunately, the significance of a radioactive tracer survey is generally easier to

comprehend than that for a temperature survey. Consequently, the associated discussion will be much briefer. Ease of interpretation, however, should not be confused with "correctness" of interpretation. The tracer tool has its own peculiarities and limitations that must be appreciated to use it effectively.

Radioactive Tracer Surveys

The radioactive tracer tool is a direct consequence of the widespread availability of radioactive isotopes that accompanied the growth in atomic physics research in the United States. An enormous surge in the application of tracers to tag materials occurred in the late forties and throughout the fifties as the operation of particle accelerators produced these materials in quantity. The high resolution provided by "radio-assay" was, of course, already well known at this time. The advantage of the gamma ray as a non-destructive tag that could be detected external to the host was also clearly established. Furthermore, the increased usage of the natural gamma ray logging tool for formation evaluation soon showed that the underground environment was also not excessively radioactive.

Most of the activity underground results from the decay of natural isotopes of potassium and thorium with some support added by uranium. Shales, where these materials concentrate, typically register about 100 API units on a gamma ray log. This activity amounts to about 6 microcuries per ton of material, an exceedingly low concentration in view of the fact that most radio assaying methods employed this amount of activity in grams of material.

The earliest use of the radioactive tracer method was to tag water so as to follow the injection of this water into open-hole completions. The tagging material was added to the water at the surface and a gamma ray logging tool, i.e, a Geiger-Muller ionization tube, was used to track the movement downhole. By the early fifties, the self-contained tool that carried its own source of tagging material had evolved.

The most widely used tagging material for water is an aqueous solution of sodium iodide, NaI, containing the isotope of iodine I-131. The decay of this isotope produces, in addition to beta particles, gamma radiation 80% of whose energy is in the 0.3 - 0.4 million electron volt range. The half-life is ideal at 8.05 days. Furthermore, in solution the iodine is a negative ion, I^-. As such, the material is not absorbed on rock surfaces which tend to be electronegative. It, thus, can be pumped into porosity and away from the wellbore out of range of the tool.

The fact that 90% of the gammas registered by a tracer tool originate from within a foot of the detector is also one of the limitations on the method. It, like all nuclear logging tools, has limited depth of investigation.

On the positive side, the tracer tool is the highest resolution flowmeter available. With this tool, vertical speeds as low as 2 feet per week can be detected. Moreover, it is the only absolute flowmeter available. The British hydrodynamist, G. I. Taylor, showed in 1954 that if a slug of tagged water is mixed uniformly over the cross section of a pipe, then the centroid of the material subsequently moves with the average or superficial velocity of the stream, $\hat{v}$. Timing the

movement of a tracer slug produces a number for $\hat{V}$ which can be converted to the volumetric rate by multiplication by the cross-sectional area of the pipe, A:

$$q = A\hat{V}$$

No calibration factor is involved for either laminar or turbulent flow. Tracer determined velocities are typically measured in units of feet per minute so that the above equation gives cubic feet per minute with A expressed in square feet. In terms of barrels per day, the expression becomes

$$q\,(BPD) = 256\,A\hat{V} \qquad (3)$$

A = Cross-sectional area, ft²

$\hat{V}$ = Average velocity, ft/min

Before further comments, the features of the modern tracer tool must be examined.

Modern Radioactive Tracer Tools: The schematic of a 1 3/8 -inch diameter tracer tool is shown in Figure 34. The assembly consists of two tools, a reservoir and pump section at the top and a detector section at the bottom made up of two gamma sensors and the associated circuity necessary to amplify and transmit the detector counts. In the figure, a casing collar locator, CCL, is placed between the two detectors. The resulting five-foot spacing between the detectors is fairly typical in domestic use. It is also not unusual to find a temperature sensor of the type described on page 2 at the bottom of the tool. In fact, all companies can run the thermometer with the tracer tool.

The reservoir section contains tagged field brine that is ejected in discrete volumes into the wellbore by a positive displaced piston driven by the electric motor shown on the figure. The amount displaced into the wellbore on a given "shot" depends on how long the operator activates the electric motor. A normal shot displaces about 1/100 of the reservoir volume, but the operator can displace the entire reservoir in one step if he so chooses. A particular tool may have one, two or four ejection orifices spaced around the tool barrel at the top of the reservoir. The orifices are plugs that can be removed for loading the reservoir at the surface. The more ejection ports the better the mixing of each shot with wellbore fluid.

At the surface, a concentrated aqueous solution of sodium iodide containing about 5 microcuries of I-131 is diluted with about one pint or 500 CC's of field brine in a metal syringe, the discharge end of which can be threaded into a hole in the tracer tool that normally contains an ejection orifice. Although sanitary, this method of loading traps air in the reservoir. This air is purged in the bottom of the hole prior to any logging operations.

A normal "shot" from a 100-shot tool will typically contain about 0.05 microcuries of I-131. In the immediate vicinity of a detector capable of such a response, this concentration would correspond to some 150,000 API units of activity which is 1,500 times background, even in

shales. It is therefore no surprise that the tool can detect even minute flows behind pipe so long as the tagged fluid is in the near vicinity of the well.

Two detectors are present on the tool of Figure 34. This is done in order to minimize timing errors whenever the tool is used for stationary measurements of fluid velocity. If the slug is timed as it goes past each detector, then the exact time of ejection from the reservoir is not required for a velocity determination.

Early versions of the tracer tool invariably used Geiger counters as gamma ray detectors. The modern trend, however, is to the use of scintillation crystals due to their higher sensitivity to gamma radiation and to their ability to measure radiation intensity as well as the number of incident gammas per unit time. These tools are likely to have only one detector.

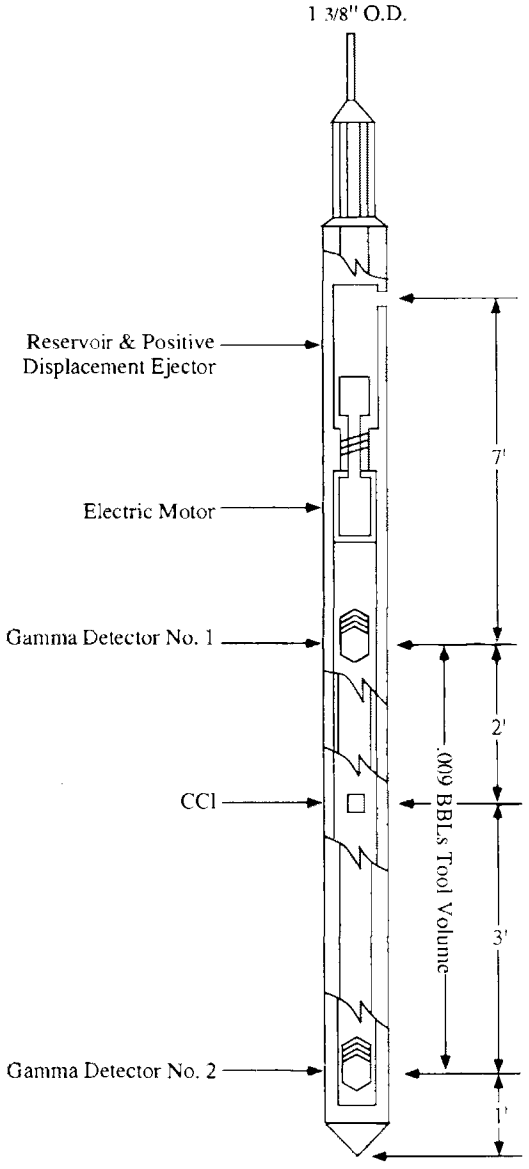

Figure 34. Schematic of a radioactive tracer tool for injection logging.

Tool Resolution: The proficiency of a gamma detector is important at both high and low count rates. A scintillation crystal is superior to a Geiger counter on both ends of the scale for gamma detection. A Geiger counter is basically a particle detection device. The passage of, say, an alpha particle through the low pressured gas in the tube ionizes the gas so a pulse of current can pass between electrodes. Gamma rays, however, being devoid of mass, are inefficient ionizers. This inefficiency establishes the low count rate threshold. Once the tube pulses, then time is required for the ions to neutralize before the next pulse can occur. If this "down time" is denoted by t seconds/count, then the count rate, C_i, registered in response to a true rate C_t is:

$$C_i = C_t - C_t \times C_i t$$

$$\text{or} \qquad C_i = C_t (1 - C_i t) \qquad (4)$$

The "down time" for an ionization tube is of the order of one-third of millisecond, i.e., $t \approx 3 \times 10^{-4}$ seconds; thus, at a true count rate of $C_t = 500$ cps, equation (4) gives an indicated count $C_i = 435$ cps, a 13% error. Consequently, the tubes are usually employed in bundles of several tubes so that at least one tube can be active at any given time.

As already mentioned, a normal shot contains about 0.05 μc (microcuries) of I-131 in about 5 grams of diluent. One curie, by definition, gives 3.7×10^{10} disintegrations per second; therefore, an unmixed shot can generate a count of $C_t = 3.7 \times 10^{10} \times 0.05 \times 10^{-6} = 1{,}850$ cps. Given dilution on ejection and counter inefficiency, the actual value is closer to 1,000 cps. The previous calculations by equation (4) showed that this is an excessive count rate for a single Geiger tube.

A scintillation crystal, on the other hand, has no such rate limitation because its "down time" is essentially zero. Furthermore, even a very low energy gamma incident upon the crystal will excite the emission of a pulse of light whose intensity is directly proportional to the energy level of the gamma. The light pulses are amplified in number by photomultiplier tubes to give an extremely sensitive detector. A crystal, however, is far more delicate and "temperamental" than an ionization tube. Consequently, Geiger counters remain in widespread usage on tracer tools.

In summary, a tool that records satisfactorily its own gamma ray log at a sensitivity of 40 API units per inch has plenty of resolution for radioactive tracer work. Geiger tube devices may be non-linear at high count rates, however.

Tool Specifications: The dimensions appearing on Figure 34 clearly illustrate a tool much longer than the temperature logger. The entire assembly typically runs about 15 feet in length with collar locator and temperature probe. If the tool is to pass into a liner, then centralizers must also be attached. This adds another 5 feet of tool. The tool diameter may therefore become the critical factor in the use of the tool. Fortunately, the same diameters are available for this tool as those listed for the thermometer, as small as 7/8-inch and as large as 1 11/16-inches. This range includes devices with scintillation detectors as well as with Geiger counters. As with the thermometer, a popular size is the 1 3/8-inch tool shown in Figure 34.

Temperature and pressure ratings are also comparable to those for the thermometer. The main difference is in the increased length of tool before sinker bar addition. The use of a single detector tool will reduce the length by 5 to 6 feet.

Logging Procedures: Logging with the radioactive tracer tool is done in two ways, both of which may be used on any given job. One way is to eject a "shot" of tracer into the injection stream and then record the location of the slug with time by successive gamma ray intensity surveys, or "drags," of the wellbore. This depth-mode logging is usually called a slug tracking procedure. It affords one a quick and easily understood picture of where the injected water is going. This fact is illustrated by the surveys on Figure 35 for a well on injection at about 600 BPD brine into a single set of perforations. For this record, a slug of tagged brine was ejected at 9,510 feet with the well on injection; then eleven successive surveys of gamma ray intensity, records A through K, along the wellbore were recorded, in this case, by the bottom detector. Each record or drag was made by the operator quickly dropping the tool until the detector passed

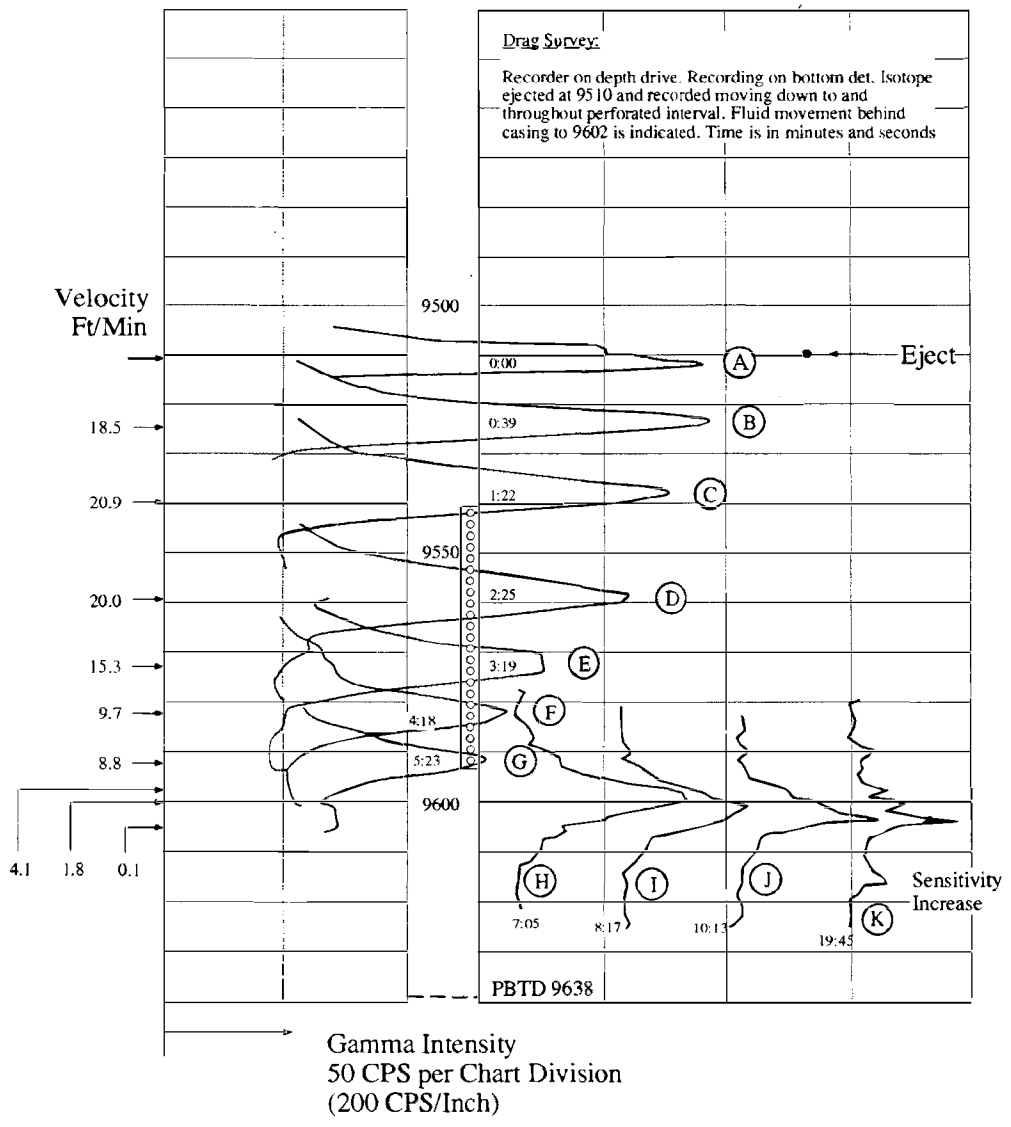

Figure 35. A radioactive slug tracking record from a well on injection at about 600 BPD water.

through the slug and then logging back upward at constant speed with the recorder on depth drive. As the detector records through the maximum or peak activity, the operator notes the corresponding time. These times are listed on the figure as minutes:seconds at the depth of maximum activity. The numbers start at 0:00 at the peak for drag A, and increase to 19:45 for drag K. The operator adjusts his logging speeds so as to "catch" the slug at 10-20 foot intervals in the full flow stream above the perforations. As the slug moves down the wellbore, even before reaching the perforations, it spreads vertically and drops in peak amplitude accordingly as a result of mixing by flow turbulence and by the movement of the logging tool through the slug two times for each drag. A visual inspection of the slug "size" alone is enough to show that practically all the injected fluid makes it to depth D, 9,560 feet, before leaving the wellbore. All the injection thus occurs over the bottom half of the perforated interval. The final survey, K, shows that some of the water has flowed all the way down to 9,605 feet, some twelve feet below the bottom perforation. In order to place the location of this flow, inside or outside pipe, the operator ejected another slug at 9,604 feet. The two logging runs on Figure 36 overlay, showing that this slug remains at the ejection depth. Therefore, the flow revealed on drags H through K is behind casing.

The slug tracking technique offers a clear picture of what is going on in and immediately around the wellbore. But, as a flow profiling technique, it obviously has poor vertical resolution. The second method of tool use overcomes this deficiency. First, however, it should be mentioned that operators are historically negligent in recording the detector sensitivity employed in surveying. The log heading stated that the drags on Figure 35 were recorded at a gamma sensitivity of 200 counts/sec per inch of chart, yet the operator apparently increased the sensitivity for the last survey, drag K. The activity of the storage spike in the perforation at 9,590 feet has increased from the previous survey even through 9 1/2 minutes of injection ensued! In fact, the operator may have increased sensitivity from survey I through K.

The second way the tracer tool is used entails stationary measurements of travel times between two detectors. To conduct such a velocity shot, the operator positions the tool so as to place the detectors at chosen locations, turns his recorder to time drive at a speed of anywhere from 1/2 inch of log per minute to 10 inches/min, and turns on both gamma detectors; hopefully, both at the same sensitivity. He then ejects a slug of tagged brine into the moving stream and continues the record until the slug passes both detectors. The resulting travel time between detectors of known spacing is an inverse velocity measurement that is free of lag error between the "firing" at the surface and actual ejection downhole.

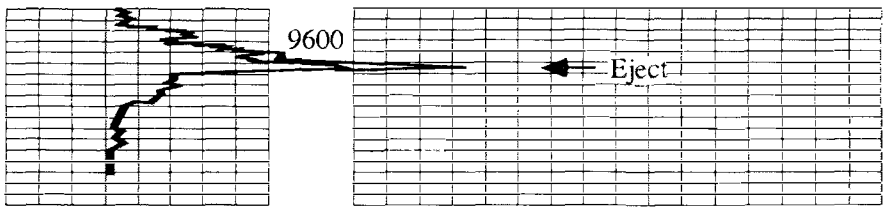

Figure 36. Slug tracking (2 surveys) below the perforations of Figure 35 well.

Figure 37 shows a velocity shot taken above the perforations in the well of Figure 35, a well on injection at some 600 BPD. The two detectors on this particular tool are spaced 5.5 feet apart. The left-hand trace is the output of the bottom detector, positioned at 9,505.0 feet, whereas the right-hand trace is from the top detector at 9,499.5 feet. The recorder is on time drive at a nominal speed of 1 inch/minute. With 10 vertical log divisions per inch, the nominal vertical scale is 60/10 or 6 seconds per chart division. A calibration, however, gave 23.5 chart divisions in two minutes of time. The vertical time scale is therefore 120/23.5 = 5.1 seconds per chart division. The ejected slug arrives first at the top detector, the maximum activity, point A, appearing some 3.5 chart divisions after the ejection marker. The maximum intensity at the bottom detector, point B, arrives later after some 6.2 chart divisions following the eject mark. The difference between arrivals A and B can be measured directly at 2.7 chart divisions without reference to the ejection marker. This, of course, is the advantage of the dual detector tool. This difference represents a nominal travel time $\Delta t = 2.7$ cd x 6 sec/cd or $\Delta t = 16.2$ seconds over 5.5 feet. In view of the calibration, the actual travel time is $\Delta t = 2.7 \times 5.1 = 13.8$ seconds, a value some 14 % lower than nominal. This travel time is representative of the full flow stream and is customarily used only as a reference for subsequent shots within the perforated interval. Consequently, the speed calibration of the chart drive is often omitted and only the nominal speed, 1 inch/minute in this case, is listed. Actually, this speed is too slow in the case of Figure 37. A drive speed of 5 inches/minute would have been more appropriate as this would have separated points A and B by some 14 chart divisions and would have allowed a more accurate evaluation of travel time.

The timing of the difference in peak values illustrated in Figure 37 is the most commonly used of five different ways that have been proposed. All five are illustrated on Figure 38. On this figure,

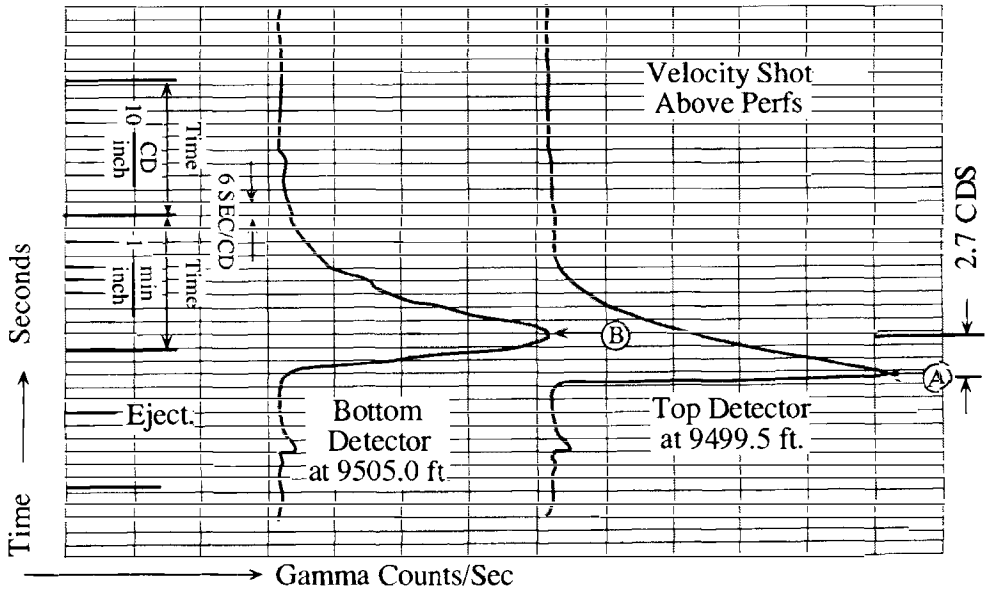

Figure 37. Velocity shot record above the perforations of the Figure 35 well on 600 BPD water injection.

the peak time is designated by point 2 and as method #2. The obvious ambiguity in the location of this point on Figure 38 is eliminated by the peak "shaping" procedure that locates point 3 by the intersection of the dashed lines on the figure. These lines are the tangents at the inflection points to the leading and the trailing edges of the pulse in activity. The remaining three methods of timing utilize "first arrivals" which are, necessarily, faster than peak travel times. If the leading-edge tangent line is continued to its intersection with the base line, then the resulting point 1 defines a "first arrival" that is independent of tool sensitivity. This is obviously not the case when one tries to locate point 5 as the "first" point at which the gamma ray activity exceeds the base line activity. Whenever the leading edge of the pulse is very sharp, as at the top detector in Figure 37, points 1 and 5 will coincide. Finally, there is a so-called "half-peak" arrival time that is determined by the intersection with the leading edge of the pulse of a line parallel to the base line and passing through a point at one-half the maximum or peak amplitude. This procedure gives point 4 on Figure 38. The intersection with the leading edge occurs near the inflection point, as Figure 38 demonstrates.

The five timing points are marked in Figure 39 on each of the pulses from Figure 37 and the corresponding travel times in chart divisions are tabulated. As the table shows, the "eyeballed" or estimated first arrival are usually the least reliable whenever the sensitivity is such that the pulses do not "peg" the recorder.

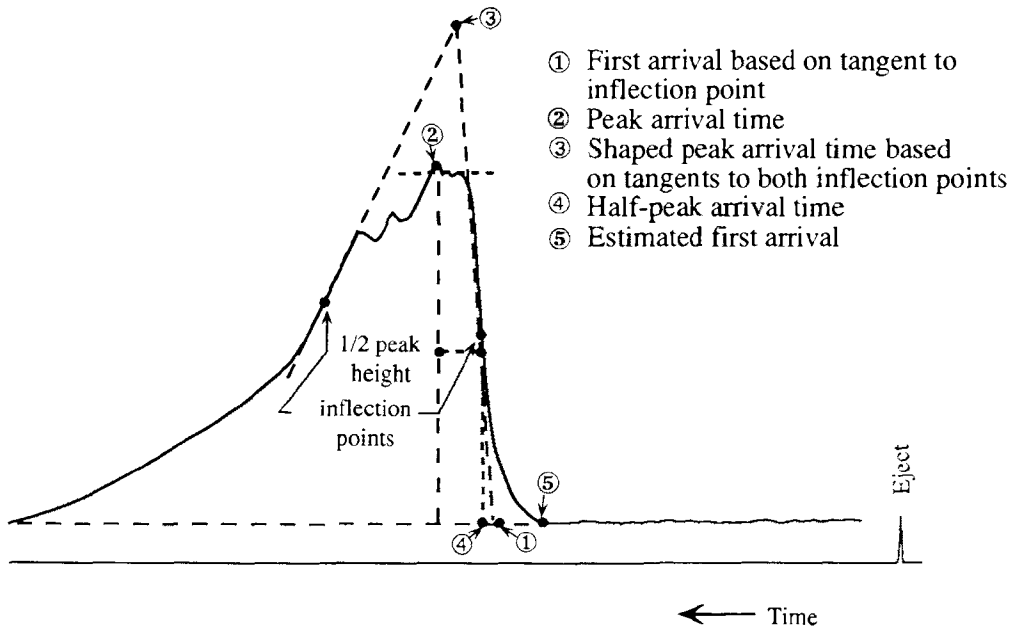

Figure 38. Five methods for timing the travel of a stationary velocity shot.

TRAVEL TIMES, Δt CHART DIVISIONS, FOR Figure 39 POINTS

Point	*Method*	*Δt*
2	Peak Arrival	2.7
3	Shaped-Peak Arrival	2.5
1	Inflection First Arrival	1.0
4	Half-Peak Arrival	1.0
5	"Eyeball" First Arrival	0.5

For pulses of the quality of those on Figure 39, nothing more complicated than peak travel times is necessary. As the pulses become more dispersed, one can usually get by with the peak shaping approach. Once the pulses have become very "strung out", at very low rates for example, then about the only consistent approach is the half-peak technique. The same method should, of course, be used for all velocity shots on a given survey.

However timed, the stationary, velocity-shot technique allows the vertical resolution to be controlled by the amount the tool is moved in the well between "shots." This is the only way that one can survey sets of perforations that are spaced twenty or less feet apart and retain any quantitative vitality. Likewise, the method is required when detailing within a short perforated interval.

The velocity shot is, however, an instantaneous sample of, typically, 30 seconds or less duration. As such, the resulting travel times are much more sensitive to rate fluctuations than are the tracked slug surveys of the type shown on Figure 35. Because the latter method samples more wellbore in a given time interval, various drags are more likely to share a common rate of injection. In the velocity shot method, it is good practice to replicate near the end of the survey some of the shots done early in the survey.

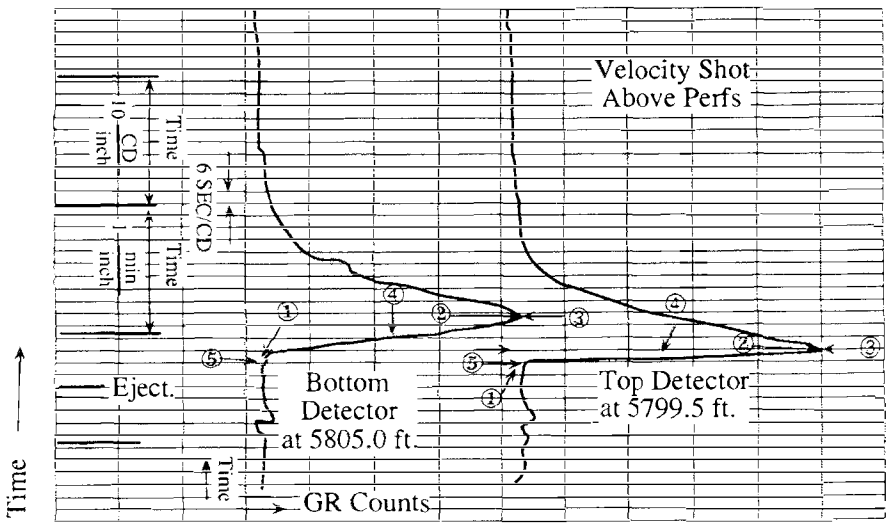

Figure 39. Location of five timing points on the records of Figure 37.

Figures 35 and 37 are demonstrations of the observation that both slug tracking and velocity shot procedures are usually employed on any given job. A lot of record is collected; consequently, it is very helpful to have a section of the log devoted to listing where and at what time each ejection occurred, the size of the shot, and the sensitivity at which it was recorded. Because this is seldom done, one has to assume that the sequence of operations proceeded from the bottom of log to the top in order of shot number.

Finally, recommended recording sensitivities are listed in Table 4. The scale common to all service companies is the API units/inch since the actual counts/second per inch will vary from company to company. Thus, the values in the table are keyed to normal gamma ray log sensitivity of 40 API units/inch.

TABLE 4. SUGGESTED GAMMA RECORDING SENSITIVITY FOR RADIOACTIVE TRACER TOOLS WITH 5 μC TOTAL CHARGE OF IODINE-131 IN WATER

Purpose of Record	API Units/Inch
Gamma Ray Log for Depth Control	40
Detection of Behind-Pipe Flow	200
Flow Profiling Inside Pipe	1000

This table states that the response to shots ejected to detect flow behind casing should be recorded at about one-fifth the sensitivity used for gamma ray logging. This choice keeps in perspective that small amount of tracer that can be squeezed behind pipe in almost any well. Likewise, the response to shots ejected to track flow inside pipe can be recorded at about one twenty-fifth normal API sensitivity. This level allows the slug to be recorded without "pegging."

The remaining "sensitivity" is the chart speed used when a stationary velocity shot is recorded. As the shot on Figure 37 illustrates, it is easy to lose precision in timing if the chart drive is too slow. The recording speed, S, should be adjusted according to fluid velocity so as to space the peaks from the two detectors about 5 - 10 chart divisions apart. If the spacing between detectors is L feet, then the number of chart divisions is approximately given by:

$$\text{No. CD's} = 10\,\frac{SL}{\hat{V}} \qquad (5)$$

$$\text{No. CD's} = 5 - 10$$

If 10 chart divisions are chosen, then Equation 5 gives the necessary chart drive as:

$$S = \frac{\hat{V}}{L} \qquad (6)$$

S = Time-drive speed, in/min
$\hat{V}$ = Fluid velocity, ft/min
L = Detector spacing, ft

For example, the water velocity associated with the shots on Figure 37 is about 20 ft/min and the detector spacing is 5.5 feet so that equation 6 gives

$$S = \frac{20}{5.5} = 3.6 \text{ in/min}$$

With available speeds of 1/2, 1, 2,5, 10 inches/min, one would therefore select a speed S = 5 in/min rather than the 1 in/min actually used on Figure 37.

With these procedural details out of the way, a more detailed look at what the surveys mean is in order.

Injection Profile from Slug Tracking: Please refer to the slug tracking survey contained on Figure 35. This survey showed that most of the injection left the wellbore over the bottom half of the 52-ft long perforated interval. The injection will now be profiled in more detail.

There are two ways that slug tracking surveys are used to profile flow. Both ways assume that the slug of tracers is uniformly mixed over the cross sectional area of the casing when ejected so that equation 3 relates the volumetric rate to the apparent slug movement. Some operators, immediately after ejecting a shot, will work the tool through the slug a few times before starting the logging operation. Others do not bother, as was the case with the operator who ran the survey of Figure 35 (page 50). The bifurcated shape of the slug recorded on drag A shows that it was not well mixed over the cross section. Furthermore, the "size" of the slug recorded on drag A is less than that recorded on the next pass, drag B. When drag A passed through the slug, most of the tracer material was on a side of the pipe away from the tool. The operator is depending on fluid turbulence and subsequent logging runs to mix the slug.

Slug Timing: The more common of the two profiling methods makes use of the peak location-time data on Figure 35 to calculate velocities for each drag after the first. Slug A is located at 9,512 feet when the clock was started. On drag B the peak had moved to 9,524 feet and 39 seconds of time had elapsed on the clock. Thus, the apparent velocity between these depths is

$$\hat{V} = \frac{(9524 - 9512)}{39} \times 60 = 18.5 \text{ ft/min}$$

In a like fashion, the velocities of slugs C through I are determined in the table below and listed on the left-hand side of Figure 35. Incomplete mixing has only minimal influence on the timing

of slugs over a twelve-foot interval. Consequently, the average velocity for slugs B, C, and D can be taken as representative of the full flow stream, i.e., for 100% injection rate the velocity is

$$\hat{V}_{100\%} = \frac{1}{3}(18.5 + 20.9 + 20.0) = 19.5 \text{ ft/min}$$

The variation in these numbers can be the result of either timing errors or actual rate fluctuations. Common practice assigns the percent flow for a particular drag to the midpoint depth of the interval between it and the preceding drag. Thus, the 100% point for drag B is assigned to a depth of :

$$9{,}512.0 + 12/2 = 9{,}518 \text{ feet}$$

This is an arbitrary practice that would be in error even if the only loss in the interval occurred at exactly the midpoint depth!

TABLE 5. SLUG TRACKING DATA FROM SURVEYS ON FIGURE 35

Drag	Peak Location	ΔL Ft.	Δt Sec.	$\hat{V}$ Ft./Min.		% Flow in Well	Interval Mid-Point
A	9512.0	---	---	---		100	---
B	9524.0	12.0	39	18.5		100	9518
C	9538.3	14.3	43	20.9	19.5	100	9531
D	9559.2	20.9	63	20.0		100	9549
E	9573.0	13.8	54	15.3		78	9566
F	9582.5	9.5	59	9.7		50	9578
G	9592.0	9.5	65	8.8		45	9587
H	9599.0	7.0	102	4.1		0	9593*
I	9601.2	2.2	72	1.8		0	

* Base of Perforations

The numbers in the above table are graphed on Figure 40 and indicate the initial impression that most of the flow is lost from the bottom half of the perforated interval was correct.

The above survey came from a section of wellbore with a constant casing size. If the cross-sectional area changes from one drag to the next, then the velocities must be corrected to a common area by multiplication by the ratio of the actual area to the reference area.

To appreciate the extent to which any discrete timing procedure can smear a flow profile, consider the following hypothetical situation. Suppose four drags, A, B, C, and D, are measured and the peaks are spaced exactly 10 feet apart. The entire stream flows over the interval from A to B

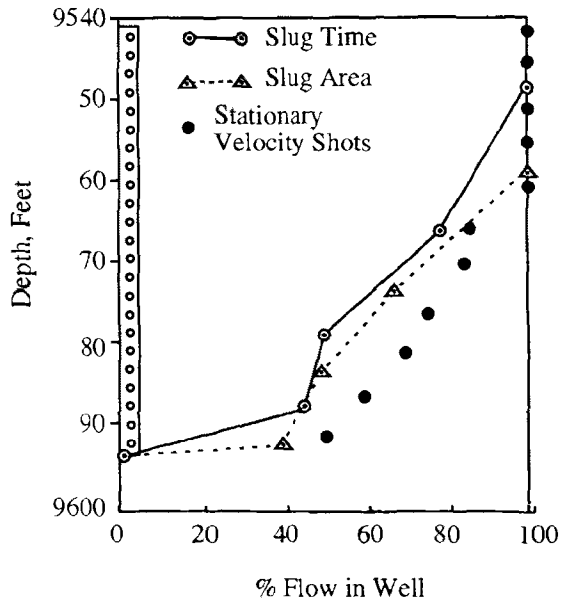

Figure 40. Profile for slug tracking surveys from Figure 35.

requiring 10 seconds for the transit. Thus, a velocity of 1 ft/sec., associated with 100% of flow as listed in the table below, is assigned to the midpoint of interval AB.

Drag	ΔL Ft.	Δt Sec.	$\hat{V}$ Ft./Sec	% Flow
A	10	10	1.00	100
B	10	10	1.00	100
C	10	15	0.67	67
D	10	20	0.50	50

Now, at the midpoint of interval BC, exactly 50% of the flow exits the wellbore and the remaining 50% continues on to C and D. The travel from B to C will thus be half the way at a speed of 1.0 ft/sec and the remaining half at only 0.5 ft/sec. Thus the travel time will be

$$\Delta t_{bc} = \frac{5\text{ ft}}{1.0\ \frac{\text{ft}}{\text{sec}}} + \frac{5\text{ ft}}{0.5\ \frac{\text{ft}}{\text{sec}}} = 15\text{ sec}$$

as shown in the table. The apparent velocity is then 10/15 = 0.67 ft/sec. The travel time from C to D will be 20 seconds. As the table shows, the resulting "profile" allocates a 33% loss, rather than 50%, to the mid-point of interval BC and carries a 17% loss over to the mid-point of interval CD where no loss actually occurred. This behavior is characteristic of any interval velocity technique. The loss from the first interval is underestimated and a little final loss is carried one interval beyond the actual.

Before looking at the second method of profiling, which avoids the dispersion inherent to timing, it should be pointed out that the velocities on Figure 35 and in the tabulated results of page 57 are the superficial velocities that are related to volumetric rates by equation 3, which is

$$q\ (BPD) = 256\ A\hat{V} \qquad (3)$$

The survey on Figure 35 is in 5 1/2-inch, 17 lb/ft casing with a cross-sectional area A = 0.1305 sq. ft. At 100% flow, the timed slug velocity is $\hat{V}$ = 19.5 ft/min. Therefore, the injection rate, q, is

$$q = 256 \text{ X } 0.1305 \text{ X } 19.5 = 651 \text{ BPD.}$$

As was pointed out in the introduction, this type of survey is the only one that gives a velocity that requires no adjustment to superficial velocity. Most pipe tables also list the pipe capacity, C, in bbls/ft directly so that the rate can be obtained by

$$q = 1440\ c\hat{V} \qquad (3A)$$

where c = Pipe capacity, bbls/ft

$\hat{V}$ = Superficial velocity, ft/min

Slug Area: The second method of flow profiling from slug tracking data makes use of the area under the recorded intensity curve for a given drag. If the gamma intensity is assumed to be proportional to the concentration of tracer, then the area under the curve is proportional to the total amount of tracer in the wellbore at a given drag location. This area would then decrease in proportion to the fluid loss from the wellbore. The assumption of direct proportionality between intensity and concentration is strictly valid only whenever a detector is surrounded by a tracer concentration that is uniform not only across the pipe cross-section but also in the vertical direction. In such a situation, loss in peak height alone would be sufficient for flow profiling. Drags A, B, and C on Figure 35 show that peak intensity alone is insufficient because this value decreases as the slug spreads vertically.

Furthermore, a gamma ray originating at a particular location can be counted from about a foot away from its origin. Thus the area under a drag curve accumulates multiple counts due to "carry-away." This influence can be minimized by use of a number proportional to the area that is obtained by multiplication of the peak height by the width of the pulse at one-half peak height.

For example, drag A on Figure 41 has a peak height of 70 millimeters as shown. At half this height, the pulse width is 5.2 mm, so the product 70 x 5.2 = 364 $(mm)^2$ is the number to be assigned as an area. In a similar fashion, the other drags through G can be measured to give the numbers in Table 6. The "growth" in slug area through drag C is the result of poor mixing after ejection. The tracer material went to the pipe wall when it squirted from the tool orifice. If not intentionally mixed upon ejection, then about three drags through the slug is needed to achieve cross-sectional mixing. Fortunately, drags C and D can be averaged to give a reference area of 490 mm^2 for the full flow stream, the 100% point.

The percentages in Table 6 are based on this reference. These percentages are graphed as dashed lines for comparison on Figure 40. They show even more of the injection leaving the wellbore over the bottom half of the perforated interval than does the timed slug profile. Note in the table that the slug area is assigned to the location of peak intensity for the drag as this measurement is instantaneous at this depth. The apparent loss of 34% between drags D and E is, of course, smeared over the 14-foot interval separating the peak location.

Table 6. Slug "Area" Data from Figure 41 Slug Tracking Survey

Drag	Location Ft.	Height mm	Weight mm	Product Area, mm^2		% Flow in Well
A	9512	70.0	5.2	364		100
B	9524	71.4	5.5	393		100
C	9538	64.0	7.6	486	490	100
D	9559	58.0	8.5	493		100
E	9573	43.1	7.5	323		66*
F	9582	37.2	6.5	242		49
G	9592	33.8	5.7	193		39

* Relative to 490 mm^2

The method does, however, confine the loss to the interval over which it actually occurs. No fluid loss is carried over to the next interval as with the timed slug method. Moreover, the method is unaffected by variations in injection rate or by changes in cross-sectional area so long as fluid jets are avoided.

The recording sensitivity and the logging speed should be kept constant for the drags that are to be used for profiling, drags A through G in the case of figures 35 and 41. Each of the drags on Figure 41 was run with the tool moving upwards as the tracer slug moves down to meet the tool. Consequently, the apparent width of a given peak will be shorter on the record than it actually is by the amount that the slug moves down while the tool passes through it. Let W denote the

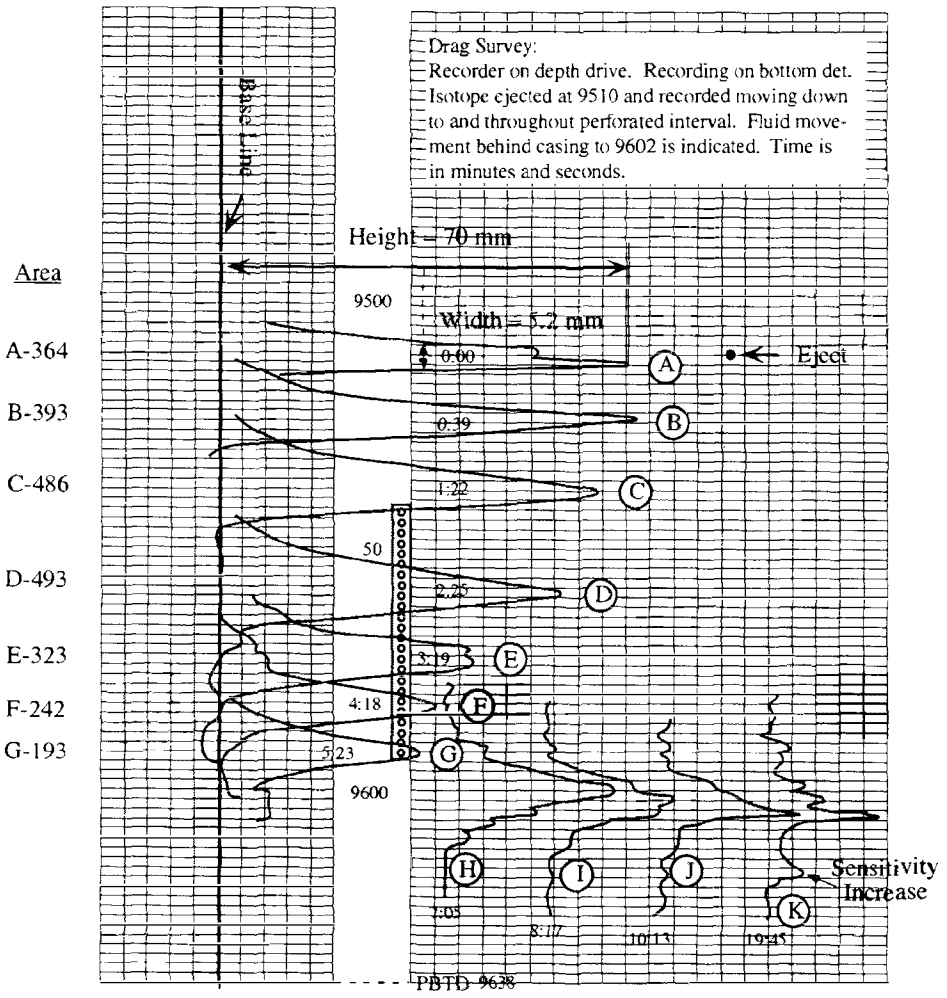

Figure 41. Injection profiling by slug "area" from a tracked slug survey.

actual slug width, W_{app} the width on the record, and δ the distance traveled by the slug as the tool passes through. Then

$$W_{app} = W - \delta$$

If V_L is the line or logging speed upward, then the time required for the tool to pass through the slug is

$$\Delta t = \frac{W_{app}}{V_L} = \frac{1}{V_L}(W - \delta).$$

During this time the slug moves a distance δ given by

$$\delta = \hat{V}\Delta t .$$

From these two equations one obtains the following expression for δ:

$$\delta = W \frac{\hat{V}}{V_L + \hat{V}}$$

from which

$$W_{App} = \frac{W}{1 + \frac{\hat{V}}{V_L}},$$

or

$$W = W_{app} (1 + \hat{V}/V_L)$$

At the logging speeds typically used for drag surveys, 200 ft/minute or higher, the correction to the apparent width as taken from the record is generally insignificant.

In spite of its approximate nature, the slug area method of profiling shown on Figure 41 gives a slightly better answer than does the times slug method of Figure 35. This is shown on Figure 40 where the two methods may be compared to the profile given by eleven velocity shots made over the perforated interval.

Injection Profiles from Velocity Shots: The increased vertical resolution afforded by stationary velocity shots is apparent from the comparison already made on Figure 40. This increased resolution is purchased with increased logging time. Consequently, the chance of including errors due to rate variations also increases. For example, the total 20 shots associated with the testing that gave the data for the velocity shots on Figure 40 were spaced over nearly half an hour. By contrast, the logging for drags A through G on Figure 41 occupied less than six minutes of time. The common procedure is to make the velocity shots in a single progression, top to bottom or vice versa, without doubling back to check on previous shots. If this check is to be done, specific instructions must be given to this effect.

The various methods for travel-time selection have already been illustrated on the velocity shot of Figure 39 taken in the 100% flow stream. The travel time of 13.8 seconds quoted for this shot was the peak travel time. This time is assigned to the depth at the mid-point of the detectors, i.e., to 5,802 feet in Figure 39. The velocity shot data are tabulated as shot number, mid-point depth, and travel time in exactly the same fashion as was the timed slug data in the table on page 57. The travel times are commonly referred to as "reaction time." Since the detector spacing is the same for all shots, the percentage profile is done with reciprocal travel time without conversion to a velocity. Thus, in the well of Figure 39, a travel time of 20 seconds, relative to 13.8 seconds for full flow, would correspond to (13.8/20) x 100 = 69% of the total rate. This is the point graphed as a solid dot on Figure 40 at a mid-point depth of 9,581 feet.

A question that usually arises is the meaning that one attaches to the velocity associated with the 13.8 second travel time for the velocity shot of Figure 39; namely how is the number

$$V = \frac{5.5 \text{ ft}}{13.8 \text{ sec}} \times 60 \frac{\text{sec}}{\text{min}} = 24 \frac{\text{ft}}{\text{min}}$$

related to the volumetric injection rate? It is obviously bigger than the superficial velocity $\hat{V}$ = 19.5 ft/min determined from the timed slug data in the table on page 57. This is not unexpected since the cross-sectional area determining V is the annular area between the tool and the casing wall. For the velocity shot in question, the tool was a 1 3/8 inch diameter instrument with a cross-sectional area of 0.0103 square feet inside casing with an area of 0.1305 square feet. An area correction on the value for V thus gives

$$V_c = \frac{0.1305 - 0.0103}{0.1305} \times 24 = 22.1 \text{ ft/min},$$

a number that is still larger than $\hat{V}$ = 19.5 ft/min. Theoretical relations between V_c and $\hat{V}$ exists but the assumptions are so restrictive that they are of little practical utility. Consequently, the rate equation for velocity shot data is usually simply

$$q = \frac{C}{\Delta t},$$

where Δt = velocity shot travel time, seconds,
C = calibration constant, BPD-sec.

The calibration constant is determined from a surface measured injection rate and a downhole travel time in the full flow stream. For example, suppose q = 650 BPD (the rate calculated from the timed slug) and that Δt = 13.8 seconds as measured by the velocity shot in the 100% flow stream, then C = 650 x 13.8 = 8,970. The velocity shot is therefore not an absolute measure of volumetric rate as is the timed slug. The reason for this is the incomplete mixing that accompanies ejection from a stationary tool followed by only about five feet of travel prior to gamma intensity measurement. If one is desperate for an estimated rate, one can assume that

$$\hat{V} = \alpha V_c,$$

where α = 0.7 - 0.9,

for the "sharp" pulses of the type shown on Figure 39 (page 54). Because of the poor mixing, the apparent travel time of the shot slug depends almost entirely on how the material is distributed by the ejection jet into the annular volume between tool and casing. Figure 42 shows two extremes of tracer placement by a tool centralized in a low velocity stream. In frame A, a high velocity jet from a single ejection port plasters the material against the wall of the pipe. The subsequent rebound, just beginning on the figure, is the only mixing the material gets. In fact, in viscous polymer water, the slug may not rebound at all! The resulting pulse that such a shot gives can

range from satisfactory to a very smeared-out, low-intensity signature with ill defined travel time. The tool on frame B of Figure 42 has four ejection ports and can place large shots at lower velocity to give much better mixing in the pipe along with a sharper pulse whose peak is clearly defined. Tracer tools are available that avoid the placement problem by virtue of slug ejection downward into the center of pipe. Such a tool is pictured on Figure 43. The decentralizing "elbow" on this instrument positions the ejector at the centerline of whatever size pipe is involved. Because this places the tracer material in the higher velocity part of the pipe, the resulting gamma intensity pulse has sharp leading and trailing edges with well-defined travel time. It is the preferred tool for profiling flows of viscous water.

Considering the work that went into the preparation of the injection profile on Figure 40 (page 58), one must also determine how representative it is of the actual injectivity. This is done in the next section.

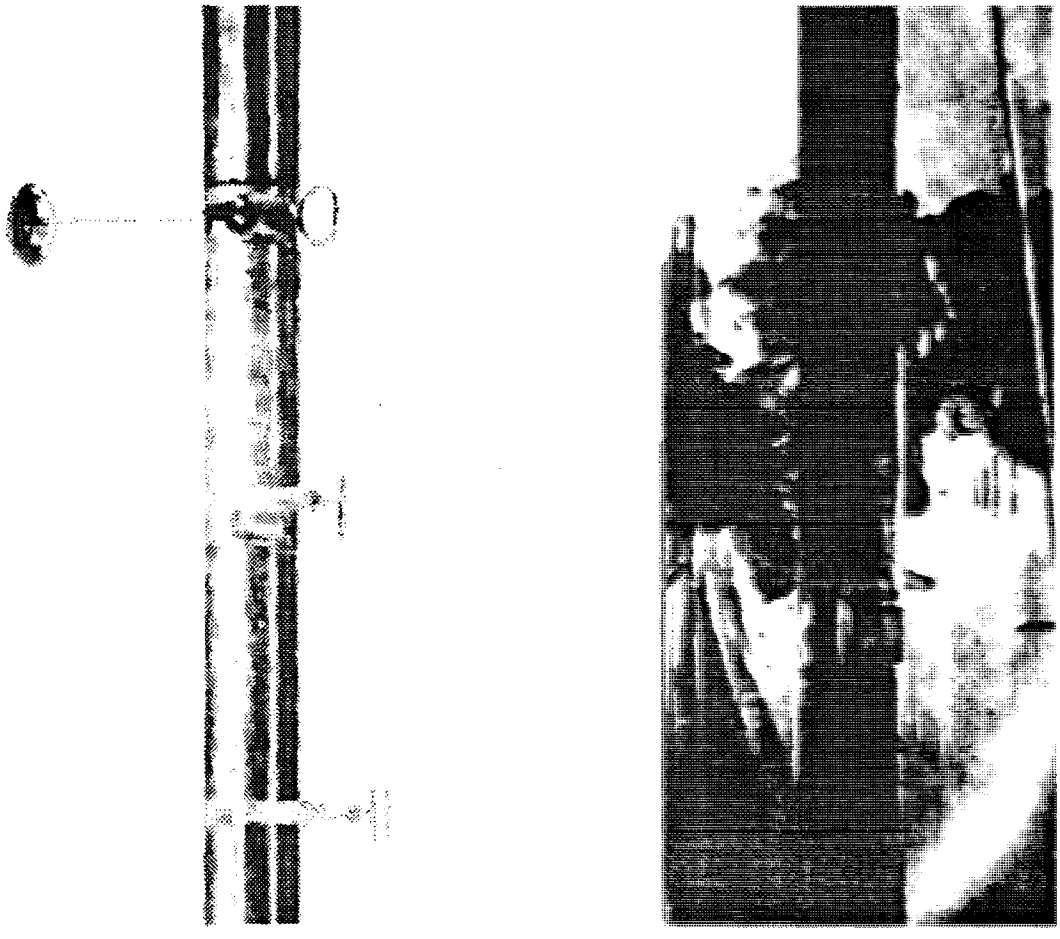

Figure 42. **Tracer placement in the annular volume between a 1.5-inch tool and a 6-inch plexiglass pipe (courtesy Atlas Wireline).**

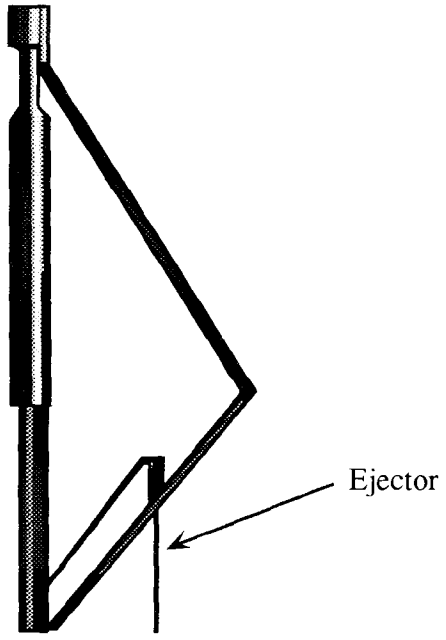

Figure 43. Tracer tool for ejecting slug at centerline of pipe (courtesy of Atlas Wireline).

Comparison of Tracer Profile with Temperature Profile: The initial drag surveys on Figures 35 (page 50) and 36 established that at least some of the injected water goes behind the pipe into porosity at 9,605 feet. The most detailed flow profile, the velocity shot data on Figure 40, places 50% of the flow exiting at the very bottom of the perforated interval. This is, presumably, the amount lost behind pipe to lower porosity. Therefore, one would conclude that only 50% of injected water is entering into the completed-interval porosity. This hypothesis can be checked. The injecting temperature survey given on Figure 44 indicates that the hypothesis is in fact, wrong! Every bit of the injected fluid is going into the porosity at 9,605 feet because the temperature survey shows no losses above this depth. Apparently, the formation has fractured downward from intended porosity into that below the completion. The tracer tool is correctly recording those depths where the water leaves the wellbore region in the fracture. The decreasing vertical velocities associated with the tracer drags on Figure 35 reflect increasing lateral velocities in the fracture itself so as to conduct the same mass rate in a form of a "spill" into the fracture. This comparison illustrates emphatically the necessity of corroborating surveys in production logging. No logging tool is an absolute, stand-alone device in all situations. Yet the belief is so strong that the "more easily interpreted" tracer data is the "right" answer that common practice is to allocate 50% injection to the completed interval even though the temperature survey is available for comparison. At least, in this example, the tagged water stayed close enough to the wellbore to be evident on the drags of Figure 35 even below the perforated interval.

But this is not always the case. Frame A on Figure 45 shows seven drags through shot #2 ejected at 5,400 feet in a well on water injection. Drag 4 already shows significant loss at the top of the

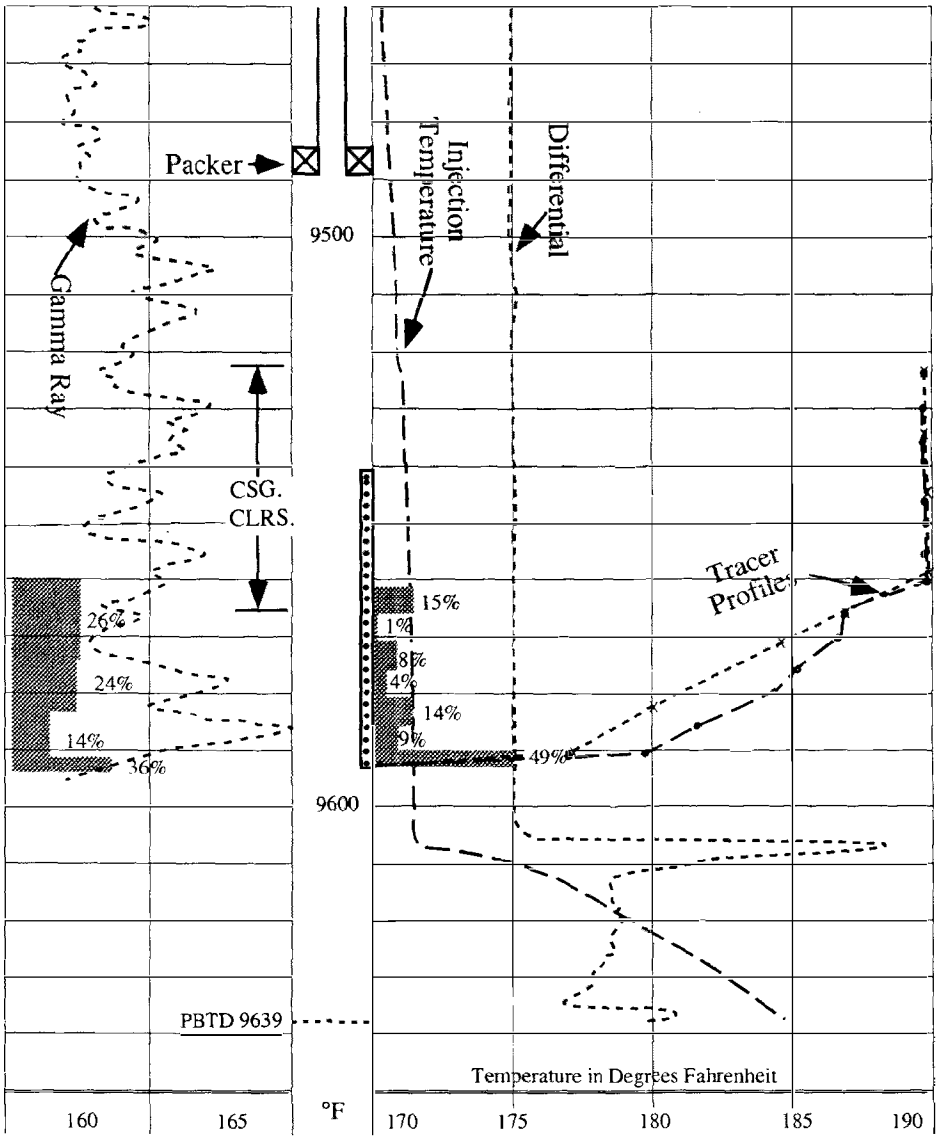

Figure 44. Injecting temperature survey from well with tracer survey shown on Figure 35.

short perforated interval at depth A on frame A. Drags 6 and 7 reveal that the vertical travel of the slug peak ceases at the bottom of the same perforations. The slug is pumped away at this location. Compare this behavior with that below the perforations in Figure 35. The velocity shot survey also showed no flow below a depth of 5,427 feet, as indicated on frame A of Figure 45. The slug travel to the bottom of the porosity of zone A at 5,431 feet apparently occurs behind pipe. As a result of the tracer survey, the entire injection was allocated to zone A. Yet the injecting temperature survey on frame B of Figure 45 shows no loss at all across this zone, depth 1 on frame B. The first loss is at depth A, the top of the thick zone of porosity evident on the

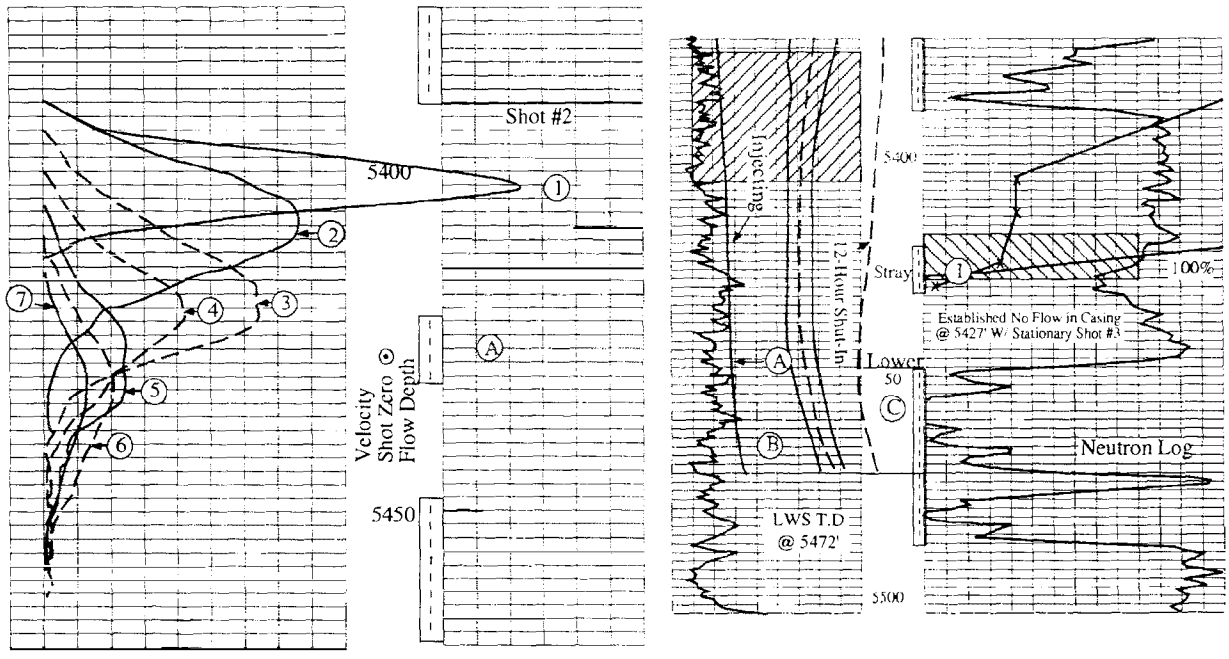

(A) Tracer Survey With Well On Injection

(B) Temperature Surveys From Same Well

Figure 45. Tracer and temperature surveys from an injection well that has been fractured inadvertently.

neutron log of frame B. The next loss is at depth B, a location in the same thick zone. Furthermore, the 12-hour shut-in temperature survey on frame B of Figure 45 shows absolutely no storage at the porosity indicated at depth 1. The only storage signature is at depth C, the top portion of the thick zone. The entire stream is actually injected into this zone not the one indicated by the tracer loss surveys on frame A. Perforations into the thick zone have plugged with continued injection, the formation has fractured from the thin zone down into the better permeability in the thick interval, and the injected stream is presently exiting the wellbore into the fracture through the thin-zone perforations. As this stream "spills" away from the wellbore, it is quickly lost to the tracer tool.

Special procedures are needed if the tracer tool is employed to demonstrate injection confinement. This is the subject of the final topic in the discussion of the radioactive tracer method. Some additional comments on the vertical resolution of the velocity shot method of surveying should be made at this time. The resolution of the shot data on Figure 40 was set by the 5.5 foot separation between the two detectors. This spacing, however, is not a restriction on the vertical resolution that can be achieved. This fact is demonstrated in the next section. The technique also allows one to limit the smearing effect already described for timed slugs to small distances.

Velocity Shots with Overlapping Intervals: Suppose the two detectors are spaced five feet apart. The tool can, of course, only measure five-foot travel times directly. If, however, the tool is only

moved by a distance of one foot after each shot, then any shot relogs four feet of the previous 5-foot interval and picks up one foot of new travel time. In this fashion, one-foot travel times, $\Delta t'$, can be calculated from five-foot times, Δt. Consider the 8.5-foot perforated interval shown on frame A of Figure 46. Suppose that injection is occurring only in the top four feet of the interval in a uniform fashion so that equal amounts are lost in each foot of interval. If 50% of the total stream is injected into the 4-foot interval and 50% continues to other sets of perforations deeper, then the true injection profile appears on frame A of Figure 46 in the form of a bar graph showing the 12.5% of the total injection that exits over each foot of the 4-foot interval. If the survey is made with the actual spacing of detectors as the interval between shots, then two shots will span the entire perforations. The resulting smearing will then be so bad that roughly 25% of the injection appears to exit over the top half of the perforations and 25% over the bottom half, i.e., the injection appears to be uniform over the entire perforated interval. This is clearly unacceptable. So, instead, velocity shots will be taken at 1-foot intervals starting with the tool positioned so that the bottom detector is just above the top perforation at location 1 on frame A of Figure 46.

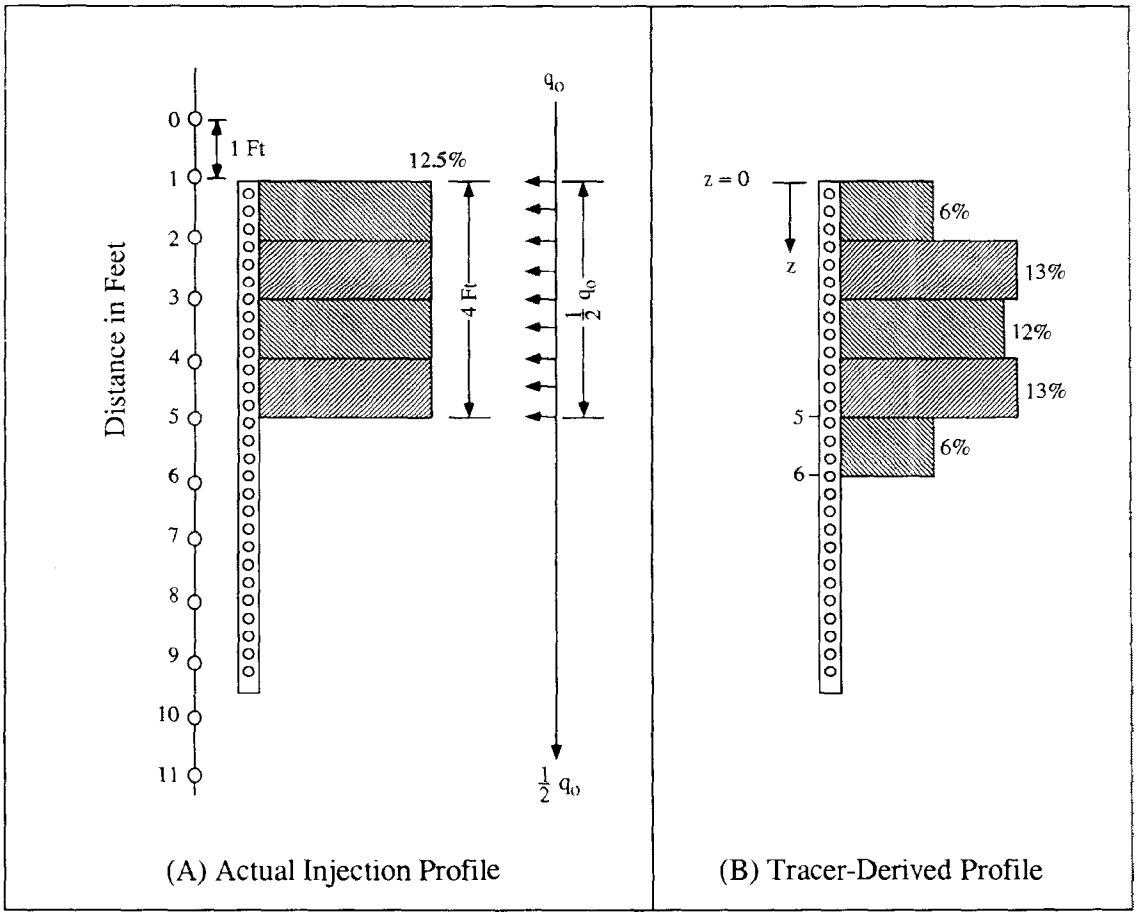

Figure 46. Control of vertical resolution by overlapping 1-ft stations with a tool having normal detector spacing.

The top detector is 5 feet above location 1. Both detectors are in the full flow stream, q_o. The first measured travel is thus the reference for 100% flow:

$$\Delta t_o = 5\Delta t'_o$$

where Δt_o is the 5-foot reference time and $\Delta t'_o$ is the 1-foot reference time for 100% flow. Therefore

$$\Delta t'_o = \frac{1}{5}\Delta t_o \text{ (at location 1)}$$

The tool is now moved so that the bottom detector is one foot deeper at location 2 on frame A, Figure 46. The resulting travel time, Δt_1, measured over five feet is

$$\Delta t_1 = \Delta t'_1 + 4\Delta t'_0$$

$$\Delta t_1 = \Delta t'_1 + \frac{4}{5}\Delta t_0$$

or $$\Delta t'_1 = \Delta t_1 - \frac{4}{5}\Delta t_0 \text{ (at location 2),}$$

This is the travel time for the first 1-foot increment into the perforated interval. This result can also be written as

$$\Delta t'_1 = \Delta t_1 - \Delta t_0 + \Delta t'_0 .$$

In this form it has an obvious geometric significance. When the tool is lowered by one foot to a current location from a previous location, the movement of the bottom detector adds an increment of one foot length. Likewise, the movement of the top detector leaves behind an increment of equal length. The last expression, stated in words rather than symbols, is:

> "The travel time for the added increment is equal to the difference in 5-foot travel times in the current and in the previous location plus the incremental travel time for the increment left behind."

In the above form the statement is perfectly general. For example, for shot #5, five feet into the perforations, the bottom detector moves from location 5 to location 6 on frame A of Figure 46. Likewise, the top detector moves from location 0 to location 1 leaving behind an increment with a travel time of $\Delta t'_o$. Thus

$$\Delta t'_5 = \Delta t_5 - \Delta t_4 + \Delta t'_0 .$$

For shot #6, the bottom detector moves from location 6 to location 7 whereas the top detector moves 1 foot into the perforated interval leaving an increment with a travel time of $\Delta t'_1$.

Consequently,

$$\Delta t_6' = \Delta t_6 - \Delta t_5 + \Delta t_1' ,$$

or, in general

$$\Delta t_N' = \Delta t_N - \Delta t_{N-1} + \Delta t_{N-5}' ,$$

where the N-5 arises from the 5-foot spacing between detectors. Shot #6, six feet into the perforations and two feet beyond the injection interval in frame A of Figure 46, is required in order for the survey to register zero injectivity in the added increment. The corresponding apparent profile is shown on frame B of Figure 46. Here we see that half the true injection is lost from the first increment of the perforated interval and is allocated instead to the increment just beyond the last increment to actually receive injection.

The profile in frame B of Figure 46 is quite simple to calculate. If a distance parameter z is measured from the top of the perforations downward as shown on frame B, Figure 46, then the velocity in the perforated interval is given by

$$V(z) = V_o \left(1 - \frac{z}{8}\right); \quad 0 \le z \le 4 \text{ ft}$$

$$V(z) = \frac{1}{2} V_o \qquad ; \quad z > 4 \text{ ft}$$

where V_o is the full stream velocity. The travel time over an increment extending from z_i to z_j is thus

$$\Delta t_{ij} = \int_{z_i}^{z_j} \frac{dz}{V(z)} = \frac{1}{V_o} \int_{z_i}^{z_j} \frac{dz}{\left(1 - \frac{z}{8}\right)}$$

recognizing that $\Delta t_0' = \frac{1}{V_0}$ minutes, we obtain after integration

$$\Delta t_{ij} = 8\, \Delta t_0' \ln\left(\frac{8 - z_i}{8 - z_j}\right); \quad z_j \le 4 \text{ ft},$$

for the interval travel time. For example, $z_i = 0$ and $z_j = 1$ for the first foot into the perforations, interval 1-2 on frame A, Figure 46. Thus

$$\Delta t_{12} = 8\, \Delta t_0' \ln\left(\frac{8}{7}\right) = 1.068\, \Delta t_0'$$

For the fifth foot, interval 5-6, $z_i = 4$ and $z_j = 5$, so that $V(z) = 1/2\, V_o$ and $\Delta t_{56} = \frac{2}{V_0} = 2\Delta t_0'$. In this fashion, the following numbers are obtained.

Shot	Frame A Interval	$\Delta t'$	% Flow in Well	% Loss to Interval
0	0-1	$\Delta t'_o$	100	
1	1-2	$1.068\ \Delta t'_o$	94	6
2	2-3	$1.233\ \Delta t'_o$	81	13
3	3-4	$1.459\ \Delta t'_o$	69	12
4	4-5	$1.785\ \Delta t'_o$	56	13
5	5-6	$2\ \Delta t'_o$	50	6
6	6-7	$2\ \Delta t'_o$	50	0

The numbers in the last column are graphed on frame B of Figure 46.

The technique of overlapping intervals must be initiated with a shot in a location where the fluid velocity is constant over the spacing between detectors. One can, of course, log upward as well as downward. The general rule stated on page 69 is independent of direction.

Quality Control in Profile Surveys: Numerous comments have been made about the tracked slug survey of Figure 35 (page 50), and the stationary velocity shot of Figure 37 (page 52). In reality, the survey quality is not all that good. The slug tracked on Figure 35 was not mixed when first ejected and a common baseline was not employed for all subsequent drags through the perforated interval. On the velocity shot in Figure 37, the time drive of 1 inch per minute is much too slow for the slug velocity.

The following example is a higher quality survey. The example comes from a well on a quite low rate of injection of some 150 BPD into two perforated intervals. The completion is 5 1/2-inch, 17 lb/ft casing. A 12-drag tracked slug survey is given on Figure 47. Tool motion was used to mix the tracer slug immediately after ejection. The baseline indicated by the double line serves as a reference for all the drags. This survey was conducted in a manner so as to insure quality from both slug area analysis and slug timing.

The peak times are not shown on the log of Figure 47. Instead, they were tabulated on a section of the log. A visual inspection of the surveys on Figure 47 shows most of the injected water is still in the wellbore on drag #7, whereas drag #8 shows considerable loss. From the relative location of the respective peaks on these drags it will not be possible to tell if this loss occurs right at the bottom of the top set of perforations or right at the top of the bottom set. The velocity shots will have to decide the issue. The data from the tracked slug survey is tabulated below. The "area" listed in column 3 of the tabulation is the product of the peak height and half-height width as illustrated on drag 1 of Figure 47.

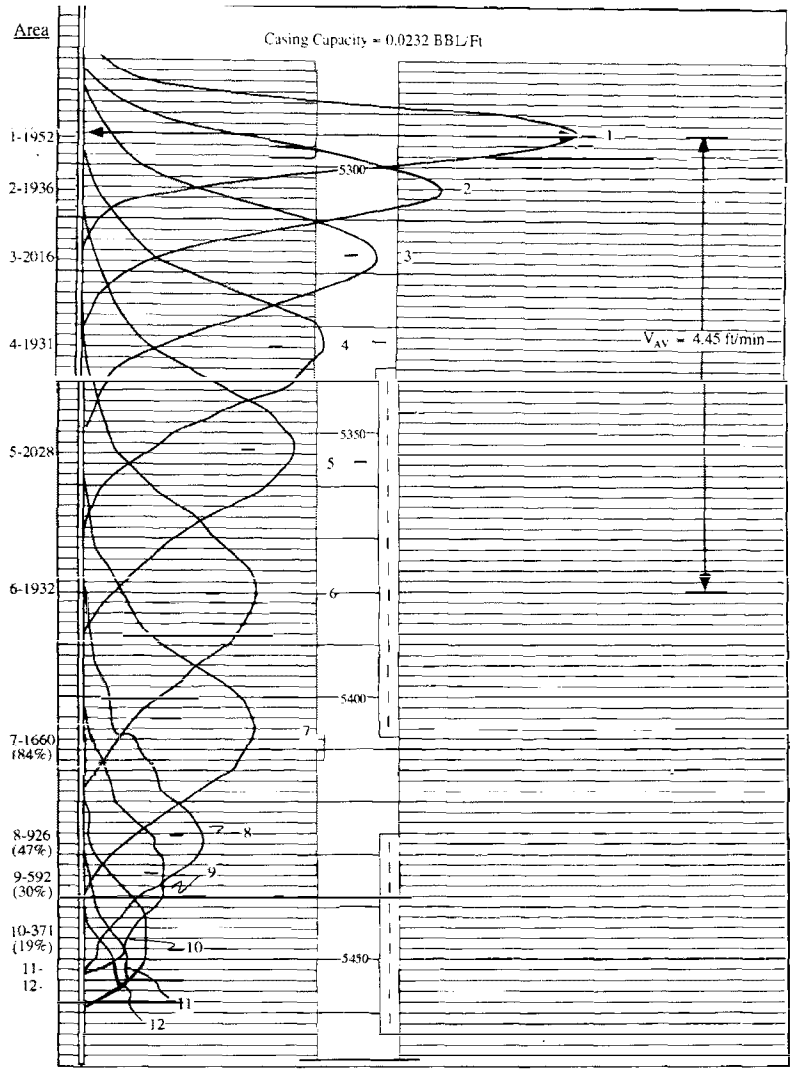

Figure 47. Good quality tracked slug survey in well on injection at 150 BPD.

Drag No.	Peak Location	"Area" mm²		% Flow	Travel Interval	Time Secs	$\hat{V}$ Ft/Min		% Flow	Depth @ Mid-Point
1	5294	1952		100		0				
2	5304	1936		100	10	132	4.55		100	5299
3	5316	2016	1966	100	12	161	4.50	4.45	100	5310
4	5334	1931		100	18	237	4.56		100	5325
5	5353	2028		100	19	270	4.22		100	5343
6	5380	1932		100	27	367	4.42		100	5366
7	5406	1660		84	26	405	3.85		87	5393
8	5426	926		47	20	496	2.42		54	5416
9	5433	592		30	7	255	1.65		37	5430
10	5446	371		19	13	626	1.25		28	5440
11	5452	176		9	6	781	0.49		11	5449
12	5453	96		5	1	755	0.08		2	5452.5

The values for this area, as a result of the mixing after ejection, are free of the initial "growth" that distorted the survey of Figure 35. The individual values for drags 1 - 6 are all within 4% of the average.

The corresponding average velocity of $\hat{V}$ = 4.45 ft/min along with a pipe capacity of C = 0.0232 bbls/foot gives by equation (3A), page 59:

$$q = 1440 \times 0.0232 \times 4.45 = 149 \text{ BPD}$$

for the injection rate. This is the same as the metered rate of 152 BPD. The injection profile data tabulated above are plotted on Figure 48. The only difference arises from the assignment of the timed slug data to the midpoint location. Had these values been assigned to the peak location instead, the two approaches would have given the same profile.

Both profiles show apparent loss between perforations which actually occurred at the perforations. As already stated, a velocity shot between the two sets of perforations is needed for correct allocation.

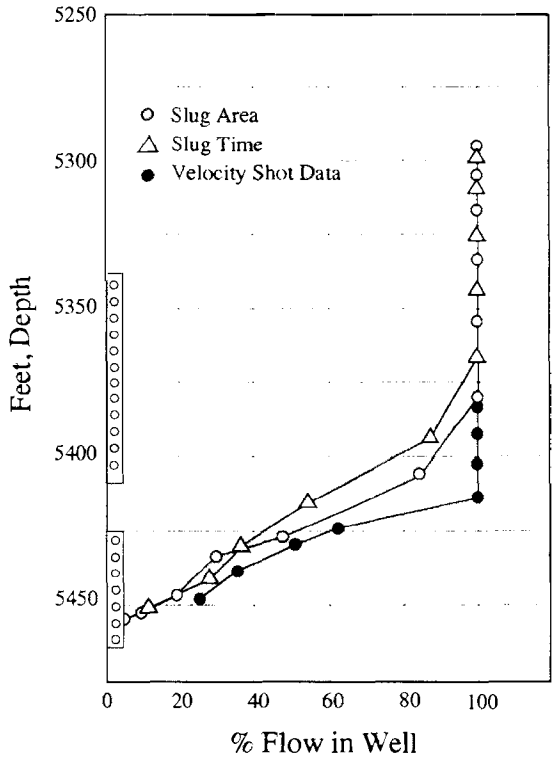

Figure 48. Injection profile for tracked slug survey of Figure 47 with injection rate of 152 BPD.

The detectors for velocity shots are spaced 5 feet apart. For the average velocity V = 4.45 ft/min given in the tabulation on page 72 for the full flow stream, the chart drive speed, according to equation (6), page 56, should be no slower than

$$S = \frac{\hat{V}}{L} = \frac{4.45}{5} \approx 1 \text{ in/min},$$

a speed that would give 10 chart divisions, roughly, between peak locations at 6 seconds per chart division. The actual time drive employed was 2 in/min for a nominal 3 seconds per chart division. A calibration, however, gave 25 chart divisions of travel in 123 seconds of time, or 123/25 = 4.92 seconds per chart division. This is the scale for all subsequent stationary shots. A total of 17 shots were made for flow profiling purposes. Two of these are illustrated on Figure 49. Frame A is a shot in the full flow stream with the top and bottom detectors at 5,300 and 5,305 feet, respectively. The pulses are turned around relative to each other so that gamma intensity on the record from the bottom detector, the left-hand trace on frame A, increases from left to right. On the other trace from the top detector, however, intensity increases in the opposite direction, right to left. For some reason, this procedure is thought to facilitate analysis and, as such, is a harmless quirk favored by many logging operators. On frame A, peaks are marked by arrows. The locations should be at the mid-point of the pulse width about the peak. Otherwise, pulse-shaping, method 3 on Figure 38, should be used to fix a peak location. On frame A, the peaks are separated by 12.4 chart divisions or 12.4 x 4.92 = 61.0 seconds. This corresponds to an apparent velocity of (5/61) x 60 = 4.92 ft/min. As things happened, 13 out of the 17 shots were in the 100% flow stream. From these an average velocity of 5.48 ft/min was determined. The tool diameter and casing size in this example are both the same as those for the velocity shot of Figure 37. Consequently, the area correction is the same as that carried out on page 32, or V_c = 0.921 x 5.48 = 5.05 ft/min. This value is again larger than the superficial velocity $\hat{V}$ = 4.45 ft/min associated with the drag surveys of Figure 47.

Frame B on Figure 49 is the velocity shot taken with both detectors located between the two sets of perforations. On this frame the peak travel time is 16 chart divisions which is longer than the 12.4 cd's associated with the 100% shot of frame A. Nominally only 12.4/16 = 0.78 of the flow passes the top set of perforations.

Actually, at the low rates involved in this example, the peak shape and apparent travel time becomes quite dependent upon the ejected tracer distribution. In such situations, those travel times that are associated with the first arrivals, methods 1, 4, and 5 on Figure 38, are much less sensitive to tracer distribution than are the peak travel times. For this reason, the half-peak points have been marked on the leading edge of all four pulses appearing on Figure 49. The travel time associated with these points on frame A is 11.0 chart divisions whereas on frame B they are separated by 10.0 chart divisions. Likewise, the travel times for the "first arrivals" are the same. No measurable injection loss occurs in the top set of perforations! The loss that appears to occur between the perforations on the profile of Figure 48 in conjunction with the tracked slug is thus associated with the top of the bottom set of perforations.

Figure 50, for velocity shot #4, shows how strung out the pulses become. For this shot, the top and bottom detectors were at 5,435 and 5,440 feet, respectively. In contrast to the pulses on

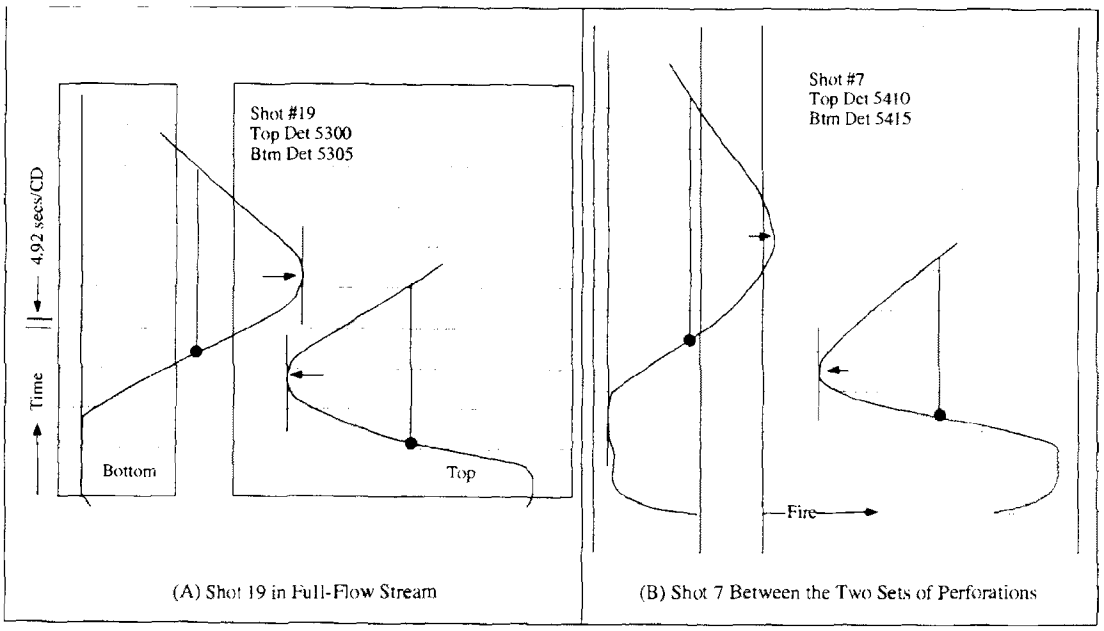

Figure 49. Velocity shots at two locations in the well giving the slug survey of Figure 47. Injection rate is 152 BPD in 5 1/2-inch, 17 lb/ft casing. Perforations at 5338-5408 and 5426-5464.

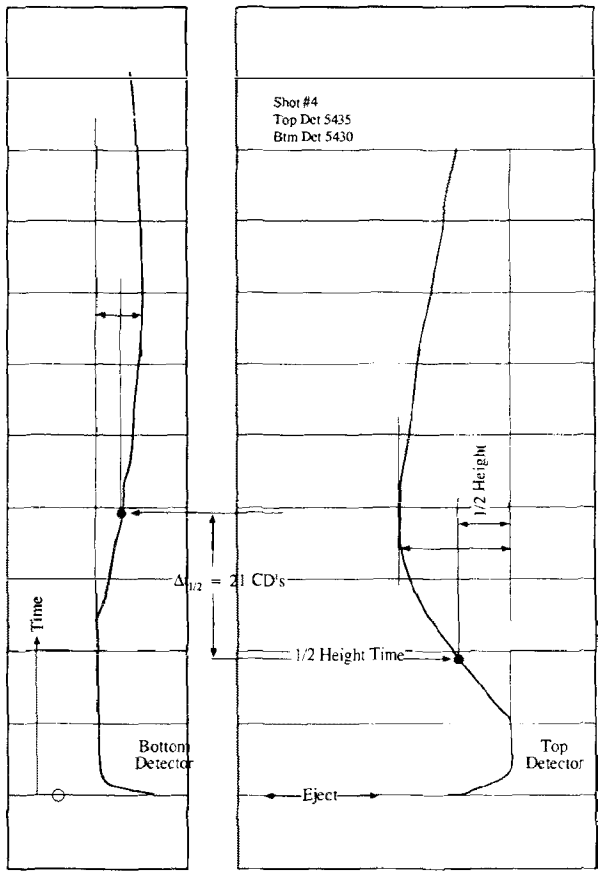

Figure 50. Velocity shot #4 with rounded (concave) leading edge typical of well-mixed shot in laminar flow.

Figure 49, the ones on Figure 50 have leading edges that are rounded over (concave) without inflection points. This shape is characteristic of a well-mixed slug in a laminar flow stream. For a velocity shot under these conditions, theory predicts that both the peak and leading edge travels at a velocity that is twice the superficial, i.e., $Vc = 2\,\hat{V}$. It has already been seen that for previous velocity shots in turbulent flows $V_c \approx \hat{V} / 0.8 = 1.25\,\hat{V}$. Consequently, one should in theory increase the travel times measured in laminar flow before comparison with those measured in portions of the well where flow is turbulent. From the above figures, the laminar peak travel times should be increased by a factor of 2/1.25 = 1.60 for comparison with turbulent peak times. In theory, the factor for leading edge travel time is 1.32.

One might then speculate that, instead of the 21 chart divisions associated with the half-peak travel time shown on Figure 50, one should use a value in the range of 28 - 34 chart divisions for comparison to the 100% value of 9.88 chart divisions listed in Table 6. Actually, the full-flow velocity of 4.45 ft/min is just in the turbulent range so that the first loss drops the stream into the laminar regime.

TABLE 7. VELOCITY SHOT DATA FOR WELL OF FIGURE 47

Shot #	Top Detector	Bottom Detector	Half-Peak Separation, CD		% Flow in Well
20	5285	5290	10.0		100
19	5300	5305	11.0		100
18	5315	5320	10.0		100
17	5325	5330	10.0		100
16	5333	5338	8.0		100
15	5338	5443	10.0		100
13	5350	5355	10.0	9.88	100
12	5360	5365	7.5		100
11	5370	5375	10.8		100
10	5380	5385	11.0		100
9	5390	5395	10.0		100
8	5400	5405	10.1		100
7	5410	5415	10.0		100
6	5421	5426	12.2		61*
5	5426	5431	14.0		53
4	5435	5440	21.0		36
3	5445	5450	29.0		26

* Relative to 9.88/1.32 = 7.48 cd's for 100% flow where 1.32 is laminar correction factor

These facts follow from the value of Reynold's number for the full flow stream. This number, N_{Re}, is defined as

$$N_{Re} = 129 \frac{\rho \hat{V}(D_p - D_t)}{\mu} \qquad (7)$$

where ρ = Density, gm/cc
D_p = Pipe inside diameter, inches
D_t = Tool diameter, inches
$\hat{V}$ = Average velocity of fluid, ft/min
μ = Fluid viscosity, centipoises

for the flow to be laminar $N_{re} \leq 2{,}000$: consequently,

$$\hat{V}_{Lam} \leq \frac{2000}{129} \frac{\mu}{\rho(D_p - D_t)} \qquad (8)$$

For D_p = 4.9 inches, D_t = 1.375 inches, μ = 0.82 cp, and ρ = 1.06 gm/cc, equation (8) gives for the onset of laminar flow

$$\hat{V}_{Lam} \leq 15.50 \times \frac{0.82}{1.06 \times (4.9 - 1.375)},$$

$$\hat{V}_{Lam} \leq 3.40 \text{ ft/min}.$$

Consequently, the large loss "between" perforations shown on the drag profile of Figure 48 will drop the flow into the laminar region because 3.40/4.45 = 0.76. It is therefore simpler to correct the 100% flow value of 9.88 chart divisions than it is to correct all readings below shot #7 in the tabular results above. This single correction is made by 9.88/1.32 = 7.48 CD's as the reference for 100% flow in the table. For example, shot #6 gives for the percent flow in the well:

$$\% \text{ Flow} = 100 \times \frac{7.48}{12.2} = 61,$$

and, likewise for the remaining shots. The velocity shot profile is shown as solid circles on Figure 48. The location for a given shot is taken at the mid-point depth between the two detectors. The velocity shot data do not show the 15%, or so, loss over the bottom half of the top set of perforations that the drag surveys indicate. This injection may be of a sporadic nature or it may not be within the ability of the velocity shot to detect a loss of this size. The tabulated half-peak travel times show variations of this magnitude. Both survey methods place the majority of the injection as exiting over the top half of the bottom set of perforations.

The injecting temperature survey of Figure 51 also does not show a loss over the top set of perforations. The first "exit" shows up at a depth A some 6 feet above the top of the bottom set of perforations. This most likely is the result of flow behind pipe upward from the top of the lower perforations. The short-time shut-in surveys indicate that such a crossflow takes place.

The injecting temperature survey also shows flow to the base of the interval at depth B. Given the large exit over the top half of the bottom set of perforations evident on the tracer survey, the flow to the base of the unit is also probably behind pipe in a fracture. The 12-hour shut-in temperature survey shows the major storage at 5,450 feet, location C, in the lower perforated interval.

However, there is a storage signature at depth D in the bottom part of the upper set of perforations. The storage in the top part of this interval around 5,350 feet is a relic of "injections past."

In summary, this example presented a good quality tracer survey with tracked slug data that was quite easy to interpret, its main disadvantage being that of insufficient vertical resolution. The velocity shots, although quite well run, then required for their interpretation a laminar correction whose validity is uncertain. So, whereas the problem of vertical resolution was eliminated, additional concerns were added. Finally, the temperature surveys revealed more details of the injection pattern.

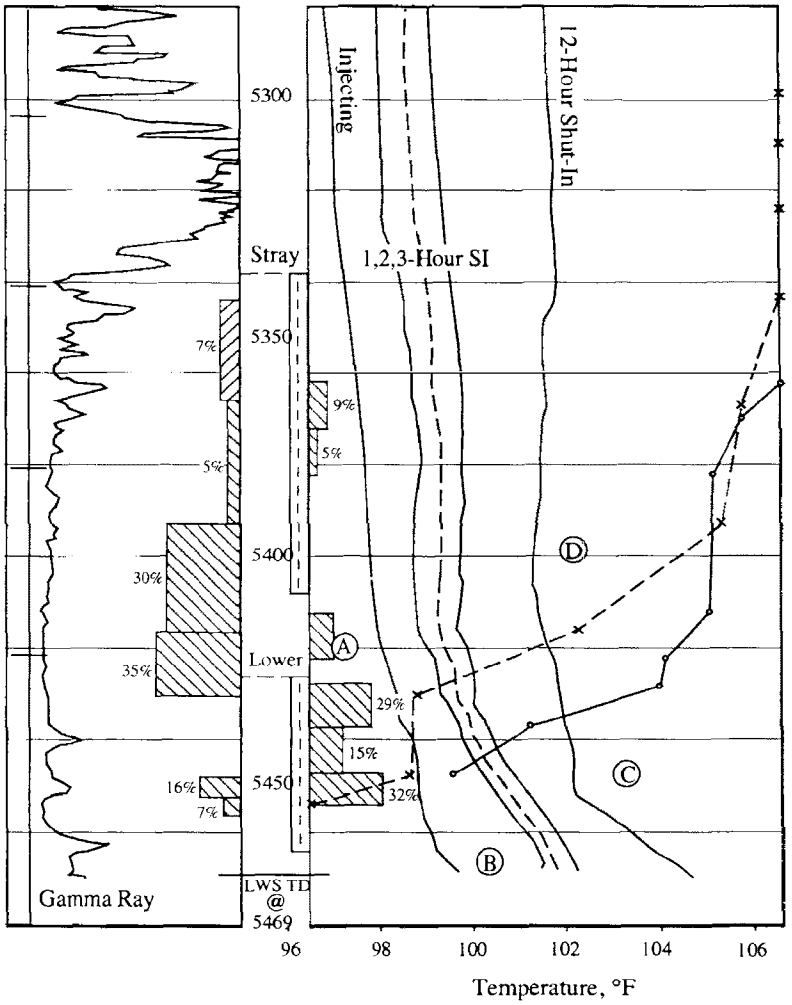

Figure 51. Temperature surveys from well on water injection at 152 BPD.

It should be added that once the well is shut off injection, a crossflow check should also be run with the tracer tool. Very small interzonal flows can be detected in the wellbore in this manner. A crossflow check on the well under discussion after three hours of shut in is given in Figure 52. Four shots of tracer were ejected as the tool was lowered past four selected locations then a logging run was made back up the well. This gave the solid line survey on Figure 52. The tool was then again lowered to the bottom of the well and, after 5 minutes of elapsed time, a second drag was made through the 4 slugs. This drag is the dashed curve on Figure 52. Note that, at the time each drag is recorded, the same number of passes upward through the slug have been made as were made downward. This procedure keeps the dispersion from tool movement symmetric about the peak. Thus, the peak, or more properly, the centroid, of the control slug #1 has not moved in the five minutes between drags. The remaining slugs have each moved upward during this same time with slug #2 travelling some 4 feet while the other two covered only 3 feet during the same time. The crossflow pattern is then mainly from the bottom set of perforations upward into the top of the top set of perforations with a little contribution from the lower portion of the top set. This pattern is shown on the left of Figure 52. The 4 and 3-foot travels in 5 minutes represent velocities of 0.80 and 0.60 ft/min, respectively. With a casing capacity of C = 0.0232 bbls/ft, equation (3A) gives for these velocities volumetric rates of 27 and 20 BPD, respectively, values shown on the left of Figure 52. The crossflow pattern is supportive of the injection profile in the sense that those zones taking injection become the source zones for shut-in crossflow.

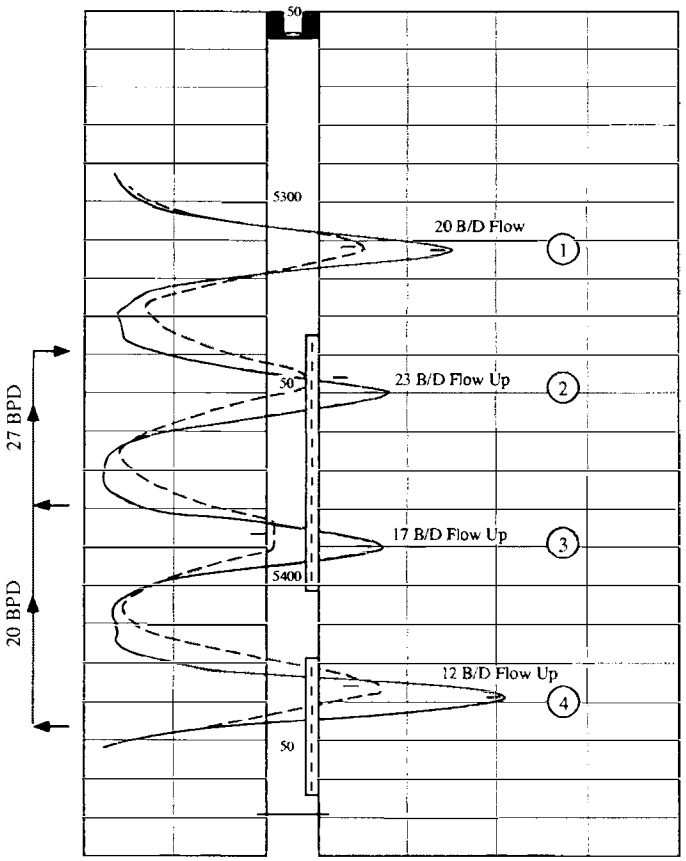

Figure 52. Crossflow check after three hours of shut-in time following water injection at 152 BPD. Drags are five minutes apart.

Logging for Casing Leaks with Well Shut-In: If an injection well has positive wellhead pressure when shut-in, then the above crossflow check procedure is the most sensitive method available for the detection of casing leaks anyplace in the wellbore. With the well shut-in, at least overnight, a slug of tracer is placed in the casing above the topmost perforations. If the pressured injection zones backflow to casing leaks, then the tracer slug will accordingly move upward in the wellbore. With proper procedure, incredibly small leaks can be detected in this fashion. Figure 53 presents five drags run on five successive days after placement of a tracer shot twenty feet above an injection zone in a shut-in well. The logging tool, of course, was left downhole during the sequence. Removal of 7,300 feet of 5/16-inch cable would allow at least an equal volume, 0.7 bbls, of inflow from injection zones below. In the 7- inch, 23 lb/ft casing, this would have displaced the slug upward by some 18 feet! Also, careful depth control is necessary, preferably by the presence of a cable "flag" placed on the line at the surface at a given depth prior to slug placement. Furthermore, the recorder should be checked for record "stretch" after each logging run.

Even the service company doing the logging did not believe the precision illustrated on Figure 53 was possible, although this was common knowledge in the early days of the tracer instrument. During the elapsed 4 days the centroid of the slug has drifted upward by at most 1 foot; consequently, any leak has a velocity no greater than 1 foot per 4 days, or

$$\hat{V} \leq 1.736 \times 10^{-4} \text{ ft/min},$$

from which

$$q \leq 9.82 \times 10^{-3} \text{ BPD},$$

a value that is about 1 cc per minute! This is in spite of the fact that a crossflow of some 50 BPD was in progress between the injection zones themselves during the logging operation.

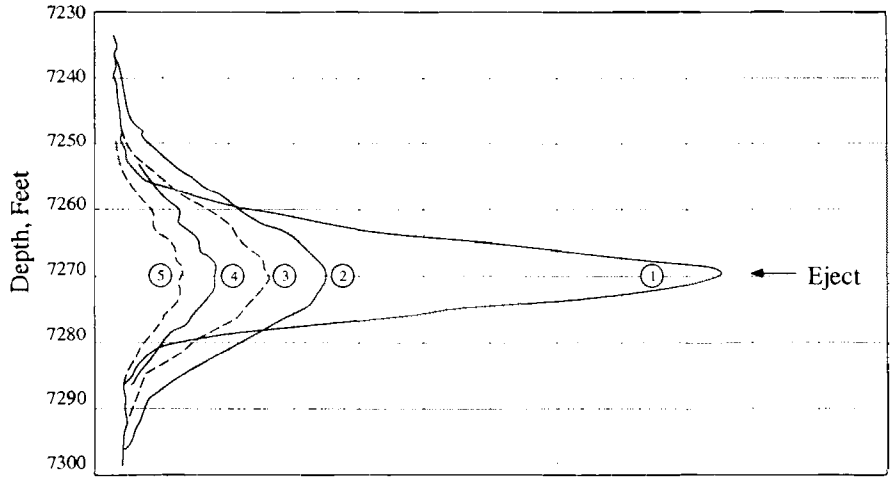

Figure 53. Drags on five successive days through a radioactive slug ejected at 7,270 feet in a shut-in injection well. Logging tool left in well between drags!

This is, therefore, the preferred method of testing tubular integrity in injection wells with positive wellhead pressure. Otherwise, the procedures described in the following section should be used.

Logging for Injection Confinement: With proper use, the radioactive tracer technique is the most sensitive method available for the detection of loss from an injection zone due to flow behind pipe. Proper use entails a realization that the tools sensitivity can be either underutilized or abused. For this reason, Table 4 (page 55) includes a recommended recording sensitivity of about one-fifth that used for a gamma ray log, namely, a sensitivity of 200 API units/inch is a good compromise for behind-pipe flow detection. At full gamma log sensitivity, even a "whiff" of tracer squeezed between the pipe and cement leaves a significant signature on the record. Any repair attempted on the basis of such a signature will cause far more damage than that which it is attempting to cure.

The limited depth of investigation of the gamma tool is another factor to keep in mind. The consequence of the exponential decrease of gamma ray intensity with distance has already been demonstrated by examples. At the recommended recording sensitivity, any gamma ray originating more than 15 inches away will appear as a statistical event lost in the overall background.

The same two techniques used for flow profiling are also employed in logging for flow behind pipe, that is, both slug tracking and stationary velocity shots are in use. The principal difference that one encounters in the case of logging for leaks is that operators who routinely use both methods while profiling will use only the stationary procedure in doing "channel checks" and "packer checks" for behind-pipe and casing leak, respectively. Yet this method is the least suited of the two for this application, as will be explained below. Consequently, the logging operator should be given specific directions as to the logging procedure to use for leak detection.

Slug Tracking Procedure for Behind-Pipe Flow: As in the procedure for profiling, this method involves the ejection of a normal shot of tracer followed by subsequent logging drags over the wellbore with the recorder on depth drive. As already mentioned, this procedure gives a very graphic, overall picture of the flow pattern in the wellbore. As such, the method allows one to distinguish true behind-pipe flow due to poor completion from tracer spreading due to vertical permeability close to the wellbore. Likewise, tracer spreading in fluid eddies often found at the base of the bottom perforated interval or immediately below a tubing string terminated by a packer can be recognized for what it actually is. These situations are all too often classified as poor mechanical integrity conditions by operators who rely exclusively on velocity shot techniques.

The operational procedure for slug tracking, however, requires some modifications to that used for flow profiling. Prior to any tracer ejection for flow profiling, a check should be made for loss behind pipe from the topmost perforations. This is done in the following way. First, a base gamma ray log is run at 200 API units per inch recording sensitivity. At this time the well is pristine relative to tracer contamination; consequently, the base log should show small excursions that correlate to the normal gamma log, sands should be recognizable from shales.

After the base log is completed, a normal shot of tracer is ejected within 20 feet above the top perforation. The slug is not intentionally mixed by tool movement so as to minimize dispersion upward. Successive logging runs are then made, at the same sensitivity as the base run, to tell if the slug, after reaching the perforations, splits with a portion returning upward behind pipe. This is all done, of course, with the well on normal injection. At the recommended recording sensitivity, the intensity will "peg" as the tool goes through the slug while it is still in the wellbore. Also, that tracer "plastered" against the casing wall at the point of ejection will be in evidence on many of the subsequent drags. Any significant amount of tracer that moves upward behind pipe will be recognizable easily from a comparison of any subsequent drag to the base survey.

The above procedure is illustrated for the injection well whose temperature surveys appeared on Figure 33 on page 45. As explained at that point, the well was new and was logged for the purpose of control on normal lithology signatures. The temperature logs showed the injection confined to the top half of the injection interval. This is now corroborated with the tracer tool. Frame A on Figure 54 repeats the completion and logging details given previously on Figure 33. The gamma ray log on this frame is an open-hole log recorded at a sensitivity of 48 API units per inch or 12 API units per chart division. Frame B of Figure 54 shows the base gamma log at 240 API units/inch that was run just prior to tracer ejection. Not only is the completed interval lithology evident on this log, but the zone of concern at depth 2 is also evident as well. This logging was conducted downward because part of the record is in the tubing set just above depth 2.

Frame C on Figure 54 shows the first two drags made after a normal shot was ejected 5 meters above the perforations. The ejection depth, 1,347 meters, is marked by an arrow. On each drag, the base log is reproduced as the solid curve whereas the current survey appears as a shaded area between curves. Above the slug, the two curves are indistinguishable as they should be. In the one minute of elapsed time represented by the two surveys, the slug has not been pumped down to the perforations.

It has, however, reached its deepest injection depth on the final five drags appearing on frame D of Figure 54. Still there is no distinction above the ejection depth between the base log and the current drag, the dotted curve. All that is shown over the 17-minute interval is that the slug is pumped away into the top half of the perforated section. This is exactly what the temperature log, Figure 33, revealed! Figure 54 illustrates a well run confinement test as far as the perforated interval is concerned.

In an older well, one would next run a "packer leak check" by ejecting a slug of tracer immediately below the end of tubing and repeating the same type of logging sequence. This procedure is illustrated in a subsequent example.

Once the leak check surveys are completed, the recording sensitivity can be reduced and any desired profile in surveys conducted. At the reduced sensitivity, any minor behind-pipe contamination is of no importance.

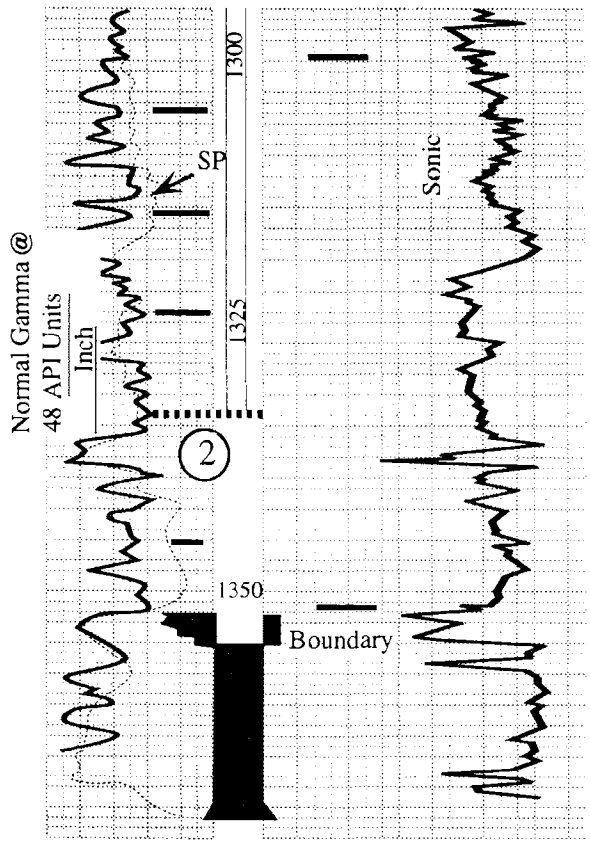

A) Completion details with gamma @ 48 API units/inch

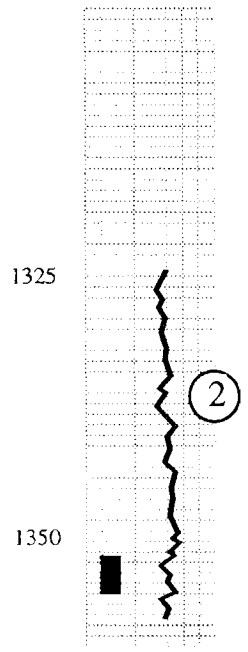

B) Base gamma @ 240 API/inch prior to ejection of tracer

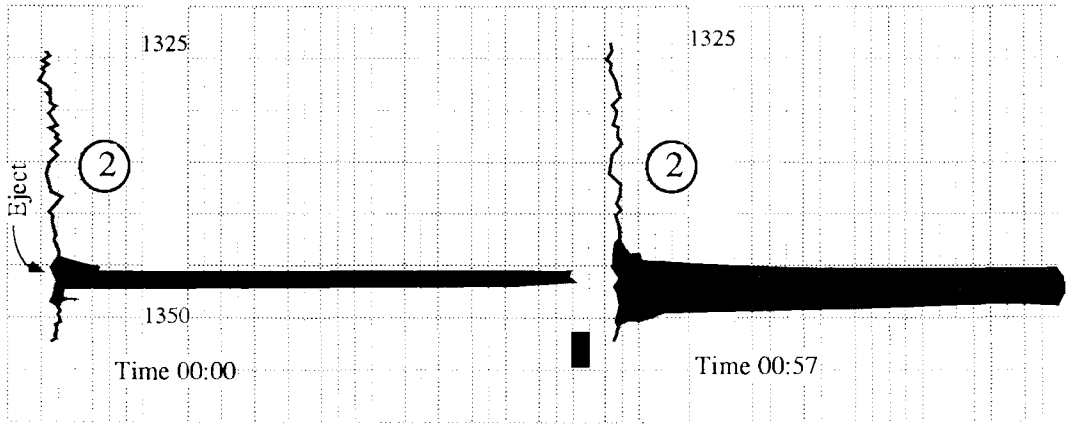

C) First two drags after shot ejection at depth of 1347 meters without mixing. Time in min:secs

Figure 54. Tracer slug tracking surveys for behind-pipe loss to zones above perforations; rate = 70 BPD.

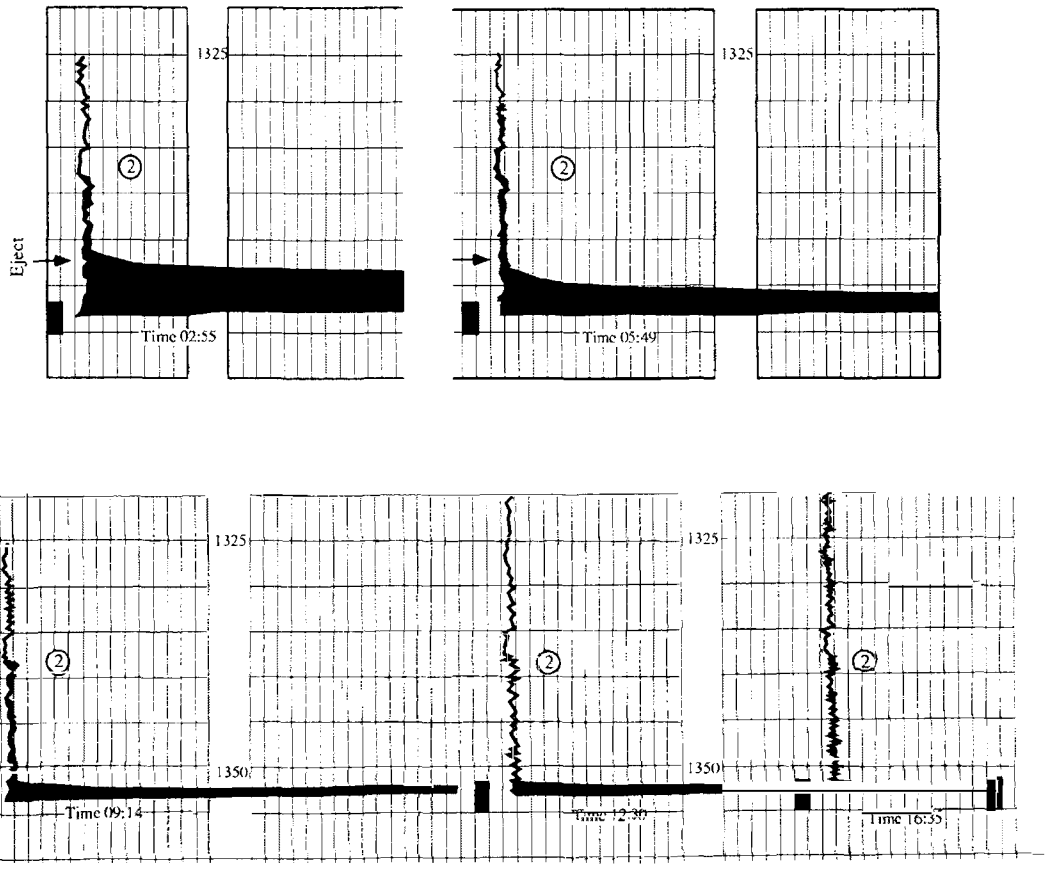

(D) Final Five Drags Through Slug After Ejection at 1347 Meters

Figure 54 (cont). Tracer slug tracking surveys for behind-pipe loss to zones above perforations; rate = 70 BPD.

After the tracer work is completed, it is a good idea to rerun the gamma ray log at normal sensitivity as a quality control check on instrumentation. The unused tracer is also dumped to prevent bringing it back to the surface. Often the two operations are combined into one final leak test. This was done in the present example. After the gamma log was rerun at 48 API units/ inch, the contents of the tracer tool was dumped by one long shot at 1,347 meters, injection was continued for an additional 10 minutes, the well was then shut-in and gamma ray log run once more. The resulting logs appear on Figure 55 where the solid curve, labeled base, is the gamma log run prior to the tracer dump and the dotted curve, labeled background, is the final gamma log run after the dump. The two logs fail to track over about four meters at depth 1 on the figure with the "prior" log being more active at this depth. The obvious question, of course, is whether this is the result of tracer put behind pipe during the confinement test but not picked up at the lower recording sensitivity. In this example, the dump test proves that this is not what happened. Equally often, however, the tracer will be dumped in the bottom of the well to decay naturally. This would leave the task of explaining why the log labeled "base" on Figure 55 is more active at depth 1 than is the original open hole log on frame A of Figure 54. Regardless of the reason for its occurrence, the anomaly that is at depth 1 on the logs of Figure 55 can be placed in perspective relative to the recommended procedure on Figure 54. Below the tubing on Figure

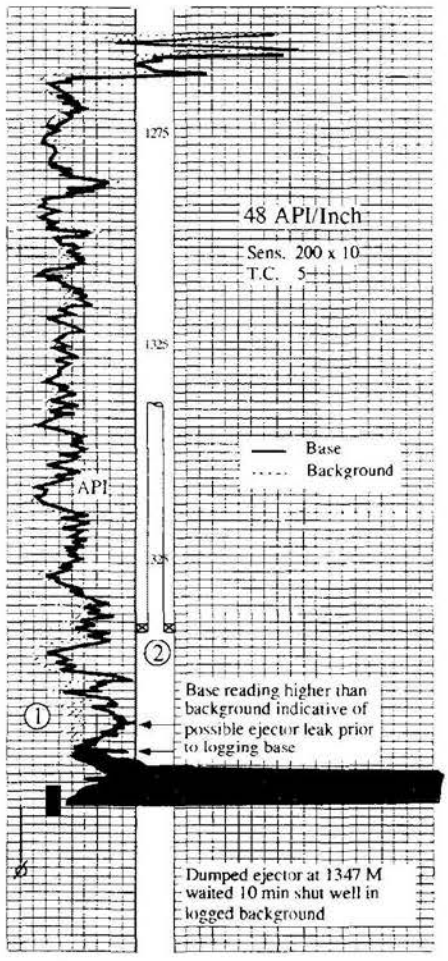

Figure 55. Surveys before (base) and after tracer dump followed by ten minutes of injection at 70 BPD.

55, the dotted trace is displaced about one chart division to the left side of the solid trace. This separation increases to about two chart divisions over the 5-meter interval at depth 1. The discrepancy is, therefore, one chart division over a 5-meter interval. Relative to the sensitivity used for the two drags on frame C of Figure 54, the discrepancy is 1 x 48/240 = 0.2 chart divisions over a 5-meter interval. This area can be compared to the "area" for the drag in frame C at 00:57 seconds as the slug appears to have been mixed to some degree at this time. The "width" of this peak is about the same 5 meters of that of the anomaly. Yet, the "pegged" amplitude alone is 28 chart divisions; consequently, the true amplitude would exceed this value by at least one-half again. The reference area would then have an amplitude of some 50 or so chart divisions. The discrepancy could thus represent a flow of at most 70 BPD x (0.2/50) = 0.3 BPD or 1/2 CC per second! Even if real, such a leak could not be squeezed with any degree of success. The 0.2 chart divisions is about the width of the line on the base log of frame B on Figure 54. The five drags on frame D, Figure 54, show numerous locations where the dotted-line survey departs from the base log by this amount due to normal statistical variation alone. The point to be made is that the sensitivity employed for normal gamma ray logs is too high for general use in confinement tests. Anything that can be dealt with will already be apparent at the sensitivity displayed on Figure 54.

This fact is illustrated by the next example. The temperature surveys on Figure 20 (page 27) revealed a loss to a zone immediately above a disposal zone that could result from either a casing leak or behind-pipe flow. The tracer survey considered next shows that the problem is the result of a leak behind casing. That this is the case is already apparent on the flow-profiling drags appearing on Figure 56. Contrary to the recommended procedure, the flow profiling was done before any channel checks or packer checks. This is an acceptable way of doing the surveys provided one can allow about one-half hour of injection between the profiling surveys and the leak check shots. The drags on Figure 56 show that most injection is leaving the wellbore over the bottom half of the perforations which is what the injecting temperature survey on Figure 20, also revealed. However, drag 4 further reveals that some tracer has split off and moved back uphole behind pipe to permeability in sand C immediately above the injection zone. This fact is even more evident on drag 5 of Figure 56. The two drags together show two permeability spikes marked by arrows on Figure 56.

Whenever a tracer material leaves the wellbore and enters pore space, some tagged material is absorbed on the rock surface and is thus held at this location for a time that depends on the strength of absorption. For the anionic iodine, I-, this absorption is a weak process.

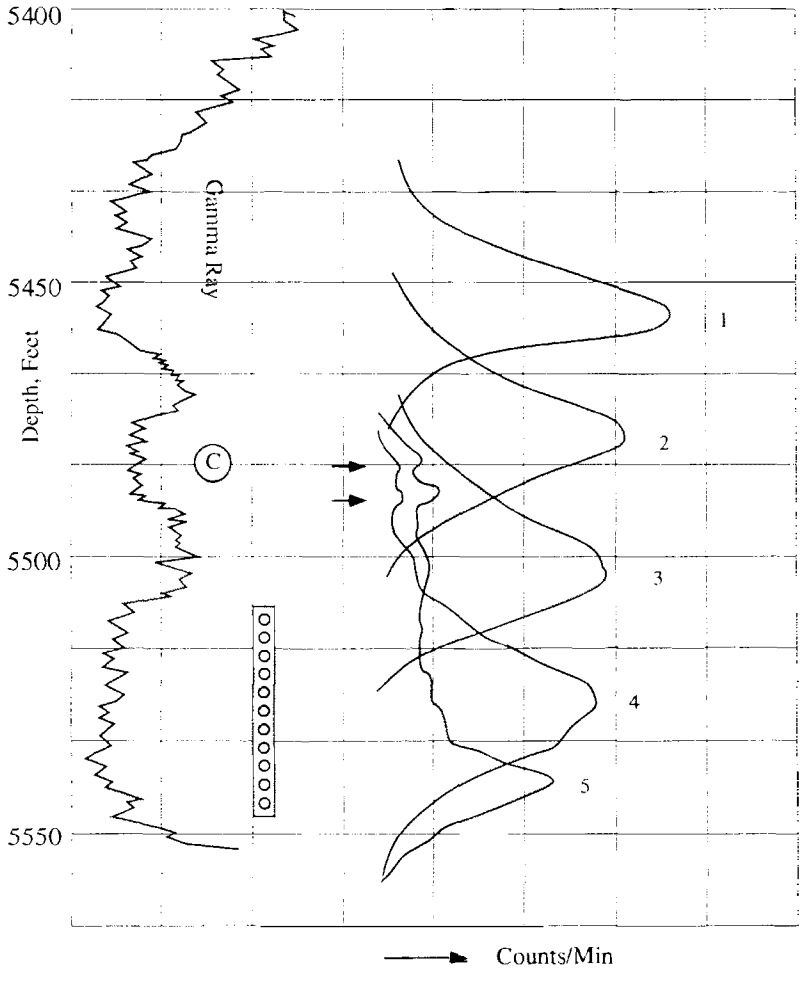

Figure 56. Five flow-profiling drags in a well on injection at a nominal 500 BPD.

Consequently, continued injection washes the surface clean and displaces the tracer into the formation. By contrast, tagged metal ions, cations, lock to the rock so tightly that they are still evident on the injection points even after a week of continuous injection.

It is the creation of the injection spikes that enables the slug tracking procedure to distinguish behind-pipe flow of tracer to porosity from spread to tracer due to vertical permeability around the well. In the latter case, tracer is already in the formation so that no discreet "exit" spikes develop on the drags. Instead, the tracer just seems to drift away from the slug like the edge of a bank of fog. An example of this behavior will be given subsequently.

In the example at hand, injection was continued for one hour after the drag survey of Figure 56 was completed before a "channel check" or confinement survey was initiated. After this time, with the well still on injection, a base log was run at 200 API units/inch with the result shown by the leftmost trace on Figure 57. At this sensitivity, the sand at C is free of tracer pollution. Consequently, a normal shot was ejected at a specified depth of 5,515 feet at the top of the perforated interval although subsequent drags showed that the material actually ejected at a depth closer to 5,520 feet. Five of the nine drags through the slug are depicted on Figure 57. The first survey through the slug, labeled 0:00, was actually made somewhat over a minute after ejection. By this time the slug has mixed and traveled nearly to the bottom of the perforations. By the time of the drag labeled 1:17, some of the tracer has split off and gone upward behind pipe and into the first of the two permeability exits already observed on Figure 56. The drags on the bottom row of Figure 57 exhibit both the permeability spikes. In fact, by 10:08 (minutes:seconds) most of the tracer had been displaced into the formations at both the perforated interval and at zone C. There remains on the record three "permeability" spikes in the bottom half of the completed zone, a residual at the depth of ejection and two "permeability" spikes in zone C.

The massive tracer dump test was not run because the behind-pipe flow appeared on all the tracer surveys. A closure gamma ray was not run for the same reasons.

The drags of Figure 57 exhibit the true signature of tracer flow behind pipe. The only feature missing is a drag before the tracer reaches exit porosity. If, on the drag of 1:17 at the right top of the figure, the permeability spike at sand C is leveled to the height behind it, then the picture is that of a slug not yet at an exit depth. The slug front is sharply defined with tracer simply stretched out behind this front. This behavior contrasts with the hypothetical figures typically presented in discussions on tracer logging. These show tracer slugs moving behind pipe with the same bell-shaped signatures as those on Figure 56 for the slug moving inside the casing. The area open to flow behind pipe is so constricted and tortuous that the bell shape is not preserved. Only in relatively large, uniform annular areas does this type of signature appear.

Because the permeability "spikes' are a significant feature, the reader is asked to go back to the tracked slug survey that started the tracer discussion, Figure 35, and examine the last drag, K, in the sequence. The four spikes at 9,605, 9,601, 9,598, and 9,590 feet are all "permeability spikes." The development of these spikes is evident on the surveys H, I, and J. These features also serve as quality control checks on procedure.

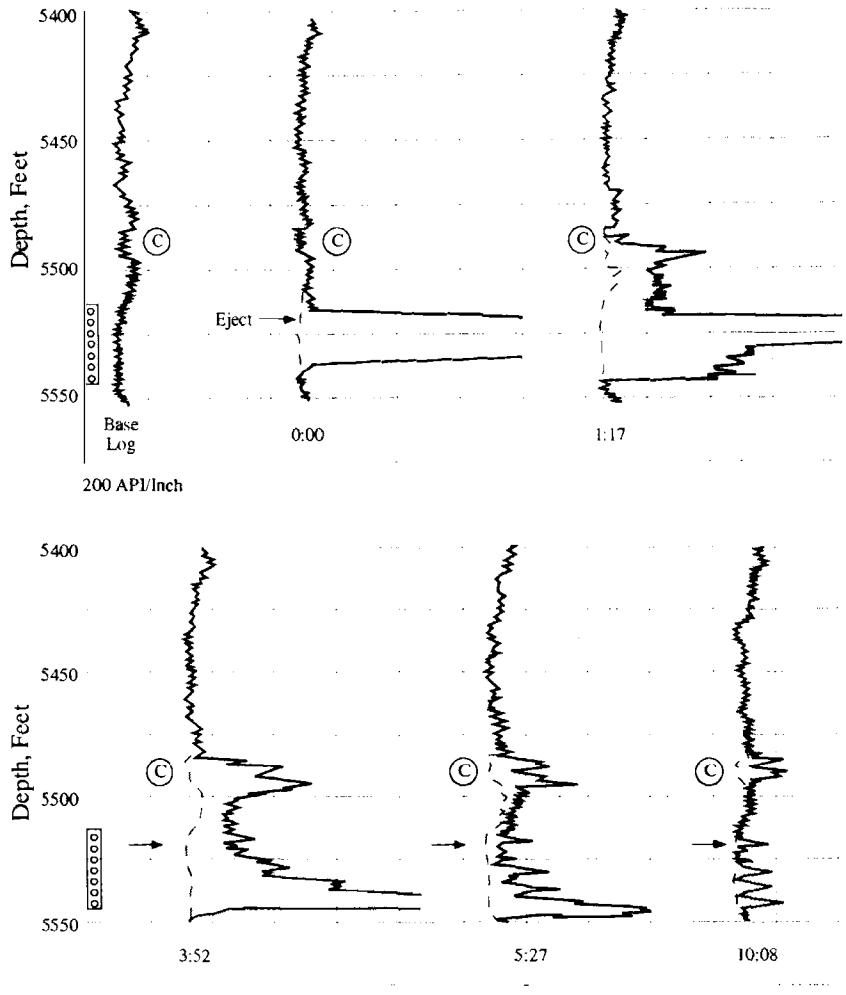

Figure 57. Behind-pipe flow detection by slug tracking in well in injection at a nominal 500 BPD.

The slug tracking method is also the preferred way to check for leaks past the packer and into the tubing-casing annulus. For this purpose, a normal slug is ejected in the tubing above its end and successive drags at a sensitivity of 200 API units per inch run to track the slug's progression. The logging is done downward so as to successfully navigate the end of tubing. An example of this type of survey is on Figure 58. The left-most trace is a gamma-ray log, labeled "correlation gamma-ray," run at 80 API units/inch because of the "hot spot" at depth 1 on the figure. This region of high intensity results from a cobalt-60 tagged cement slug behind pipe at this depth. The base gamma ray log, labeled as such, was run before any tracer ejection at 400 API units/ inch. This is not sufficient sensitivity to show any of the lithology character evident on the correlation gamma, but was again a compromise to avoid domination by the tagged cement. With the injection rate steady at 720 BPD a normal shot of tracer was ejected in the tubing at depth 2, 4,250 feet, a location 28 feet above the end of tubing. Seven consecutive surveys were then run from 4,200 feet to total depth. The times listed below each drag are the times that the logging started at 4,200 feet. The first survey, run #1, was started at 3:30 pm very quickly after the slug was ejected. Full stream velocity in the tubing is 129 ft/min; in the casing 22 ft/min; and

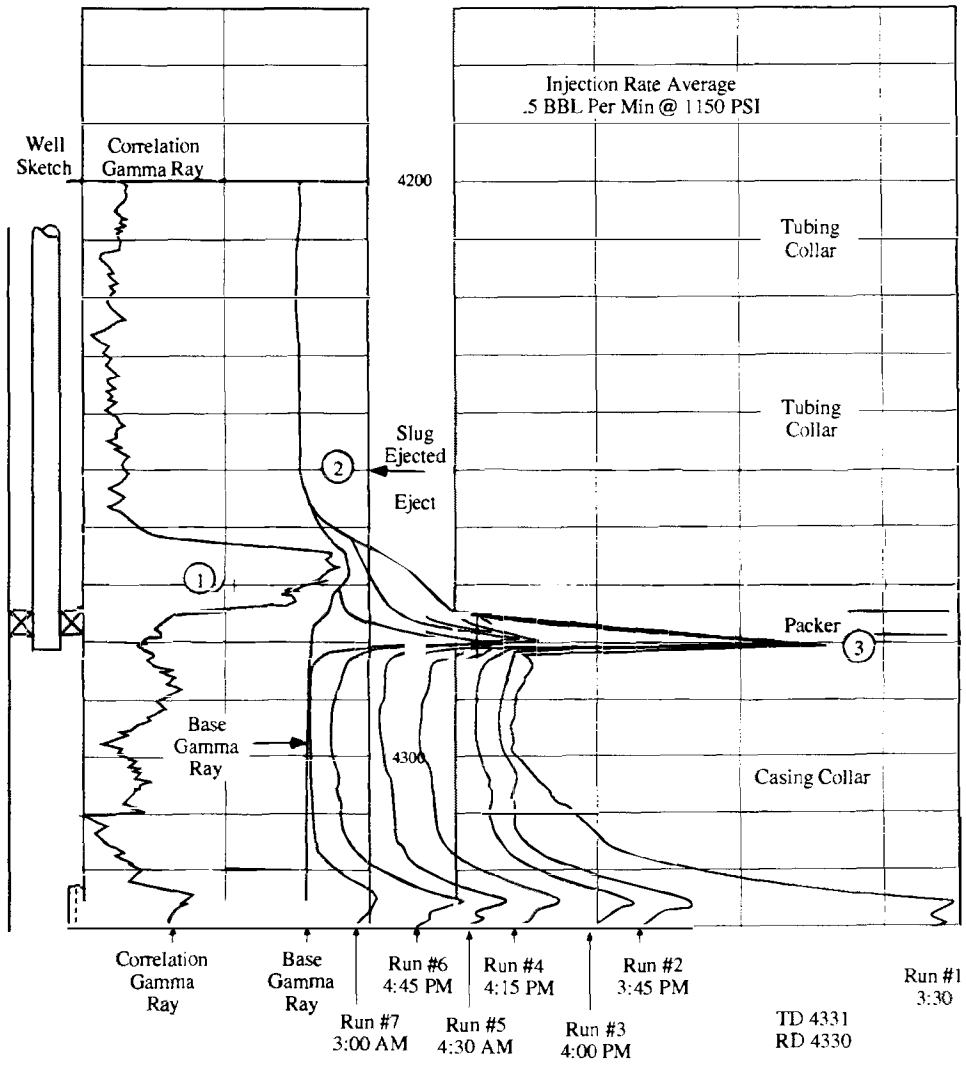

Figure 58. Packer leak check by the slug tracking method in well on injection at 720 BPD.

in the annulus 28 ft/min. In the 3+ minutes required to log from 4,200 feet to 4,330 feet at 40 ft/min, the main part of the slug has reached the perforated interval at 4,321-4,330 feet and two permeability spikes are developing. Two things should be noted about drag #1. First, the activity due to tagged cement adds to the tracer activity thereby distorting the shape of the intensity curve across region 1. In fact, without the prior gamma logs, run #1 alone would suggest flow up the backside of the tubing to about 4,260 feet, a depth nearly eighteen feet above the packer! The second feature to note on run #1 is the large slug of tracer at depth 3, a location immediately below the collar signature of the end of tubing. Subsequent drags, on fifteen minute intervals, show that the slug is stationary at this location. Furthermore, the concentration of tracer at depth 3 remains nearly unchanged through run #4, a drag started 45 minutes after ejection.

Actually, there is a third feature to drag or run #1 that is easily overlooked. The intensity below the slug at depth 3 decreases to a value much larger than the background level on the base log.

In fact, run #6, one hour and 15 minutes later, is still above base line activity from depth 3 all the way to the perforations, where injection spikes persist at high levels.

Here is what has happened. As the tracer slug exited the end of the tubing, a large portion was trapped in a turbulent eddy circulating under the packer. This material was then slowly, but continuously, washed out of the eddy and carried down to the perforations by the continued injection.

The skeptical reader can accept the above argument and still ask how one can be confident that the eddy did not also slowly drain upward into region 1 as well. The additive nature of gamma emissions from independent sources allows us to correct the drags after ejection for the distortion from the cement emissions. The increased activity due to cement that is evident on the base log is subtracted from the activity recorded for the drag under correction. The result of this correction to run #1 is given on Figure 59. Here, the peak asymmetry is clearly downward, not upward.

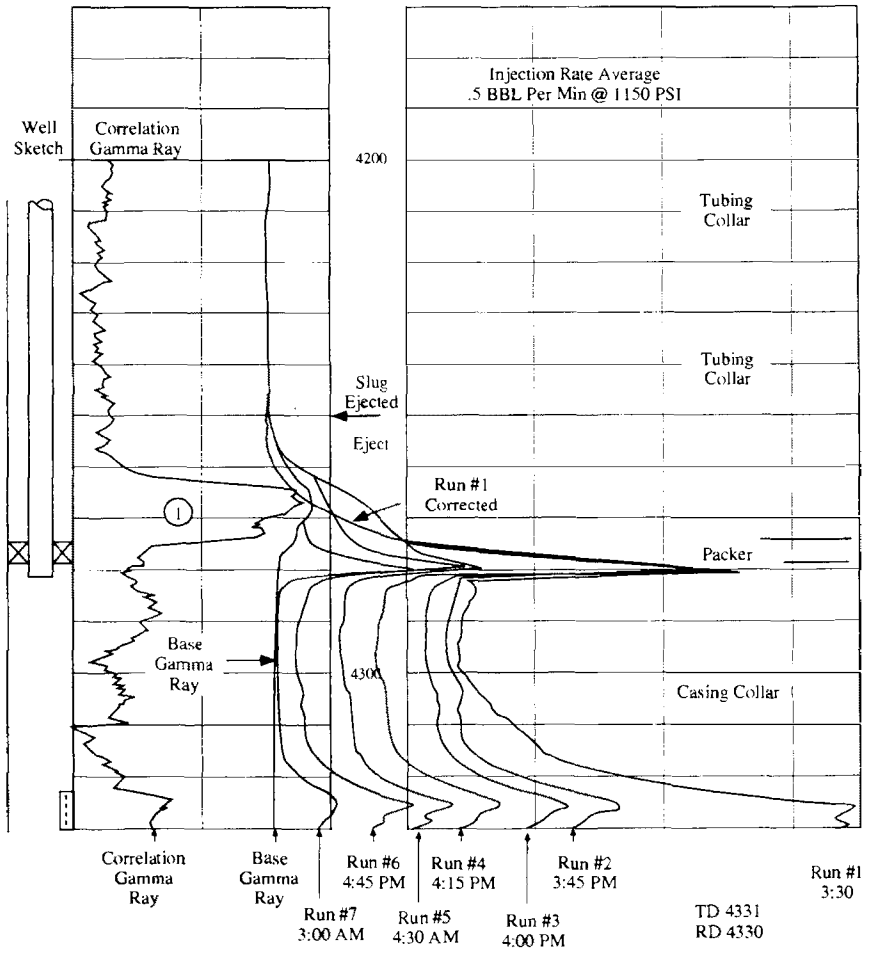

Figure 59. Corrected run #1 with spurious base activity subtracted.

Figure 58 thus demonstrates a case of a perfectly valid verification of packer integrity by a test that, thanks to the quirks of completion and flow pattern, is easily misconstrued. In fact, the figure is a testimonial to the ability of the slug tracking method to reveal the "big picture." Had only a stationary, velocity shot packer check been made, the eddy would have been incorrectly identified as a "slow " packer leak.

A shut-in crossflow check that reveals movement past the end of a tubing string is given on Figure 60, where three drags run on 15 minute intervals are depicted. Four slugs of tracer were injected, the first slug being placed immediately under the packer and the remaining three spotted over the interval of open perforations. Slug 1 was intended to be a control shot; however, its behavior was interpreted as evidence of a leak past the tubing packer at 4,347 feet into the squeezed perforations in the casing above the packer. There is, certainly, movement inside the casing. During the 30 minute period slug #2 moves upward 27 feet with an irregular velocity averaging 0.9 ft/min. For a casing capacity C = 0.0232 bbls/ft, the corresponding volumetric rate is q = 1440 x 0.0232 x 0.9 = 30 BPD. The three surveys through slug #1 show two things:

1) The slug is in a stagnant location because its peak is stationary, but tracer material is being washed out of the slug because its peak is rapidly dropping in intensity.

2) The presence of slugs 1' and 1" show that this washed material is carried upward; presumably, by the flow from the perforations that moves slugs 2 and 3.

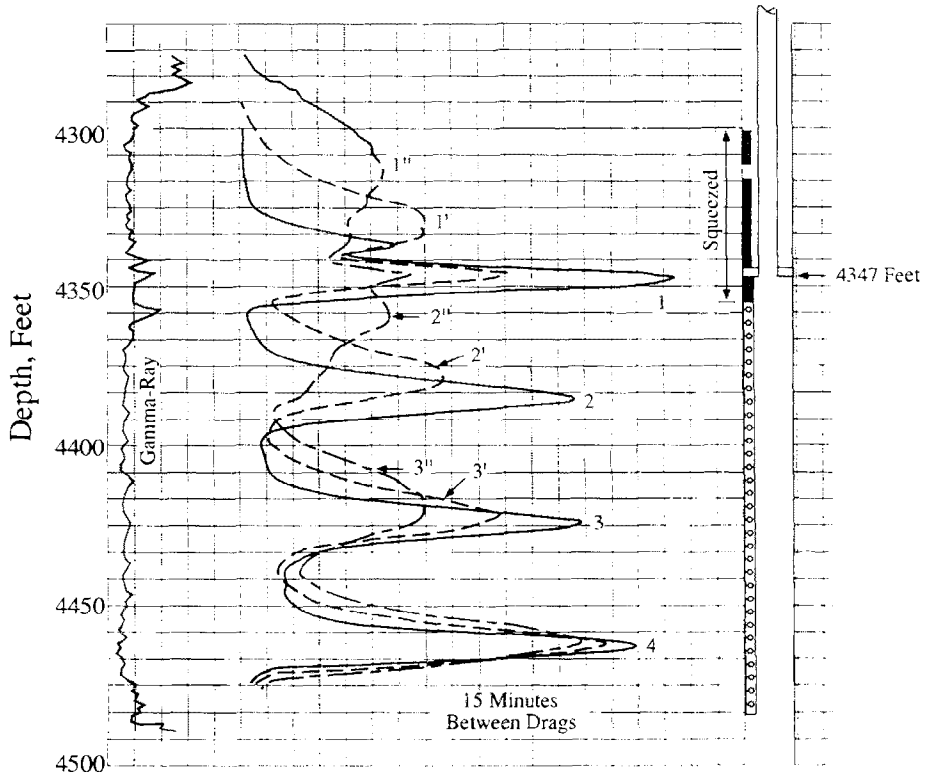

Figure 60. Crossflow check after one hour shut-in period on 900 BPD injection well.

The shape of drags 1' and 1" has the same bell-type signature as the ejected slug; consequently, the flow is inside pipe somewhere, the question is where! The location that would immediately come to mind is the annular space between the tubing and casing with flow into the squeezed intervals shown on Figure 60. There are, however, three features to the surveys that rule out this type of crossflow:

- First, drags 1' and 1" show no injection spikes even though tracer covers the entire squeezed interval;
- Second, the tracer drag 1" shows no slowing down that is necessary for it to accommodate the lithology on the gamma-ray log that shows a porosity limit at 4288 feet;
- Third, and most important, a flow past the packer would not leave the stagnant pocket of tracer at location 1.

The flow depicted is therefore into the tubing string and upward, not behind tubing. The well does have positive pressure. Hence, the behavior could signify a tubing-to-casing-to-environment leak at shallower depths.

Figure 60 illustrates one of the problems most common to unsupervised tracer surveying; namely, the failure to carry through on an observed situation to the point that one knows what one is seeing. The behavior may be the result of nothing more than failure to seal around the logging cable at the surface or failure of the wing valve to completely shut-off backflow from the well. Lack of annular pressure when the well is on pump certainly suggests this is the case. Furthermore, had the logging operator run two more drags, he would have established that slug 1 did not stop at the top of the unit containing the squeezed perforations. A "procedure" called for three drags, and three drags were run, no more nor less!

The point of Figure 60 is that tracer transport that does not require the flow to squeeze past or around obstacles maintains a simple slug shape as a characteristic signature. This shape is not maintained, for example, on Figure 57, once the tracer starts to move behind pipe.

In combination, Figures 59 and 60 illustrate another point. One often hears or reads statements to the effect that tracer surveys, either radioactive or activation type, give results that "are easy to interpret." The correct statement should be worded differently: The surveys give the most graphic and most easily comprehended picture available. The reasons for what is seen on the survey, however, can be just as obscure as on any other logging procedure. This point is generally not emphasized sufficiently in most discussions on production logging.

For the above reasons, the next method of leak check, the stationary velocity shot procedure, is the least preferred way of confinement demonstration.

Velocity Shot Procedure for Behind-Pipe Flow: The stationary or velocity shot method of leak checks is by far the more popular technique among logging engineers simply because it is easier to perform than is the slug tracking technique. One stops the tool, say, just above the top

perforation, and, with the well on injection, ejects a slug of tracer into the moving stream. With the recorder on time drive, the operator can observe the slug go past the two stationary detectors on its way to the perforations. This far, we have a standard velocity shot. However, for the leak check, the recording is continued sufficiently long to insure that no tracer doubles back behind pipe and, again, passes the detectors on its way up. With one detector close to the perforation, the record length can be held to a minute or so duration without fear of failure to detect leaks.

A sensitivity of 200 API units/inch is again recommended for the stationary record. Because two detectors are available, common practice uses the higher sensitivity on only one detector record. This allows the other one to record the slug shape inside the casing without pegging.

A similar procedure is employed to check packer integrity while the well is on injection. This technique is illustrated on Figure 61 for the same well that appeared on the shut-in test of Figure 60. The tool is stopped with the ejector port located at 4,238 feet as shown on frame A of Figure 61. The top detector was located four feet deeper at 4,342 feet whereas the bottom detector was at 4,347 feet at the end of the tubing string. The top detector output was recorded on an insensitive scale on the right-hand side of frame B, that provides very little information other than the fact that the slug passed the detector within 1 chart division, or 1.18 seconds, after

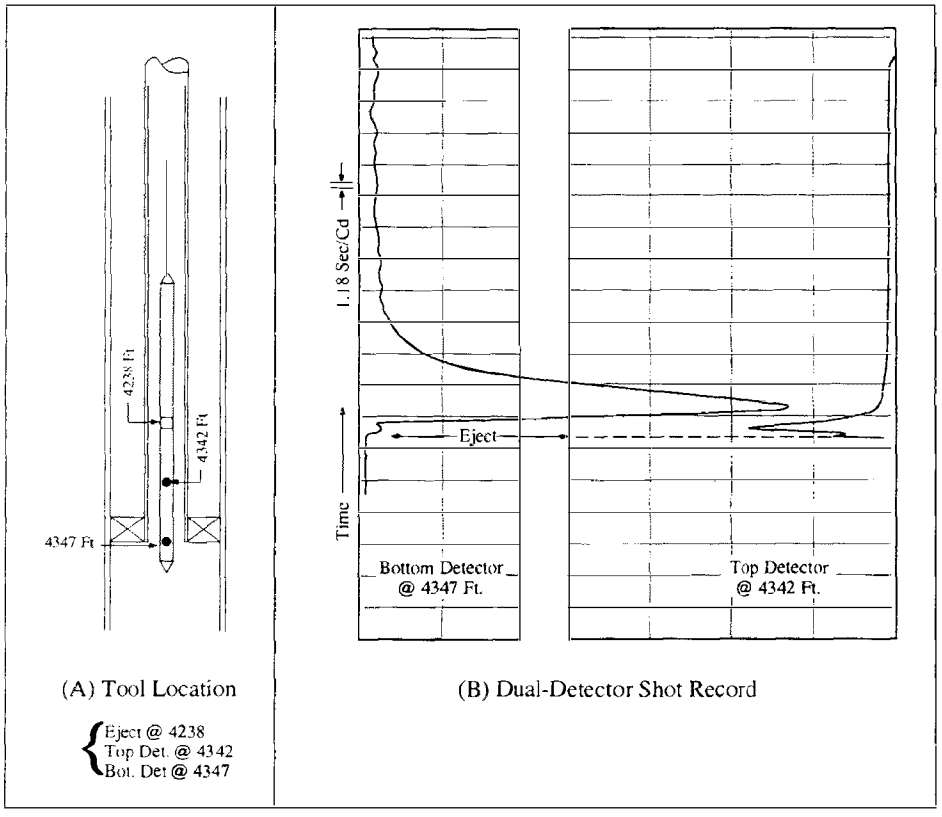

Figure 61. Stationary velocity-shot check for packer leak for well of Figure 60 while on injection at a nominal rate of 900 BPD.

ejection. The record from the bottom trace is at higher sensitivity although still not at the 200 API units/inch appropriate to behind-pipe logging. With the bottom detector at the end of the tubing, any doubling back at the packer would have added to and distorted the primary record from the passing slug. As no such distortion is in evidence, we must conclude that the packer is sealing. The record was continued for 57 chart divisions, or 68 seconds, after the slug passed the bottom detector. Had this detector been located, say, five feet above the end of tubing, then the record length would have been too short. The packer check alone does not eliminate the possibility of leaks higher in the tubing. Consequently, it is puzzling that the logging operator did not pursue the shut-in flow detected on Figure 60 for this well. All that the results of the packer check proves is that a leaking packer is not responsible for this flow.

A somewhat better technique of stationary packer check is illustrated on Figure 62 for the same well that was the subject of the behind-pipe tests of Figures 56 and 57. The end of tubing in this well is located at a collar log depth of 4,341 feet. For a quick packer test, the operator stopped the tracer tool with the bottom detector at 4,340 feet, a location 1 foot above the end of tubing. The output of this one detector was then recorded at a sensitivity of 200 API units/inch for some

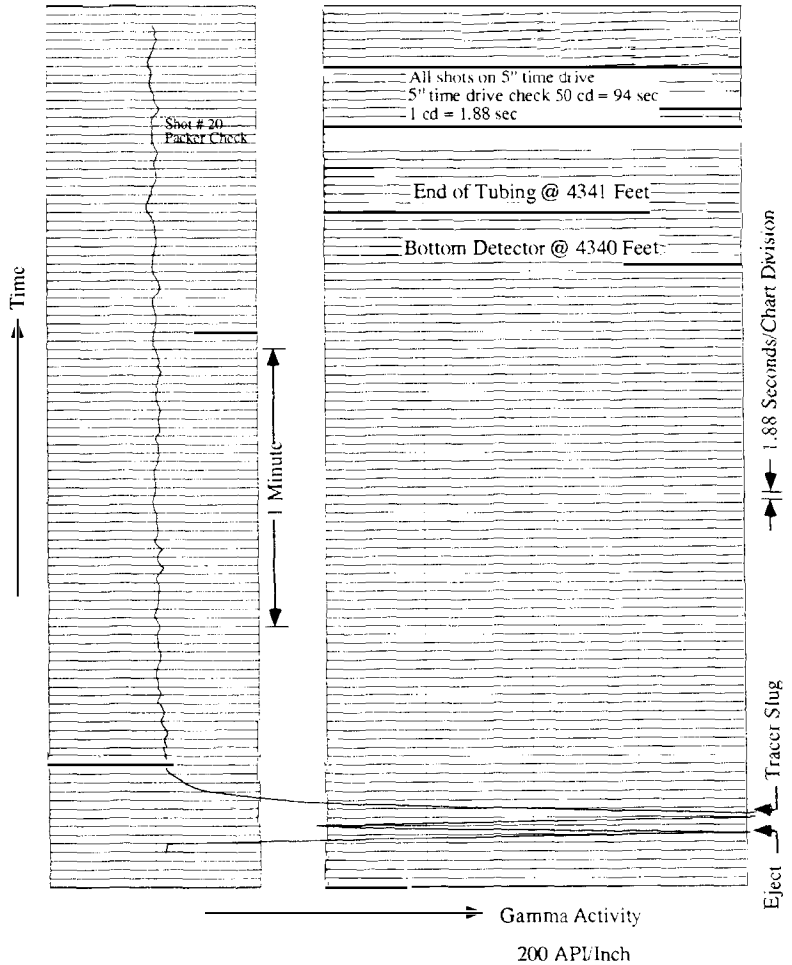

Figure 62. **A properly scaled, stationary v 'ocity shot test for packer integrity with an annular velocity resolution of 0.35 ft/min leak rate.**

three minutes after a shot ejection in the tubing above the detector. During this procedure, the well remained on injection at 500 BPD nominally. The record shows no return past the detector for the 92 chart divisions or 2.88 minutes after-shot duration. Any packer leak is then at a velocity of less than 1/2.88 = 0.35 ft/min. For an annular capacity of C = 0.0178 bbls/ft, any leak rate is therefore less than 9 BPD. This resolution is typical for operators who are not given specific directions on how long to record on a stationary leak check test.

As long as the stationary packer checks are benign, they are a fast, simple way of surveying. If "leaks" are indicated, however, one is wise to switch over to the tracked slug procedure to chase down the reason for the behavior. For example, we can draw a hypothetical velocity shot for the packer check that was done on Figure 58, by the slug tracking method. Suppose a single detector tool was positioned with the detector located one-foot above the tubing end and a shot of tracer ejected above the detector. From what is seen on Figure 58, the expected gamma response at the detector would be as shown on Figure 63. The high level of activity caught below the packer in the eddy would give a reading at the detector that would make one suspect a "slow" leak through the packer. At this point one would run drag surveys to establish that the activity originated in the "stagnant" eddy as was done on Figure 58.

Stationary velocity shots are also commonly used as so called "channel checks" for flow behind pipe above and below perforations. The procedure is illustrated on frames B and C of Figure 64.

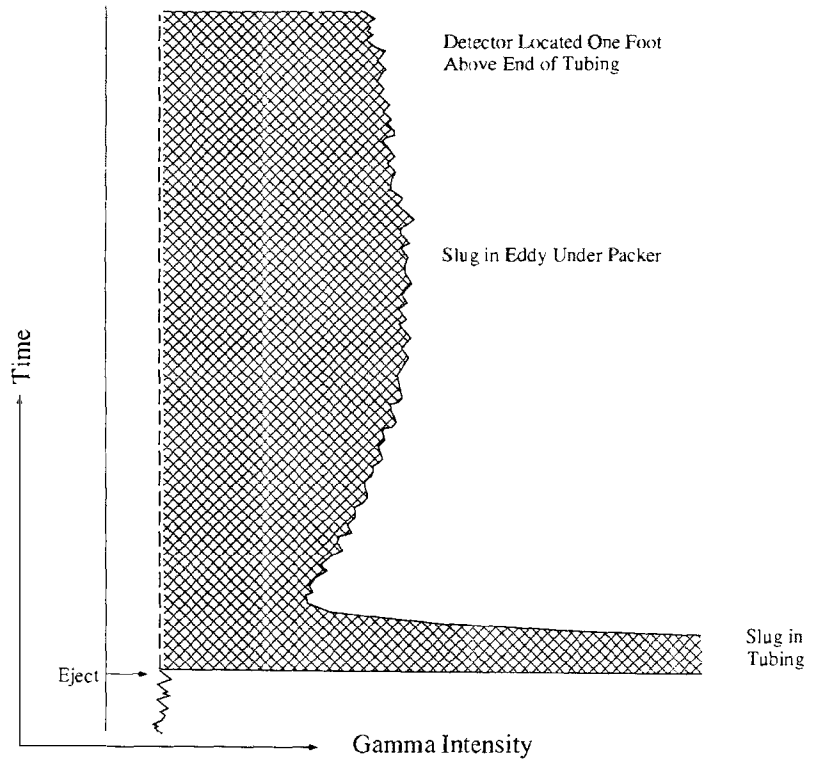

Figure 63. Hypothetical velocity shot response to stagnant slug caught under packer on Figure 58.

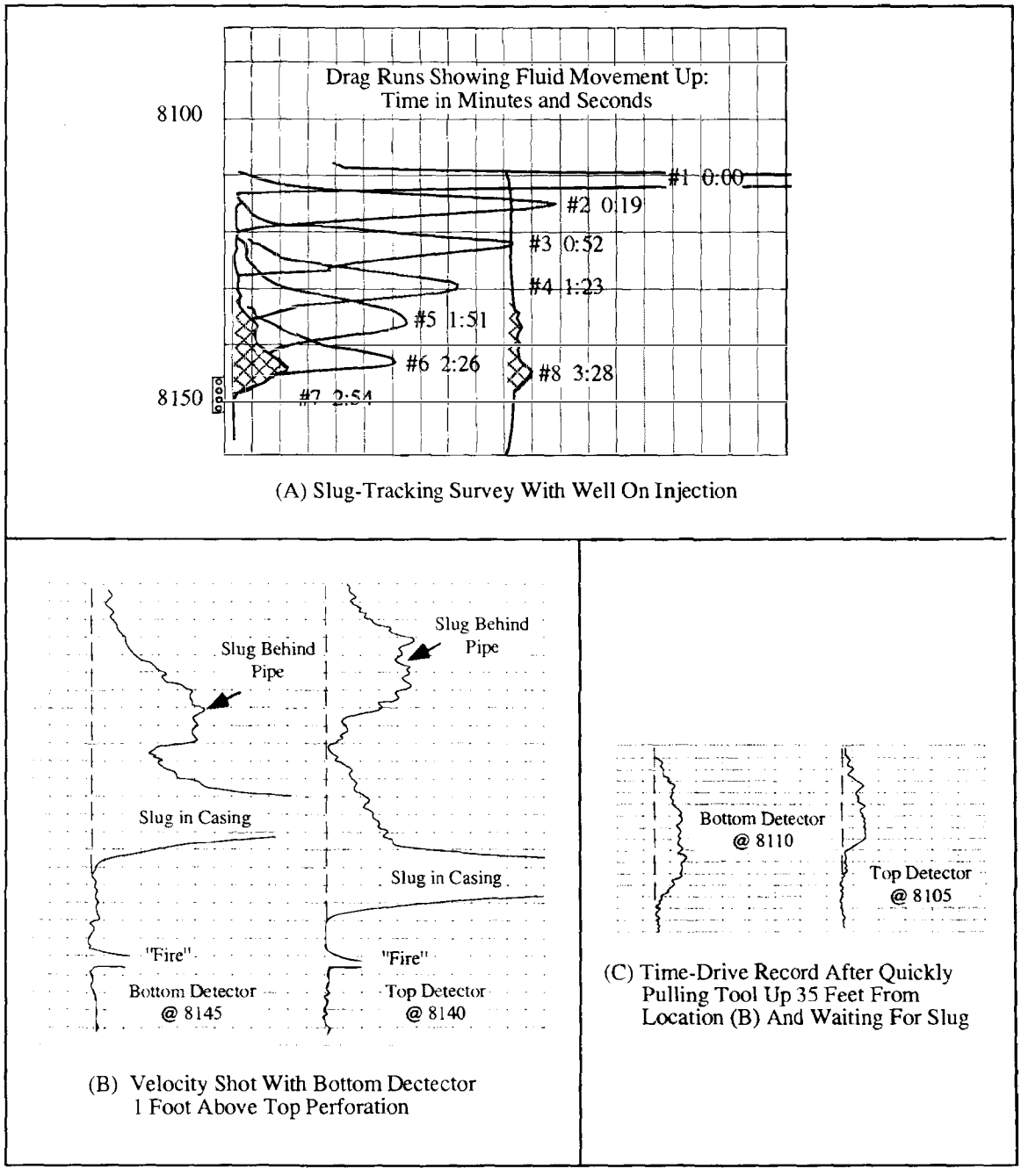

Figure 64. Channel checks on well of Figure 32 with well on brine injection at 400 BPD.

These surveys come from the same well whose temperature surveys, Figure 32 (page 44), showed crossflow behind casing from an oil zone perforated at 8,146-52 feet. The well was killed in preparation for workover and a pump-in tracer test was run to corroborate the temperature surveys. Frame A on Figure 64 shows a slug-tracking survey done initially for

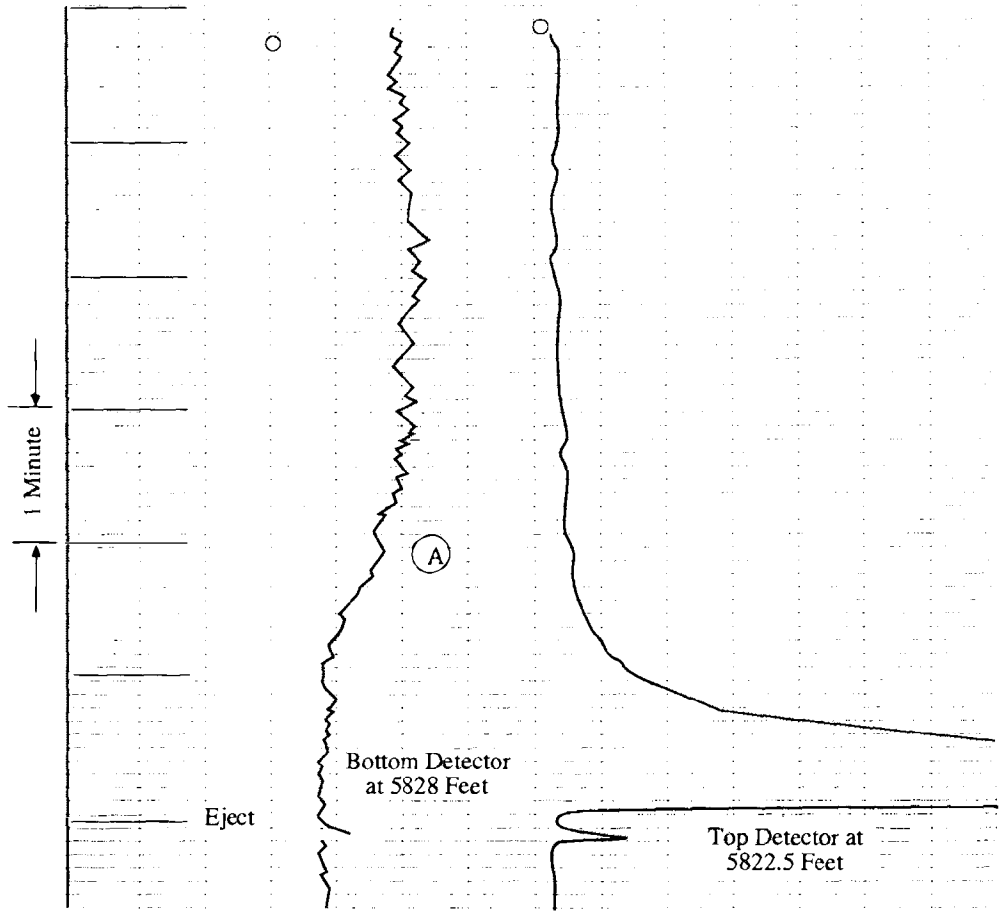

Figure 65. Channel check by velocity shot method below perforations at 5,820 - 25 feet with well on injection at 600 BPD.

injection rate estimation. By the time of drag 6, tracer has reached the perforations. Drags 7 and 8 show this material spreading upward behind pipe. After the drag survey was completed, injection at 400 BPD was continued another half hour to flush the tracer behind pipe. Then, with injection maintained, the tool was positioned with the bottom detector one foot above the top of perforations and the velocity shot of frame B, was carried out. The output of both detectors were recorded at high sensitivity. On the journey downward inside the casing, the ejected slug passes the top detector first. An additional travel time of 18 seconds is required for the tracer slug to pass the bottom detector. Very shortly after passage of this sensor, the tracer doubles back over the 1-foot distance from the top perforation to reappear at the bottom detector. In 13 seconds more the tracer passes the top detector. Once this happened, the logging operator quickly pulled the tool upward stopping with the lower detector at 8,110 feet. With the recorder on time drive, he then waited for the tracer to arrive as shown on frame C.

From the condition of the slugs on frame C, a location 40 feet above the perforations, it is apparent that they cannot be tracked much farther up the wellbore. To do this, the tool contents should be dumped just above the perforations and slug-tracking surveys initiated. In this fashion, a large shot can be followed behind pipe for some 2,000 feet before it is too dispersed for accurate detection.

Frame B also illustrates the fact that, in passing a fixed location, the tracer behind the pipe exhibits the same type of "shape" as that inside pipe. This presentation mode is the source of the misconception, previously mentioned, that this is the "shape" over distance of the tracer distribution behind the casing. Frame A shows, of course, that this is not correct.

The velocity shot channel check, while fast and easy to run, suffers from the same limited "scope of vision" as does the packer check by the same procedure. The velocity shot of Figure 65 was made at the base of perforations in a well on injection at about 600 BPD. The shot serves as a "channel check" at the base of the bottom set of perforations located at 5,820 - 25 feet. The top sensor was positioned at the midpoint of the interval at 5,822.5 feet. This allowed the bottom detector, 5.5 feet deeper, to be positioned at 5,828 feet, three feet below the bottom perforations for a channel check. Accordingly, its output was recorded at a greater sensitivity than was the output from the top detector. The traces show that the leading edge of the tracer arrived at the top detector some 1.5 chart divisions or 1.5 x 6 = 9 seconds after ejection. Likewise, a small concentration of tracer "arrives" at the bottom detector some 15 chart divisions or 90 seconds after ejection, time A. If the differential time of 81 seconds is allocated to the travel over the three foot distance from the bottom perforation to the detector, then the associated velocity is 2.2 ft/min. Consequently, if the tool is dropped another five feet down the hole, the tracer should get to the bottom detector by 2.5 minutes after relocating. Unfortunately, the logging operator was content to say that the signature was due to a small channel and "close shop."

The signature on Figure 65 from the bottom detector has the same slowly dispersing behavior shown of Figure 63 for the tracer ensnared by the eddy current beneath a packer. In fact, the signature is the result of the same type of phenomenon. Figure 66, an 11-drag slug-tracking survey from the same well, helps to understand what is happening. Drags 1 through 5 show that practically all injected water reaches the bottom set of perforations before exiting the wellbore. This rapid change in flow direction over a five-foot long interval sets up turbulence in the form of eddies that can scour the wellbore for a significant distance below the perforations. Drags 7 through 11 show that the slug peak slows down to a stop at the bottom perforations. However, a comparison of the leading edges of these same drags with that for drag 6 reveals that at the same time the slug starts to slow down its leading edge starts to disperse below the base of the perforations. By the time of drag 11, this dispersion has carried tracer some 14 feet below the base. Some of this spread is obviously the result of logging repeatedly through the tracer slug; however, the situation is clearly more severe than that of previous examples, say, for instance, that shown by drag 8 on frame A of Figure 64. After viewing Figure 66, the reader should not be surprised to see the appearance of tracer on Figure 65 at a detector situated only three feet below the base of perforations. This would probably not have happened if a good portion of the injected water exited the wellbore at the top set of perforations. The condition is a result of the particular state of flow in the well.

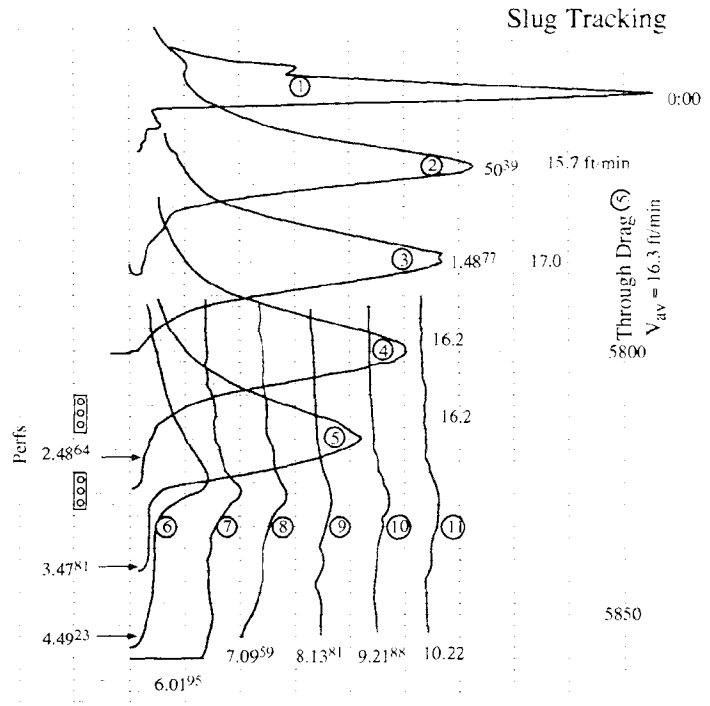

Figure 66. Slug tracking survey from same well as velocity shot of Figure 65 with same injection rate of 600 BPD.

The same slowly dispersive behavior shown on the trace from the bottom detector on Figure 65 is also characteristic of the signature produced by velocity shot "channel checks" in formations with good vertical permeability. If the tracer can spread through porosity either upward or downward from the perforations, then this movement will be detected provided the flow is within about one foot of the wellbore. On a stationary, velocity-shot channel check, this situation is very difficult to distinguish from that due to a small, behind casing leak. Failure by the logging operator to follow such flow has resulted in many unnecessary workover attempts. The "leak" will only extend to the top or bottom of the porous interval if it is the result of vertical permeability. Consequently, one should always provide open-hole or cased-hole lithology logs to the operator if there is the possibility of tracer spread by vertical flow in a formation.

For example, the gamma-ray log on the left-hand side of Figure 67 shows that the top set of perforations are located at the bottom of a lithological unit that extends upward from the shale at 11,611 feet to a second shale "break" at 11,464 feet at the top of the log. Furthermore, this unit is known to have good vertical permeability. The temperature surveys on the right-hand track confirm the presence of vertical permeability. These surveys were run after 536 barrels of water had been injected into a previously static well at about 2 bbl/min rate. An injecting log was not run; however, the shut-in surveys show that some injected water reached the total depth of 11,653 feet. Likewise the surveys show that most of 536 barrels stayed in porosity in the interval identified as BE on the temperature surveys. This interval is seen to be a subunit on the gamma-ray log. The topmost perforations are into the bottom of this subunit. The surveys further show

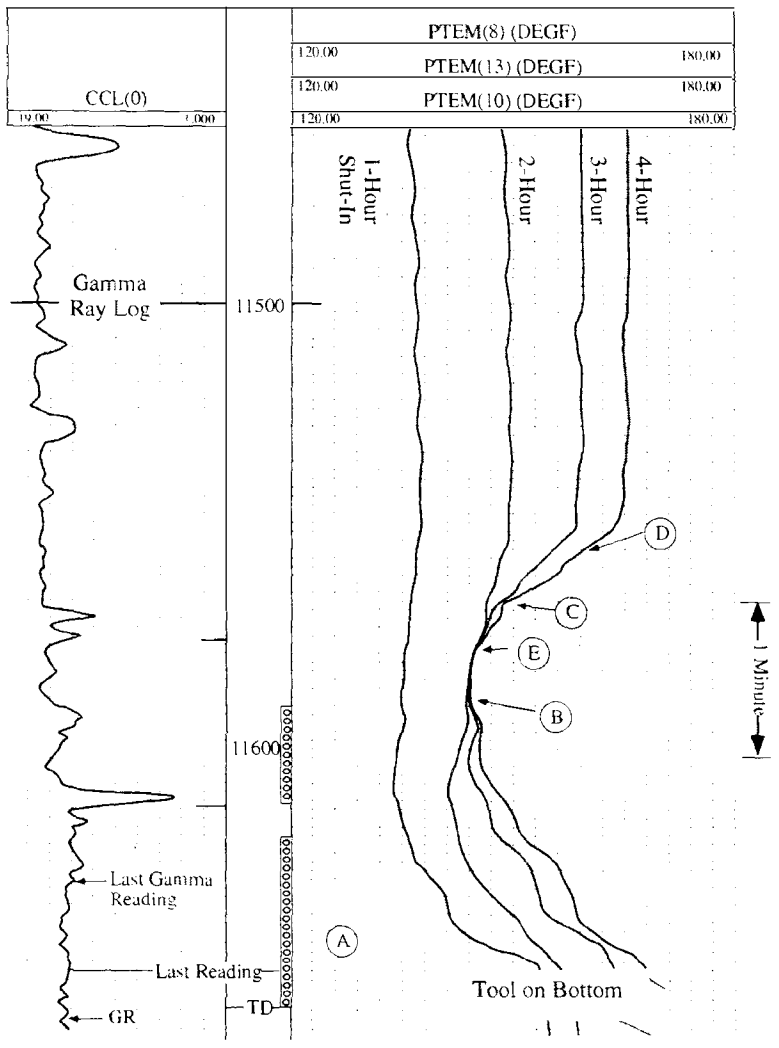

Figure 67. Temperature surveys from a well after 536 barrels of water injected and well shut-in.

some injection up to depth C, 11,566 feet, and the possibility of the injected water reaching as far up as depth D at 11,555 feet. Because the well had been static prior to injection, the relative behavior of the shut-in surveys also reveal that the water reached interval BE by vertical flow through the formation, not by flow directly behind pipe. Had the latter been the case, the injection "cold" would have been in direct contact with the wellbore and would have been in clear evidence on the 1 and 2 hour shut-in surveys. The small amount of storage at the bottom of the top set of perforations does appear on these traces.

The third of three velocity shots made as "channel checks" while injecting into the well is illustrated on Figure 68. The logging tool makeup and its location for this shot is shown on frame A of the figure. Three detectors, one above the ejector and two below, are identified by the numbers 1,2, and 3 on frame A. The output from each of these sensors is labeled correspondingly on frame B. The output for detector 1 is recorded at normal gamma log sensitivity of 40 API units per inch whereas a sensitivity of 100 API units per inch is employed

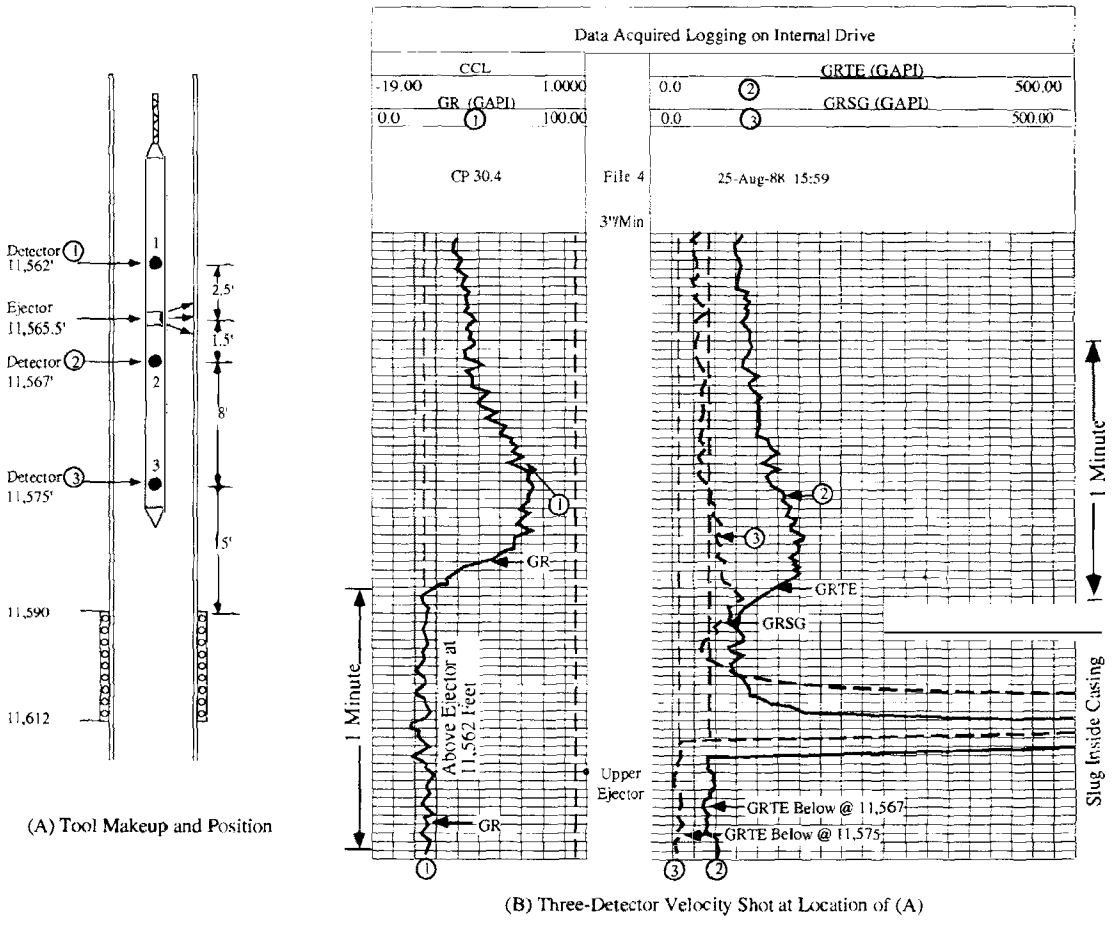

Figure 68. Channel check, velocity-shot survey with well injecting 2 BBL/min.

for the other two detectors. All three record sensitivities therefore exceed the recommended 200 API units per inch and, accordingly, each will respond to quite small tracer concentrations. The ejected tracer slug, of course, "pegs" the output of detectors 2 and 3 as it moves down past these sensors inside the pipe. The leading edge of the slug moves over the eight-foot spacing between the two detectors in about 2 chart divisions or 2 x 2 = 4 seconds of time. The peaks require 3 x 2 = 6 seconds for an apparent velocity of 80 ft/min. The downward traveling slug does not appear on the record from detector 1 because it is ejected below this detector. Tracer, however does double back and reappear on all three records in the order 3-2-1 as an upward-traveling slug. The leading edge arrives back at detector 3 about 12 chart divisions, or 24 seconds, after it passes going down inside the casing. For this slug to reach the perforations while inside casing required 4 sec x (15/8) = 7.5 seconds. The return then used 24 - 7.5 = 16.5 seconds. This corresponds to a frontal velocity of (15/16.5) x 60 = 55 ft/min. Likewise, the 4 foot progression from detector 2 to detector 1 required at most 1.5 chart divisions, or 3 seconds, thus averaging 80 ft/min. The low level of intensity of the return tracer on all detectors means that, for the flow to be directly behind pipe, only a small part of the original slug broke away to move upward. At the frontal velocities estimated above, we would anticipate that the tracer would simply move on past as it did on frames B and C of Figure 64, with a frontal velocity of only 20-30 ft/min. Instead, the tracer "tails" out more like the behavior of the captive slug on Figure 65.

Two additional velocity shots at locations below that on frame B of Figure 68 showed the same type of behavior; namely, return slugs of low amplitude, high frontal velocity, and slowly dispersed trailing edges. Of these three characteristics, the "strung-out" trailing edge would, therefore, seem to also be the velocity-shot signature of tracer spread by virtue of vertical permeability around the wellbore.

With only the results of frame B, Figure 68 known, an analyst could not tell what the "picture" meant for sure. Poor completion integrity would certainly be a possibility. Of course, what the logging operator should have done was dump the remaining tracer just above the top set of perforations and then track the slug going upward to see if it stopped at the unit top, i.e., at about 11,470 feet on the gamma-ray log of Figure 67.

From the tenor of the last three examples, the reader may have guessed already that sloppy procedure is a problem in the application of the tracer tool for behind-pipe flow detection. The problem arises inadvertently. The tool produces such a graphic "picture," the tendency is to jump to the most obvious conclusion of what the picture means. Work is thereby terminated before alternate conclusions can be discredited. In a very real sense, the tool is "too good." The closing section will discuss this problem further.

The next sequence of logs will illustrate the combined use of the temperature and tracer logs to diagnose a complex combination of tubing and casing failure. The temperature log on Figure 69 is from a new well that had undergone only brief periods of injection but still should have a wellbore temperature colder than static. This is clearly not the case below a zone at depth C that had served as a mud disposal zone at the time the well was drilled. In fact, the temperature log shows crossflow from depth B in the open-hole section up to the disposal zone at depth C. The most obvious interpretation of the log is that shown by the dashed line on the wellbore sketch, namely flow from depth B in the open-hole completion past the packer and up the tubing-casing annulus to a casing failure at depth A. Because this depth is above the cement top behind the casing, the flow can then continue unimpeded to the disposal zone at depth C. This interpretation, however, was not supported by a temperature survey run after 40 barrels of mud were pumped down the tubing. This log, shown on Figure 70, revealed a tubing failure at a collar at 12,900 feet, depth A on the figure. During the survey, the logging tool encountered an obstacle it could not pass at 13,170 feet.

In view of these additional complexities, the entire length of the tubing was then checked with the tracer tool. Velocity shots were taken every 1,000 feet. The tool was positioned and the mud pumps started. When the rate was up to 0.5 bbls/min a slug of tagged water was ejected and the travel time to a single detector 4 feet below was recorded. This sequence of operations could be run quickly without a lot of mud loss. The tracer survey showed tubing integrity from surface down to the failure seen on the temperature survey of Figure 70 at 12,900 feet. Three of the velocity shots are reproduced on Figure 71. The records on frames A and B were obtained with the detector above the suspect collar. The tracer slug on both records traverses the 4-foot spacing between injector and detector in one chart division or in about 3 seconds. However, when the detector is located at 12,900 feet, a travel time of 10 cd's or 60 seconds is required for the same journey. Most of the mud, obviously, exited the tubing between the depths associated

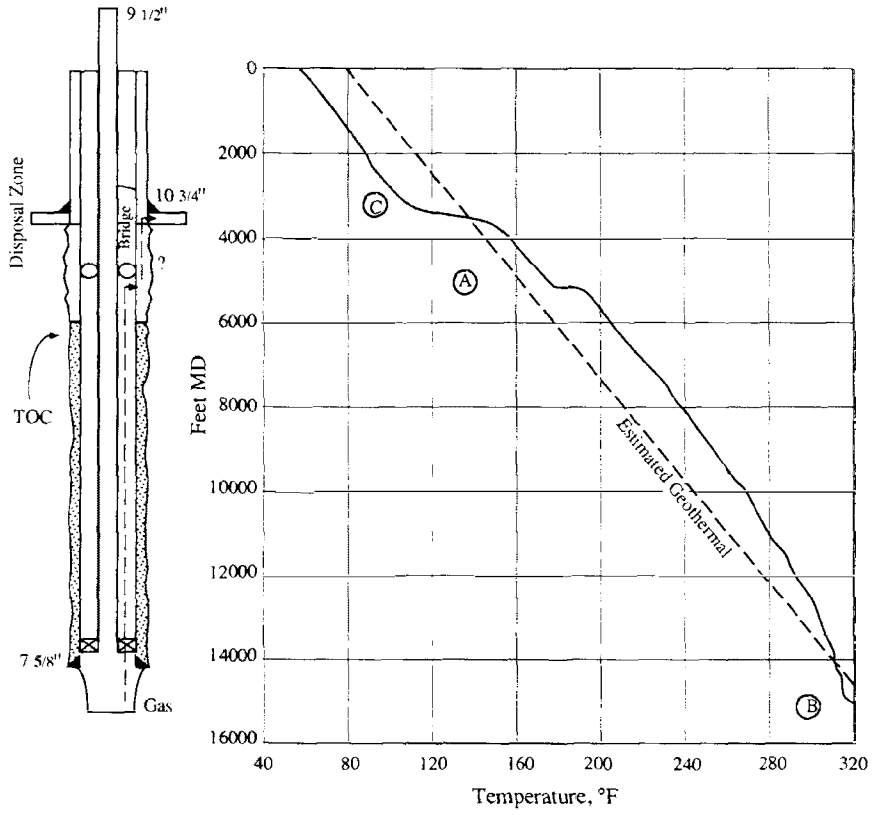

Figure 69. Shut-in temperature survey on a new well.

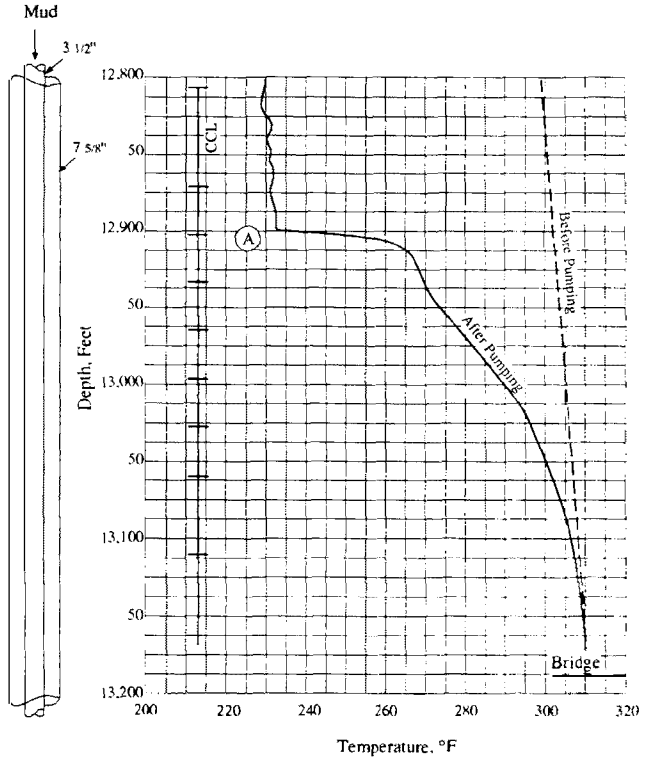

Figure 70 Temperature surveys before and after 40 BBLs of mud pumped down tubing.

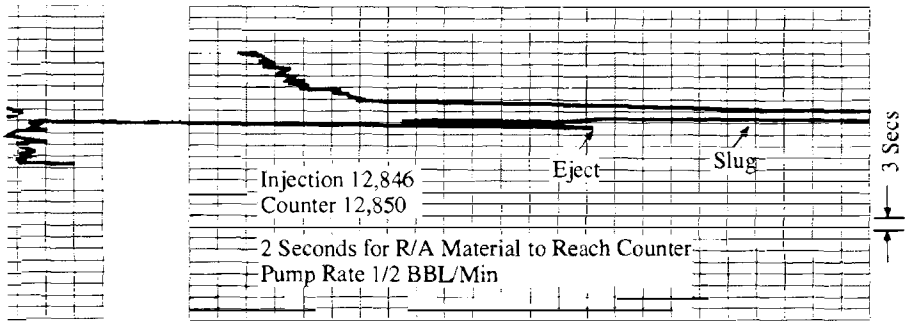

(A) Detector at 12,850 Feet and Time Drive at 2 Inches/Minute

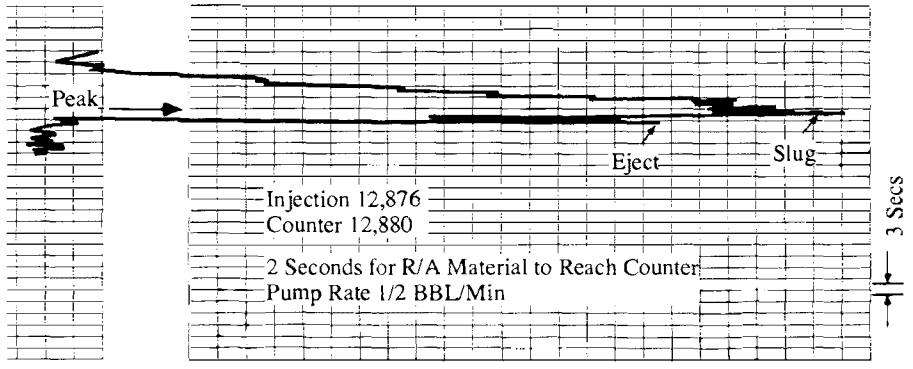

(B) Detector at 12,880 Feet and Time Drive at 2 Inches/Minute

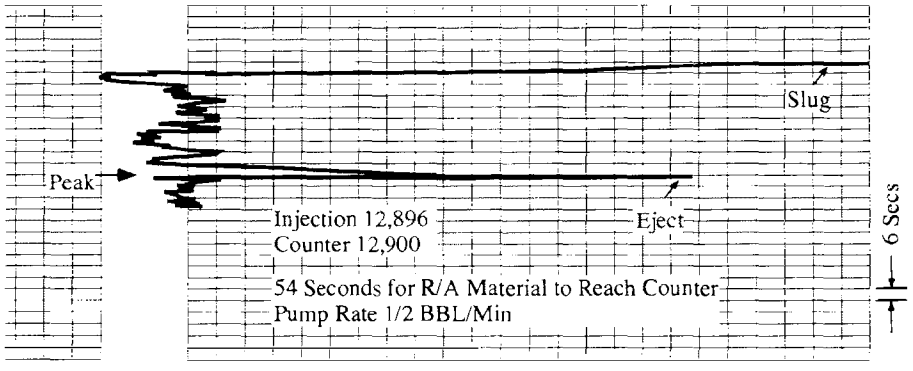

(C) Detector at 12,900 Feet and Time Drive at 1 Inch/Minute

Figure 71. Three velocity shots in well of Figure 70.

with frames B and C, i.e., between 12,880 feet and 12,900 feet. The recorder was put back on depth drive and a short collar log record obtained. This log appears on Figure 72. The leaking collar is at depth A, 12,888 feet. Note that this depth is 4 feet shallower than the location shown for the same collar on the CCL record of Figure 70, the temperature survey. The tracer tool, in essence, has been employed for depth control. Consequently, a marker was put on the logging cable with the detector located at the bad collar. This marker is the reference for subsequent logging work.

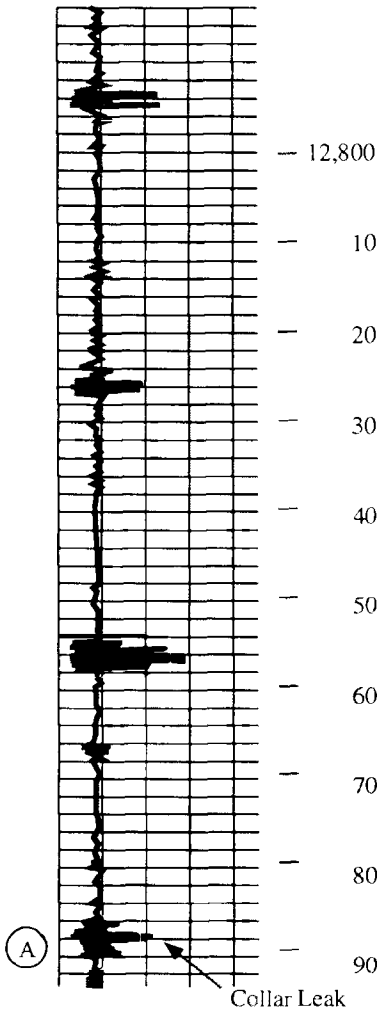

Figure 72. Collar log run after velocity shots on Figure 71.

The next sequence of operations involved the use of the tracer tool to find out where the mud goes once it exits the tubing. One would expect the mud to go upward, from what is seen on the temperature log of Figure 70. To check this expectation, the tracer tool was positioned with the detector at 12,800 feet, a location 88 feet above the bad collar. Injection rate was brought up to 1 bbl/min and a shot of tracer "fired." Frame A on Figure 73 shows the result. At the 6 sec/chart division record speed, the ejection mark on frame A is indistinguishable from the activity caused by the passage of the slug moving down inside the tubing. The reappearance of the slug moving upward in the annulus between the 3 1/2" tubing and 7 5/8" casing is evident as a well defined slug with relatively high amplitude on frame A. The centroid of the slug passes the detector some 22 chart divisions after its initial appearance on the way down. This is a travel time of 6 x 22 = 132 seconds for the double back over the 88-foot distance from the detector to the collar. The transit time inside the tubing can be determined from the velocity shot data of Figure 71

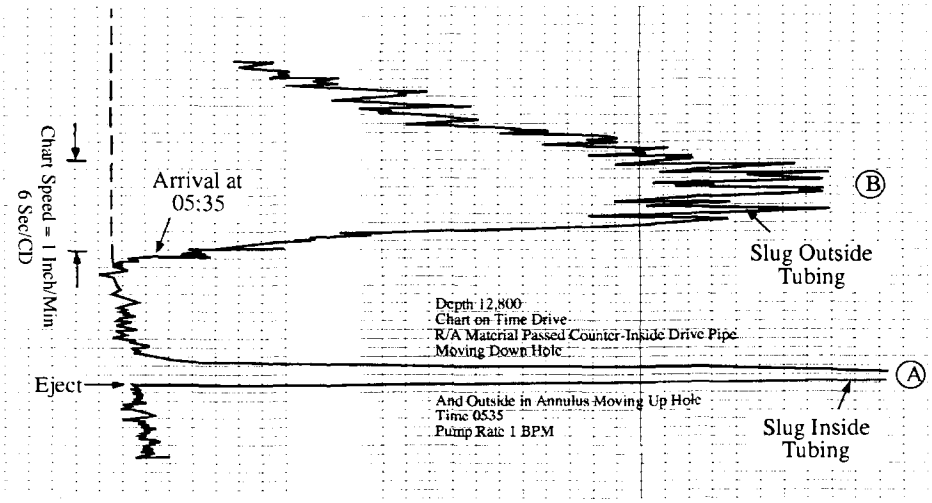

(A) Detector at 12,800 Feet (88 Feet Above Bad Collar) With a Time Drive of 1 Inch/Min.

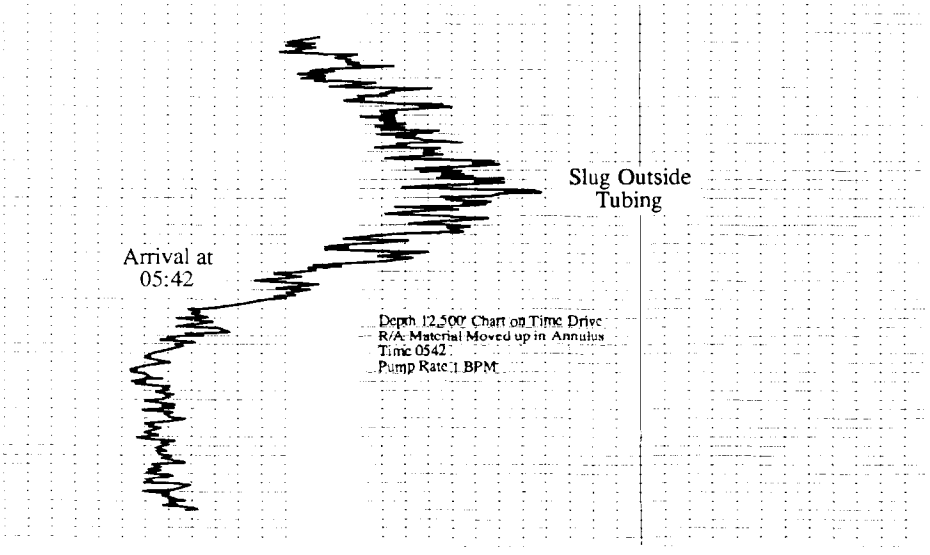

(B) Detector Quickly Moved to 12,500 Feet Depth, Time Drive at 1 Inch/Min.

Figure 73. Velocity shots above tubing leak @ 1 BPM rate.

taken at a rate of 0.5 BPM. At this rate, the slug went the four feet from ejector to detector in 3 seconds. Thus, the 88-foot travel at twice the rate would require a time

$$\Delta t_{in} = \frac{88}{4} \times \frac{0.5}{1} \times 3 = 33 \text{ seconds.}$$

This leaves for the outside, annular travel a transit time

$$\Delta t_{out} = 132 - 33 = 99 \text{ seconds,}$$

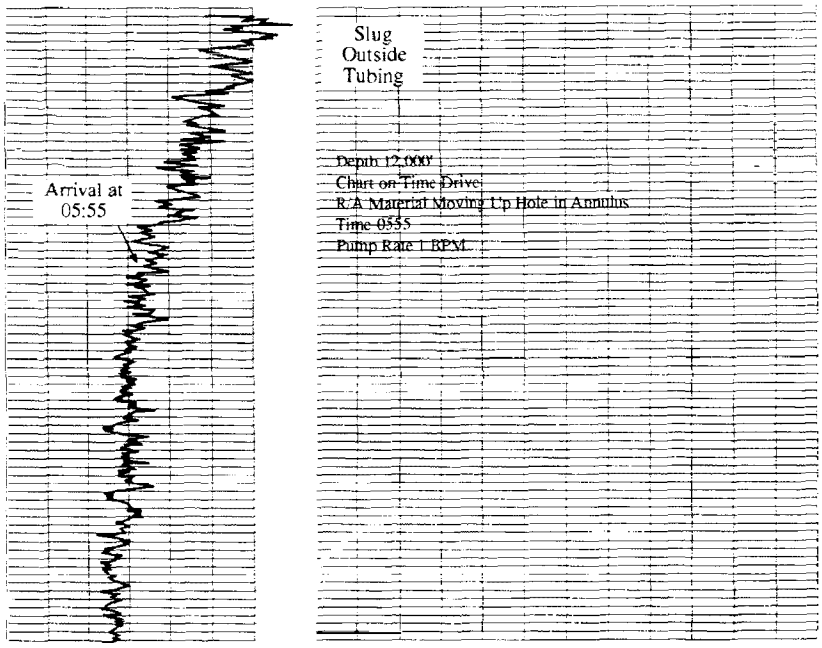

(C) Tool Pulled to 12,000 Feet and Detector Put on Time Drive at 1 Inch/Min.

Figure 73 (continued). Velocity shots above tubing leak @ 1 BPM rate.

or

$$V_c = \frac{88}{99} \times 60 = 53 \text{ ft/min}$$

for the apparent fluid velocity associated with the annular area between tubing and casing. According to the results of page 63

$$\hat{V} \approx 0.8\ V_c = 0.8 \times 53 = 42.4 \text{ ft/min.}$$

The annular capacity is 0.0307 bbl/ft from pipe tables. Consequently, the volumetric rate associated with the upward traveling slug is

$$q = 0.0307 \times 42.4 = 1.3 \text{ bpm}$$

Because the nominal pump rate was 1 bpm, one can conclude that, once out of the tubing, all the injected mud goes upward behind the tubing. The record on frame B of Figure 73 was obtained with the detector quickly repositioned 300 feet farther up the well at 12,500 feet. The slug arrives some 7 minutes after it was detected at 12,800 feet. It still has a cohesive appearance and a relatively high amplitude even after traveling some 388 feet in the annular space. The apparent velocity between the two positions is 300/7 = 42.9 ft/min, the same as previously estimated after correction. The slug is well-mixed at this juncture. Frame C is a similar record with the detector

at 12,000 feet. The leading edge of the slug has dispersed considerably over the 833-foot journey. The trailing edge, which was not recorded, would be even more spread out. The thirteen minutes travel time between the stations on frames B and C represents a velocity of 500/ 13 = 38.5 ft/min, a value representing a volumetric rate of 1.2 bpm.

After the tracer work was completed, an impression block was run to determine the nature of the "obstacle" that was encountered on the logging run of Figure 70 but not on the run of Figure 69 one day earlier. The "obstruction" was only a tight spot due to a kink, or "dogleg," in the tubing.

In a turn-about of sorts, the tracer tool has been used to help decide what the original temperature survey of Figure 69 revealed. The flow exits the tubing at 12,900 feet at the bad collar, then continues up the annular space between tubing and casing to a failure in the casing at depth A on Figure 69. From here flow goes upward behind the casing to the disposal zone at depth C.

In this example, you will also note a philosophy at work which is directed towards use of the tools in a fashion that illuminates the overall problem piece by piece. Each speculation is verified before adding the next one. In complex situations, this approach will generally lead to a resolution quicker than will an attempt to do everything in a single survey. This example is also well suited to the slug tracking tracer procedure; however, application of the velocity shot method minimized the amount of mud usage.

Quality Control Revisited: Figure 60 (page 91) presented a drag survey that possibly missed a tubing-casing leak because the survey was not properly carried to a conclusion. Likewise, the velocity shots for the two examples depicted on Figures 65 and 68 both suffer from the same lapse in procedure. This is the most common type of error in quality control and is easily prevented by proper supervision. Basic errors can, however, creep into the most unlikely situations as the final example will illustrate.

Figure 74 shows a slug tracking survey consisting of 13 drags in a well on injection at a rate of 950 BPD. A comparison of drags 5 and 6 shows that most of the water exits the wellbore at the top set of perforations. An injection spike appears about the middle of these perforations at depth A on drags 6 and 7. The 100 % superficial velocity from drags 3 and 4 is 41.3 ft/min, whereas the value from drags 5 and 6 is 13.6 ft/min. Consequently, at least 100 (1-13.6/41.3) = 67% of the injection exits over the top perforations. Drags 7 through 13 clearly show the centroid of the tracer distribution stopping at depth B, 4,478 feet. In fact, a close inspection of drag 6 shows that it has split into two parts. One peak is at 4,452 feet whereas the second is already at depth B with the remaining drags. This latter peak has thus moved faster than the slug peaks in the full-flow stream. The accumulation at depth B must then include tracer that flows behind the casing. Yet no injection spikes develop on any of the drags below depth B. Furthermore, all drags from 6 on show tracer dispersing downward below depth B, again without the development of injection spikes. This vertical spread continues to depth C, 4,525 feet, and the logging operator has chosen to "channel" it on down to depth D at 4,576 feet.

Yet the injecting temperature survey on Figure 75 shows that the bulk of the water got to and no deeper than depth A, 4,500 feet. Furthermore, the 4 hr. shut-in log reveals that the porosity that

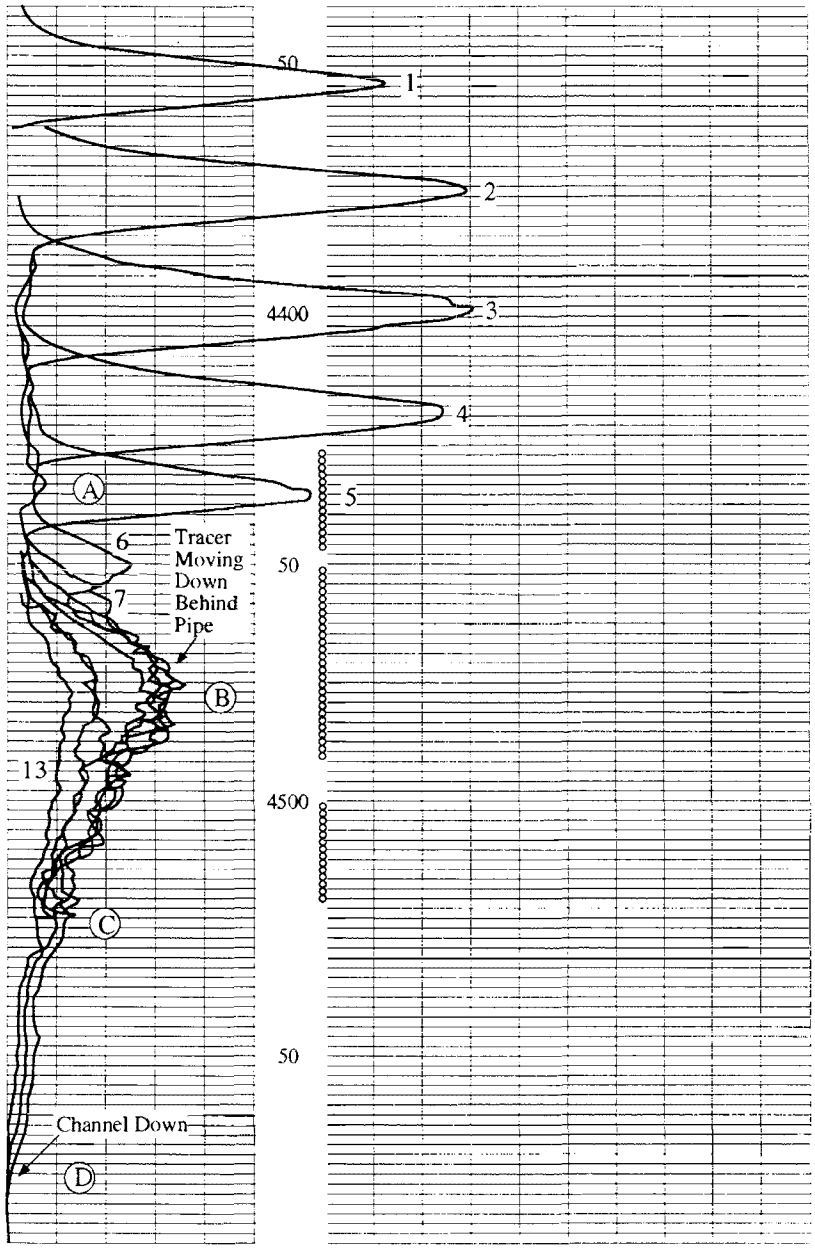

Figure 74 Slug tracking survey from well on injection at 950 BPD.

stores present or past injected water is confined to the interval from depth B, 4,440 feet, down to depth A, 4,500 feet. The operator is so biased by the tracer survey, however, that he has labeled a "channel" down to depth C, 4,614 feet. This is an incorrect interpretation.

The two different surveys indicate that the well is fractured from the differences in apparent depths at which water is "lost" from the wellbore. There is also no difficulty in the continuation

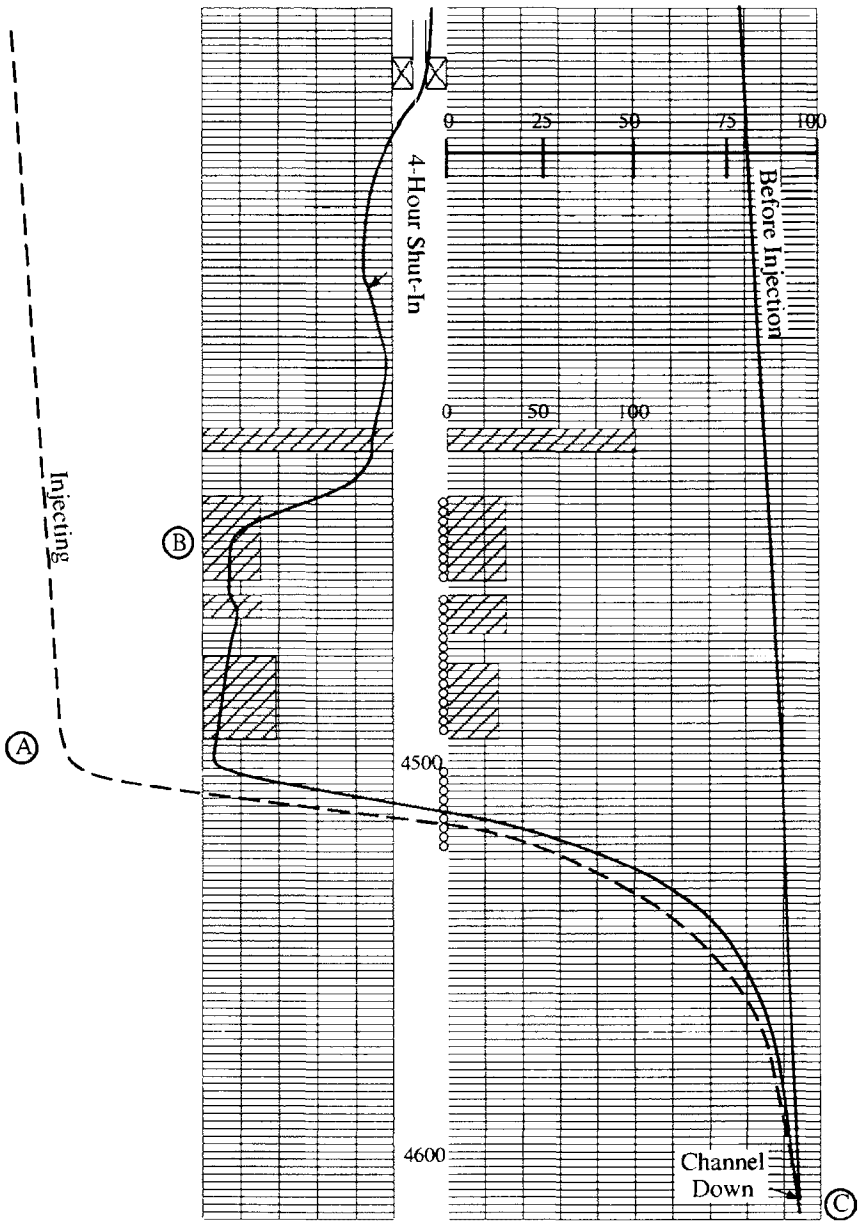

Figure 75. Temperature surveys from well of Figure 74 (recorded @ 2F/inch).

of behind-pipe flow down to 4,500 feet on the tracer survey of Figure 74 so as to agree with what the temperature surveys of Figure 75 show. The difficulty arises in the attempt to explain the dispersion of tracer at least 30 feet below 4,500 feet. This spread is uncorroborated on the temperature surveys.

A crossflow check with the well shut-in, as discussed previously, is also an excellent quality control indicator. It offers the key to what is going on in this particular example.

Figure 76 shows the location of two slugs, 2 and 3, ejected at 4,470 feet and at 4,542 feet, respectively, with the well shut off injection. Three drags were run through the bottom slug 3 at

the elapsed time in minutes as listed. Seven drags were made through the top slug 2 in a sequence that was incomprehensible to the individual subsequently redrafting the log in final form as only four times are listed. Two things are clear: first, both slugs are stationary. This is no surprise because it had been decided from the injecting survey of Figure 74 that most movement below 4,450 feet was occurring behind casing. The second feature on Figure 76 is the surprise. In dropping the tool downward so as to log upward, the operator has smeared tracer out over the entire interval to be logged. He has apparently done the same thing in the stagnant area of the wellbore below depth B on Figure 74. The vertical resolution of the survey is thereby destroyed. This problem would have been difficult to pin down, however, without control slug 3 on Figure 76.

In fact, the dispersion of tracer below depth B on Figure 74 closely resembles the signature produced on slug tracking surveys by tracer spread through vertical permeability around the wellbore. The only distinction is the large amplitudes.

A final feature evident on the drag surveys of Figure 74 is the paucity of "permeability," or injection, spikes. This is characteristic of fractured wellbores. Most of the tracer moves away from the wellbore region in the fracture before entering formation porosity.

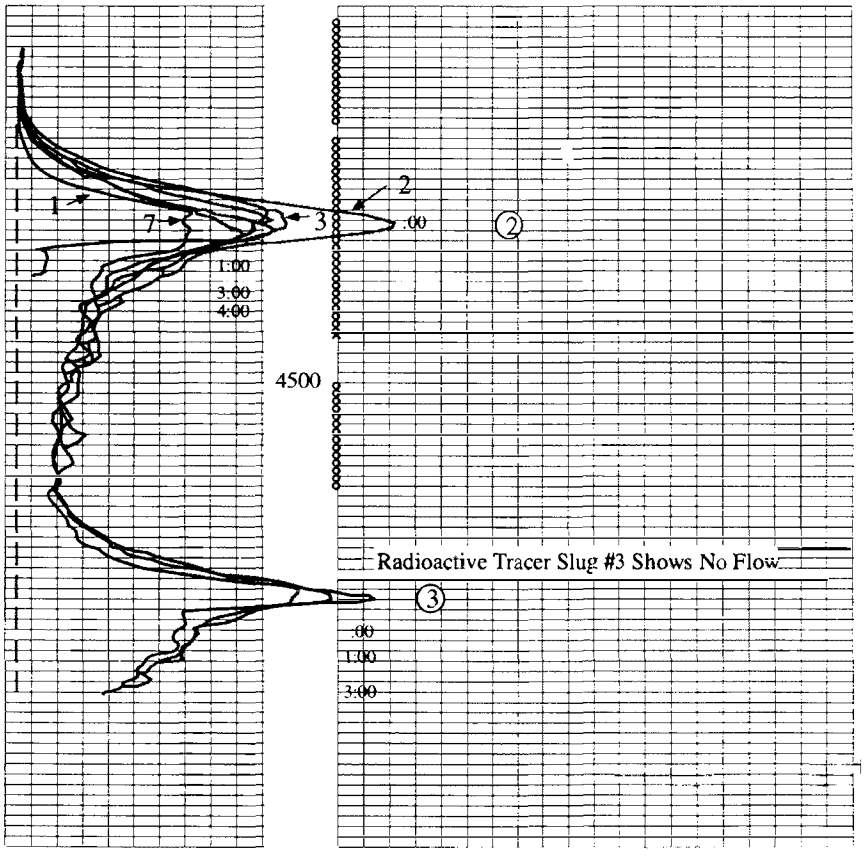

Figure 76. Shut-in crossflow check on well of Figure 74.

This final example concludes the discussion of radioactive tracer surveying of injection wells. The limited scope prohibited a general discussion of the wide selection of tracers available that can be made water, oil, or mutually soluble. Gaseous tracers are also commonplace. All these variations evolved for application to either producing wells or gas injection wells rather than to water disposal wells. There has been no discussion of the use of multiple tracers that emit gamma rays of different energy levels and, accordingly, can be identified by spectral logging techniques. The application of this technology is still limited primarily to the evaluation of staged, well stimulation treatments.

At this point, attention is directed to the final surveying tool, the noise logging tool, that utilizes the sound created by fluid turbulence as a "tag" to follow flow downhole.

Noise (Sound) Surveys

The sounds of moving fluids are so commonplace in everyday life to go almost unnoticed. Only when the movement influences our well being do we tend to bring these sounds to the conscious forefront. Who, for example, cannot recall being lulled by the soothing gurgle of a shallow stream of water on its way along an irregular path. In contrast, the sharp clap of thunder following a nearby bolt of lightening is startling in the extreme. The same sound, when heard from a distance, is little more than an ominous rumble, the higher pitches having been attenuated by the intervening air. Likewise, the intense scream of a jet plane's exhaust is quite painful in proximity but quickly resides to more of a bothersome roar with distance from an airport. These emotions are but a few of the myriad elicited by a single source, fluid turbulence.

It is therefore not surprising that this turbulence can be used to detect flow; particularly, flow behind-pipe where the cramped space and numerous constrictions give the high velocities and sudden expansions necessary for significant levels of turbulence. Actually, noise surveys first came into widespread application for a particular type of problem, the bubbling of a small amount of gas upward through liquid. The need to detect such flows was an unwelcome side effect of deep drilling that started in earnest domestically in the early sixties. The operation of cementing from great depths to surface proved difficult. All too often gas pressure appeared on the annuli of intermediate casing "strings" before the drilling itself was even completed. At this point, the resulting small gas flow was more of a nuisance to be dealt with than a threat to the well integrity. Nonetheless, the location of the source of gas was a challenge that led to the evolution of the noise logging tool.

Because of this mode of evolution, a stigma has been attached to the noise logging tool to the effect "that it is no good for anything except gas." As with most myths, there is some truth to this contention. The correct statement would be that the tool has its greatest sensitivity to the flow of gas upward through liquid, an application for which its resolution is typically about 10 cu. ft/day or 3 cc/sec volumetric rate. For the detection of single-phase flow, gas, water, oil, or whatever, the tool relies on the turbulence created as the fluid is forced across a constriction or past an obstacle. The acceleration of the flow across a localized pressure drop is an effective source of turbulent sound. The intensity of this sound, however, depends on both the volumetric rate and the pressure differential that accelerates this rate. Thus the tool resolution becomes

dependent on pressure differences as well as on rate and a unique lowest rate alone cannot be specified. This feature will be described in detail under a section devoted to tool resolution. The material in this section will allow an estimation of the rate resolution for each particular situation.

The noise tool does have two advantageous features for water flow that are lacking in the case of the tracer instruments. The first of these is the greater depth of investigation offered by the sound source. The frequency range of the tool is such that practically all the sound attenuation is the result of geometric spreading of sound intensity away from the source. Thus, the squared amplitude attenuates as the reciprocal of squared distance. The amplitude drops, accordingly, as the reciprocal of distance, a much lower attenuation rate than the exponential rate associated with gamma rays. Therefore, the tool can "hear better at a distance." More strings of casing can intervene between tool and sound source.

The second advantage enjoyed by the noise tool is the fact that the flow of water past the tool inside casing or inside the annular space between tubing and casing does not create much turbulent noise. In fact, with a 1 11/16 - inch tool in 5 1/2 - inch casing, an injection rate of 850 BPD with a velocity $\hat{V} = 25$ ft/min past the tool is required to raise the sound level above the normal ambient level typical of commercial tools in "dead" wells. This low level of sound is characteristic of any single-phase flow in straight conduits with constant cross-sectional area. The tool can, therefore, easily distinguish flow behind pipe from flow inside pipe. Furthermore, behind-pipe flow, either up or down, can be detected with the well on injection, provided the injection pumps themselves are not so noisy that logging is impossible.

The above comment raises the issue of the complicating influence of extraneous sources of noise, especially that due to surface machinery, on the quality of a noise survey. The failure to recognize such sources is characteristic of an inexperienced logging engineer. Otherwise, the interpretation of a noise log is just as straightforward as a tracer survey. The underlying physical principles are even simpler.

Noise Logging Tools: A commercial noise logging sonde is nothing more than a microphone that is constructed in a way that will withstand the abuse to which a logging tool is subjected. A schematic of the instrument appears on frame A of Figure 77. The piezoelectric crystals convert the oscillating pressure associated with sound transmission within the wellbore to an oscillating voltage that is input directly to an amplifier - cable driver combination. The latter sends the oscillating voltage up the logging cable to surface recorders. The sonde is therefore quite simple in construction and, consequently, is very reliable.

The piezoelectric transducers, pictured individually on frame B, are hollow cylinders made up of ceramic matrix containing a small amount of a highly polar compound, typically, lead zirconate. When the crystals are deformed by a force on their surface, the bound charges on the lead zirconate are separated and the surface becomes charged. A radial compression, for example, causes the inner surface of the crystals of frame B to become electropositive relative to the outside surface, thus, the crystals convert sound to voltage.

Frame C shows six crystals assembled for encapsulation in an epoxy, cast cylinder that gives the strength necessary to withstand wellbore pressure. As shown, the crystals are wired in parallel for purposes of electrical redundancy. So long as one crystal remains intact, the package will function normally. The more sophisticated tools utilize a pressure balanced housing for the crystals. A bellows transmits wellbore pressure to silicone fluid that completely surrounds the individual transducers. All tools have a covering over the microphone section in the form of a thin metal sheath or a teflon sleeve as protection against wellbore fluid.

Frame A shows that at the surface the microphone output goes to a speaker, or more typically to a set of headphones, that allows the logging operator to listen to the acoustical environment downhole. The human ear remains one of the most "diagnostic" of all sonic instruments! This also allows the operator to hear any tool creep that continues after the tool is supposedly stopped to take a sound level measurement.

Surface Processing of Microphone Output: At each location, stationary sound level measurements are made in a way that reveals the pitch content or frequency structure of the transmitted signal. As illustrated on frame A of Figure 77, the signal is input to at least four high-pass filters simultaneously. Each of these filters reject those oscillating voltages with frequencies below its cut-off setting and output those with higher or equal frequencies. The

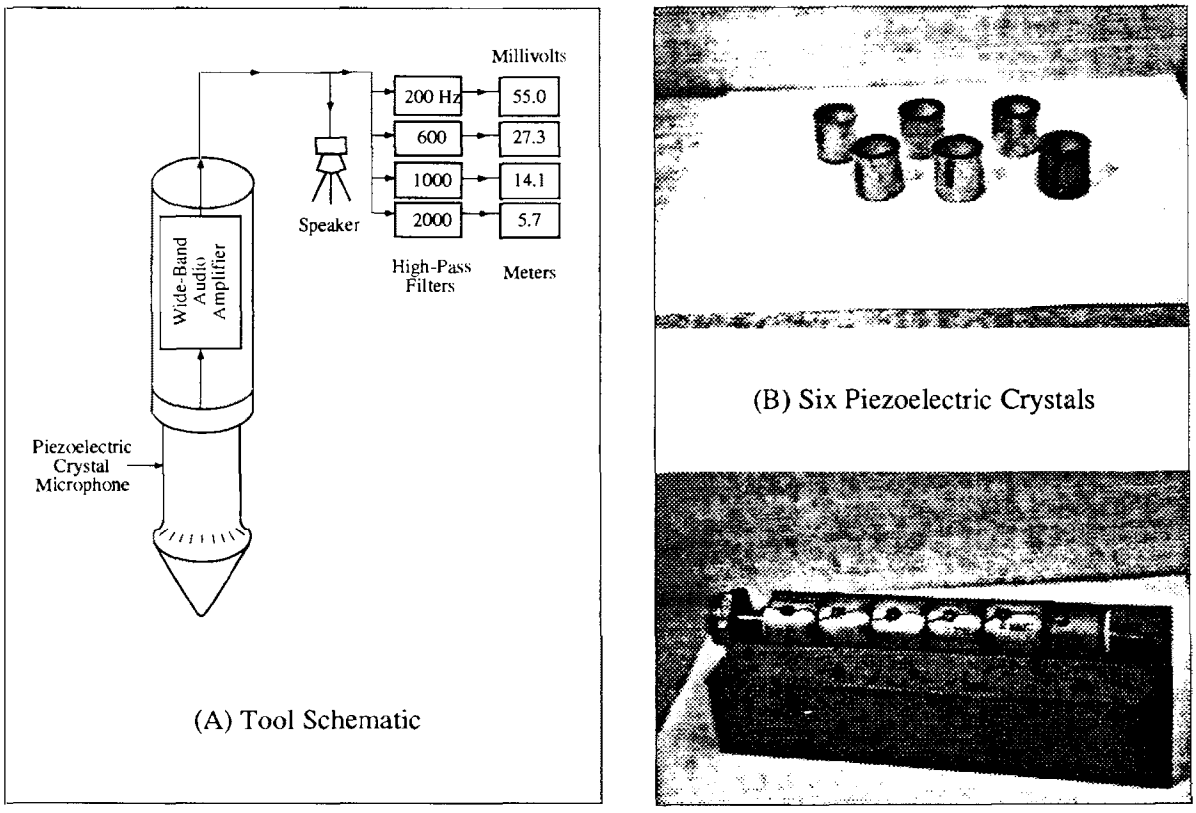

Figure 77. Noise (sound) logging sonde with piezoelectric detection elements shown separately.

settings shown on frame A, Figure 77, are standard for most companies, the lowest cut-off being 200 Hz. The remaining filters reject below 600, 1,000, and 2,000 Hz, respectively. In this sequence, the filters progressively remove from the low end of the audible sound range up to about the start of what would correspond to the soprano range in music. The amplitude of the output from the filters must then decrease in the same progression from 200 to 2,000 Hz as shown by the figures labeled "millivolts" on frame A.

The output of each filter, typically, serves as the input to its own millivolt meter, which, in turn, has a visual display of the light-emitting diode digits form. Once the meters have settled down after the tool is stopped, the operator activates the recording system that averages the output amplitude from each filter for a fixed period of time and then stores this average. The manner in which numbers are retained varies from pad and pencil, to paper tape, to magnetic tape depending on the particular company doing the logging. All the companies preserve at least the four frequency cuts illustrated on Figure 77, frame A, at each stop along with a depth reading.

The frequencies associated with the filters depicted on frame A are not arbitrarily chosen. The lowest setting, 200 Hz, eliminates most of the logging truck vibrations, for example, that are transmitted down the taut logging cable but is still low enough to detect the action of gas moving upward through liquid. The other settings are based on experimental data as to how best to distinguish the gas-through-liquid situation from the single-phase situation. More comments on this topic appear in a subsequent section on frequency content of sound from flow behind pipe.

Narrow band filters are not used generally to provide numbers for a noise log. The broad band readings tend to mute the influence of the resonant peaks that are inevitably present in the sound amplitudes.

One service company uses a digital processing scheme that divides the microphone output into ten frequency bands, corrects each band for cable attenuation, then recombines the bands required to represent the high-pass readings on frame A. These numbers are tabulated as "cable corrected" values along with the uncorrected measurements; however, it is usually the latter values that appear on the actual log.

Another company uses a software processing package with their noise tool that requires a sequence of band pass readings at four different high cut-off frequency settings but at the same low frequency cut-off of 100 hertz. Their "window" W6 band passes amplitudes from 100 Hz to 10,000 Hz and is a number analogous to the 200 Hz high-pass amplitude shown in connection with frame A. In fact this number is relabeled as WIH, window-1 high pass, on their log presentation. Their windows W3, W2 and W1 are bandpass amplitudes at 100-2,000 Hz, 100-1,000-Hz, and 100-600 Hz, respectively. These readings are used to generate the remaining three high-pass values shown on Figure 77. Thus, on their logs, the following four numbers replace the 200,600, 1,000 and 2,000-Hz readings of Figure 77:

$$W1H = W6, \qquad (100 - 10k\ Hz)$$

$$W2H = \sqrt{(W6)^2 - (W1)^2}, \qquad (600 - 10\ kHz)$$

$$W3H = \sqrt{(W6)^2 - (W2)^2}, \quad (1{,}000 - 10\ kHz)$$

$$W4H = \sqrt{(W6)^2 - (W3)^2}, \quad (2{,}000 - 10\ kHz)$$

Tabulated values on these noise logs contain numbers for two additional bandpass measurements, windows W4 and W5, which span the ranges 100-4,000 Hz and 100-8,000 Hz, respectively. Two additional high-pass values are computed from these and tabulated as W5H, a 4-kHz high-pass value, and W6H, an 8-kHz cut. Because logging cables severely attenuate signals with frequency components as high or higher than 10 kHz, the above scheme would appear, at first glance, to be the same as the simpler method of Figure 77. But there is a big difference in the results! The lower frequency components of the sound, whatever their origin, have amplitudes that are usually more variable with time than are the amplitudes at higher frequencies. Furthermore, extraneous noise sources are more intense at the lower frequencies. Each measurement in the above scheme is "polluted" by these frequencies. Consequently, the "noise" level in the noise itself can be unacceptably high. A higher frequency "cut" can exceed in value a lower frequency "cut," a clearly impossible situation for the instantaneous "cuts" of frame A on Figure 77. Tool resolution is compromised by the surface processing of tool output, a situation all too similar to that described in the notes for digitally recorded temperature logs.

Tool Sensitivity: This topic would normally appear under tool specifications but it is important enough to consider separately. Whatever the manner of signal processing, there is a standard unit of reference for the noise logging system. In this standard system, the logging tool is immersed in water along with a sound source. A sinusoidal pressure oscillation in the water with an amplitude of 1×10^{-6} PSI (root mean square) and a frequency anyplace in the range 200-2,000 Hz will produce a reading of 1 millivolt on the appropriate meter. In the past, companies have attempted to maintain their tools at this standard level within $\pm$ 3 decibels. Thus:

$$1 \times 10^{-6}\ PSI \Leftrightarrow 1 \times (10)^{\pm 3/20} = 0.7077 - 1.414\ Millivolts\ (RMS).$$

With the hard economic times, companies have become sloppy in their attention to quality control. At this time, only one manufacturer supplies a calibration certificate with each tool. The actual calibration is done at Naval Facilities in San Diego, California. Relative to the usual specification units, the above standard millivolt system output is equivalent to a sensitivity of – 134 decibels relative to 1 volt per micro pascal.

The proliferation of digital processing programs has also degraded standardization. These programs are generally written to process sinusoidal signals at unit net gain and are seldom tested with actual flow noise. Consequently, the most that can be said at present is that companies supposedly record at sensitivities of 1/2 to 1 times standard units. Because of the wide range of signal levels to which the tool must respond, most companies have a provision to decrease tool sensitivity by a fixed factor of 10.

Tool sensitivity is important because it determines the output level to be expected for a tool in a shut-in well that is totally free of any flow. This is the so-called "dead well" or "ambient"

output. All quality control checks for extraneous noise must, or course, be referenced to this level.

Finally, it should be mentioned that one company measures the tool output in decibel units with 1 millivolt representing 70 decibel units. In this system, an output of X decibels is therefore the following number of millivolts:

$$\text{Millivolts} = 10^{Y}$$

$$Y = 1/20\,(X - 70)$$

$$X = \text{No. of decibels}$$

These decibel values are then presented on a linear log format rather than on the logarithmic format that is typical for the noise log.

Noise Log Format: A Typical noise log format displays four numbers for the four high-pass readings on frame A of Figure 77 in millivolts for each stationary measurement. These numbers are usually given on a logarithmic scale as illustrated by the frames on Figure 78. The records on both these logs come from "dead" wells and illustrate ambient behavior under two completely different conditions. Frame A on Figure 78 is a portion of a log from an injection well that has been shut in for 24 hours. The ambient level is, accordingly, low-ranging from 1 to about 2

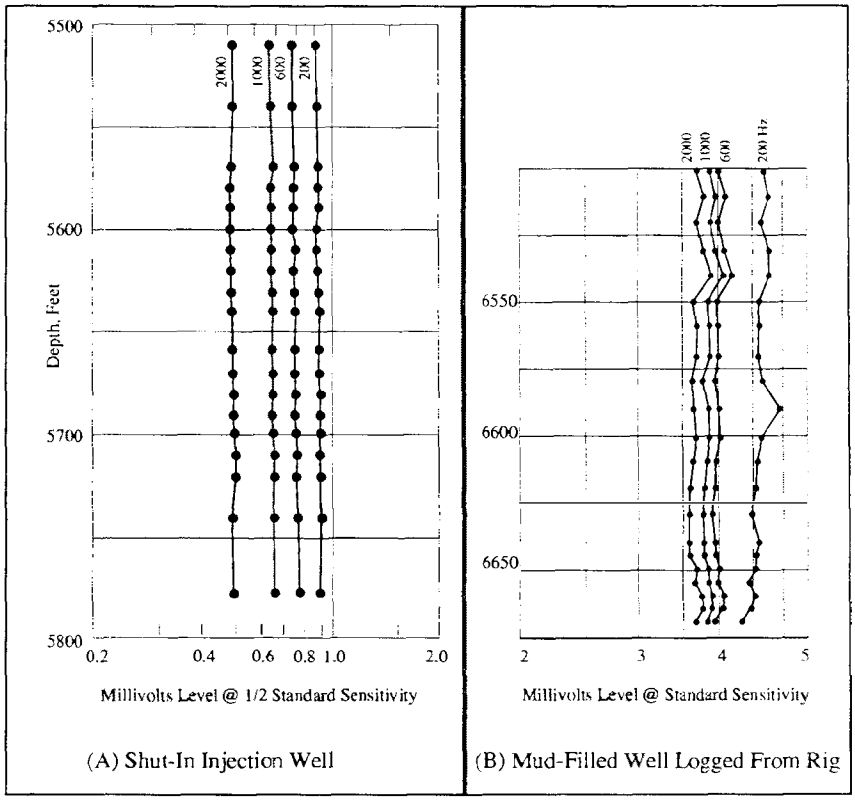

Figure 78. Noise log format illustrating typical ambient or dead well levels.

standard units. In contrast, the record on frame B is from a noisier environment, namely, an open-hole section beneath a drilling rig. Here, the ambient levels are in the range of 4 to 5 standard millivolts. Note also that the variation in noise level from station to station is greatest on the lowest frequency curve, the 200-Hz trace. This fact was claimed without any demonstration in the previous discussion on data processing. The high-pass method employed restricts this variation to the frequency cut to which it actually belongs.

For comparison, Figure 79 shows a noise log from a shut-in well that has a behind-pipe crossflow of water upward into a gas zone that was pressure depleted from production. Only at the top of this log, above the water level, are the noise levels on all cuts at about dead-well values. At the bottom of the log, a location over 1,000 feet away from the noise source at depth A, only the 2,000-Hz cut has decayed to ambient level. The lowest frequency cut, the 200-Hz curve, still has an amplitude that is 36% of the peak value at depth A. This is an illustration of the already mentioned ability of the tool to "detect from a distance."

The log also shows that most of the 250 PSI pressure differential between the sands is dissipated at one constriction located at depth A. This is an unusual situation for flow behind pipe. Also, the behavior of the four high-pass readings at the peak, depth A, shows that the sound amplitude drops very little from the 200-Hz reading through the 1,000-Hz reading. Yet the 2,000-Hz values is only about 1/3 of the 1,000-Hz value. This behavior means the most intense components in the sound occur at a pitch, or frequency, near 1,000 Hz. The spectrum peaks at

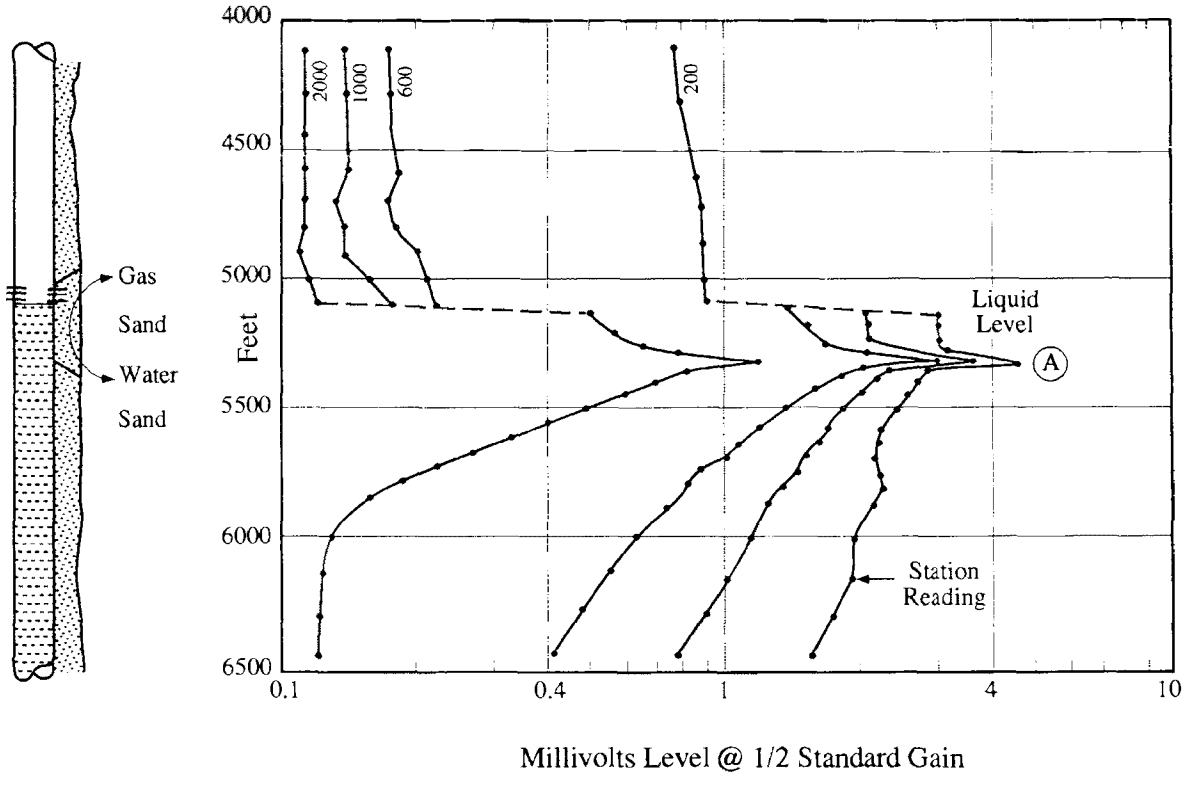

Figure 79. Noise log format with a 20-BPD water flow behind pipe into a gas zone depleted by 250 PSI.

ncy. Most single-phase flows produce dominant pitches of 100 Hz or higher when
ıg over a constriction. We have, therefore, partially justified the filter setting depicted
ʌ of Figure 77, the tool schematic.

level exerts an enormous influence on the log character on Figure 79. The loss in
l that occurs when the detector leaves the water column is the result of two factors.
the sound in water, a pressure wave exerts a force on the sound much greater than an
ːity oscillation in gas would produce because of the larger water density. The "so-
ıpling is better with water around the microphone. Second, the water surface itself
through interfacial tension any oscillations that attempt to cross. This noise log
t an interface is brought up because it is not unusual to have a water level in an
ell.

ː ambient noise levels on all three logs are slightly to either the high or low side of 1
illivolt level. This is typical for dead-well levels free of extraneous noise.
tly, this level serves as a quality control check on noise logging procedure. Every log
e locations with levels already ambient or decaying towards ambient. Exact values
t also depend on the length of logging cable on the reel and on its size. This is why
t values at the top of the log on Figure 79 are somewhat smaller than those on frame
ː 78 even though both logs were recorded at one-half standard sensitivity. Corrections
ngth are discussed in the next subsection.

ıuation: The tool schematic on frame A, Figure 77, shows that the amplified voltage
ıe microphone is transmitted directly up the logging cable of the surface unit.
the wide range of signal level over which the tool must operate, no attempt is made to
tage levels to spikes as was done with the thermometer. Consequently, the logging
acts as filter attenuating the higher frequency components of the tool output more
ın the lower frequency ones. AC current is lost from the cable primarily by
ːtorage in the insulating material that separates the conductor from the outside wire
· example, a logging ːable 7/32-inch in diameter and 24,000 feet long has over 1
capacitance in this insulating material. The insulation acts like a capacitor that shunts
n the conductor to ground, i.e., to the outside sheath. Also, the "resistance" that a
ffers to an AC current is inversely proportional to the signal frequency.

ɔrrect way to account for cable filtering is to divide the signal into narrow-band
orrect the amplitude of each segment according to its center frequency, and then
ːhe segments. This is a tedious operation because the recombination must account for
ıift also due to cable capacitance. Fortunately, it is not necessary to go to this degree
ːecause the cable correction is generally small, it is usually not even made. When it is
ıuch simpler procedure can be used that is perfectly satisfactory.

numbers measured at each station, one can correct only that value whose high-pass
ıency is closest to the dominant frequency. For example, on the log of Figure 79, the
ːh A has a dominant frequency not much larger than 1,000-Hz. This cut, whose
ː 2 x 3 = 6 standard millivolts, would be the one corrected for cable attenuation by a

factor appropriate to 1,000-Hz frequency. Such factors, labeled F_L, appear on Figure 80 fc common sizes of production logging cable, 7/32-inch diameter for the left-hand figure and inch on the right-hand figure. The cable length, L, on the abscissa of each figure is expres thousands of feet. A line is present on each figure not only for the four high-pass filter set in general use, but also for two higher frequency settings, 4 and 6 kHz, that are present on company panels in case they are needed for better vertical resolution.

Use of the correction factors is straightforward. The log on Figure 79, for example, was recorded on a truck that had 23,600 feet of 7/32-inch cable on its reel. For this length, the hand figure on Figure 80 gives, from the 1,000-Hz line, $F_L = 1.65$, thus, the corrected nois associated with the peak at depth A on Figure 79 is

$$N_{1,000} = 3x2 \times 1.65 = 9.9 \text{ std. mv},$$

A value that will be of use in the section on rate resolution. A correction on any other of t three remaining numbers measured at depth A on the log of Figure 79 with the factors fro Figure 80 is inappropriate. For example, at 200-HZ, $F_L = 1.20$, whereas the log peak value millivolts. Thus

$$N_{200} = 4.5 \times 2 \times 1.2 = 10.8$$

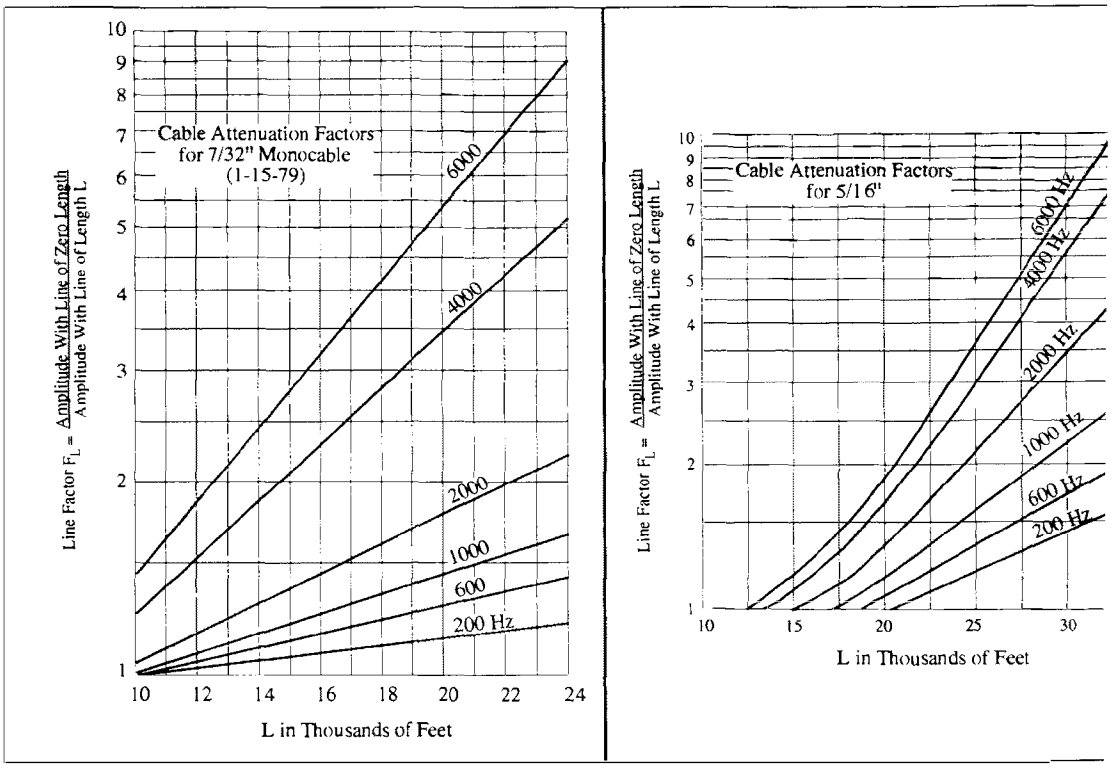

Figure 80. Logging cable attenuation factors for two wireline sizes.

Although seemingly valid, this number has no meaning because the dominant pitch contributing most of the amplitude to this measurement is closer to 1,000 Hz.

In the past, noise logging tools were manufactured with so-called "line-compensating" features. These tools contained signal generators that, when activated, would produce a constant voltage tone at each of the four frequencies, 200, 600, 1,000 and 2,000 Hz. In the surface panel, gains were adjusted to give the same output from each filter. This approach, however, allows the logging operator too much flexibility in "knob turning."

At the present time, variations from company to company in tool sensitivity are generally greater than variations due to cable filtering. The corrections may, therefore, not be sufficient to bring two companies logs into agreement.

Tool Specifications: The most important of the tool's specifications, its fixed sensitivity, has been discussed in some detail already. Suffice it to say that the ± 3 decibel tolerance quoted allows, in the extreme, the output in millivolts of two tools to differ by a factor of 2. Most companies exert better control than this in-house, but it is not uncommon to see this level of variation from company to company.

Noise logging instruments are available in diameters that range from as large as 1 11/16 inches (1.69 inches) to as small as 1 inch. The 1 3/8-inch diameter is also popular for this tool. The microphone section itself is generally less than 8-inches in length so that even in the usual combination with a thermometer, one still has a very compact instrument, generally less than 5-feet long.

The better noise logging sondes are rated for operation at 400 °F and 20,000 PSIG. A more common temperature rating is in the range of 300° to 350 °F, a rating that will accommodate practically all injection wells but may be too low for deep production wells, especially gas wells.

Logging Procedures: The noise logging tool does not need to be run with centralizers. Furthermore, direction of logging is of no consequence to the taking of stationary readings. The most obvious procedural question is related to the proper spacing between readings. In general, spacing is not all that critical a factor because of the long-distance carry away that is already evident on the log of Figure 79. A coarse grid of stops can be selected so as to accommodate the total interval to be logged and then additional time can be dedicated to more detail at crucial locations such as cement tops, casing shoes, perforations, zones of interest or around noise peaks.

A single station measurement will typically require from 3 to 4 minutes from time of arrival to completion. Add to this about 1 minute for tool relocation and you have a logging rate of about 15 stations per hour. A four hour long logging run would thus accommodate 60 measurements. Suppose we have 3,000 feet to survey. A coarse grid of stations 100 feet apart would use 30 of these 60 and leave 30 stops for detailing, which is usually sufficient. At this density, no noise peak could be located more than 50 feet from a measuring station. It is obvious from the log behavior on Figure 79 that very little would be inadvertently skipped over by such a spacing. The lines on Figure 81 allow a more specific answer as to what might be missed. This figure

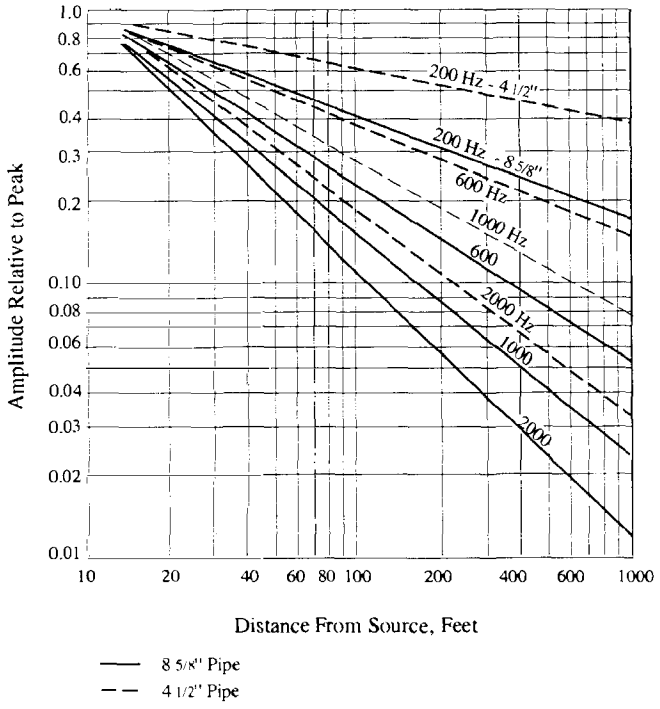

Figure 81. Sound carry-away from a source in water.

shows, for two casing sizes, the amount of sound carry-away with distance as a fraction of the peak value at the source. For each pipe size, four lines are present, one for each frequency on the noise log. The figure shows, for example, that in 8 5/8-inch casing the 1,000-Hz sound level fifty feet from a source is still 0.26 of the peak value. Suppose the ambient 1,000-Hz level is the 0.14 millivolt reading associated with the log on Figure 79. Then for a peak to be lost in this background, its amplitude could be no greater than $0.14/0.26 \approx 0.6$ millivolts. In such a fashion, the sample spacing and its consequences can be determined prior to the actual logging operation.

The use of a fine station spacing embedded in a coarser grid is illustrated on the log in frame A of Figure 78. This survey was actually run to determine if any non-related crossflow was occurring between sands located at 5,600 and 5,700 feet. A 30-foot station spacing is used in the approach to the sands, both from above and from below. Twenty feet above a sand, the station spacing is reduced to 10 feet and retained at this value through the zone and for 20 feet below it. This procedure was repeated at each of the two sands with one 20-foot spacing between the two. In frame B of Figure 78, the location of interest is at the bottom of the log. A 10-foot sample interval is used in the approach to this depth with a reduction to 5-foot intervals over the last thirty feet of log.

The log on Figure 79 shows four different stations spacings. A 250-foot interval appears on the approach to the perforation from above. This interval is reduced to 100 feet with the tool still 400 feet from the perforations. A further reduction of 50-foot intervals is made when the noise level increased as the tool enters the water column. This spacing is carried on for 400 feet below the peak at depth A. At this point, the 2,000-Hz level is almost back to ambient value so the operator increases the sample interval to 150 feet over the bottom part of the log. The immediate

symmetry about the peak value at depth A means that the actual peak is located very near the station stop depth. Its location appears to be a bit off the regular 50-foot spacing; consequently, the logging operator most likely searched for this location. Had he measured only at the stations on either side of the peak, then the largest amplitude would have been 0.8 millivolts on the 2,000-Hz curve rather than the 1.2 millivolts measured at depth A. The apparent peak would be 67% of its actual value. At a regular 50-foot spacing, a peak would be within 25 feet of a measurement. The 2,000-Hz line on Figure 80 for 4-1/2-inch pipe shows that the apparent amplitude is about 50% of true value.

The logs on figures 78 and 79 were recorded with the well shut in. This is the correct way to log for non-related, behind-pipe flow. If an injection well has positive wellhead pressure, it is also a good way to log for injection confinement. A packer check can easily be run in such a situation. For an injection confinement test, the well should also be logged on injection . A "channel check" is possible with the tool in the casing; however, the flow velocity past the tool in the tubing will generally create too much noise for a valid packer check while on injection. The logs on figures 78 and 79 utilize a range of station spacing that is typical, 5 to 250 feet. The particulars in spacing arrangement are worked out relative to the situation at hand.

Noise Log Characteristics: There are three features to every noise log that are pertinent to what the log means. These are: (1) sound levels on all four cuts, (2) variation in level on a particular cut from station to station, and (3) the frequency content of the sound at a peak in level. These three features can be referred to succinctly as loudness, character, and pitch, respectively. Loudness relates to the severity of the problem, character to how flow is taking place, and pitch to the type of flow-single phase or gas through liquid. Each of these features is discussed in some detail because, in combination, they form the basis for noise log interpretation.

Loudness: The measured sound levels on a noise log are significant for two reasons. In the first place, the level increase above ambient is obviously related to the severity of the problem. For example, at depth A on the log of Figure 79, there is a peak in noise level to values from 1.2 to 4.5 millivolts for the four cuts. These are considerably higher levels than ambient, for which the same four cuts range from 0.12 to 0.8 millivolts. Although one cannot associate a degree of severity with the increase at this point in development, one would agree that if another run six months down the road gave levels at depth A that were three times higher, this would signify an increase in the flow rate. The actual relation to rate is given in subsequent sections devoted to specific flow situations, but for now it is the low end of the loudness range that will be discussed.

In the second place, the level of sound on a noise log is the best quality control index available. Ambient levels under proper logging conditions have been demonstrated to fall just on either side of the 1 millivolt level, depending on environment and logging cable. If this level does not appear anywhere on the log with the well shut in, then there usually will be an extraneous noise source that has gone unrecognized. The log will either be useless, or worse, will lead the interpreter to incorrect conclusions.

The log on Figure 82 is from an oil well that is shut-in with a tubing pressure of 815 PSIG. Only at the deepest station do the values of noise level appear to be settling down to ambient values.

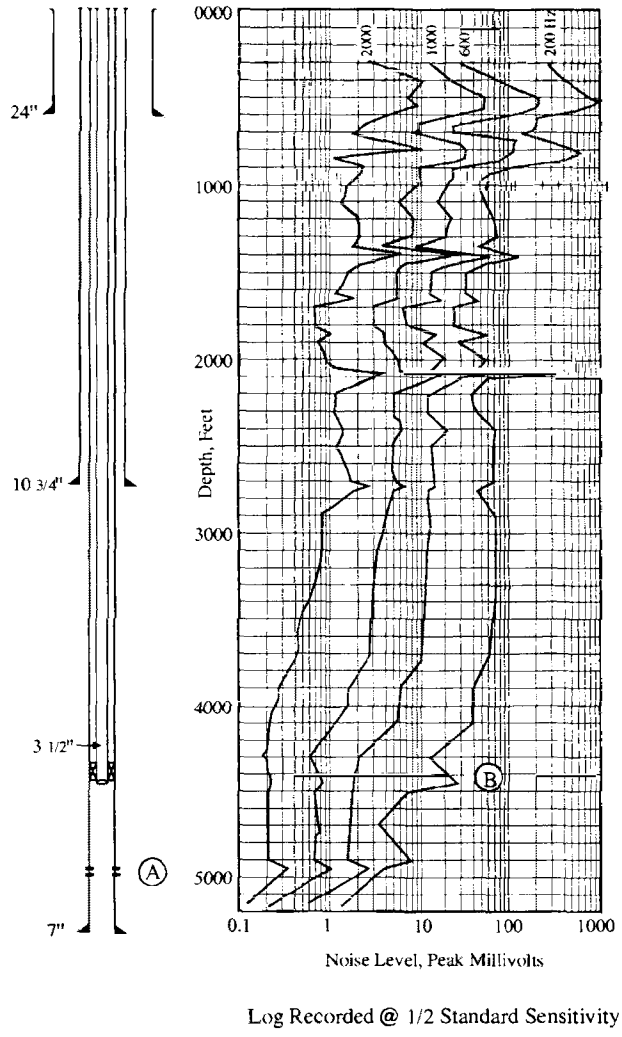

Figure 82. Noise log from a shut-in oil well with 815 PSIG tubing pressure.

Even the perforations at depth A are producing. The sustained levels above the end of the tubing, depth B, indicate that this flow is entering the tubing and flowing through the narrow space between tubing and logging tool. From what is seen at shallower depths, this flow reaches all the way to the surface. Finally, the flow appears to go in surges as witnessed by the many peaks. Steady flow up the tubing would not exhibit this character. In short, what this log shows is the result of a lubricator seal at the surface leaking sporadically. More specifically, one sees on the log the extreme sensitivity that the tool has to the movement of gas through liquid. A slight loss of seal pressure allows carbon dioxide and nitrogen to flash from the oil and bubble upward. Each time this happens the flow surges. All this confusion is the result of attempting to log a high pressure well without the use of a grease-injection controlhead. Sloppy procedure!

The term "peak millivolts" that appears on the abscissa of this log is a common way to designate a tool with one-half the standard sensitivity. Likewise"peak-to-peak" is sometimes used to designate standard sensitivity.

The log on Figure 82 is also typical of what can happen in a shut-in injection well that has positive tubing pressure. A loss in seal pressure will allow dissolved air to flash.

Compare the noise level on Figure 82 with that on Figure 83. The lower part of the log on Figure 83 was shown on frame B on Figure 78. The levels on Figure 83 are 10 to 25 times lower than the values on Figure 82. At the worst, location 3, the levels on Figure 83 rise only about 25% above ambient values. Yet the control demonstrated above and below locations 1-4 is sufficiently good that significance can be attached to the peaks at these locations. As a check, a second pass was made over the interval 6,325-6,475 feet to insure that the peaks repeated. The four peaks are, in fact, at depths of closest approach to a well blowing out of control nearby, with the closest approach being at location 3.

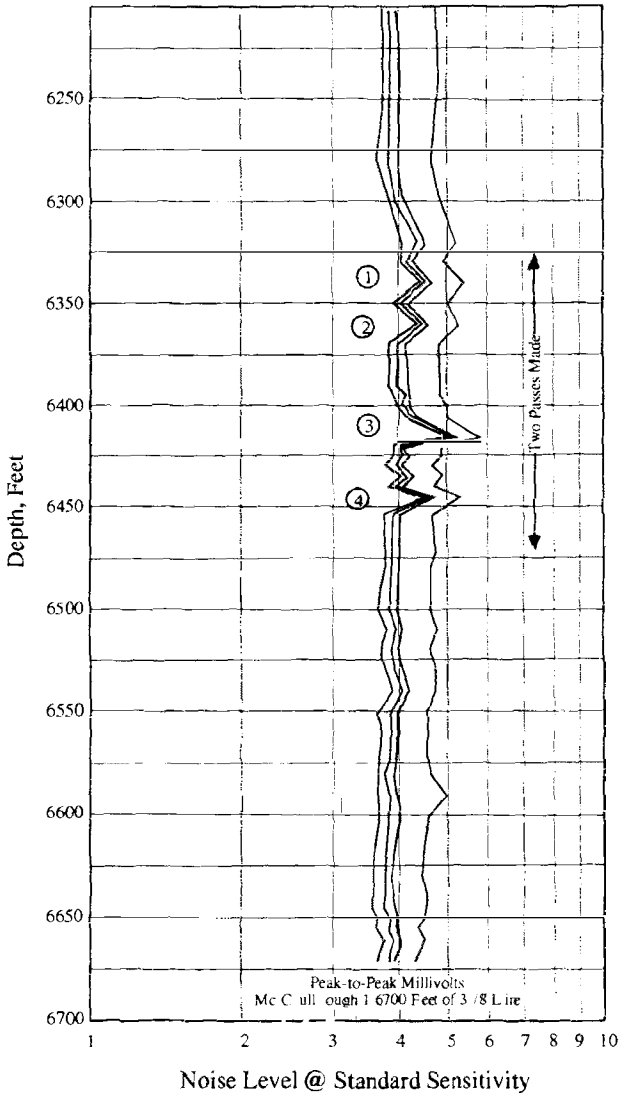

Figure 83. Noise log from mud-filled open hole in the vicinity of well blowing out of control.

The significance attached to loudness on a noise log is therefore relative to not only problem severity but also to procedural quality control.

Character: It has already been indicated that the variation in level of sound on a particular "cut" from station to station is related to the path followed by a steadily flowing stream. This fact is incorporated into the hypothetical situation of behind-pipe flow illustrated on Figure 84. A crossflow is depicted from zone A to zone C past a single constriction at location B. An acceleration occurs across a pressure drop at each of these locations, on entry to the wellbore region behind pipe at depth A, on passage through the tight spot at depth B, and on exit from wellbore at depth C. Accordingly, a peak in the sound level occurs at each of these locations, the magnitude of which is directly proportional to the pressure drop at that location. Most of the pressure difference between zones A and C is dissipated at these three locations. Had the flow occurred inside the casing, then the peak in sound level at depth B would not be present. Also, an actual situation may be such that the pressure drop at either the entry, depth A, or the exit, depth C, or at both may be so small that the associated peak is not recognizable above the residual sound carry-away from the peak at depth B.

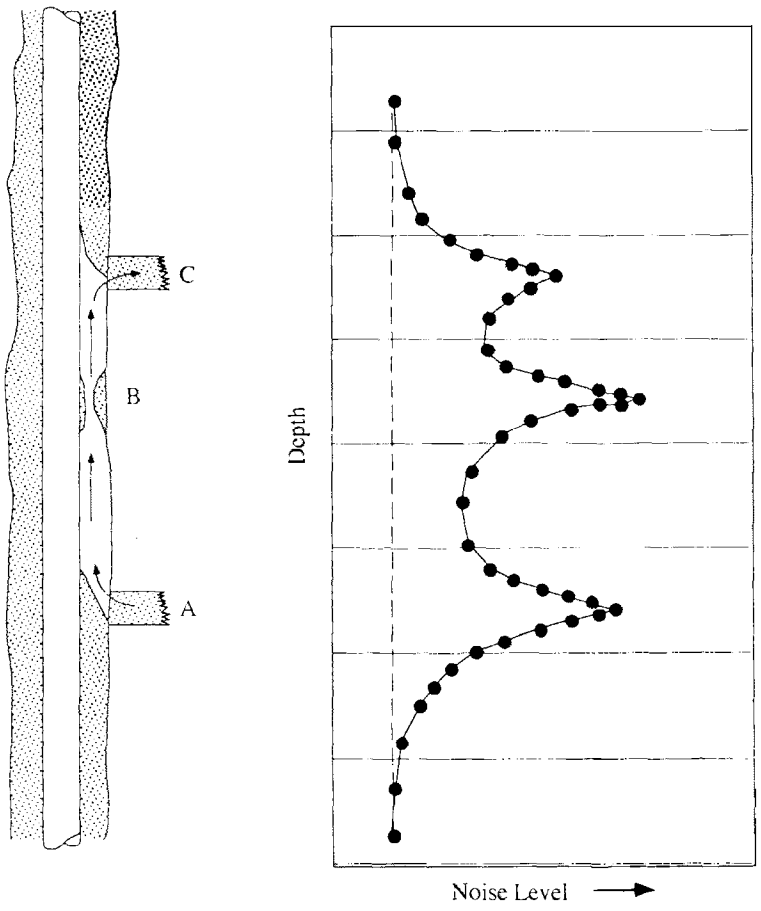

Figure 84. Noise log character as related to flow path.

The type of information available from record character is demonstrated by the next two examples, both of which involve the flow of water behind casing.

Figure 85 shows a noise log from a well experiencing an underground blowout that commenced when the drill bit penetrated an abnormally pressured water zone at the bottom of the open hole section. This water is charging porosity in a normally pressured zone at depth A. Above this location, sound levels decay to ambient levels slightly to the high side of the 1 millivolt value. Within the crossflow interval below depth A, the number of peaks in any one curve is limited only by the station spacing in use, not by the actual number of constrictions which apparently are numerous indeed. The flow is therefore behind the intermediate string of 9 5/8-inch casing shown at 17,000 feet. It is the cement and not the casing itself that has failed. The crossflow rate of 500 BPD was estimated from a rate measured when the water flow was diverted to the surface.

Compare the character on the log of Figure 85 with that appearing on Figure 86, another example of water crossflow behind pipe at a much higher estimated rate of 5,000 BPD. The cut on Figure 86 with the best vertical resolution, the highest frequency curve at 2,000-Hz shows on two locations, D and E, in nearly 4,000 feet of interval at which peaks in noise level occur. As will be seen shortly, the single peak at depth D is associated with an entry from a source aquifer located at this depth whereas the double-peak structure at depth E results from two exits into porosity at two locations in the same shallow aquifer. Not a single tight spot is evident in

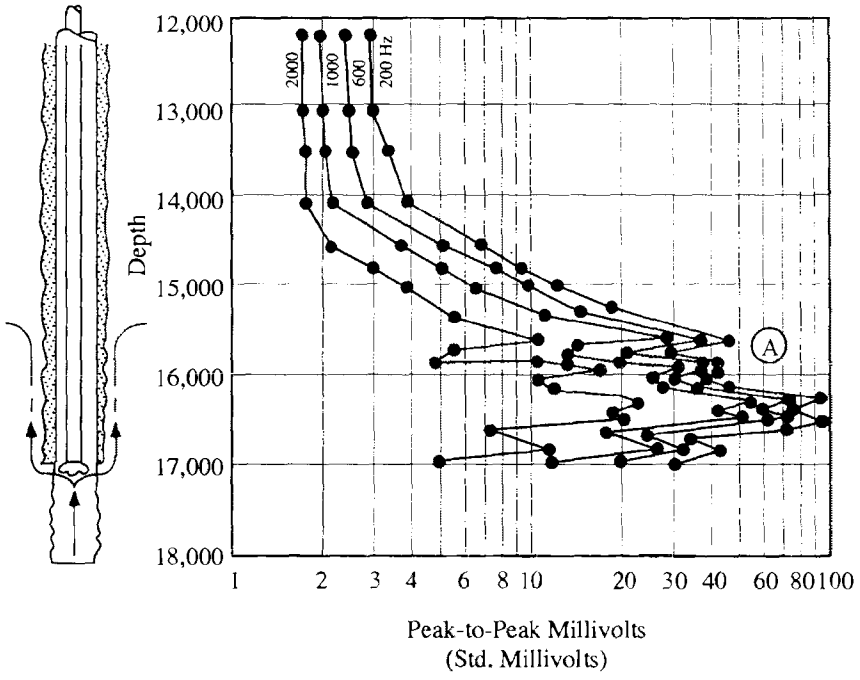

Figure 85. Noise log from a 500-BPD flow of high pressure water behind 9 5/8-inch casing in a well being drilled.

between! The flow is obviously taking a path of nearly constant cross-sectional area. The well completion sketch on the left-hand side of Figure 86, unfortunately, shows several possible routes satisfying this requirement.

Two temperatures surveys from this well appear on Figure 87. The log on frame A was run 1.4 months after the well was shut off production, the same time at which the noise log of Figure 86 was recorded. The survey shows the water flow as originating at depth D and progressing to depth E with a minor loss at depth F. The noise log of Figure 86 shows that there is very little pressure differential left at the location of minor loss, depth F. Most of the charging has apparently already happened!

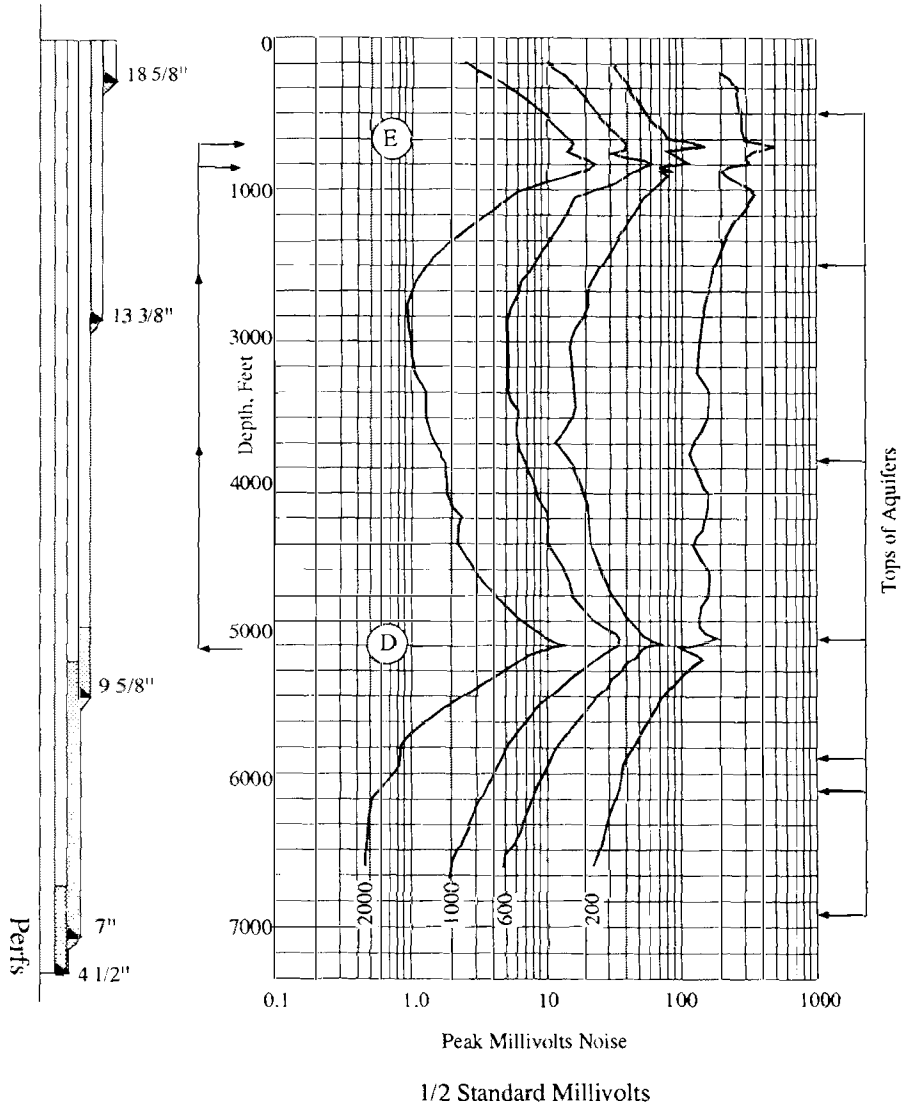

Figure 86. Noise log from shut-in well with water flow behind-pipe at an estimated rate of 5,000 BPD.

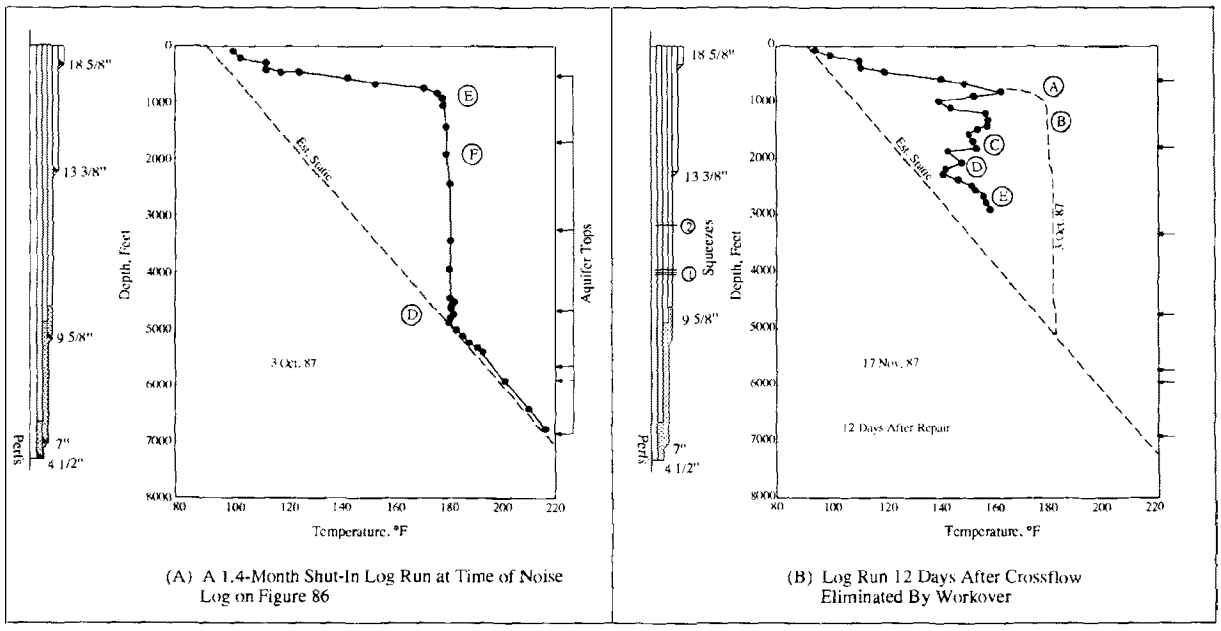

Figure 87. Temperature surveys on well of Figure 86 before and after a workover to eliminate behind-pipe flow from deep aquifer into shallow aquifers.

After a workover, the well was left shut-in for 12 days so that the survey shown on frame B of Figure 87 could be run. Storage signatures associated with porosity taking water are marked on the log. Locations A and B on this figure correspond to the peak locations on the noise log of Figure 86.

Finally, the log on Figure 88 allows one to compare on the same log the character in noise levels to flow along a tortuous path to that along a smooth path. The log was run with a small annular gas flow in progress. The lack of character to levels above the cement top, located at depth A, relative to those below the cement top is very evident.

As the log on Figure 82 demonstrated, character can also be introduced by extraneous noise sources that are intermittent in nature. Common sources of this type will be covered in a final section on quality control.

Pitch: The third feature to a noise log that is essential to interpretation is the pitch or frequency content at a particular peak in noise level. Whenever the flow is occurring behind pipe, frequency content is an excellent indicator of single-phase flow as opposed to the flow of gas upward through liquid. This fact is illustrated by the experimental data appearing on Figure 89. These data are from an experimental assembly consisting of a joint of casing with a flow channel in the cement behind the joint. A string of 2-inch tubing is inside the casing and the logging sonde is inside the tubing. The entire assembly is filled with water.

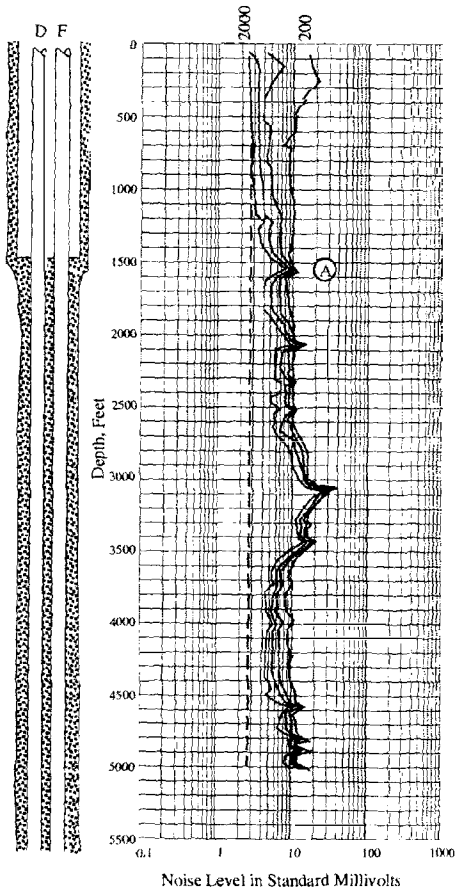

Figure 88. Noise log from well with a very weak gas blow from annulus (D-string logged).

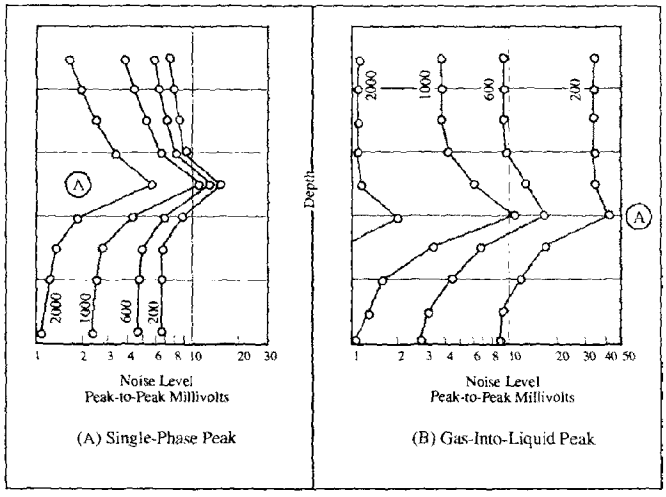

Figure 89. Frequency content (pitch) at a noise peak produced by two different types of flow behind pipe.

The record on frame A of Figure 89 resulted from water acceleration into the channel from a porous plug located at depth A. The first three measurements at 200, 600, and 1,000-Hz are "bunched together" in the 10-16 standard millivolt range whereas the 2,000-Hz cut has dropped to 5.5 standard millivolts. Thus, the dominant frequency of the sound is near 1,000 Hz. This type of behavior is typical of the turbulent sound generated by high velocity, single-phase flow behind pipe. At least three "cuts" through 1,000-Hz will be bunched together and all four may be if the dominant frequency moves up into the 2,000-Hz range. Lower velocity flow of water inside casing generates much lower frequency sounds until the rates become quite high.

A comparison of the frequency behavior at the peak at depth A on Figure 79, with the 20 BPD water flow, frame A of Figure 89, indicates that the behavior is the same. Likewise, at any of the peaks on Figure 85, the 500 BPD water flow, the first three readings are bunched together in the same fashion as are those on frame A of Figure 89. For the gas flow behind pipe shown on the log of Figure 88 all four "cuts" are crowded together at most of the peaks. Thus, the dominant frequency is closer to 2,000-Hz for this case. This is not a distinction between single-phase gas as opposed to water alone, because water can also generate peaks with frequencies this high or higher. Higher velocities are, of course, required for water because of the higher viscous attenuation in water.

The frequency behavior exhibited on frame B of Figure 89 resulted from a small rate of gas bubbling from the porous plug into a water-filled channel. In contrast to those on frame A, the levels at the peak on frame B are spread out over a range from 2 to 42 standard millivolts. There is obviously quite a bit of sound at the lower frequencies. In fact, the level in the band from 200 to 600-Hz alone

$$N_{200} - N_{600} = 42 - 17,$$

$$\Delta N = 25 \text{ std. millivolts},$$

exceeds the level associated with all frequencies above 1,000-Hz, i.e.

$$\Delta N > N_{1,000} = 11 \text{ std. millivolts}.$$

This strong component of lower frequency sound is generated by the collapse of liquid upon itself during the cycle of uplift and fallback of water associated with entry and subsequent rise of each discrete bubble or slug of gas. This process accompanies a particular slug of gas as it rises through the water; consequently, the level on the 200-Hz curve remains at a high value even above the entry depth A on frame B of Figure 89.

The frequency behavior exhibited on this frame is a characteristic of a gas-liquid system and will be manifest for flow either inside or outside casing. As gas velocity increases, the churning action in the liquid also increases to the point that the liquid begins to foam or froth. From this point, the frequency character starts a transition from that of frame B back to that of frame A. Rapidly decreasing sound levels also accompany this transition back to single-phase type

behavior. Most behind-pipe flows of gas through liquid exhibit frame B type frequency behavior until the gas simply lifts the liquid out of the flow path.

The third noise log with water flow behind pipe examined, Figure 86, had an estimated crossflow rate of 5,000 BPD. Yet the peak frequency structure at both the source depth D and the exit depth E is of the "spread out" type of frame B on Figure 89, for gas moving through liquid. Note also that the 200-Hz level is practically constant from the source throughout the 4,000-foot interval to the exit peaks. The noise logging tool is responding to the dissolution of gas, nitrogen and carbon dioxide, at the entry depth D, and the subsequent travel of gas upward. Evidence of gas cooling at the source is evident on the temperature log on frame A of Figure 87, at depth D.

The type of frequency character exhibited on Figure 86, is not that unusual in connection with behind-pipe flow of ground water. Gas flow through liquid is such a strong sound source that a little gas evolution will dominate the noise log levels. This actually increases the sensitivity of the tool above that which it has for single-phase flow alone, provided the gas does not stay dispersed as very tiny bubbles that move with the water.

The example logs considered so far are sufficient to show that, in combination, the three features, loudness, character, and pitch determine what a noise log means from a qualitative standpoint. But one must relate the loudness to flow rate for the tool to be effective.

Sound Level-Flow Rate Relation: Compare once again the sound level at the peak, depth A, on Figure 79 with the levels at the peaks on the log of Figure 85, all of which have a dominant pitch of about 1,000 Hz, the same as that of peak on Figure 79 (page 118). On the latter figure, the level is only $N_{1,000} = 6$ standard millivolts even though the sound source is directly behind the casing in which the tool is located. This value is considerably less than the level at 1,000-Hz of any of the five peaks appearing on Figure 85, which from depth A downward reads 30, 31, 54, 51, and 27 standard millivolts, respectively, and this with the tool removed by two strings of pipe from the sources located behind the casing. Intuition would therefore attribute more behind-pipe flow to the situation on Figure 85 than to that producing the log on Figure 79. However, the pressure drops associated with the peaks are quite different. The single peak on Figure 79 accounts for 250 PSI pressure difference whereas the five peaks on Figure 85 combined dissipate some 2,000 PSI of abnormal pressure. Consequently, the levels cannot be related to rate alone. The necessary relationships are given in the following subsections.

Water Flow Behind Casing: The turbulence created by the acceleration of a single-phase fluid past a constriction is directly proportional in intensity to the power expended to achieve the acceleration. This is simply a statement of energy conservation because all the power is lost to fluid frictional dissipation. Thus, the level of sound at a peak is proportional to the rate of pump work creating the peak, that is, to the product $\Delta p \times q$, where Δp is the pressure drop across the constriction and q is the volumetric rate. The constant of proportionality between sound level, N, and pump power, Δpq, is determined experimentally with apparatus of the type that was described in connection with Figure 89. If the 1,000-Hz cut is chosen as the calibration level, then the relationship takes the specific form

$$\Delta p \times q = 1{,}100\ Np \times (N_{1,000} - 6), \qquad (9a)$$

where

Δ_p	=	pressure drop across, peak, psi
q	=	volumetric rate, BPD
N_p	=	number of pipe strings between tool and noise source
$N_{1,000}$	=	level at peak on 1000-Hz cut, standard millivolts

The experimental basis for the above relationship is given by the correlation on Figure 90 for $N_p = 1$, i.e., for the water flow behind the same casing in which the tool is located. Equation 9a represents the straight line shown on the figure for noise levels greater than 7 standard millivolts on the 1000-Hz cut. For example, at $N_{1,000} = 15$ the line shows $\Delta p \times q = 10 \times 10^3 = 10{,}000$ whereas equation 9a gives $\Delta p \times q = 1{,}100 \times 1 \times (15\text{-}6) = 9{,}900$. The scatter of data on Figure 90 arises from the presence of values for many different types of geometric configurations to the flow path behind pipe. This causes an uncertainty in rate of about a factor of 2 within the value given by equation 9a; however, geometry behind cemented pipe is never known with any degree of confidence.

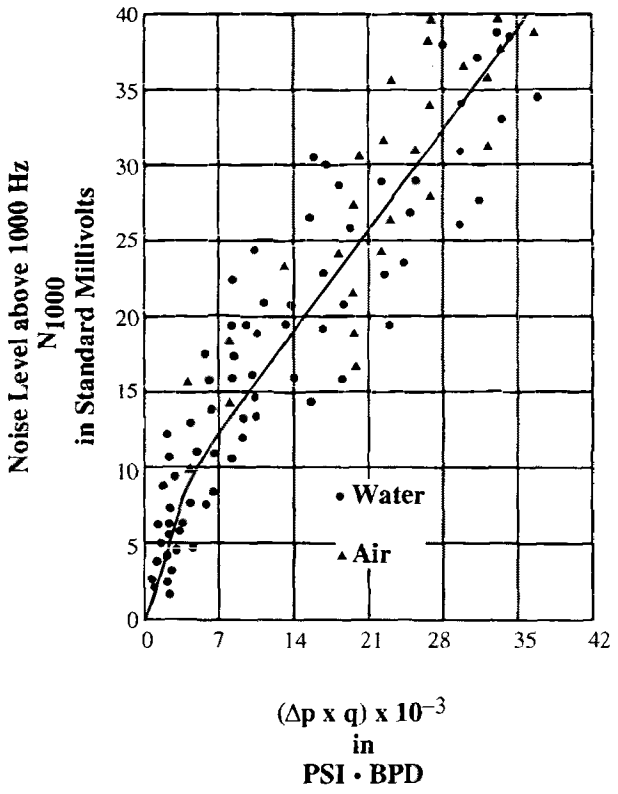

Figure 90. Sound level-rate correlation for water flow behind the pipe in which sonde is located ($N_p = 1$).

The relation expressed by equation 9a can be applied directly to the peak at depth A on the log of Figure 79. After cable correction, the value for $N_{1,000}$ was:

$$N_{1,000} = 3 \times 2 \times 1.65 = 9.9 \text{ std mv.}$$

It had also been noted that this peak had dissipated the known 250-PSI pressure deferential between zones so that $\Delta p = 250$ PSI for the peak, with $N_p = 1$, equation 9a gives

$$250\ q = 1{,}100 \times 1 \times (9.9 - 6),$$

$$q = 17 \text{ BPD.}$$

A value that, fortuitously, is close to the estimated rate of 20 BPD. From the scatter on Figure 90, one could expect $\Delta p \times q$ to be in the range of 1,800 to 7,000 with corresponding rates of 7-28 BPD.

Refer now to the log on Figure 85. If one attempts to apply equation 9a to a particular peak, the appropriate value for Δp is unknown because all that is known is the total pressure difference of 2,000 PSI over all the peaks. This total pressure drop, however, is the sum of the individual drops at each peak. From the form of equation 9a, if Δp_{TOT}, the total drop, is used, then the corresponding noise level is the sum for the individual levels, i.e.,

$$\Delta p_{TOT} \times q = N_p \sum_{i=1}^{5} (N_{1000_i} - 6),$$

where the $N_{1,000_i}$, are the individual 1,000-Hz cuts at the five peaks on Figure 85. This particular log was run on 25,100 feet of 7/32 inch logging cable. The corresponding attenuation correction factor from Figure 80, is $F_L \simeq 1.75$ at the dominant frequency of 1,000 Hz. Thus, the corrected peak values of the 1,000-Hz cut are, in order from Depth A on Figure 85, downward:

$$\sum_{i=1}^{5} (N_{1000_i} - 6) = (30 \times 1.75 - 6) + (31 \times 1.75 - 6) + (54 \times 1.75 - 6) + (51 \times 1.75 - 6) + (27 \times 1.75 - 6)$$

$$\sum_{i=1}^{5} (N_{1000_i} - 6) = 308 \text{ std. mv.}$$

With 2 strings of pipe between the sonde and the leak, $N_p = 2$, and we have

$$\Delta p_{TOT} \times q = 1{,}100 \times 2 \times 308 = 677{,}600.$$

For an estimated Δp_{TOT} = 2,000 PSI, the corresponding rate is

$$q = \frac{677{,}600}{2000} = 339 \text{ BPD},$$

a value to the low side of the estimated 500 BPD rate.

It should be noted that the use of the 1,000-Hz cut on Figure 90 and in equation 9a is simply a matter of choice. There are data points on the figure for peaks with dominant frequencies in the 2,000-Hz range similar to the peaks appearing on the log of Figure 88. Consequently, the cable correction factor by which the $N_{1,000}$ levels are multiplied should be that appropriate to the dominant frequency. In the case of Figure 88, the cable factor at 2,000 Hz is the proper one.

At noise levels below about 8 standard millivolts, the correlation on Figure 90 is represented by

$$\Delta p \times q = 350\, N_p \times N_{1,000} \qquad (9b)$$

for $N_{1000} \leq 8$ std. mv.,

which gives a convenient expression for the resolution that a noise log from a shut-in well has to water flow behind pipe. If it is considered that, for recognition $N_{1,000} \geq 2\, N_{1,000}$ (BKG), i.e., a peak must exceed twice background level, then the previous expression gives

$$q \geq 700 \frac{N_p \times N_{1000}(BKG)}{\Delta p} \qquad (10)$$

where q = minimum detectable rate, BPD

N_p = number of pipe strings between logging tool and leak

$N_{1,000}$ (BKG) = background noise level above 1,000-Hz, std. mv.

Δp = pressure difference available for behind-pipe flow

This expression allows the tool resolution for any particular situation to be estimated in advance. It also shows that the tool efficacy is completely dependent upon the pressure difference available to drive flow. As Δp becomes small, the detectable rate increases rapidly.

At a background level of 1 standard millivolts and a driving differential Δp = 100 PSI, equation 10 gives $q \geq 7\, N_p$, a condition that makes the noise logger comparable to temperature and tracer tools. If, however, the pressure difference drops to Δp = 10 PSI, then $q \geq 70\, N_p$ and the tool is no longer comparable to the other two.

Water Flow Past Tool: If the noise log is run while the well is on injection, then the noise generated by flow past the tool may determine the appropriate background level whenever the tool is above the perforations. Likewise, carry-away from this source may dominate the background below the perforations.

For example, the noise log on Figure 91 came from a water flood well on injection at a rate of 26,800 BPD at 1,300 PSI tubing pressure. This rate produces, in the 7-inch casing, a velocity of 508 ft/min past the logging tool. This velocity is sufficient to produce a dominant frequency at the same 1,000 Hz previously observed for behind-pipe flow. Furthermore, the level of sound is quite high, 1,300 millivolts at 0.1 standard sensitivity. In terms of the previous logs, $N_{1,000}$ = 13,000 standard millivolts!

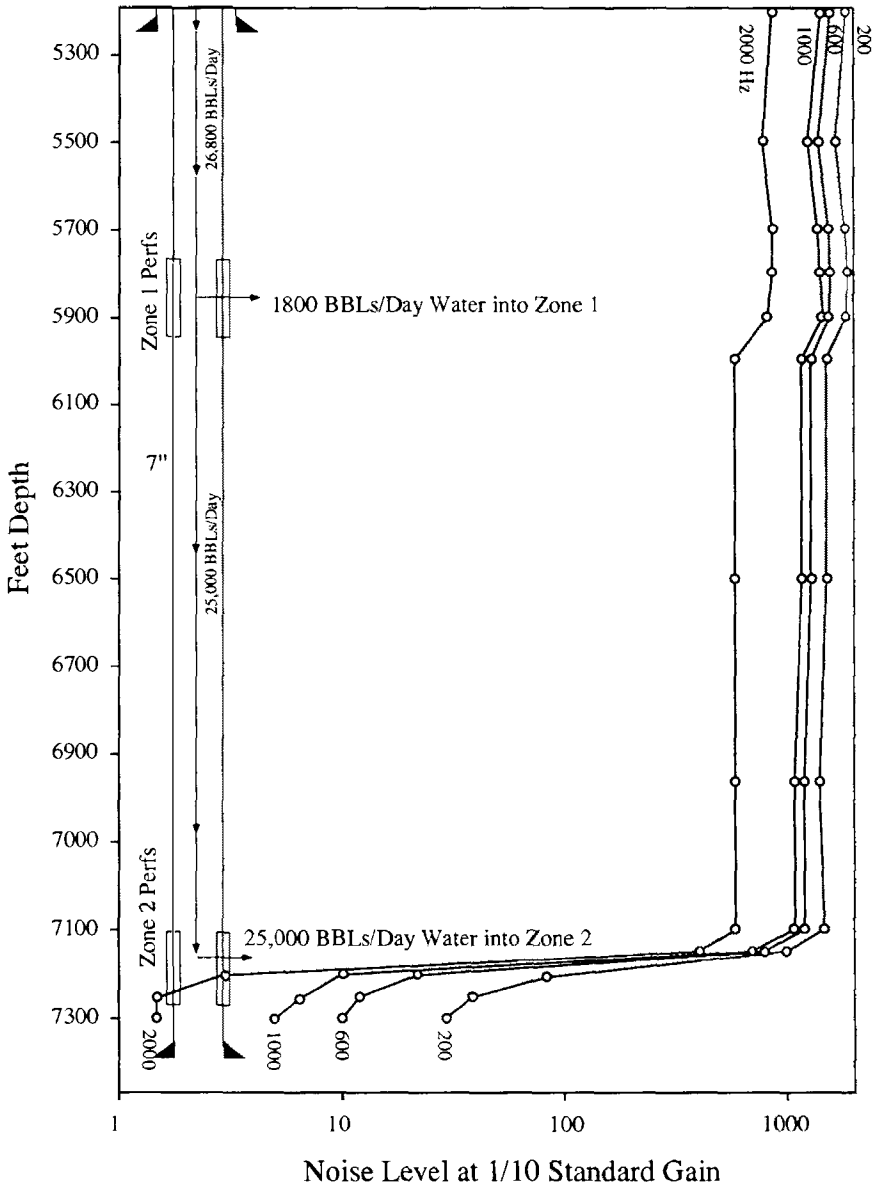

Figure 91. Noise log from well on water injection at 26,800 BPD and 1,300 PSI in 7" casing.

At this injection rate, the log gives an excellent injection profile. A small amount of water is lost to the perforations and into zone 1, but the vast majority of the injected water leaves over about the top one third of the perforated interval in zone 2. Above zone 2 the injection noise is still $N_{1,000}$ = 11,000 std. mv.

According to equation 9a, this level could hide any flow doubling back upward outside the casing whose rate did not exceed

$$q = 1100 \times \frac{1100 \text{ std. mv.}}{1750 \text{ psi}} = 7{,}000 \text{ BPD}$$

where 1,750 PSI is the total injection head. This rate resolution is about the same as the 20% of flow that the temperature log can detect during injection.

If, however, the injection rate to the bottom perforations was only 10,000 BPD, then the noise due to flow past the tool would drop to 700 standard millivolts. At the same injection pressure, the resolution would be $q \geq 440$ BPD or 4.4% of injection rate. At 5,000 BPD, the resolution for behind-pipe flow would further increase to 2% of the injection rate.

The above statements make use of the relationship for noise level due to water flow past the tool that will now be developed. In a smooth geometry, the turbulent pressure drop, Δp, in equation 9a can be expressed in terms of a friction factor, f, per foot of pipe as

$$\Delta p = f \rho V^2 = f \rho \left(\frac{q}{A}\right)^2,$$

where ρ is the fluid density and A is the area between the tool and the casing. Thus, equation 9a is of the form

$$N_{1000} = B\rho \frac{q^3}{A^2}$$

where B is a calibration constant. For a water density of 62.5 lb/ft^3, the combined value ρB as experimentally determined gives the following relationship for the noise level caused by flow past the tool:

$$N_{1,000} = 3.3 \times 10^{-11} (q^3/A^2) \qquad (11)$$

where
- $N_{1,000}$ = 1,000-hz cut in std. millivolts
- q = volumetric rate, BPD
- A = cross-sectional area between tool and pipe.

For a given volumetric rate, tool size, and casing size, equation 11 can be used to estimate the sound level resulting from water flow past the tool. As an aid to the use of this expression, the cross-sectional areas for common tool sizes are listed in Table 8:

TABLE 8. CROSS-SECTIONAL AREA FOR NOISE LOGGING TOOLS

Tool Diameter Inches	Cross-Sectional Area
1	0.0054
1 3/8	0.0103
1 1/2	0.0123
1 5/8	0.0144
1 11/16	0.0155

These values can be subtracted from pipe areas given in commonly available tables. For example, the 7-inch, 23 lb/ft casing on Figure 91 has an area of 0.221 sq. ft. A 1 11/16-inch tool was used to log the well. Therefore, in equation 11

$$A = 0.221 - 0.0155 = 0.2055.$$

For a rate q = 25,000 BPD, the level from equation 11 is

$$N_{1000} = 3.3. \times 10^{-11} \times \frac{(25{,}000)^3}{(0.2055)^2}$$

$$N_{1000} = 12{,}200 \text{ std. millivolts}$$

This value is as close to the measured level of 1100 x 10 = 11,000 standard millivolts as can be expected without specific tool calibration.

Equation 11 provides the relation needed to convert the noise levels through, say, the bottom set of perforations in zone 2 into a flow profile. Because $q \propto \sqrt[3]{\text{level}}$ by equation 11, it is simple to construct the injection profile shown on Figure 92. For this profile, the 2,000-Hz cut has been used as the one with the best vertical resolution. Zero flow has been assigned to $N_{2,000} = 1.5$ millivolts as Figure 91 indicates. Still, Figure 92 indicates that, relative to the spinner survey, sound carry-away has "smeared' the profile downward somewhat. Nevertheless, the noise log profile is quite acceptable. Equation 11 also shows that more typical injection rates like 2,000 BPD will not raise the noise level in the wellbore by very much. For example, 5 1/2-inch, 17 lb/ft casing has an area of 0.1305 sq. ft, so that with a 1 11/16-inch logging tool A = 0.1305 - 0.0155 = 0.115. At q = 2,000 BPD, equation 11 gives $N_{1,000} = 20$ std. millivolts. Consequently, the tool, even above the perforations, has a resolution for behind-pipe flow that by equation 9a is :

$$\Delta p \times q = 15{,}400 \text{ PSI} \cdot \text{BPD},$$

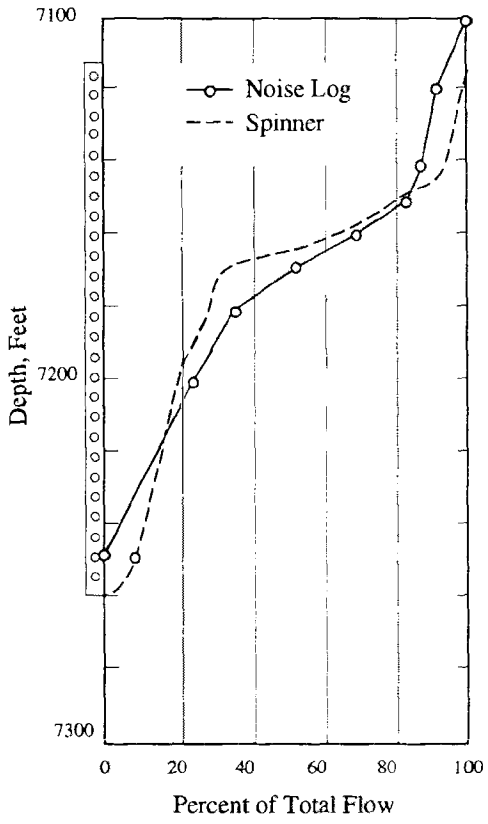

Figure 92. Comparison of noise log and spinner survey injection profile for a rate of 25,000 BPD.

•

while the well is on injection. For a 500 PSI injection head, this is equivalent to a 31 BPD rate behind casing, a value plenty low enough for surveillance purposes. This is obviously not the case when the tool is located in the tubing. Suppose a 1 11/16-inch tool is in 2 3/8-inch tubing. Then A = 0.02171 - 0.0155 = 0.00621 sq.ft. For a 2,000 BPD rate, equation 11 gives $N_{1,000}$ = 6,850 std mv. A packer check is, therefore, not possible with the well on injection. Most injection zones, however, will be over pressured at an injection well itself. Consequently, a packer check can be made during shut-in.

The influence that the dissolution of a small amount of gas that coalesces into rising bubbles or slugs can have on the noise levels associated with water flow outside pipe has already been seen on at least one noise log, Figure 86. Likewise, the log on Figure 82 showed what an even smaller amount of gas flow upward through oil inside the casing could do to the levels. This influence is put on a quantitative basis in the next sub-section.

Gas Flow Through Liquid: The discussion associated with Figure 89 established that gas movement upward through liquid produced a large component of sound in the band $\Delta = N_{200} - N_{600}$ between the lowest two frequency cuts. In fact, for gas rates below about 1,000 ft^3/day at flow conditions, the gas rate is directly proportional to the sound level in this band. The appropriate relationships are:

$$q_{gas} = \frac{N_p \Delta}{2}; \text{ flow behind casing} \qquad (12A)$$

$$q_{gas} = \frac{\Delta}{15}; \text{ flow inside casing} \qquad (12\ B)$$

where q_{gas} = gas rate, cu. ft./day, at downhole temperature and pressure
Δ = $N_{200} - N_{600}$, std. millivolts, noise level between 200 and 600-Hz cuts
N_p = number of pipe strings between tool and flow

These expressions are based on measurements from the same type of apparatus described in connection with Figure 89, and are approximate in nature.

On Figure 86, at the source depth D, 4,800 feet,

$$\Delta = 2 \times (170\text{-}70) = 200 \text{ std mv}$$

The source is at least 2 pipe strings removed from the tool so that

$$N_p \simeq 2$$

From equation 12A $q_{gas} = 2 \times 200/2 = 200$ cu. ft./day

at a depth of 4,800 feet and a temperature of 180 °F (Figure 87). At standard conditions, this rate would be about 150 times larger, i.e.,

$$q_{gas} = 30{,}000 \text{ scf/d},$$

or about 6 scf/bbl of water, which is not an unreasonable value for flashed carbon dioxide.

The log on Figure 82 is the result of a small surface leak through the tubing. At depth in the tubing $\Delta \simeq 2 \times (70\text{-}10) = 120$ std mv. From equation 12 B, $q_{gas} = 120/15 = 8$ ft^3/day. This figure may make the leak hypotheses a bit more palatable.

Vertical Resolution On Noise Logs: Any event may be lost in the background sound or in the carry-away from a nearby peak. No explanation of why this happens was given because the concept is widespread in everyday life. Everyone is familiar with the bedside units that generate synthetic sounds that supposedly mimic pleasing natural sounds such as surf or rainfall, the intent being for these to "drown out" disturbing background noise. Because sound amplitude is oscillatory, the only way that the level from two separate sources could be the sum of the individual levels is for the two sources to be in phase with each other. Otherwise, some destructive interference results from the combinations.

This property of sound creates no problem in the vertical resolution of sources having comparable amplitudes. This fact is demonstrated on Figure 93 that shows the 2,000-Hz cut alone as the tool passes two sound sources of equal magnitude but spaced at different distances apart. Even at the closest spacing shown, 2 feet apart, the two peaks are clearly resolved at a 1-foot sample interval. The resolution would be even better with a sample interval of 0.5 feet.

The problem comes with peaks of unequal magnitude, a situation in which the presence of a small amplitude source is not evident above the residual from another much higher amplitude source. A progression to this condition is apparent at the top peak on Figure 94, which is located ten feet away from a second peak whose amplitude is the larger of the two. In frame B, the top peak at 12 millivolts amplitude is barely evident above the residual from the 56 millivolt peak ten feet away. On frame C, the 5 millivolt peak at the top location is unrecognizable above the 9 millivolt residual from the deeper peak.

The attenuation with distance shown by the sound levels on both Figures 93 and 94 is more rapid than that indicated on Figure 81 (page 122), for sound carry-away because the sources are in the casing with the logging tool and, thus, "blow" directly upon the microphone as it passes.

In order to obtain better vertical resolution, most companies have two more high-pass filters in addition to the normal four. These two pass at frequencies above 4,000 Hz and 6,000 Hz, respectively, and can be switched to two of the voltmeters normally used for the regular four cuts. These two values can, therefore, be added to the normal four numbers at any station. This procedure is illustrated on the flowing noise log of Figure 95. The log was run to profile the

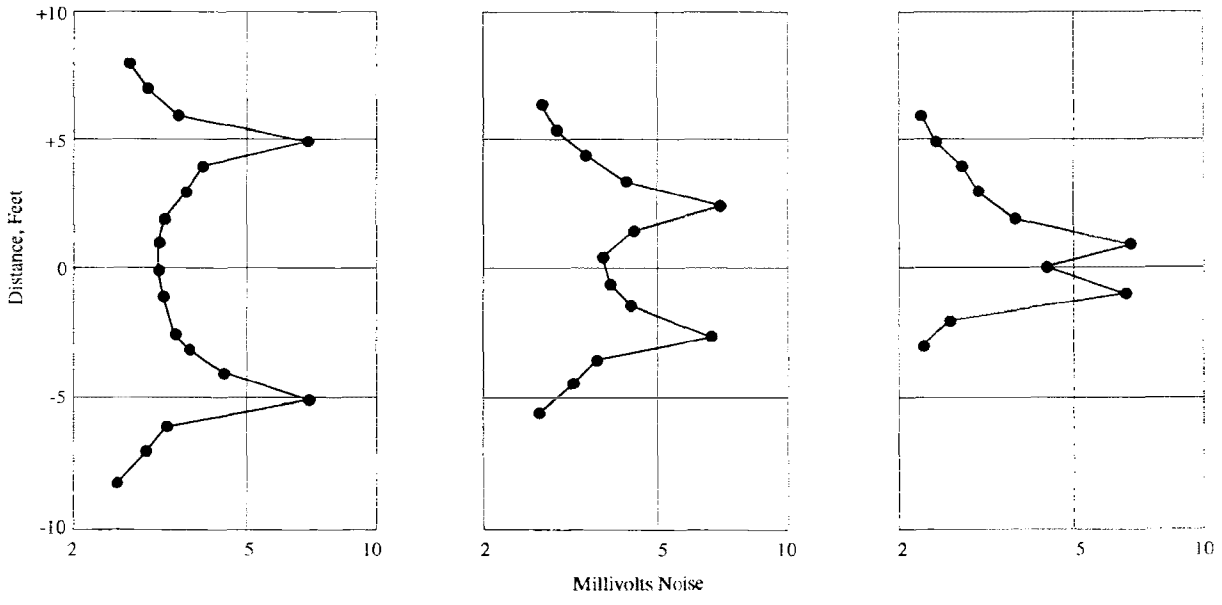

Figure 93. 2000-Hz noise "cut" for two independent sound sources of equal magnitude but different distances apart inside casing.

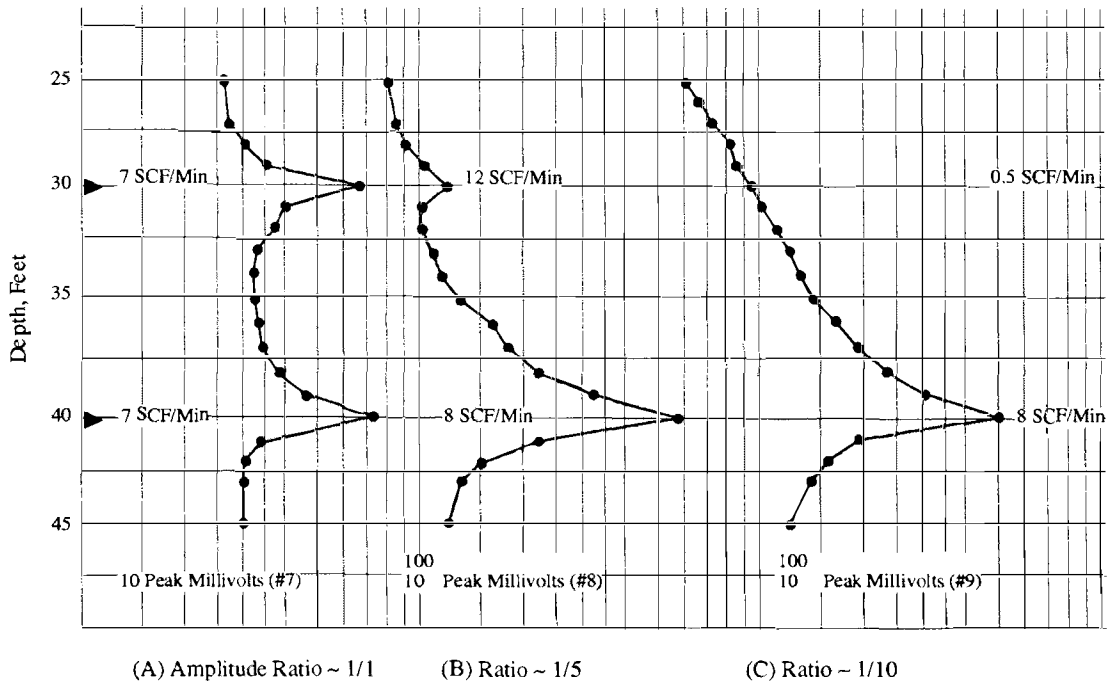

Figure 94. Submergence of weaker source beneath the residual from a stronger one ten feet away. Both sources are inside casing.

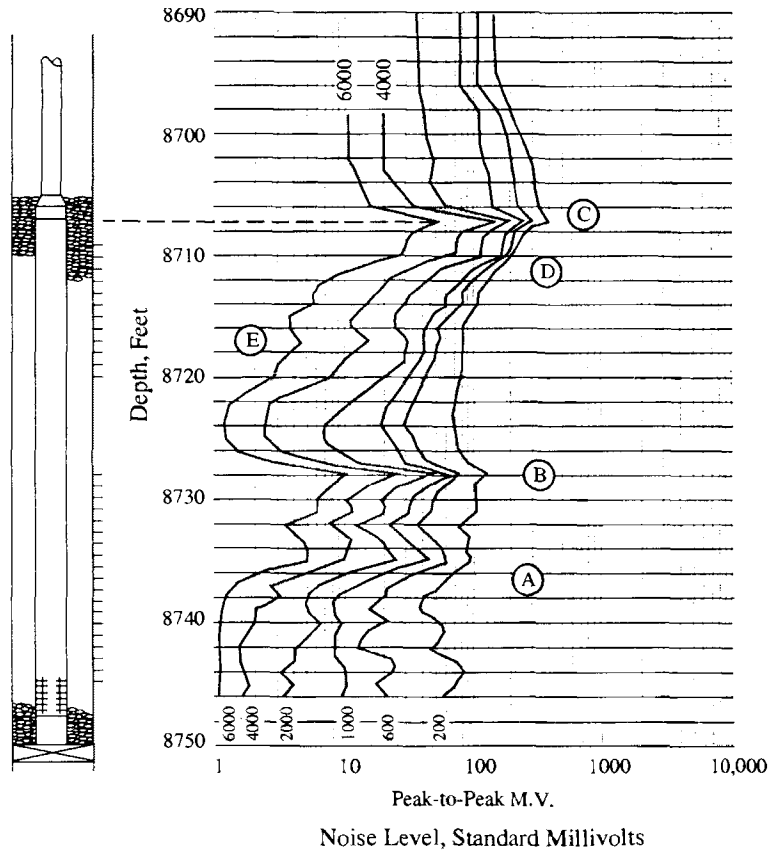

Figure 95. Noise log with 4 and 6-kHz cuts for improved vertical resolution from a gravel-packed gas well flowing three million std. ft³/day.

production of gas from a gravel-packed completion in casing with two intervals perforated. The perforations were logged with 1 foot station intervals at a dry gas rate of 3 million SCF/day. The 4 and 6-kHz values were added to the normal four from 8,698 feet down. None of the six cuts resolve individual peaks very well in the highest productivity interval, AB, over the top half of the bottom set of perforations. However, at depth E, a peak that is just beginning to be ill defined by the 2,000-Hz cut is well defined on the 4,000 and 6,000 cuts. On the latter, a second peak appears just above depth E that is not evident on any of the lower frequency cuts. The entry into the screen at depth C is above the topmost perforations in the casing. This suggests that both the screen and the perforations in the top set may be nearly plugged by fines.

All the material presented so far has been in preparation for the next two sections that deal with the use of the noise survey to demonstrate either injection confinement or the lack of non-related crossflow behind casing. Whereas the radioactive tracer tool is the preferred complement to the thermometer for injection confinement surveys, there are situations where the injection occurs behind the string of pipe in which logging tools must be run. Dual completions, for example, fall in this category. Here, the noise log becomes of use as an inexpensive way of surveying with a tool that does not have to be either "fished" out or cemented in place in the event it is lost downhole.

Noise Surveys For Injection Confinement: Most injection zones are over pressured to some degree. This can be true for wells that do not stand full during injection, that is, for wells that inject on "vacuum." Salt water with a gradient of 0.50 PSI/ft. over-pressures a formation about 40 PSI for each 1,000 feet of water column. Thus, a zone at 3,000 feet will have 80 PSI excess pressure even though the brine level in the wellbore stands 1,000 feet below the surface. Consequently, a noise survey on the injection well shut off of injection will have a higher sensitivity to loss behind pipe to zones above the target interval than will a survey run while injection is in progress. This supposes that the injection rate exceeds about 2,000 BPD. At rates no larger than 2,000 BPD, an injecting survey will be more sensitive. As with all generalizations, these can be wrong. They are given to justify to the reader that, like the other tools discussed, noise surveys should also include both injection and shut-in surveys if the tool is used to evaluate confinement. Unlike temperature surveys, shut-in noise logs can be run as soon as injection ceases.

The best way to proceed from here is to simply examine cases of both confined injection and unconfined injection.

The noise survey of Figure 96 was run with a well on injection at a rate of 10,800 BPD and 1,400 PSI tubing pressure. Two intervals are targeted for injection as indicated on the figure. The survey shows all the injection entering the top portion of the top set of perforations. Within the tool resolution, there is no indication of flow upward behind pipe from the perforations. The signature is thus one of confinement to the top zone. Above the perforations, the noise level is N1,000 $\simeq$ 1,200 std mv whereas the net injection head at the 1,400 PSI tubing pressure is about 1,250 PSI. Equation 9A indicates a rate resolution behind pipe of:

$$q \geq 1100 \times \frac{1200}{1250} \approx 1100 \text{ BPD},$$

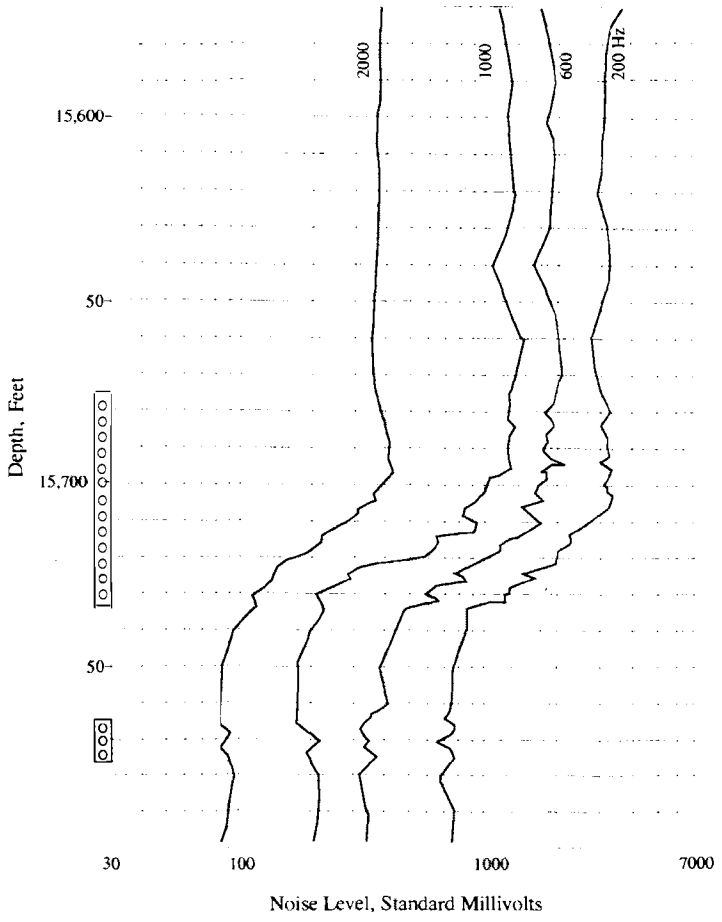

Figure 96. Noise survey with well on injection at 10,800 BPD and 1,400 PSI. Casing is 7-inch, 29 lb/ft and tool is 1 1/2-inch.

or about 10% of total rate. The behavior of the 2,000-Hz curve indicates that this may be a conservative estimate, however. The speed up of exiting water is evident by the increased level over the entire top half of the upper set of perforations. This suggests that by adding the 4,000 and 6,000-Hz cuts, we could obtain excellent sensitivity to behind-pipe flow even while injecting at this high rate.

The cross-sectional area of the 7-inch, 29 lb/ft. casing is 0.2085 ft^2 whereas the tool cross-section is 0.0123 ft^2. Thus, in equation 11, A = 0.2085 - 0.0123 = 0.1962 ft^2. Therefore,

$$N_{1000} = 3.3 \times 10^{-11} \times \frac{(10{,}800)^3}{(0.1962)^2}$$

$$N_{1,000} = 1{,}080 \text{ std. mv.}$$

as compared to the measured value $N_{1,000}$ = 1,200 std. mv. Note also that this value is only about 1/3 the value of the 200-Hz cut. The dominant frequency is in the 600-1,000 Hz range for the inside casing flow. As a result, the four cuts are more spread out relative to each other.

The four cuts are even more spread out on Figure 97, a noise survey with the rate reduced to 5,000 BPD. The dominant frequency at this rate is near 600 Hz. The injection is again seen to be confined to the upper portion of the top set of perforations with no indication of loss behind pipe from the top interval. The movement behind pipe within the upper half of the top perforations is even more evident on the 2,000-Hz curve of Figure 97. Also, some fluid acceleration in this same location is now evident on the 200-Hz curve. Obviously, the sensitivity to flow behind pipe is greater at this lower rate. Above the perforations, $N_{1,000} = 150$ std. mv. whereas the injection head has dropped to 575 PSI; consequently, equation 9A predicts

$$q \geq 1100 \times \frac{(150 - 6)}{575} = 280 \text{ BPD},$$

as compared to 1,100 BPD at 10,800 BPD. Again, this figure is conservative given the behind-pipe noise evident within the perforations. Still, it is only 5.6% of the injection rate.

The flow noise from 5,000 BPD inside the casing is given by equation 11 as $N_{1,000} = 110$ std. mv. as compared to the measured value of 150 std. mv.

On both figures 96 and 97, the sound levels below the perforations do not decay very rapidly. The levels reduce to about 20%-30% of the peak values at a distance of about 50 feet and then

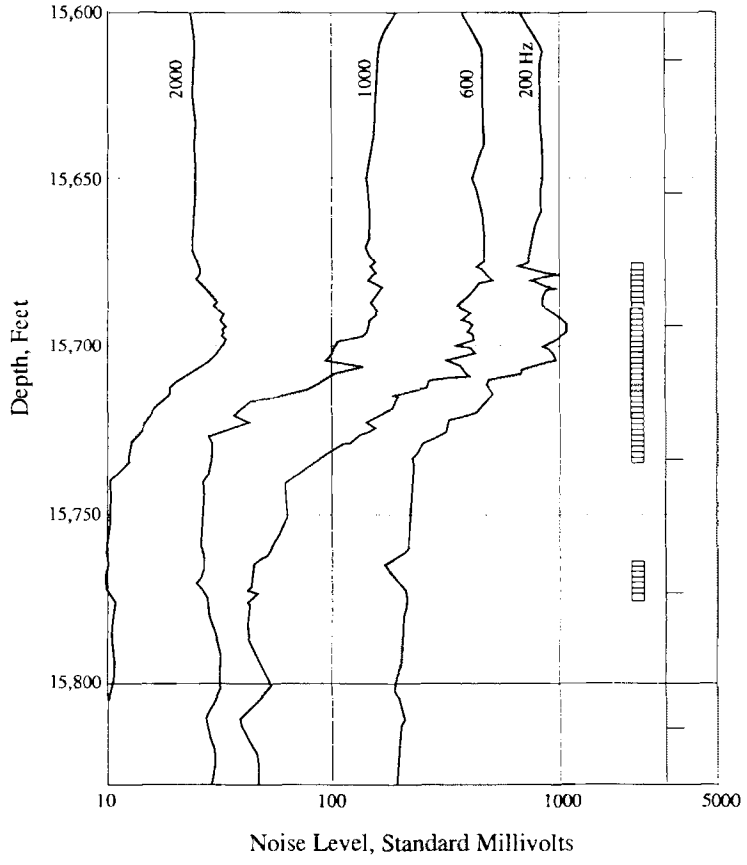

Figure 97. Noise survey from well of Figure 96 with injection rate reduced to 5,000 BPD.

settle down at relatively constant levels. This behavior is not in accordance with the carry-away pattern depicted on Figure 81 for behind-pipe sources. In fact, the residual levels on figures 96 and 97 are the result of waveguide transmission away from the flow noise source inside the casing above the perforations. A level at about 20% of full flow noise is typical of the mode of transmission in water.

When the injection well was shut in, the water level in the 3 1/2 inch tubing dropped to a stable level that placed 135 PSI excess pressure at the injection zones. The noise survey of Figure 98 was then run. This survey included a "packer check" as well as a "channel check." At a background noise level $N_{1,000} = 1.5$ std. mv., equation 10 establishes a leak rate resolution of

$$q \geq 700 \times \frac{1 \times 1.5}{135} = 8 \text{ BPD},$$

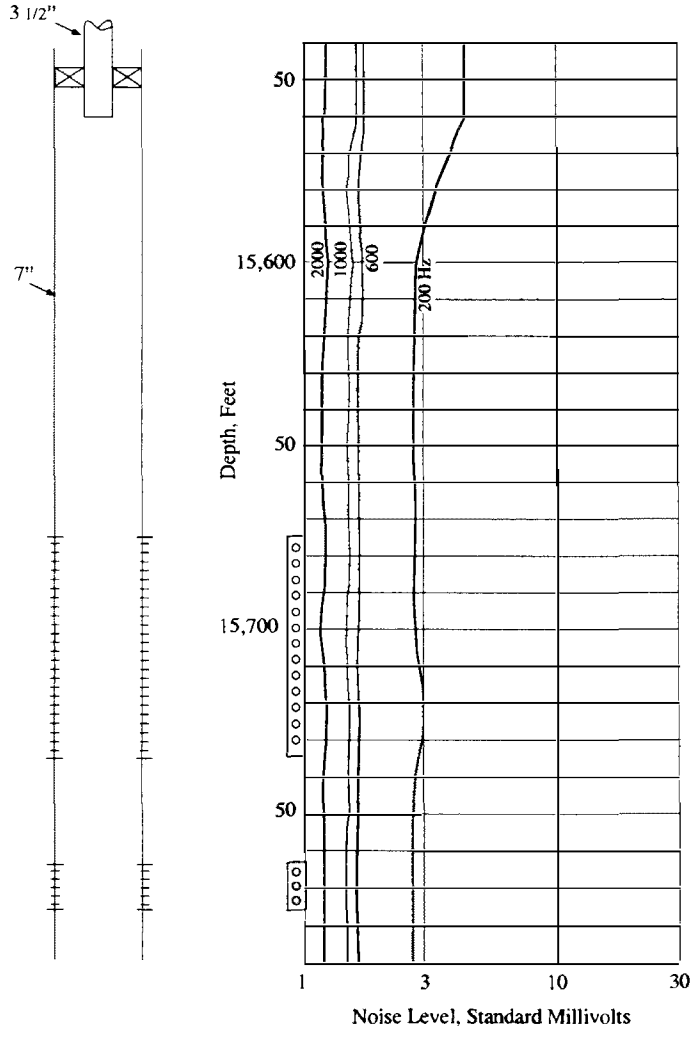

Figure 98. Shut-in noise survey on Figure 97 well with 135 PSI excess pressure on injection zones.

a value that shows the advantage of having charged the zone above normal pressure. Had this not been the case, the injection rate could have been further reduced to about 1,000 BPD and the well surveyed while on injection. At this rate, the flow noise at 1,000-Hz would be about at the 1.5 std. mv. background level.

The next example involves an injection well that is about one year old. Current injection rate is 5,000 BPD at some 200 PSI net injection head. This particular well had been acid fractured in an attempt to insure that injection reached all three zones perforated, either inside or outside the 7-inch, 32 lb/ft casing. Flowmeter and temperature surveys appear on Figure 99. Note that the temperature surveys include both injection and shut-in passes and the shut-in times include both short and long times. The latter, at 28 hours, is in the recommended range listed in Table 3 for a 1 year old injection well. The spinner survey on frame A of Figure 99 shows that all the injection leaves the wellbore over the upper half of the top perforated interval with nothing,

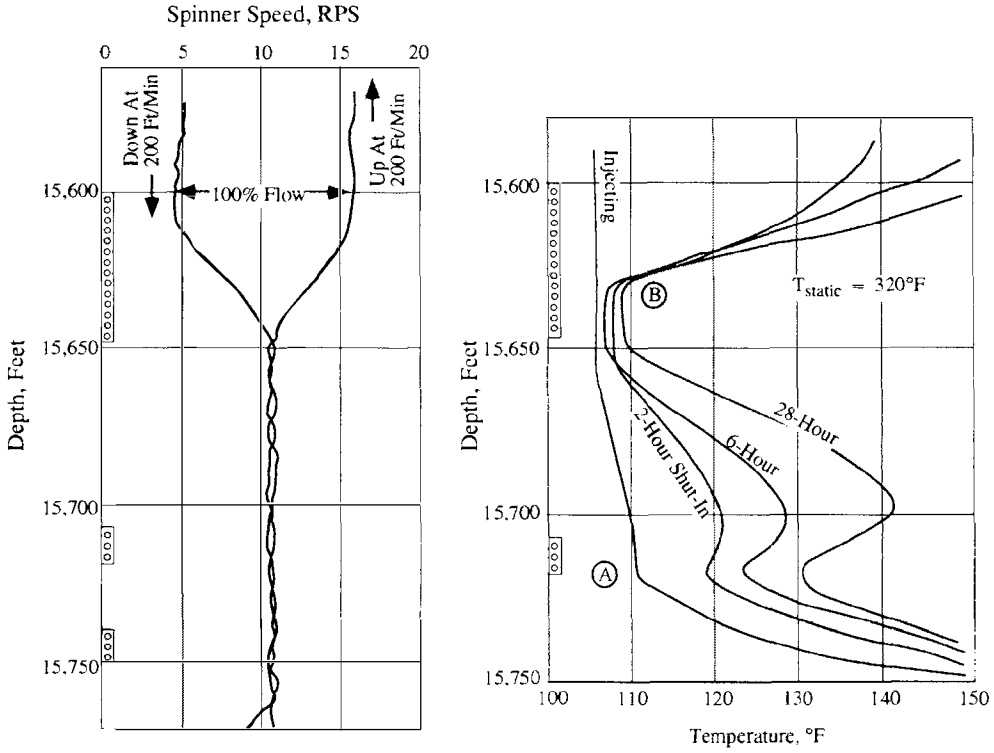

(A) Spinner Survey on Injection

(B) Temperature Surveys Both on Injection and Shut In

Figure 99. Surveys on a one-year old injection well with a current injection rate of 5,000 BPD.

within tool resolution, reaching the lower two intervals.

The temperature surveys on frame B of Figure 99 show that, although most of the injection stays in porosity located in the lower part of the top perforated zone, some of the injected water reaches the perforated interval just below 15,700 ft. Slopes on the injection temperature survey correspond to about 10% of the total rate, or 500 BPD, flowing to this depth. As this amount is within spinner resolution, we would conclude that this flow occurs in an acid fracture outside the 7-inch casing.

This outside-of-casing flow is confirmed by the noise survey of Figure 100, run with the well on injection at about 3,500 BPD. The behind-casing flow is clearly evident on all cuts at levels above the noise created by the flow inside casing. The level created on the 2,000-Hz cut by the flow outside is at some locations nearly 3 times the level from flow inside even though only about 10% of the total gets behind the casing.

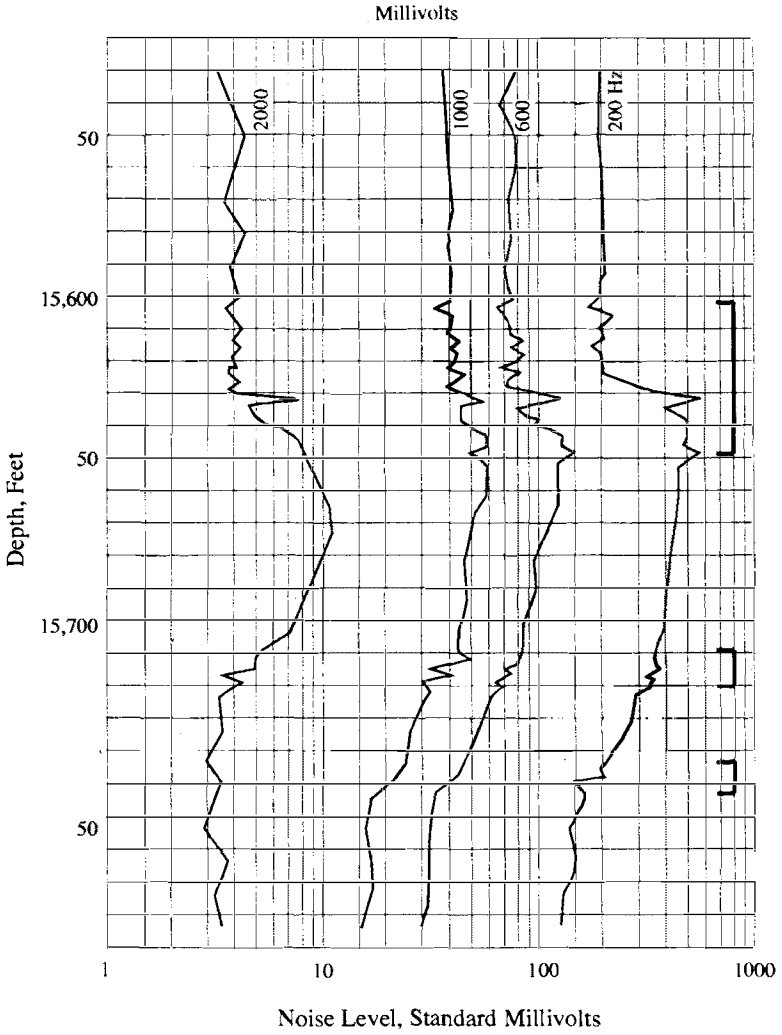

Figure 100. Noise log from well on water injection at 3,500 BPD with a flow of about 350 BPD behind casing from top perfs to the zone at middle perfs through an acid frac.

The curve with the best vertical resolution, the 2,000-Hz cut, shows that the behind-pipe flow stops at the middle set of perforations. Someone looking at the lower frequency cuts might be tempted to carry on to the bottom perforations, yet the levels on all cuts at this location are close to the expected carry-away levels from the chart on Figure 81 for large pipe and a 30 ft distance between the 15,700 ft. location and the bottom interval.

Another feature evident on the noise log of Figure 100 is the way statistical variations in flow sound take on an "air" of importance whenever the sample density increases. This is dramatically illustrated by the apparent activity on all cuts in the record over the top 20 feet of the upper perforations relative to the activity above, where stations are more widely spaced. Within the 20 feet, the same variance is being sampled more often than above, yet it "looks" more significant. The spinner survey on frame A of Figure 99 clearly shows that very little flow is lost from the wellbore over the top 20 feet of perforations, however. This is verified on the noise log by the fact that the average level on any cut within the top 20 feet of perforations is no different from the level above.

An example of a casing leak appears on the noise log of Figure 101, which was run in a shut-in injection well completed as shown with a 9 5/8 inch injection "string." The well had the same 840 PSI shut-in pressure on both the 9 5/8 inch "tubing" head and the 9 5/8 x 13 3/8 inch annulus. The purpose of the logging was to find the location of the leak in the 9 5/8 inch injection string. The noise tool was dropped to a depth of 4,000 feet and a reading taken with the annulus pressure undisturbed. As the points on left-hand side of the log show, the sound level was at ambient value. The actual readings ranged from 0.22 to 1.5 millivolts at one-fifth of standard sensitivity, or from 1.1 to 7.5 standard millivolts. The annulus was then opened sufficiently to flow 300 BPD water with a small amount of gas. The noise level at 4,000 feet increased to the values shown on the right-hand side of the log on Figure 101. These high levels are quite obviously not the result of a 300 BPD water flow past the tool. At 4,000 feet, the noise band

$$\Delta = N_{200} - N_{600} = 450 - 100 = 350 \text{ mv}$$

has more amplitude than everything above $N_{1,000} = 50$ mv. This, of course, is the signature of gas moving upward through liquid. The high noise levels are thus the result of gas dissolution from the water. In terms of standard units:

$$\Delta = 350 \times 5 = 1{,}750 \text{ std mv}$$

According to equation 12B

$$q_{gas} = 1{,}750/15 = 117 \text{ ft}^3\text{/day}$$

at the pressure and temperature existing at 4,000 feet. This would correspond to about 16,000 std. cu. ft./day, which is not much gas.

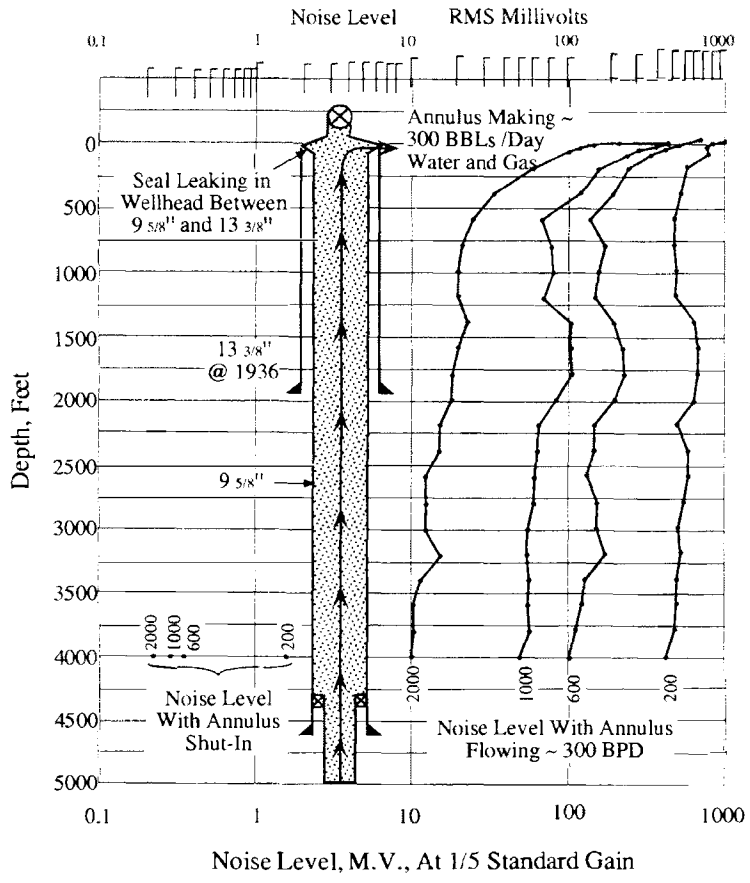

Figure 101. A shut-in noise survey on an injection well with leak in hanger assembly of wellhead.

With the annulus on flow, the well was logged upward from 4,000 feet on 200-foot station intervals without any decrease in levels all the way to the surface. The leak is therefore in the seal assembly of the wellhead itself.

Noise Surveys For Noninjection Related Flow Behind Pipe: Logging for noninjection related crossflow behind pipe is done with the well-shut-in. Under these conditions, some portions of the wellbore should be at ambient or dead-well levels on every log. Thus, a quality control check is available on the log itself. One has the background level for use in the rate resolution estimation available from equation 10. Suppose, for example, that the background is $N_{1,000} = 3.8$ std. mv. and that the polluting zone is 70 PSI higher in pressure than the depleted zone into which it crossflows. Then $\Delta p = 70$ PSI in equation 10 and the tool would have a resolution of :

$$q \geq 700 \times 3.8/70 = 38 \text{ BPD}$$

for flow immediately behind the casing string containing the sonde, i.e., for $N_p = 1$. If the tool is located in tubing which is inside casing with the leak outside the casing, then $N_p = 2$ and the resolution is only 76 BPD. The background level would have to be further reduced if the resolution is to be improved. This may not be possible in some situations; consequently, at pressure differences below 100 PSI, the noise tool resolution will generally not be as good as that available from the temperature tool.

Example noise logs from shut-in wells with water flow behind pipe at rates from 20 BPD up to 5,000 BPD have already been examined on figures 79, 85, and 86. Consequently, only one more example of non-related flow is considered.

This example involves a well that had been sitting closed in for some 6 months after drilling and cementing of production casing had been completed. During this time, 70 PSIG of water pressure built up on the annulus between 5 1/2 inch production casing and 8 5/8 inch surface casing. With the annulus open and the pressure at 0 PSIG, the well would flow water at approximately 400 BPD. The source of this flow was to be identified before a workover was undertaken. For this purpose, a combined temperature-noise survey was conducted. Static surveys were run one day, then the well was relogged the next day with the annulus flowing. The program called for the entire 4,500 feet of wellbore to be logged. Stations 100 feet apart were used for the course noise log grid. This was to be reduced to 20 foot stations for 100 feet on either side of the calculated top of cement at 2,500 feet behind the 5 1/2 inch production casing. This would leave at least five station stops for detailing across the 8 5/8 inch shoe at 300 feet or wherever necessary. The shut-in noise log showed only dead-well levels, the four cuts "straddling" the 1 mv. level. The log run with the annulus on flow at rates from 340 to 520 BPD is shown on Figure 102. At the bottom of the well, the 1,000-Hz and 2,000-Hz levels have settled down to values close to the ambient levels from the previous day. The two lower frequency cuts at 600 Hz and 200 Hz are still decaying from higher levels above.

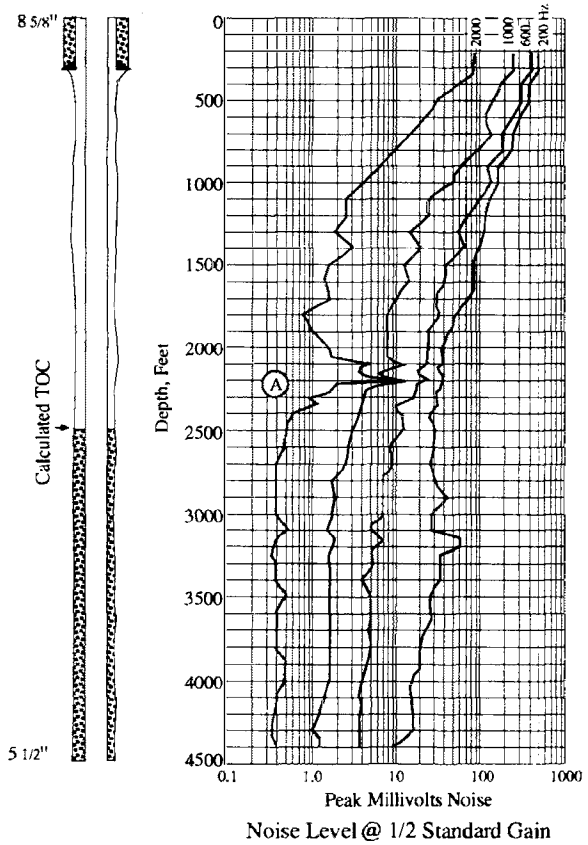

Figure 102. Noise log with water flow at surface of ~ 400 BPD from 5 1/2 x 8 5/8 annulus under 70 PSI differential.

The source of flow was detected before the cement top was reached and the detailed logging was done at depths of 2,000-2,300 feet. The 2,000-Hz curve shows two peaks in this interval, one at 2,100 feet and the other at 2,200 feet. Above 2,100 feet the 2,000-Hz curve does not decay back to ambient value before it becomes influenced by carry-away from the largest sound source, which is the flow through the annulus valve at the surface.

From the relative positions of the 1,000 and 2,000-Hz readings at 2,200 feet, depth A of Figure 102, the dominant frequency of the source is 2,000-Hz or higher. Likewise, the peak at 2,100 feet depth shows a dominant frequency closer to 1,000 Hz. Consequently, there is a single-phase flow of water alone, according to the discussion related to Figure 89. Note, however, that these two peaks do not show on the 200 and 600- Hz curves. The carry-away from the source at the surface is concealing the peaks on these two cuts! The shallowest measurements on the log are at 200 feet. The levels at 1,200 feet are generally in agreement with the 1000-ft. residuals as predicted by the lines on Figure 81, for 4 1/2 inch pipe.

The values on Figure 102 were recorded at one/half standard sensitivity on a truck whose reel contained 17,100 feet of 7/32-inch logging cable. For this cable length, Figure 80 gives the following correction factors:

$$F_L = 1.30 \text{ at } 1{,}000\text{-Hz},$$

$$F_L = 1.55 \text{ at } 2{,}000\text{-Hz}.$$

The corrected readings at the two peaks on Figure 102 are therefore:

$$\text{at } 2{,}100 \text{ ft.} : N_{1000} = 12 \times 2 \times 1.30 = 31 \text{ std. mv.}$$

$$\text{at } 2{,}200 \text{ ft.:} \; N_{1000} = 13 \times 2 \times 1.55 = 40 \text{ std. mv.}$$

These are the values needed in equation 9A along with $N_p = 1$, $\Delta p = 70$ PSI, to give

$$q = 1{,}100/70 \times [(31-6) + (40-6)] ,$$

$$q = 927 \text{ BPD} ,$$

whereas the actual rate was closer to 500 BPD. As was mentioned in connection with equation 9A, a factor of 2 is not unusual.

A rate resolution can also be estimated from the log on Figure 102. The 2,000-Hz cut could drop to 0.5 mv. on the log before being lost in background. Thus, the peak value of 9 mv. at depth A, 2,200 ft., could drop by a factor 9/0.5 = 18. For the same pressure differential of 70 PSI, the rate resolution is:

$$q \geq 500/18 = 28 \text{ BPD} ,$$

a value not too different from the 38 BPD previously estimated.

Temperature surveys from the well appear on Figure 103. The log taken with flow from the annulus shows production that commences at a depth of 2,250 feet. This location is at the bottom of a water sand according to the open-hole logs from the well. Likewise, the noise log spike at 2,200 feet is already at the top of this sand. The sound sources are apparently at locations where the borehole wall has collapsed around the casing.

The character on the flowing survey of Figure 103 is the result of the unsteady rate as noted on the curve. A comparison of the shut-in and flowing surveys shows no flow from below depth B, 2250 feet. Although the surveys are separated by about 3 °F, they track each other perfectly below depth B. The separation is most likely an operator inconsistency in "log scaling," that is, in setting up the log scale relative to the temperature measurement with the tool stationary at the top of the well. Alternately, the difference may be the result of the need to "manually shift" the recording pen several times to accommodate the 70+ degree range. Each time the trace starts off scale to the right-hand side of the chart, it is shifted back to the left-hand side of the chart. On "analog" trucks this process is accomplished by hand, so if the trace wanders a bit off-scale before the operator notices, then absolute error can creep into the record. This is of no consequence so far as interpretation is concerned.

The important point is that the "anomalies" need not be at the same location on the temperature and the noise surveys whenever the flow is behind casing.

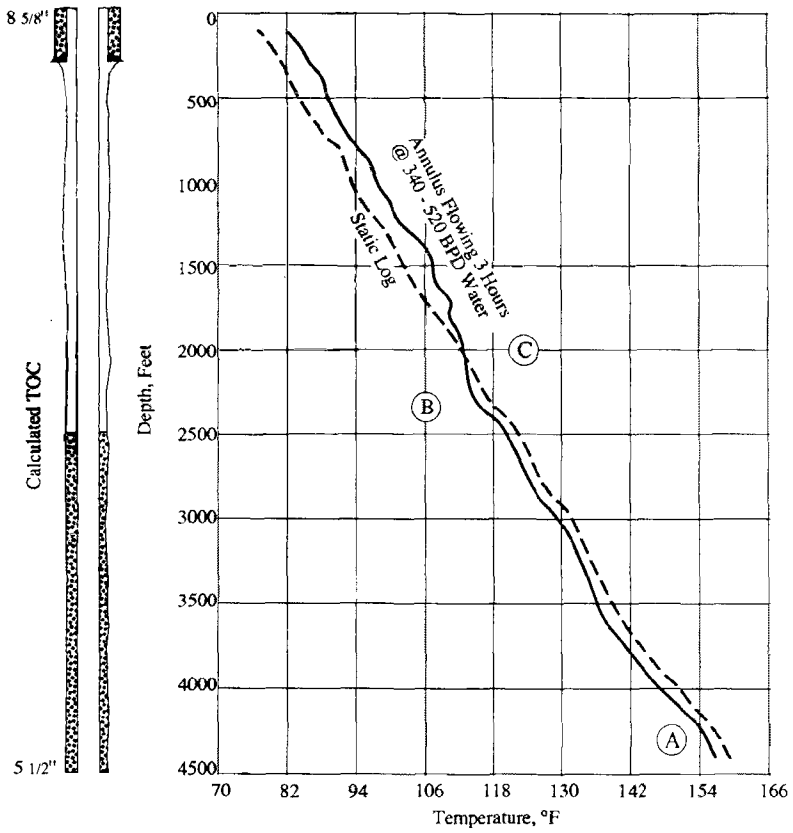

Figure 103. Temperature surveys run one day apart, first with annulus shut-in at 70 PSIG and then with annulus on flow at 340-520 BPD water.

The temperature survey would have been even more influenced by the non-related flow had it been run when pressure first appeared on the annulus. At this time the well was less than one month old and was still disturbed from static. The movement of water to pressure the annulus would have returned the temperature to static at depth B, 2,200 ft., even on a shut-in log.

In the U.S., normal water sands in an area with hydrocarbon production can become overpressured because of blowouts on wells being drilled and as a result of leaks from oil or gas wells already in existence. Noise logs showed gas-in-water flow signatures that conformed to the pattern shown at the peak in frame B of Figure 89. There is an exception to this signature that is described in the next section.

Attenuation by Gas Dispersed in Water: The signature demonstrated on frame B of Figure 89 and on the actual logs of Figures 86, and 101, is the result of the buoyant movement of gas through water. If there is no relative movement, then the source of noise is not present. This can happen when gas that comes out of solution in water remains dispersed as small bubbles in the water and moves with the water. Even worse, a dispersion of this type is "dead" acoustically in that it attenuates severely the frequencies employed in noise logging. This phenomenon is easily demonstrated by means of a glass of water, a spoon, and an "alka-seltzer" tablet (a chemical source of carbon dioxide). First, tap on the side of the glass with the spoon to hear a clear ring in the form of a bell-like "ding, ding, ...ding." Now drop the "alka-seltzer" tablet into the glass of water, at the same time continuing to tap the side with the spoon. The tablet hardly drops below the water's surface before all the "ding" is gone and your tapping produces only a hollow sounding "thunk, thunk,...thunk."

The noise log on the top, frame A of Figure 104, illustrates the deadening influence above the water entry into the wellbore at depth B. When the watered-out well is on production at 3,830 BPD water, gas that comes out of solution is swept along with the high velocity water and remains dispersed as small bubbles in the water. This fact is evident from the relative attenuation on either side of the peak due to entry at depth B on frame A. Below this depth, the log shows normal carry away from the peak. In contrast, the sound levels above depth B quickly attenuate to low levels that are less than those caused by water alone at 3,800 BPD.

All the frequency behavior on frame A is that of single-phase flow. However, with the well shut-in, the entry appears on frame B at depth A as a normal gas in-liquid signature. At a reduced water velocity, the gas bubbles have time to coalesce and move relative to the water. In this example, we have a situation in which a lower rate of water flow could create more noise than would a higher rate.

The same type of behavior can occur at the source of non-related water flow behind pipe. This is illustrated by the next example. The problem is water pressure on the 4 1/2" x 8 5/8 " annulus of a new well that has no production tubing. When opened, the annulus flows brine at rates approaching 1,000 BPD. A disposal zone located at about 4,500 feet was suspected as the brine source. A flowing temperature log was provided in frame A of Figure 105. The rate of flow from the annulus at the surface was 823 BPD average with ± 100 BPD fluctuations. The temperature survey shows at depth A, 4,360 feet, the warming that is caused by water flowing to

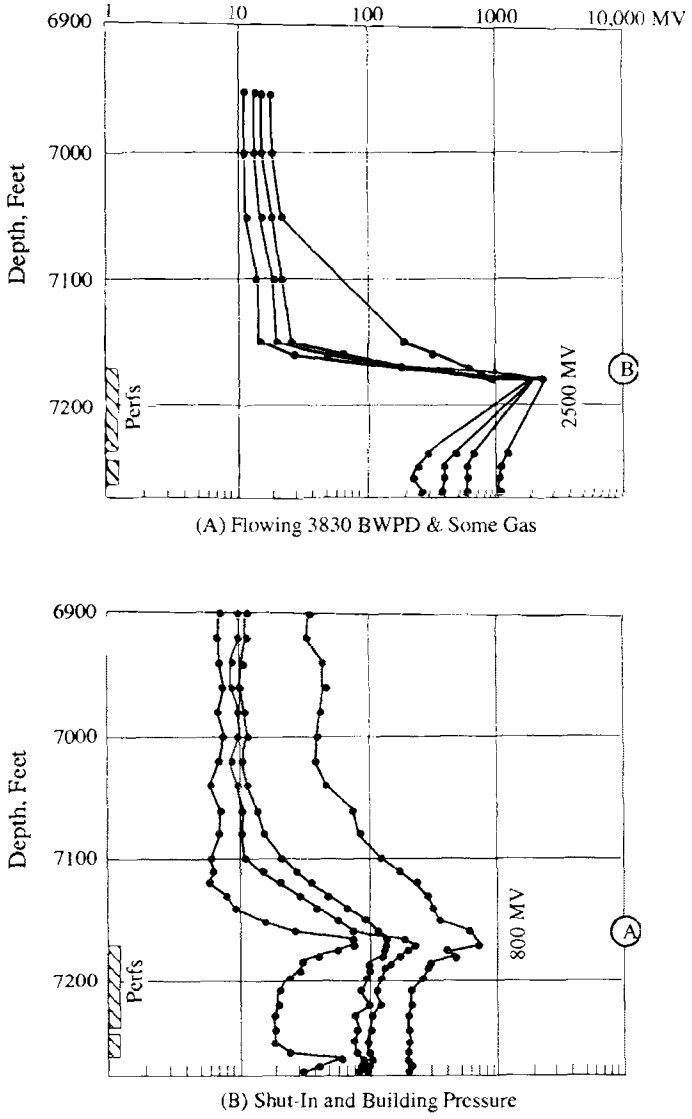

Figure 104. Noise logs, flowing and shut-in, from a watered out-gas zone produced to hold back water.

the wellbore of a new well that is still to the cool side of static. This source is nearly 200 feet above the disposal zone, but the latter was still "suspect" because it was the "only pressured zone around." The noise log on frame B shows what the actual situation is. A compact depth scale is used on the noise log to better show the rapid attenuation above the source, depth A, relative to that below this depth. Note also the low signal levels. The noise log signature is that of gas dispersed in water. The zone at 4,360 feet has been over pressured as a result of having been charged with gas at some other location, presumably from a blowout on a well being drilled. This is another situation in which lower rates of flow would give higher noise levels. At 800 BPD rate, the brine made it all the way up to 1,000 feet before enough gas had coalesced to give a gas-in-liquid signature on the noise log.

In closing the treatment of the noise logging tool, the topic of quality control must be discussed so as to "rehash" comments already made and to add some new ideas not yet introduced.

Quality Control Revisited: Quality control in noise logging is perhaps more subtle in some ways than it is for the temperature and radioactive tracer tools. Poor quality can occur in spite of the best of intentions. For example, compare again the logs on Figures 105 and 88. The latter looks like the better quality of the two, but it actually is not. The station sampling interval of 100-foot stops on the log of Figure 105 was designed to accommodate the 4,500 feet of wellbore with at least 15 stations on closer spacing about the cement top or the 8 5/8" shoe as needed. As things developed, the close spacing was actually used on either side of the source depth A. The procedure, thus, adapted to the situation. On the other hand, the well on Figure 88 (page 130) is surveyed on a constant interval density of one measurement every 50 feet. With over 7,500 feet of wellbore to potentially survey, a total of 150 measurements would be needed, which is more than can be done in a normal day. Consequently, the operator ran out of time before he ran out of hole! He never got to the source of the gas blow at the surface. A better quality sampling scheme would use a coarse density with 200 foot intervals to within about 200 feet of the estimated top of cement. Then the interval could be reduced to 50 feet across the cement top and past the 8 5/8-inch shoe. This would have shown that the source was below the cement top. The interval could have been increased again to 200 feet to total depth with a second fine density where the deepest peak appeared. Detail can always be added at locations where it is needed.

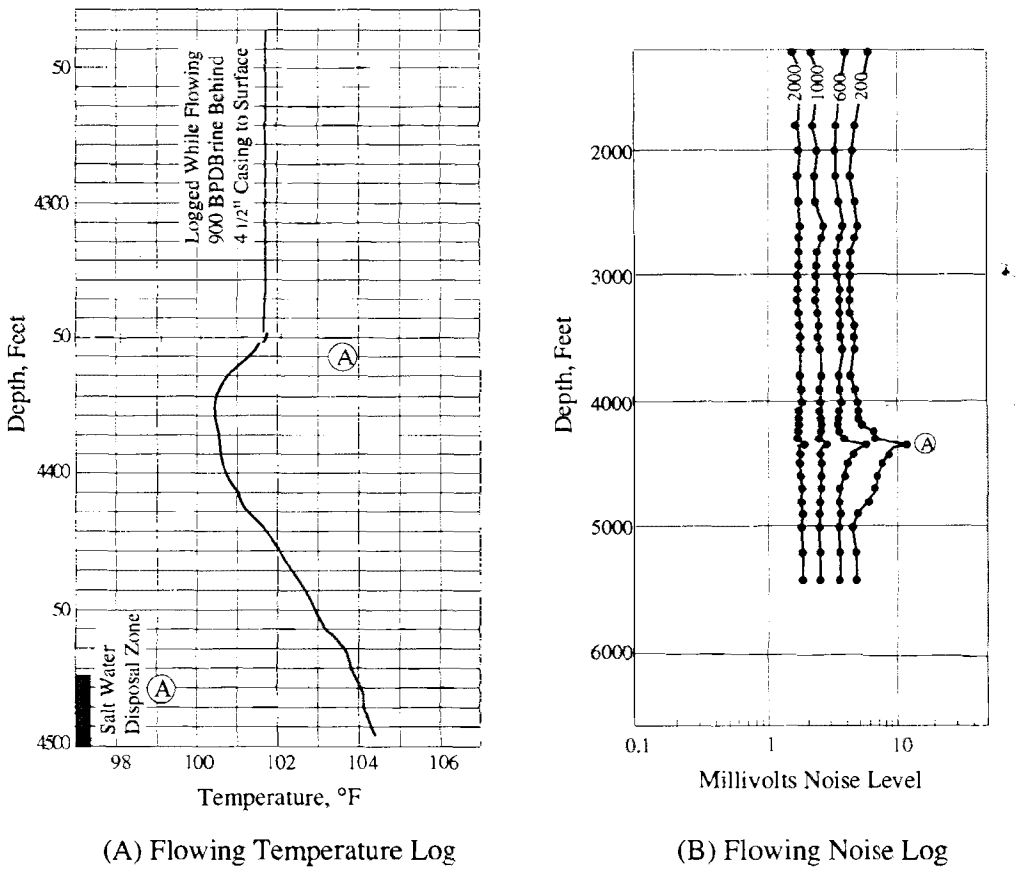

(A) Flowing Temperature Log

(B) Flowing Noise Log

Figure 105. Temperature and noise surveys from a shut-in well with an 800-BPD water flow behind 4 1/2-inch casing from 4,360 feet to the surface.

Another example of poor quality spacing appears on the two logs of Figure 106. These logs are from a dual tubingless, gas well that has pressure on the annulus. Both production strings were shut off production overnight before the logging, which was done in the longer of the two, string H. The liquid level in the annulus is evident on both logs, at depth A on the log of frame A and at depth B on frame B. This means that there is flow in the annulus in both cases although the annulus was shut-in for the log on frame A. The completion picture on the left-hand side of Figure 106 shows three locations that require logging on close station spacing: the shoe at 1,500 feet, the estimated top of cement at 3,000 feet, and the F-string perforations at 4,160 feet. If 30 measurements were devoted to these locations, then about 30 more would be left for a coarser density. With a potential 6,000 feet to survey, the latter density would require station intervals of 200 feet spacing each. The resulting seven measurements in interval from the top of the well to the 1,500-foot shoe would have given plenty of detail over a location where no sound sources are expected anyway. Instead, the operator expended 25 of his stops in this part of the well. The rest of the well will, of course, be inadequately covered. He zips across the cement top on a 500-

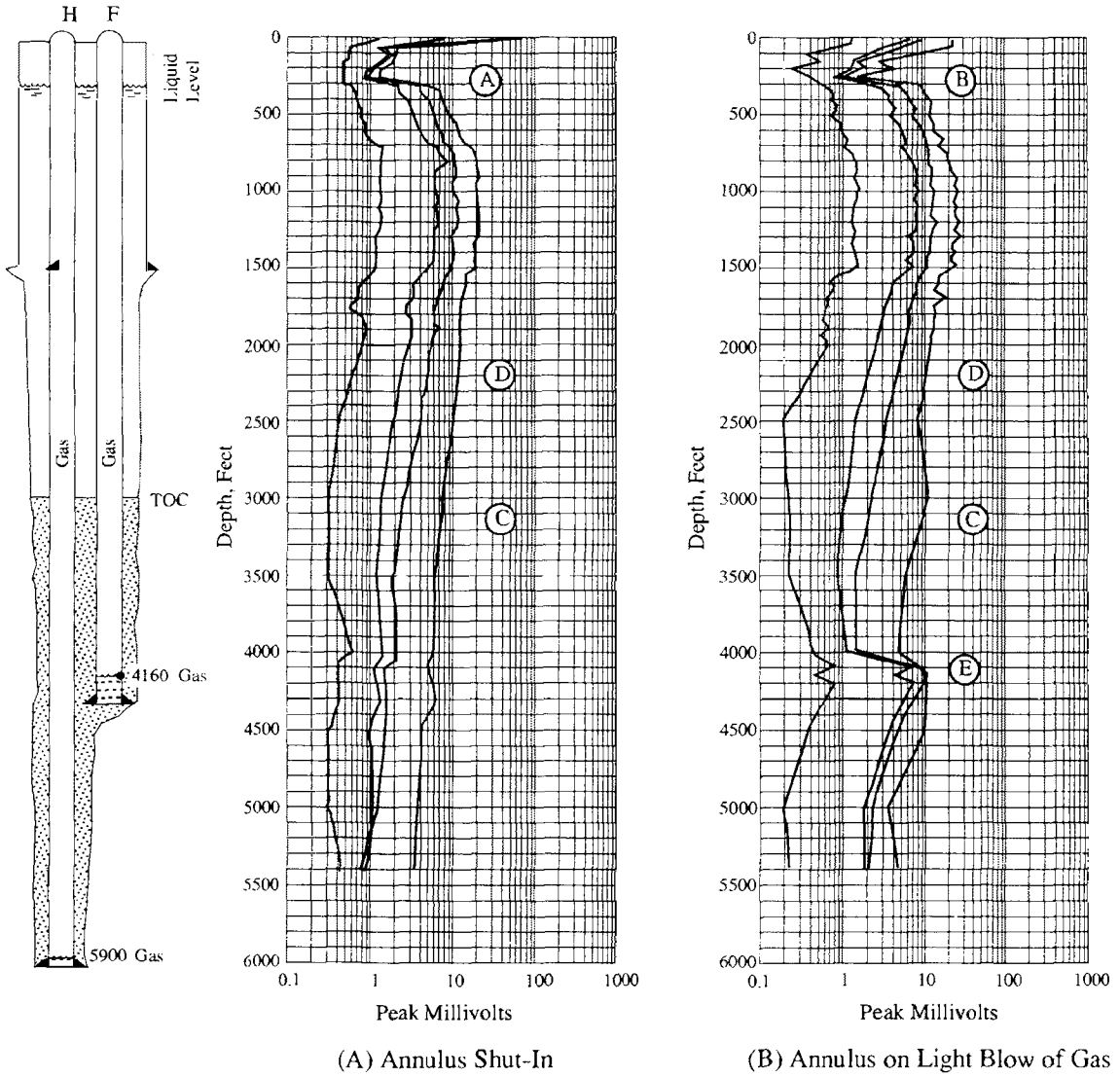

Figure 106. Noise logs from long string, H, of shut-in gas well with pressure on annulus.

foot interval. The behavior at the two stations at 2,000 and 2,500 feet "cries out" for more detail over the interval. The 2,000-Hz cut shows that the stations straddle a source. This is most likely a charged zone that is maintaining the annulus pressure.

A comparison of frames A and B shows that the operation of venting the annulus starts a small amount of gas moving at the liquid level at the perforations in the short string, depth E of frame B. Again, the definition is poor at this location because of the widely spaced measurements, but this behavior means that there is probably a small tubing leak someplace above the cement top. This may be the source of noise missed at depth D. Overall, the logging leaves us not quite sure why there is annular pressure on the well.

The above losses in quality resulted from poor planning before actually logging. Other losses can occur during actual logging. It has already been seen what leaks in the lubricator can do to the quality of a noise log. Flow line leaks can do the same thing.

Tool movement during measurement is another common type of noise pollution, particularly for operators who allow computers to do the logging and never actually listen to what they are recording. A little reel creep can generate a lot of noise. Wind gusts at the surface can also cause the lubricator to sway and move the tool. When a well is logged from the floor of a drilling rig, the top sheave, or wireline pulley, is customarily attached to the travelling block and pulled up about 20 feet above the rig floor. This creates a long pendulum, from the travelling block to the crown block, to "swing in the breeze" from wind action on the surface of the travelling block. If a noise log is to be run, it is a good idea to pull the travelling block with sheave to the top of the derrick near the crown so that the pendulum swing is reduced to a minimum.

Some noise sources cannot be eliminated. The situation leading to the log of Figure 102 is one such case. The variance on this log is higher than desirable on all the cuts. This is particularly evident on the log at 3,000 ft. and is the result of flow instability induced variance in the large sound source created by the surface venting operation. The unstable flow is, unfortunately, a fact that cannot be changed.

Likewise, the motion of a fixed platform offshore causes the drilling template on bottom to grind against the casing of wells completed through the holes in the template. On a calm day, this level is low enough for logging to be done. By a depth of 1,500 feet or so, the background will have decayed to the normal ambient levels of about 1 millivolt. In rough weather, this noise will carry down many thousands of feet, however.

If the logging is done from a floating vessel, such as a drillship or a semi-submersible rig, the only thing that can be done is to take measurements at the trough and crest of each heave when the tool is momentarily stationary.

The sound of the grease injection pump that pressures the leak control held on top of the lubricator will carry down several hundred feet. Consequently, the top portion of a well is logged when the pump is not running.

Good operators quickly learn about the things discussed above, but one cannot depend on having experienced people anymore, no matter what company is used. In fact, the customer himself must assume responsibility for the quality of any production survey he runs, not just for noise surveys.

Summary of Procedures for Temperature, Radioactive Tracer and Noise Surveying

The procedures listed in Table 9 are intended to serve both the well operators need for injectivity information and the regulatory agency's need for integrity information. Any particular situation may, therefore, require only a certain part of a given procedure. The appropriate part can be identified from the column in the table that tells what the corresponding logging operation is supposed to show.

The procedures represent the minimum logging operations required to accomplish the stated goals. Each listed procedure can be enriched by additional logging in almost every specific situation. Likewise, a procedure may need to be modified slightly for special circumstances. However, failure to collect the type of logs that give the stated information will generally result in uncertainty in the question of confinement and integrity because these features are the most sensitive to procedure.

TABLE 9. LOGGING PROCEDURES FOR TEMPERATURE, RADIOACTIVE TRACER, AND NOISE SURVEYING

Reason for Logging: Demonstrate injection confinement and allocate injected water to various zones.

Tool Combination: Temperature and Radioactive Tracer

LOGGING PROCEDURE	WHAT LOGS SHOULD SHOW
(1) Leave well on injection while rigging up. Shut-in only long enough to hang tools in top of well,	
(2) Inject 1/2 hour before logging,	
(3) Run injecting temperature log going in hole at 20-40 ft/min. Record at 1 degree F/inch sensitivity	(3) Where injection is leaving wellbore from surface to total depth.
(4) Run depth correlation logs,	(4) True depth of surveys.
(5) Run radioactive tracer channel check above perforations with slug tracking method at a sensitivity of 1/5 normal gamma ,	(5) Behind-pipe flow above perforations.

(6) Run velocity shot packer check at same sensitivity with 5-minute record,	(6) Packer or tubing leaks.
(7) Do flow profiling work and bottom channel check,	(7) Injection profile among various zones
(8) Shut well off injection and run 2-hr shut-in temperature survey from 200 feet above perforations down to total depth as per step (3),	(8) Porosity taking current injection.
(9) Run shut-in tracer crossflow check by slug tracking method,	(9) Quality control and casing leaks.
(10) Run two longer time shut-in temperature surveys as in step (8) but at times according to the intervals in Table 3,	(10) Porosity taking injection outside perforated interval and long-time injection locations inside perfs.
(11) If confinement uncertainty still exists, return well to injection and run tracer dump test,	(11) Corroboration of previous surveys.

Tool Combination: Temperature and Noise

LOGGING PROCEDURE	WHAT LOGS SHOULD SHOW
(1) Run injecting temperature survey as per steps (1)-(3) above,	(1) Where injection is leaving wellbore.
(2) Run injecting noise survey from total depth to end of tubing. Allow 20 measurements on a coarse station interval and 15 measurements on finer grid just above top perforations and within perforations,	(2) Where injection is leaving casing below tubing. Check behind-pipe resolution by Eq. 9A or 9B.
(3) Shut well off injection and run 2-hr shut-in temperature survey as per step 8 above,	(3) Porosity taking current injection.
(4) Run shut-in noise survey at same spacing density as in step (2) of this procedure, but add four fine grid points past packer location in tubing,	(4) Behind-pipe loss from injection zone and packer leak. Check rate resolution with Eq. (10).
(5) Run two long-time shut-in temperature surveys per step (10) in the previous procedure,	(5) All porosity taking injected water.

Reason for Logging: Detection of non-related flow behind pipe in an existing injection well

Tool Combination: *Temperature and Noise*

LOGGING PROCEDURE	WHAT LOG SHOULD SHOW
(1) Shut well in overnight before logging,	
(2) Run shut-in temperature logging down at 30-50 ft/min depending on suspect interval to be logged. Start 200 feet above top of interval of interest and carry 200 feet below,	(2) Regions returning to static more rapidly than normal.
(3) Run shut-in noise log over same interval. Plan stations to give 40 measurements on coarse grid and 20 on finer grid at critical points like suspect formations, cement tops, casing shoes, etc,	(3) Pressure-driven flow behind pipe. Check tool rate resolution with Eq. (10).
(4) Keep well shut-in for additional 12 to 24 hours and run second temperature survey per step (2) in this procedure,	(4) Cross-flow behind pipe when used in conjunction with log from step (2).

Reason for Logging: Detection of non-related flow on new well.

Tool Combination: *Temperature and Noise*

LOGGING PROCEDURE	WHAT LOG SHOULD SHOW
(1) Log well within two weeks of completion or circulate prior to logging,	(1) A non-static wellbore.
(2) Proceed from step (2) in above procedure,	(2) Any crossflow behind pipe.

Ex. II – 42

Specialized Applications of Noise Logging

R.M. McKinley, SPE-AIME, Exxon Production Research Co.
F.M. Bower, Exxon Production Research Co.

Introduction

A 1973 paper[1] described how the noise logger can detect flow through poor-quality cement behind pipe. This idea is illustrated in Fig. 1. Turbulence generated by fluid moving from Sand A to Sand C creates within the tubing a sound field whose intensity is greater than the ambient noise level in the wellbore. The logging sonde, which is simply a microphone, transmits this sound level to the surface, where it is decomposed into frequencies characteristic of the type of flow. A depth record of noise level will reveal peaks at those locations where the fluid rapidly changes velocity. For example, see entry point (A), constriction (B), and exit point (C) in Fig. 1.

For this type of application, the noise log complements the temperature log very well. But this tool has other uses, too. We have found that the noise log is a valuable aid to logging methods that track fluid movement in the wellbore. The purpose of this paper, therefore, is to extend noise logging technology into the general area of flow inside casing. Specifically, we discuss how to calibrate the sonde for use in the following situations: (1) axial flow past the sonde, (2) flow from perforations, (3) liquid production from gas perforations, (4) sand production from perforations. For each case, the particular calibration coefficients refer to the standard detector sensitivity and load described by McKinley *et al.*[1]

0149-2136/79/0011-6784$00.25

Noise From Axial Flow Past Sonde

Single-Phase Flow

Suppose that the logging sonde is hanging in a wellbore down which water is being injected. The velocity increase acquired by the water while flowing past the sonde will generate turbulence. This can be detected as noise. Recall the familiar hiss from overhead pipes in steam-heated buildings. We can expect a similar sound from flow past the logging tool. The experiments described in Ref. 1 show that a single-phase fluid accelerating across a constriction radiates a noise intensity directly proportional to the pump work required to move the fluid. The same concept applies here. If Δp is the pressure differential required to flow a volumetric rate, q, past the sonde, then the resulting noise level should be proportional to the product Δpq.

This is, in fact, the case, as Fig. 2 shows. Data in Fig. 2 were measured in a flow loop with a vertical test section whose diameter varied over the range indicated. Flow rates varied from 0.1 to 30 Mcf/D. From the data correlation, we have $N^*_{600} = A \times \Delta pq$, where A is a constant and N^*_{600} is the noise level (at standard sensitivity) above 600 Hz. For turbulent flow, $\Delta p = B\rho(q/A_s)^2$, where B is a drag coefficient, ρ is the fluid density, and A_s is the cross-sectional area for flow between the pipe wall and sonde.

This paper describes the use of the noise logging technique to monitor flow inside casing. Calibrations for the following flow situations are shown: axial flow past the sonde, flow from perforations, liquid production from gas-zone perforations, and sand production from perforations. The forms of the correlating equations are independent of specific tool design.

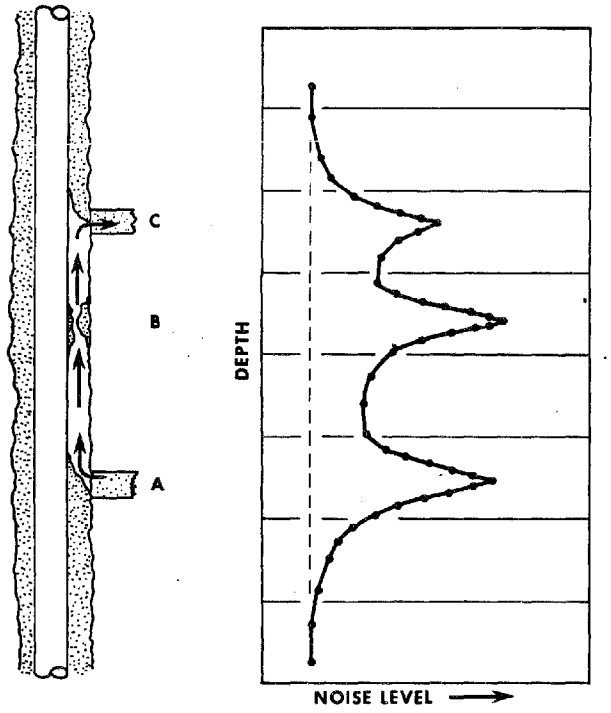

Fig. 1 – How crossflow behind tubing affects the noise level inside tubing.

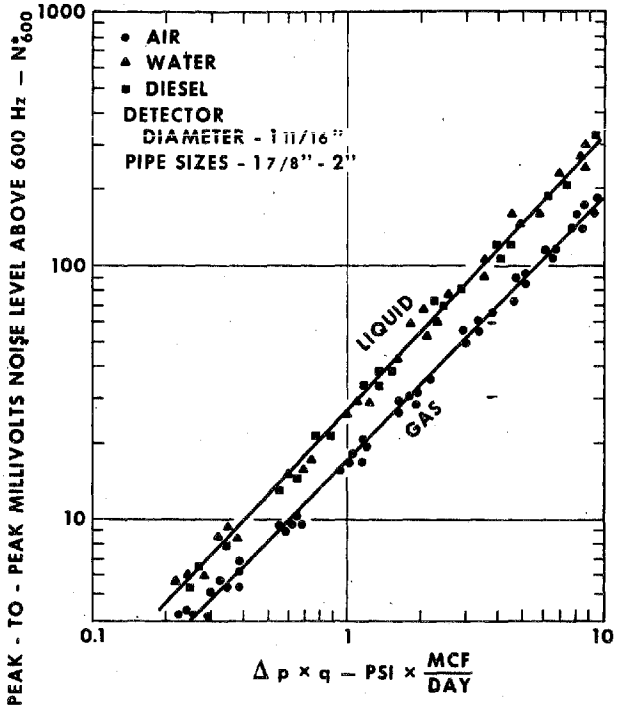

Fig. 2 – Noise level generated by flow past a detector.

Combining these two relationships gives

$$N^*_{600} = C\frac{\rho q^3}{A_s^2}, \quad \ldots\ldots\ldots\ldots\ldots\ldots\ldots\ldots (1)$$

where C is a constant analogous to a drag coefficient. As happens to the latter, the value of C decreases with increasing Reynold's number until the flow becomes turbulent. For Reynold's number greater than 6,000, we find that for gas or liquid, $C=(4\pm 1.5)\times 10^{-6}$. Thus,

$$N^*_{600} = 4\times 10^{-6}\frac{\rho q^3}{A_s^2}. \quad \ldots\ldots\ldots\ldots\ldots\ldots (2)$$

Inverting this,

$$q = 63\left(\frac{A_s^2 N^*_{600}}{\rho}\right)^{1/3}, \quad \ldots\ldots\ldots\ldots\ldots\ldots (3)$$

where q is in units of thousand cubic feet per day at flowing temperature and pressure, ρ is in pounds per cubic foot, A_s is in square feet, and the noise level above 600 Hz is in standardized peak-to-peak (p-p) millivolts. For the SI metric system of units, the numerical coefficient of Eq. 3 becomes 0.25.

These are the calibrating equations. Significantly, they show that noise level is a function of flow rate or velocity cubed. This is the advantage the tool has over linear meters. The noise level will be a sensitive indicator of small changes in an otherwise high flow-rate situation, as illustrated in Fig. 3.

The 600-Hz noise level measurements were obtained from a well on injection at 25,000 B/D water. A spinner survey had shown that a lower perforated interval (below 8,900 ft) was taking most of the water, while only about 1,000 B/D appeared to be entering the perforations shown in Fig. 3. This 1,000 B/D is 4% of the total flow, which is at the resolution of the spinner. On the other hand, the change in noise level across the interval is 19%. Furthermore, the noise level indicates water is going into the top half of the perforated interval. To ascertain the amount of injection, we apply Eq. 3 to the noise levels above and below the interval. Above the interval, $N_{600}=1{,}610$ RMS mV. Before this value can be used in Eq. 3, it first must be converted from RMS millivolts to peak-to-peak millivolts. This entails multiplying the value by 2.83. Next, the value must be corrected for attenuation caused by the loging cable and for the specific gain of the particular logging sonde. These factors (available from each logging company offering the service) are 1.6 and 2.0, respectively. The total correction factor is 9.06. Therefore, $N^*_{600}=14{,}490$ p-p mV, while below the interval, $N_{600}=1{,}310$ and $N^*_{600}=11{,}773$.

The 7-in. wellbore pipe has a 6.37-in. ID while the OD of the tool is 1.69 in. Therefore,

$$A_s = \frac{\pi}{4}\frac{(6.37+1.69)(6.37-1.69)}{144}$$
$$= 0.206 \text{ sq ft } (0.0191 \text{m}^2),$$

and

$$A_s^2 = 0.0424 \text{ (ft)}^4 \ (3.65\times 10^{-4}\text{m}^4).$$

At the injection temperature, $\rho=61$ lbm/cu ft (977 kg/m^3). Substituting these values into Eq. 3, we obtain a flow rate above the perforations of

$$q = \left(63\frac{0.0424\times 14{,}490}{61}\right)^{1/3}$$
$$= 136 \text{ Mcf/D} = 24{,}230 \text{ B/D } (0.044 \text{ m}^3/\text{s}),$$

which compares closely with the spinner total injection of 25,000 B/D. Below the perforated interval, the flow rate is

$$q = 24{,}230 \times \left(\frac{11{,}773}{14{,}490}\right)^{1/2}$$

$$= 22{,}610 \text{ B/D } (0.042 \text{ m}^3/\text{s}).$$

The net injection into the interval, therefore, is $\Delta q = 24{,}230 - 22{,}610 = 1{,}620$ B/D (0.003 m^3/s), which illustrates the tool resolution for this type of application.

However, the same cubic relationship that ensures this type of sensitivity also means that the tool will not detect low flow rates. At 600 Hz, the ambient noise level in a typical well is $N^*_{600} = 2$ p-p mV, which means that for 7-in. casing, the minimum detectable rate is

$$q = 63\left(\frac{0.0424 \times 2}{61}\right)^{1/2}$$

$$= 7.03 \text{ Mcf/D} = 1{,}250 \text{ B/D } (0.0023 \text{ m}^3/\text{s}).$$

This situation could be improved by adding turbulence generators to the tool body.

In the above example, the agreement between the spinner rate and that estimated from the noise log is closer than is usually the case. For water injection rates down to 5,000 B/D in 7-in. casing, the noise-log derived rates have been within 25% of the flowmeter rates, provided, of course, that the injection equipment itself is not the dominant noise source. Nearby injection pumps can create mechanical vibrations that carry to total depth in a well. Furthermore, at low flow rates, the noise level at a particular depth may be the result of carry-away from noise sources located at other depths within the well. This is the situation, for example, on the log in Fig. 4 from a flowing oil well. The noise levels above the topmost perforations are much too large to result from the 1,400-B/D flow past the sonde. This high residual noise results from the high values at the perforations.

Finally, here are a few comments on the use of the 600-Hz level. A complete spectrum for this type of axial flow would show a peak amplitude at about 600 Hz for the lower flow rates; consequently, this cut will pick up these lower rates better than a higher frequency cut. Moreover, this frequency is sufficiently low so that for liquids the numerical value for the coefficient C should be independent of pipe size. Our field data verify this. For gases, however, some dependence of the coefficient C on pipe size occurs. The value given seems to be correct for tubing up to 2⅞ in., which is the limit of our field data.

Gas/Liquid Flow

We also have calibrated the sonde for gas/liquid two-phase axial flow, but the results are not very useful.

NOISE LOGGER SENSITIVE TO SMALL RATE CHANGES

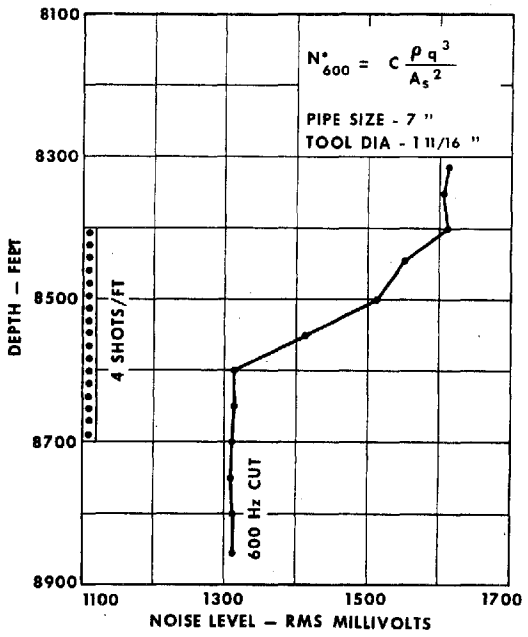

Fig. 3 – Noise profile across a perforated interval, taking 4% of total injection.

NOISE LOGGING FOR PERFORATION FLOW

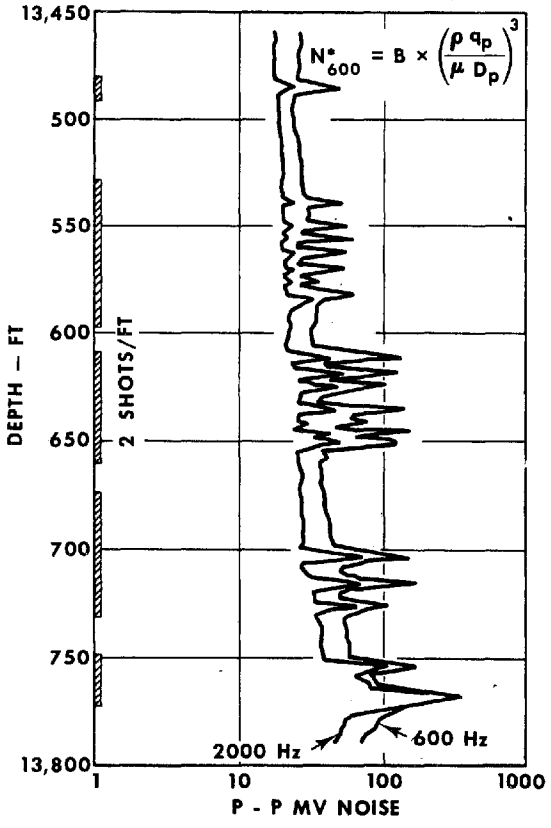

Fig. 4 – Noise log from an oil well flowing 1,400 B/D.

NOISE LOGGING WITH GAS — LIQUID FLOW

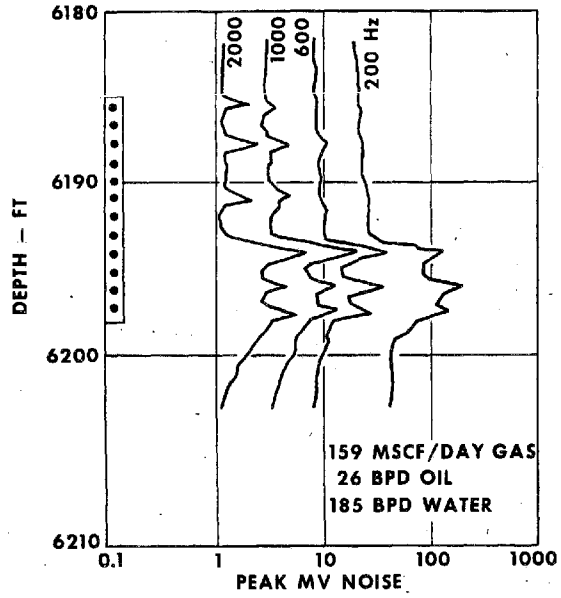

Fig. 5 — Noise log from a well flowing gas and liquid at 2,160 psi and 180°F bottomhole conditions.

More often than not, the state of the gas/liquid mixture is determined by the tangential fluid velocity at the perforations rather than by axial velocity in the tubing. The log in Fig. 5, taken over the perforated interval of a well producing considerable gas and water with a lesser amount of oil, illustrates the influence of the perforations. The loss in noise level above 6,194 ft results from foam generation at this point with the subsequent decoupling of sonde from fluid. The lower frequency cuts lose character. This foam persisted all the way up the wellbore until the pressure dropped to a point where expansion broke the foam. This is not uncommon. Consequently, we will not pursue the flow-loop correlations. Rather, we proceed to the topic of flow from perforations.

Flow From Perforations

Single-Phase Flow

Consider a perforation at least 6 in. deep and 0.5 in. in diameter. Even at formation porosities as low as 5%, the porous surface area of the perforation tunnel is still several times greater than the cross-sectional area. This means that the velocity of fluid entering the perforation tunnel is less than that of the fluid leaving the hole in the casing. Because maximum velocity determines noise level, the hole in the casing wall acts as an isolated noise source, just as any orifice does. This hole is acoustically independent of the formation. Thus, we again may write $N^*_{600} = A' \times (\Delta p q)$, where A' is a constant of proportionality. For an orifice with coefficient B':

$$\Delta p = B' \rho \frac{q^2}{A_p^2} = \frac{16B'}{\pi^2} \frac{\rho q^2}{D_p^4},$$

so

$$N^*_{600} = C' \frac{\rho q^3}{D_p^4}, \quad \ldots\ldots\ldots\ldots\ldots\ldots\ldots (4)$$

where D_p is the perforation diameter and C' is an acoustical orifice coefficient. A jet stream from a perforation actually transports the turbulent field to the sonde, a process whose effectiveness depends on the jet cohesiveness. The latter in turn is inversely proportional to the kinematic viscosity, μ/ρ, of the fluid in the pipe. Hence, we need $\rho q/\mu$ rather than q in Eq. 4. This substitution gives

$$N^*_{600} = C'' \left(\frac{\rho^4 q^3}{\mu^3 D_p^4} \right), \quad \ldots\ldots\ldots\ldots\ldots\ldots\ldots (5)$$

or

$$N^*_{600} = C'' \left(\frac{\rho^{1.33} q}{\mu D_p^{1.33}} \right). \quad \ldots\ldots\ldots\ldots\ldots\ldots\ldots (6)$$

To test this relationship, we constructed a core holder similar to those used in standard perforation evaluation[2], with the exception that the holder could be fastened to and could admit flow into a section of casing. Perforations were drilled into the core sections along with equal-sized holes in the casing wall. In this fashion, we ran flow tests on cores whose permeabilities ranged from 1 to 3,000 md, with perforations of diameter ranging from 1/16 to ½ in. and depths from 1 to 10 in. The size dependency given by Eq. 6 is needed to correlate the resulting data in its entirety. But in a field situation, one hardly ever will know the perforation diameter, D_p, with any degree of precision. For gases, the same is true for the density, ρ, at bottomhole conditions. We therefore simplify Eq. 6 to

$$N^*_{600} = C'' X_p^3, \quad \ldots\ldots\ldots\ldots\ldots\ldots\ldots (7)$$

where $X_p = \rho q_p / \mu D_p$.

This accomplishes two things. First, it removes some of the pretentiousness from estimating the influence of perforation diameter. But more important, the need for estimating downhole density of gases is eliminated because $\rho q = (\rho q)_{sc}$. Use of density at standard conditions gives the volumetric flow rate at these same conditions. An expression like Eq. 7 is satisfactory for perforation with diameters in the range of ¼ to ½ in., as Fig. 6 demonstrates. The composite data are represented by Eq. 8:

$$N^*_{600} = 3.84 \times 10^{-5} X_p^{2.86}, \quad \ldots\ldots\ldots\ldots\ldots\ldots\ldots (8)$$

which inverts to

$$\begin{cases} X_p = 35 (N^*_{600})^{0.35} \\ \quad = \dfrac{\rho q_p}{\mu D_p}, \end{cases} \quad \ldots\ldots\ldots\ldots\ldots\ldots\ldots (9)$$

where q_p (Mcf/D) is the volumetric flow rate from the perforation, ρ (lb/cu ft) is the fluid density, μ (cp) is the fluid viscosity, and D_p (in.) is the perforation diameter. For the SI metric system of units, the coefficient in Eq. 9 becomes 7234 instead of 35. The flow rates appearing in Fig. 6 range from 0.1 to 20 Mcf/D. Once more, the nearly cubic dependence of

noise level on flow rate assures that the most prolific perforations will stand out.

An excellent illustration of this is given by Robinson[3] in his Fig. 15. Robinson shows a log from a flowing gas well producing 5.9 MMscf/D dry gas. The perforations are 12 single shots spaced sufficiently far apart so that each one is recognizable on the log. Noise levels at the perforations are given in our Table 1. Four perforations near the middle are flowing a high percentage of total gas. Some of the noise levels are more than 10 times higher than our data in Fig. 6. Therefore, we are extrapolating in these instances with Eq. 9 for values of X_p.

To obtain the total production from the summed X's, we use the following values:

$$\rho_{sc} = 0.045 \text{ lbm/cu ft } (0.721 \text{ kg/m}^3),$$
$$\mu = 0.024 \text{ cp } (0.000\,024 \text{ Pa·s})$$
$$D_p = 0.45 \text{ in. } (11.4 \text{ mm})$$

Then,

$$q_{sc} = \frac{\mu D_p}{\rho_{sc}} \Sigma X_p$$
$$= \frac{0.024 \times 0.45 \times 18{,}762}{0.045}$$
$$= 4.5 \text{ MMscf/D } (1.47 \text{ m}^3/\text{s}).$$

The 25% error is within the accuracy of Eq. 9. Such close agreement generally will not be obtained because of the tool's inability to resolve noise peaks associated with closely spaced perforations. The important point is illustrated by the magnitude variation of the noise levels in Table 1. Four centrally located perforations are producing almost 50% of the gas.

For a second application of Eq. 9, we refer to the log shown in Fig. 4 from an oil well flowing at 1,400 B/D. Since this well has thick-walled casing perforated with a through-tubing gun, we would expect the spotty production evident in the figure. There are about 20 points of major productivity with the second and third intervals being the biggest contributors. Furthermore, the bottom peak appears to result from a plugged perforation. The sound pitch at this point is considerably higher than elsewhere, as the 2000-Hz curve illustrates. Discounting this last peak for the moment, we find for the remaining 19 peaks that $\Sigma X_p = 5{,}609$ (1.6×10^6), which, with the values $\rho = 51$ lbm/cu ft (817 kg/m^3), $\mu = 0.6$ cp $(6 \times 10^{-4}$ Pa·s), and $D_p = 0.2$ in. (5.08 mm) gives an oil rate of

$$q = \frac{0.6 \times 0.2 \times 5{,}609}{51}$$
$$= 13 \text{ Mcf/D} = 2{,}350 \text{ RB/D } (4.33 \times 10^{-3} \text{ m}^3/\text{s}),$$

whereas the actual rate was

$$q = 1{,}400 \times 1.25 = 1{,}750 \text{ RB/D}.$$

TABLE 1 – NOISE LEVELS AT 12 PERFORATIONS IN A GAS WELL FLOWING 5.9 Mscf/D (Ref. 3)

N^*_{600}	X_p(Eq. 9)
7,150	782
13,325	972
18,850	1,097
113,000	2,054
139,000	2,208
188,000	2,455
188,000	2,455
58,500	1,630
42,250	1,456
52,000	1,566
45,500	1,494
3,250	593
Total	18,762 (3.88×10^6)

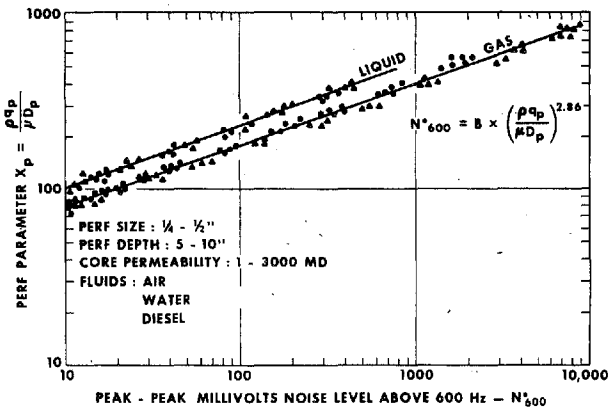

Fig. 6 – Noise level generated by single-phase flow from a deep perforation.

Single-Phase Flow from Plugged Perforations

When flowing, a gas well perforation 6 in. deep would emit an "organ tone" with a pitch of

$$f = \frac{c}{4\ell} \approx \frac{1{,}000}{4 \times 0.5} = 500 \text{ Hz}.$$

This tone would not be emitted by a plugged or very shallow perforation. We illustrate this difference with the noise spectra in Fig. 7, where the tone at 450 Hz is evident on Spectrum A, the unplugged perforation. Therefore, we can learn to recognize plugged perforations in gas wells from their flowing spectra. But even a loose pack in a perforation will eliminate the organ tone without adding much incremental pressure drop along the perforation. The important question is: How much flowing pressure loss results from the plug? To help answer this question, we have prepared the correlation in Fig. 8, which shows the incremental pressure loss per unit rate in 6-in.-deep perforations as a function of the 4000-Hz noise cut at the perforation. The form of the correlation occurs as follows:

$$N^*_{4000} = A \times (\Delta p q_p),$$

thus,

$$\frac{\Delta p}{q_p} = A' \frac{4{,}000}{q_p^2},$$

TABLE 2 – ESTIMATES OF PERFORATION PRESSURE LOSS FROM PLUGGING FOR THE OIL WELL IN FIG. 4

Depth (ft)	N^*_{4000}	N^*_{4000}/q_p^2	$\Delta p/q_p$ (Fig. 8)	Δp (psi)
13,486	15.4	64	0	0
13,585	22.0	91	3	0
13,620	36.3	150	18	9
13,762	60.0	249	70	34
13,754	72.0	298	100	49
13,770	203.0	841	260	127

$$q_p = \frac{1750 \times 5.615}{20 \times 1000} = 0.49 \text{ Mcf/D/perf}$$

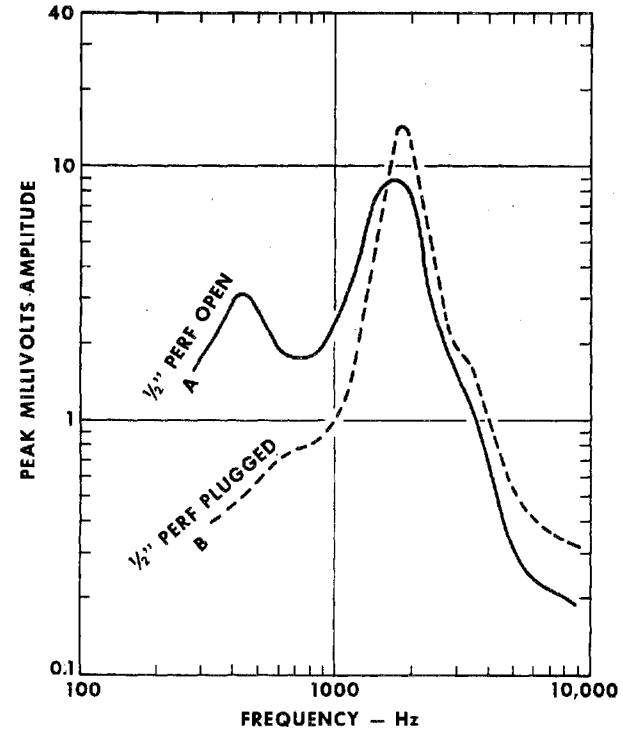

Fig. 7 – Flowing noise spectra for open and plugged perforations.

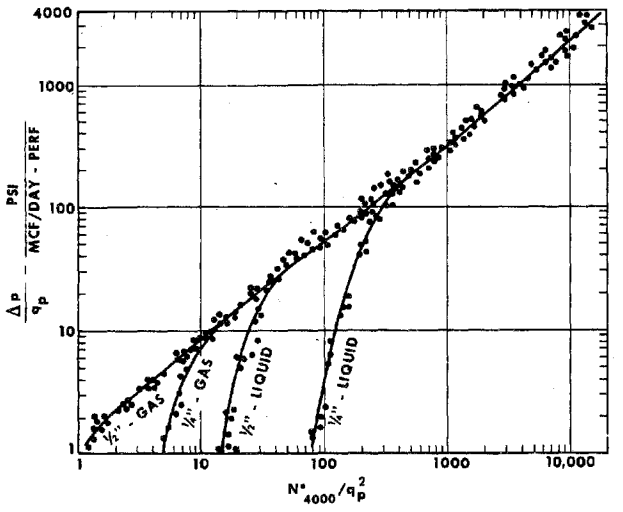

Fig. 8 – Correlation of 4000-Hz noise level with incremental pressure drop caused by perforation plugging.

where Δp (psi) and q_p (Mcf/D) are at bottomhole conditions. We return now to the oil well in Fig. 4. Table 2 summarizes values for N^*_{4000} at selected depths along with the incremental values of Δp obtained from Fig. 8 (¼-in. liquid curve). The estimated pressure loss across the plugged perforation at 13,770 ft is 127 psi. This represents nearly one-half the total flowing drawdown for this particular well. Thus, the perforation is flowing at only about one-half its potential rate.

Liquid Production From Perforations in Gas Zone

In some wells, a perforation flowing gas and liquid produces the liquid as discrete droplets that are carried away. In other wells, the liquid may be produced into a foamy environment. In either situation, the liquid incident on the sonde enriches the noise with higher frequency components, giving a log similar to that opposite the plugged perforation in Fig. 4. We have found that for an open perforation flowing dry gas,

$$\frac{N^*_{2000}}{X_p^3} \le 3 \times 10^{-5}; (3 \times 10^{-12}) \text{(dry gas)}, \quad \ldots . (10)$$

where $X_p = (\rho q_p / \mu D_p)$ gas. As one would expect, increasing values above the Eq.-10 threshold reflect increasing concentrations of water in the jet stream. Our data give a relationship approximated by

$$q_{liq} = 1.5 D_p \frac{N^*_{2000}}{\sqrt{X_p}}, \quad \ldots . (11)$$

where q_{liq} is the liquid flow rate in barrels per day and D_p is in inches. For the SI metric system of units, the constant becomes 1.56×10^{-3}, rather than 1.5.

For example, a log from a gas well flowing 1 MMscf/D showed that 20 perforations produced most of the gas. The well also was producing 200 B/D salt water. We estimate that

$$\left(\frac{\rho q_p}{\mu}\right)_{gas} = \frac{0.054 \times 1{,}000}{0.018 \times 20} = 150,$$

$$X_p = \frac{150}{0.45} = 333(6.88 \times 10^4).$$

At all entry points except one,

$$\frac{N^*_{2000}}{X_p^3} \le 1 \times 10^{-5}(1 \times 10^{-12}),$$

while at this one perforation the ratio increased to 19×10^{-5}. At this location, $N^*_{2000} = 7{,}050$ p-p mV. These values, when substituted into Eq. 11 with $D_p = 0.45$ in., give

$$q_{liq} = \frac{1.5 \times 0.45 \times 7{,}050}{\sqrt{333}}$$

$$= 261 \text{ B/D } (4.80 \times 10^{-4} \text{ m}^3/\text{s}).$$

Consequently, this perforation probably was producing most of the water. A workover verified this.

Gas-Liquid Flow From Perforations

Whenever liquid is the continuous phase in the wellbore, a perforation jet stream with gas creates such a high level of noise inside the casing that the condition of the perforation itself is of minor consequence. However, the noise contains information about the jet stream. As McKinley *et al.*[1] explained, the noise in 200- to 600-Hz band is proportional to gas rate, while Eq. 11 shows that liquid content of the jet is related to the higher frequency noise. The correlation in Fig. 9 uses these ideas. This figure, on which the actual data points are omitted, shows percent by volume, y_{gas}, of gas in the jet stream as a function of the ratio of noise levels, $\Delta^*/\sqrt{N^*_{2000}}$, *where* $\Delta^* = N^*_{200} - N^*_{600}$ is the noise level in the 200- to 600-Hz frequency band. The gas percentage could not be correlated totally independent of liquid production rate. This is the reason for the parametric values shown on the curves. Also, note the gas rate restriction ($q_{gas} \leq 0.6$ Mcf/D/perf) that results from the tendency of the fluids to become foamy.

Fig. 9 helps us to diagnose what is happening in the well illustrated in Fig. 5. We also have a density log and a spinner survey from this well. The former showed gas production from the entire perforated interval. This production and the resulting wellbore turbulence complicates the spinner interpretation.

Looking at the noise log in Fig. 5, we see the gas flow from the lower perforations. This flow is evident from the separation between the 200- and 600-Hz curves. Energy in this band is greater than everything above 1000 Hz. We have mentioned already the foam production at 6,194 ft, which suggests this depth is the point of oil entry. Altogether, there are six major entry points. We then may estimate the liquid rate per entry point as

$$q_{liq} = \frac{185 + 26}{6} = 35 \text{ B/D/perf.}$$

From the water curves in Fig. 9, we find the jet-stream gas concentration shown in Col. 4 of Table 3.

Ignore for the moment the last two columns in Table 3. The estimated gas percentages, y_{gas}, show relatively lower gas concentrations at the bottom of the interval (6,198 ft) and at 6,194 ft. This further suggests that these depths may be the water and oil entry points, respectively. To confirm this, we will need flow rates from these locations. The noise log will help estimate these rates.

Figs. 10A and 10B show correlations of gas flow rates at downhole conditions as a function of Δ^* and N^*_{2000}, respectively, with liquid rates as parameters. These charts are for gas/water flow from perforations with the indicated diameter range. We have similar charts for smaller perforations as well as for gas/oil flow. These are not needed here because the liquid in our example is almost all water.

From Fig. 10A, we see that the relationship between Δ^* and q_{gas} is not very sensitive to liquid rate. This rate is reflected more strongly in the N^*_{2000} values in Fig. 10B. This figure then is sufficient to establish values for both q_{gas} and q_{liq}. The charts are

TABLE 3 – ANALYSIS OF RESULTS FROM THE NOISE LOG IN FIG. 5

Depth (ft)	Δ^*	N^*_{2000}	y_{gas} (Fig. 9) (%)	q_{gas} (Mcf/D)	q_{liq} (B/D)
6,198	365	84	22	0.10	100
6,196	633	70	40	0.15	35
6,194	378	126	20	0.10	100
Totals				0.35	235

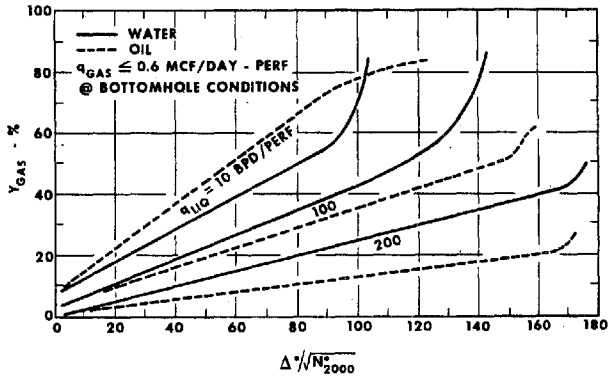

Fig. 9 – Volume percent of gas in perforation jet stream vs noise ratio.

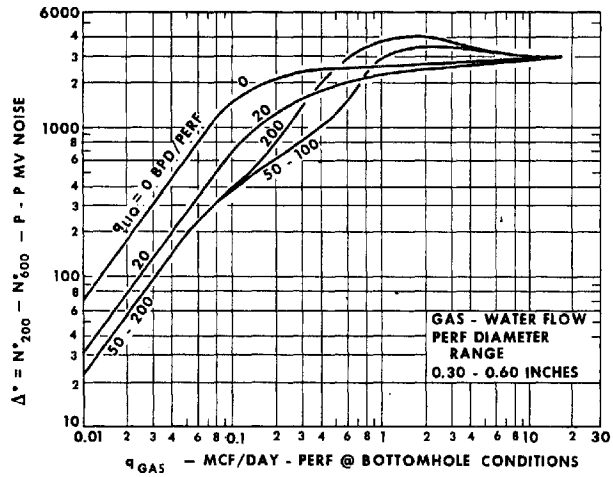

Fig. 10A – Low-frequency noise level as a function of gas/water flow rate from perforations.

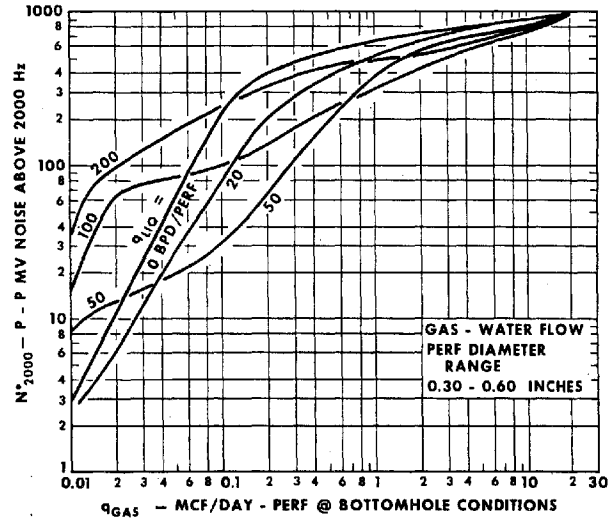

Fig. 10B – High-frequency noise level as a function of gas/water flow rate from perforations.

used in the following manner: All possible solutions consistent with the measured value of Δ^* first are read by projecting this value horizontally across Fig. 10A. These values of q_{gas} and q_{liq} then are transferred to Fig. 10B to give a set of predicted values for N^*_{2000}. The correct solution is the one with N^*_{2000} nearest the measured value. For example, we see from Table 3 that at 6,198 ft, $\Delta^* = 365$ p-p mV, and $N^*_{2000} = 84$ p-p mV. Entering the first of the values onto Fig. 10A gives the possible solutions shown in Cols. 1 and 2 below.

q_{liq}	q_{gas} (Fig. 10A)	N^*_{2000} (Fig. 10B)
0	0.034	31
20	0.060	36
50	0.10	32
100	0.10	100
200	0.094	230

If these values now are transferred to Fig. 10B, we find the numbers for N^*_{2000} in the last column above. Comparing these numbers with the measured value, $N^*_{2000} = 84$, gives the solution at 6,198 ft of

$$\begin{cases} q_{gas} = 0.10 \text{ Mcf/D} \\ q_{liq} = 100 \text{ B/D} \end{cases}$$

In a like manner, we establish the other two entries in the last two columns in Table 3. At 6,196 ft, a liquid rate of either 20 B/D or 50 B/D is consistent; thus, the average is listed. We observe from Table 3 that comparable amounts of liquid are produced at both 6,198 and 6,194 ft. Therefore, the 6,198-ft depth is not the only point of water entry. A squeeze and reperforate workover was tried without success.

Table 3 shows the deepest three entry points producing the observed total liquid (211 B/D) along with an amount of gas equal at standard conditions to

$$q = 0.35 \times 130 = 45.5 \text{ Mscf/D } (0.015 \text{ m}^3/\text{s}).$$

Much of the gas must, therefore, enter at the top three peaks. Dry-gas jetting into a foamy environment is similar to single-phase flow. Our data show that for dry-gas flow into foam, the gas jetstream group is related to noise level by

$$X_p = 47 \times (N^*_{1000})^{0.35}, \quad \ldots\ldots\ldots\ldots\ldots\ldots (12)$$

where the 1000-Hz cut is used rather than the 600-Hz cut. For the SI metric system, the constant 47 in Eq. 12 should be replaced by 9714. Using Eq. 12 at the top three entries, we find $\Sigma X_p = 670$ (1.38×10^5).

This, in turn, gives

$$q_{sc} = \frac{0.018 \times 0.45 \times 670}{0.054},$$

$$= 100 \text{ Mscf/D } (0.033 \text{ m}^3/\text{s}).$$

This amount added to that produced from the lower perforations accounts for the observed gas rate of 159 Mscf/D.

The individual rate estimates as above can be considerably in error for several reasons. First, the individual perforations may be resolved poorly because of (1) either the distance between stops during the logging operation or (2) the interference from adjacent perforations. Secondly, at higher flow rates, noise level becomes only a weak function of flow rate, as shown in Figs. 10A and 10B. This is the result of foam production in the wellbore. We have, therefore, found that the estimated rates are more useful in the relative sense, illustrated by the previous example.

Sand Production From Perforations

Above 4000 Hz, noise created by fluid movement – even water droplets impacting on the tool – decays very rapidly as frequency rises. This results from fluid viscosity. Such is not the case when sand grains hit the sonde or the casing wall. These impacts produce a very broadband noise spectrum whose major peaks are the result of tool resonances. The rate at which noise level decreases with frequency is, therefore, a good indicator of sand in a perforation jet stream. If we define a decay ratio as

$$R = \frac{N^*_{4000}}{N^*_{4000} - N^*_{6000}}, \quad \ldots\ldots\ldots\ldots\ldots\ldots (13)$$

then a jet stream with entrained sand has the following threshold values in our experimental chamber.

Single-Phase Flow

$$R > 2.5. \quad \ldots\ldots\ldots\ldots\ldots\ldots\ldots\ldots (14)$$

Gas/Liquid Flow

$$R > \begin{cases} 3.5; X_p < 100(2.0 \times 10^4) \\ 2 \log X_p - 0.5; X_p \geq 100, \end{cases} \quad \ldots\ldots\ldots\ldots (15)$$

where

$$X_p = X_{p_{liq}} + X_{p_{gas}}.$$

These relationships, which assume a jet noise level at least four times ambient values, provide criteria for detecting sand production.

We also can relate noise level to sand concentration in the jet stream:

$$C_{sand} = B\left[\frac{N^*_{4000}}{X_p^3} - 1 \times 10^{-5}\right], \quad \ldots\ldots\ldots\ldots (16)$$

where

$$C_{sand} = \frac{\text{lbm/D sand}}{\left(\frac{\rho q_p}{\mu}\right)_{fluid}}. \quad \ldots\ldots\ldots\ldots\ldots (17)$$

The coefficient B, which equals 3.5×10^4 for 16-20 mesh sand, varies inversely with mesh size. In the SI metric system, the coefficient B equals 3.1×10^8, while the threshold value 1×10^{-5} becomes $1 \times$

10^{-12}. The sand rate then is in kilograms per second rather than pounds per day. All the above correlations come from laboratory data and have not been field tested.

Conclusions

We have illustrated how the noise log can be calibrated for flow inside casing. The forms of the calibration equations are more important than the particular numerical coefficients which will change as the tools evolve. In general, for single-phase flow, noise level increases as the cube of the volumetric flow rate and decreases as the square of the cross-sectional area normal to flow. Gas/liquid flows are more complex.

Specifically, we show how to use noise levels to estimate (1) axial flow rate past the sonde for single-phase flow, (2) flow rate from perforations for single-phase or gas/liquid flow, (3) pressure drop across a plugged perforation, (4) liquid flow rate from perforations in a gas well, and (5) sand production rate from perforations.

Those correlations using jet-stream noise at perforations are especially useful when standard methods fail to give a clear diagnosis. We do not wish, however, to leave the impression that the noise log is a substitute for standard flowmeter surveys. Instead, this device should be viewed as a relatively inexpensive complement that provides estimates of flow rates. The accuracy of these estimates will depend on how well a particular tool is calibrated for a particular problem.

Nomenclature

A_s = cross-sectional area, normal to flow, sq ft (m^2)
C_{sand} = sand concentration defined by Eq. 17
D_p = perforation diameter, in. (m)
f = frequency, Hz
N_f^* = noise level, peak-to-peak millivolts, above frequency f at standardized sensitivity
p = pressure, psi (Pa)
Δp = pressure difference, psi (Pa)
q = volumetric flow rate, at flowing temperature and pressure, Mcf/D (m^3/s)
q_{liq} = liquid flow rate, B/D (m^3/s)
q_p = volumetric flow rate, from a single perforation, Mcf/D/perf (m^3/s)
q_{sc} = volumetric flow rate, at standard conditions, Mscf/D (m^3/s)
X_p = jet-stream group defined by Eq. 9 (dimensionless in consistent units)
y_{gas} = percent gas, by volume, in perforation jet stream
$\Delta^* = N_{200}^* - N_{600}^*$ = noise level in 200- to 600-Hz band
μ = fluid viscosity at bottomhole conditions, cp (Pa·s)
ρ = fluid density at bottomhole conditions, lbm/cu ft (kg/m^3)

References

1. McKinley, R.M., Bower, F.M., and Rumble, R.C.: "The Structure and Interpretation of Noise From Flow Behind Cemented Casing," *J. Pet. Tech.* (March 1973) 329-338.
2. *API Recommended Procedure 43,* 2nd ed., American Petroleum Inst., Dallas (Nov. 1971).
3. Robinson, W.S.: "Field Results from the Noise Logging Technique," *J. Pet. Tech.* (Nov. 1976) 1370-1376.

SI Metric Conversion Factors

B/D	× 1.589 873	E−01	=	m^3/d
cp	× 1.000*	E−03	=	Pa·s
cycles/sec	× 1.000*	E+00	=	Hz
°F	(°F − 32)/1.8		=	°C
ft	× 3.048*	E−01	=	m
in.	× 2.540*	E−02	=	m
lbm/cu ft	× 1.601 846	E−02	=	kg/m^3
Mcf/D	× 2.863 640	E−02	=	$10^3 m^3/s$
psi	× 6.894 757	E+00	=	kPa
scf/D	× 2.863 640	E−02	=	std m^3/s
sq ft	× 9.290 304	E−02	=	m^2

*Conversion factor is exact.

JPT

Original manuscript received in Society of Petroleum Engineers office Sept. 15, 1977. Paper accepted for publication April 21, 1978. Revised manuscript received Aug. 24, 1979. Paper (SPE 6784) first presented at the SPE-AIME 52nd Annual Fall Technical Conference and Exhibition, held in Denver, Oct. 9-12, 1977.

Ex. II - 43

Exponent®
Engineering & Scientific Consulting

Robert A. Carnahan, P.E.
Principal Engineer | Materials & Corrosion Engineering
5401 McConnell Avenue | Los Angeles, CA 90066
(310) 754-2715 tel | robcarn@exponent.com

Professional Profile

Mr. Carnahan specializes in failure analysis of engineering components and systems by combining expertise in metallurgical engineering, corrosion, materials science, and mechanical engineering.

Mr. Carnahan has performed failure analysis of a wide variety of machinery and equipment related to aerospace, automotive, construction, maritime, pipeline, power generation, and petrochemical industries. Mr. Carnahan has investigated failures of petrochemical plant equipment including heat exchangers, pressure vessels, and HF storage hardware, and has investigated failures of oil and natural gas pipelines and oil and gas well casings. Mr. Carnahan has performed failure analysis of various gas turbine components. He has investigated failures of various types of water and sewage piping, including cast iron, PVC, and asbestos cement. Mr. Carnahan has investigated failures of fire protection system components including sprinklers, piping (steel and CPVC), and couplings. He has also analyzed a multitude of plumbing product failures.

Mr. Carnahan's skills include fractography, microscopy, microstructural analysis, welding and joining, mechanical testing, and stress analysis. Mr. Carnahan also has experience with laboratory evaluation of microbiologically influenced corrosion (MIC) and has worked on a number of MIC related projects, including oil pipelines, sanitary sewer piping, and heat exchangers.

Prior to joining Exponent, Mr. Carnahan performed metallurgical failure analysis and corrosion investigations of nuclear power plant components for the General Electric Company.

Academic Credentials & Professional Honors

M.S., Metallurgical Engineering, University of Michigan, Ann Arbor, 1980

B.S., Materials and Metallurgical Engineering, University of Michigan, Ann Arbor, summa cum laude, 1979

General Electric Honors Cooperative Program

Tau Beta Pi

Clarence A. Siebert Scholarship, University of Michigan

Licenses and Certifications

Licensed Professional Mechanical Engineer, California, #M31519

Licensed Professional Mechanical Engineer, Arizona, #62030

Licensed Professional Mechanical Engineer, Nevada, #024746

Licensed Professional Mechanical Engineer, Texas, #132350

Licensed Professional Engineer, Utah # 9855287-2202

Licensed Professional Engineer, Michigan # 6201068806

Certified Corrosion and Materials Professional (API 571), American Petroleum Institute

Prior Experience

Senior Engineer, General Electric Company, Nuclear Energy Division, 1980-1986

Senior Engineer, General Electric Company, Aerospace Division, 1987-1988

Professional Affiliations

ASM International (formerly American Society for Metals) (member)

National Association of Corrosion Engineers (member)

American Society of Mechanical Engineers (member)

Society of Plastics Engineers (member)

Publications

McDonald B, Ross B, Carnahan RA. The Bellevue crane disaster. Engineering Failure Analysis 2011 Oct; 18(7):1621-1636

Dracup B, Reza A, Carnahan RA, Christiansen E, Ross B. A case study of two shiploader fires in a coal and pet coke facility. 11th International Conference, Fire and Materials, January 2007.

Kadlec R, Westmann R, Carnahan RA, Haghi M, Deyerl E. Failure analysis of heavy truck trailer axle tubes. Experimental Model Research and Testing of Thin Walled Structures, 1997.

Andrew S, Carnahan RA. Fitness-for-service of chloride ton containers. NACE Corrosion '96, Paper No. 650, 1996.

Foulds J, Carnahan RA. Examination of Sabine 2 hot reheat pipe seam weld cracking. Electric Power Research Institute, RP2253-17, Final Report, June 1994.

Carnahan RA. Alternative alloys for BWR pipe applications. Appendix J, Electric Power Research Institute Report NP-2671-LD, October 1982.

Presentations

Carnahan RA. Tribological coating development for SP-100 sliding interfaces. 5th Symposium on Space Nuclear Power Systems, Albuquerque, NM, 1988.

Carnahan RA. Field piping sensitization surveillance. International Workshop on Low Temperature

Sensitization, Electric Power Research Institute, Palo Alto, CA, 1982.

Selected Reports

Moore D, Rau C, Carnahan RA. Triumph air repair / World Airways arbitration. Exponent FaAA Report, February 2006.

Carnahan RA. Whiting motorcycle headlight examination. Exponent FaAA Report to the United States Department of Justice, May 2005 (Rule 26B Report).

Hertzberg J, Reza A, Carnahan RA. Robertshaw TS-11 and 7000 series gas valve investigation. Exponent FaAA Report, October 2004.

Carnahan RA. Investigation of the whitefly screen damage at Houweling's Nursery. Exponent FaAA Report, March 2004.

Carnahan RA. Investigation of the August 2003 skeg cracking on the M/V St. Lucia. Exponent FaAA Report, March 2004.

Carnahan RA. Monrovia Villas copper pipe failure investigation. Exponent FaAA Report, November 2003.

Carnahan RA. Investigation of Disney Concert Hall exterior panel staining. Exponent FaAA Report, September 2003.

Carnahan RA. Steam turbine blade failure investigation. Exponent FaAA Report, July 2003.

Colwell J, Carnahan RA. Conveyor belt fires at the Wilmington Calciner — Preliminary Report. Exponent FaAA Report, May 2003.

Carnahan RA, Shekerlian S, Saraf V. Investigation of the Cedar Point Insane Tower collapse. Exponent FaAA Report, June 2002.

Rau C, Carnahan RA. Evaluation of the JT8D-200 compressor blade failures. Exponent FaAA Report, March 2002.

Carnahan RA, Moore D. Evalution of the potassium carbonate contactor (V501) failure at the Nuevo Energy Rincon Onshore Facility. Exponent FaAA Report, October 2001.

Carnahan RA. Investigation of La Prensa Grafica printing press bearer damage. Exponent Failure Analysis Associates Report, April 1998.

Carnahan RA, MacNab A. Low NOx burner performance, Boiler No. 3, Century City. Failure Analysis Associates, Inc. Report, August 1994.

Foulds J, Carnahan RA. Examination of failed expansion joint bellows from Craig Station, Unit 2. Failure Analysis Associates, Inc. Report, December 1993.

Carnahan RA. The effect of copper based fungicides on pitting corrosion behavior of aluminum piping. Failure Analysis Associates, Inc. Report, March 1993.

Carnahan RA. Analysis of the couch roll bearing failure at Gaylord Container Corporation. Failure Analysis Associates, Inc. Report, July 1992.

Ross B, Carnahan RA. Examination of Durham Grange fuel storage tanks. Failure Analysis Associates, Inc. Report, September 1989.

Ross B, Carnahan RA. Evaluation of Accupac (hex pump) character toothpaste dispenser failures. Failure Analysis Associates, Inc. Report, August 1989.

Carnahan RA. Examination of a cracked jet pump beam from Peach Bottom 3. General Electric Company Report, July 1983.

MF Aleskey, Carnahan RA. Improvements in jet pump hold-down beam service life. General Electric Company Report, December 1981.

Carnahan RA, Cutt JC. Millstone Point 1 isolation condenser and shutdown cooling system piping cracks. General Electric Company Report, May 1981.